HOMOTOPY-BASED NUMERICAL SOLUTION METHODS FOR THE LOAD FLOW PROBLEM IN LARGE-SCALE ILL-CONDITIONED POWER SYSTEM MODELS

ALISSON LIMA SILVA

PhD THESIS ON ELECTRICAL ENGINEERING

ELECTRICAL ENGINEERING DEPARTMENT

TECHNOLOGY FACULTY

UNIVERSITY OF BRASÍLIA

UNIVERSITY OF BRASÍLIA
TECHNOLOGY FACULTY
ELECTRICAL ENGINEERING DEPARTMENT

HOMOTOPY-BASED NUMERICAL SOLUTION METHODS FOR THE LOAD FLOW PROBLEM IN LARGE-SCALE ILL-CONDITIONED POWER SYSTEM MODELS

ALISSON LIMA SILVA

ADVISOR: PROF. FRANCISCO DAMASCENO FREITAS, PhD

PhD THESIS ON ELECTRICAL ENGINEERING

PUBLICATION: PPGEE TD 209/24
BRASÍLIA/DF: DECEMBER - 2024

Universidade de Brasília
Faculdade de Tecnologia
Departamento de Engenharia Elétrica

Homotopy-based Numerical Solution Methods for the Load Flow Problem in Large-scale Ill-conditioned Power System Models

ALISSON LIMA SILVA

TESE DE DOUTORADO SUBMETIDA AO PROGRAMA DE PÓS-GRADUAÇÃO EM ENGENHARIA ELÉTRICA DA UNIVERSIDADE DE BRASÍLIA COMO PARTE DOS REQUISITOS NECESSÁRIOS PARA A OBTENÇÃO DO GRAU DE DOUTOR EM ENGENHARIA ELÉTRICA.

Orientador: Prof. Francisco Damasceno Freitas, D.Sc. (UnB)

APROVADA POR:

Prof. Kleber Melo e Silva, D.Sc. (UnB)
(Presidente)

Prof. Fernando Augusto Moreira, D.Sc. (UFBA)
(Examinador Externo)

Prof. João Alberto Passos Filho, D.Sc. (UFJF)
(Examinador Externo)

Prof. Francis Arody Moreno Vásquez, D.Sc. (UnB)
(Examinador Interno)

Prof. Fernando Cardoso Melo, D.Sc. (UnB)
(Suplente)

Brasília/DF, 16 de dezembro de 2024.

FICHA CATALOGRÁFICA

LIMA-SILVA, ALISSON

Homotopy-based Numerical Solution Methods for the Load Flow Problem in Large-scale Ill-conditioned Power System Models. [Brasília/DF] 2024.

2024xiv, 151p., 210 x 297 mm (ENE/FT/UnB, Doutor, Tese de Doutorado, 2024).

Universidade de Brasília, Faculdade de Tecnologia, Departamento de Engenharia Elétrica.

1. Power flow problem
2. Newton-Raphson
3. Ill-conditioned
4. Homotopy

I. ENE/FT/UnB
II. Título (série)

REFERÊNCIA BIBLIOGRÁFICA

LIMA-SILVA, ALISSON (2024). Homotopy-based Numerical Solution Methods for the Load Flow Problem in Large-scale Ill-conditioned Power System Models. Tese de Doutorado, Publicação PPGEE TD 209/24, Departamento de Engenharia Elétrica, Universidade de Brasília, Brasília, DF, 151p.

CESSÃO DE DIREITOS

AUTOR: Alisson Lima Silva

TÍTULO: Homotopy-based Numerical Solution Methods for the Load Flow Problem in Large-scale Ill-conditioned Power System Models.

GRAU: Doutor ANO: 2024

Alisson Lima Silva

Universidade de Brasília (UnB)

Campus Darcy Ribeiro

Faculdade de Tecnologia (FT)

Departamento de Engenharia Elétrica (ENE)

Brasília, Distrito Federal, Brasil

CEP 70919-970

Dedico a minha esposa Emília e minha filha Alice.

ACKNOWLEDGEMENTS

Agradeço a Deus pela saúde que me permitiu realizar este sonho e pelas oportunidades incríveis que colocou em meu caminho.

Agradeço à minha esposa, Emília, por me incentivar a trilhar essa jornada. Essa caminhada foi mais leve porque você esteve sempre ao meu lado, compartilhando cada passo e comemorando cada pequena conquista.

À minha mãe, Denice, exemplo de força e determinação, sou profundamente grato por nos apontar a educação como caminho para transformar nossa realidade. Sua dedicação e trabalho árduo sustentaram toda a nossa trajetória, da escola à graduação.

Aos meus irmãos, Poliana, Alfredo e Gabriel, agradeço por estarem comigo em todos os momentos, oferecendo apoio e companheirismo.

À minha tia Dirce, que acompanhou de perto toda essa jornada, incentivando e celebrando cada conquista como se fosse sua, meu sincero agradecimento.

Ao professor Francisco Damasceno, muito obrigado por todo conhecimento compartilhado. O senhor é um exemplo de professor e pesquisador. Sua gentileza, educação e empatia são qualidades que admiro e que desejo levar adiante em minha trajetória acadêmica.

Agradeço também aos professores que compartilharam conhecimento e promoveram discussões em sala de aula, contribuindo para o meu desenvolvimento técnico e crítico.

Ao Departamento de Engenharia Elétrica da UnB, seus técnicos e colaboradores, registro minha gratidão pela eficiência e dedicação com que suportaram e atenderam às demandas, demonstrando a excelência do programa.

Sou grato à Fundação de Apoio à Pesquisa do Distrito Federal, FAPDF, que financiou a viagem para apresentação dos resultados da minha pesquisa no evento IEEE Power & Energy Society General Meeting (PESGM), realizado nos Estados Unidos em julho de 2023.

A todos vocês, muito obrigado!

ABSTRACT

This PhD thesis presents numerical methods based on the homotopy approach to solve the Power Flow Problem (PFP) in large-scale ill-conditioned power system models. For this goal, static and dynamic homotopy-based approaches are employed to embed the nonlinear algebraic equations of the PFP. The static approaches are grounded in Newton-Raphson method (NR) resolutions, while the dynamic methods use numerical integration techniques. The states computed in the dynamic homotopy step are assumed as initial estimates and are refined in a second step by running an NR scheme for finally calculating the PFP solution. This refining step was also employed in a version of a static homotopy-based scheme when a low tolerance is imposed at the last point of the homotopy pathway. As in the dynamic solvers, in this version of the static scheme, a term based on a Fixed Point Vector (FPV) function to embed and enforce the initial estimate of the iterative PFP was inserted in the homotopy function. Studies of simple integration methods were carried out because they were used in the dynamic homotopy approach. The implicit Backward Euler's method (BE) demonstrated adequate qualities for use among the investigated techniques, including explicit and implicit methods. The performance of the techniques was evaluated through experiments conducted on several test systems, which included large-scale ill-conditioned models such as 13k-, 54k-, 70k-, 82k-, and 109k-bus networks. The static homotopy approach combined with the FPV function successfully solved all simulations, including a modified three-slack power system model. In turn, a simpler dynamic homotopy-based method was notable for its low computational cost in solving the PFP. However, while incorporating the beneficial features of the static version with FPV, another dynamic version resulted in a high computational burden. According to the problem formulation, the proposed techniques are appropriate for solving problems related to contingency and others involving inherent modeling by homotopy.

Keywords: Power flow; Newton-Raphson method; ill-conditioned systems; homotopy; MATPOWER.

RESUMO

Título: Métodos Numéricos Baseados em Homotopia para a Solução do Problema de Fluxo de Carga em Modelos de Sistemas de Potência de Grande Escala e Mal Condicionados.

Esta tese de doutorado apresenta métodos numéricos baseados na abordagem de homotopia para resolver o problema de fluxo de potência (PFP) em modelos de sistemas de potência mal condicionados e de grande-porte. Abordagens estáticas e dinâmicas baseadas em homotopia são usadas para incorporar as equações algébricas não-lineares do PFP. As primeiras são baseadas em resoluções do método de Newton-Raphson (NR), enquanto as últimas usam técnicas de integração numérica. Os estados determinados na etapa de homotopia dinâmica são assumidos como estimativas iniciais e são refinados em uma segunda etapa executando um esquema de NR. Esta etapa de refinamento também foi empregada em uma versão de um esquema baseado em homotopia estática Assim como nos solucionadores dinâmicos, nesta versão do esquema estático, um termo baseado em uma função de vetor de ponto fixo para incorporar e impor a estimativa inicial do PFP iterativo foi inserido na função de homotopia. Estudos de métodos de integração simples foram realizados porque eles foram usados na abordagem de homotopia dinâmica. O esquema backward Euler (BE) implícito demonstrou qualidades adequadas para uso entre as técnicas investigadas, incluindo métodos explícitos e implícitos. O desempenho das técnicas foi avaliado em diferentes cenários incluindo redes com número de barras de 13k, 54k, 70k, 82k e 109k. A abordagem de homotopia estática combinada com a função FPV permitiu a resolução com sucesso de todas as simulações, incluindo um modelo de sistema de potência com três barras slacks. Por sua vez, um método baseado em homotopia dinâmica mais simples foi mais eficiente por seu baixo custo computacional na resolução do PFP. As técnicas propostas são apropriadas para resolver problemas relacionados à contingência e outros envolvendo a modelagem inerente por homotopia.

Palavras-chave: Fluxo de carga; método de Newton-Raphson; sistemas mal-condicionados; homotopia; MATPOWER.

TABLE OF CONTENTS

LIST OF FIGURES

LIST OF TABLES

LIST OF SYMBOLS

$\Delta\mathbf{x}^{(i)}$	Mismatch
ϵ	Solution error
μ	Iwamoto optimal multiplier
Ω_k	Set of m buses adjacent to the k bus
$\overline{I}_k$	Current phasor at bus k
$\overline{V}_k$	Voltage phasor at bus k
$\overline{Y}_{km}$	Complex-valued element of bus admittance matrix
θ_{km}	Angular difference between θ_k and θ_m at buses $\#k$ and $\#m$
θ_k	Voltage angle at bus $\#k$
θ_m	Voltage angle at bus $\#m$
$\mathbf{f}(\mathbf{x})$	Compact notation for the set of nonlinear equations
$\mathbf{J}(\mathbf{x}^{(i)})$	Jacobian matrix
$\mathbf{x}$	Network state
$\mathbf{y}^s$	Specified power vector
B_c	Charging capacitance
b_k^{Sh}	Shunt susceptance at bus k
B_{km}	Imaginary part of $\overline{Y}_{km}$
G_{km}	Real part of $\overline{Y}_{km}$

max_{iter} Maximum number of iterations

N_b Number of buses

N_{PQ} Number of PV bus

N_{PV} Number of PQ bus

P_k Net active power injected into bus $\#k$

Q_k Net reactive power injected into bus $\#k$

V_0 Voltage at slack bus

V_{im_k} Imaginary part of voltage phasor $\overline{V}_k$ at bus k

V_{r_k} Real part of voltage phasor $\overline{V}_k$ at bus k

PQ Load Bus

PV Generations Bus

GLOSSARY

AC Alternating Current. 11, 82

BE Backward Euler's method. vi, vii, 26, 62, 66–68, 96–99, 101–106, 108, 112, 114, 118, 119, 126, 128, 149, 151

CN Continuous Newton's philosophy. 2, 25

CPU Central Processing Unit. 84, 103, 115, 116, 125, 129

DC Direct Current. 11, 23, 24, 81, 82, 130

DG Distributed Generation. 55, 58

EHV Extra-high Voltage. 21, 23, 24

FDPF Fast Decoupled Power Flow. 20

FDXB NR fast decoupled. 68, 101, 102, 105, 112, 113, 116, 126, 128

FE Forward Euler's method. 25–27, 62, 66, 68, 96–99, 101–104, 128, 149

FPV Fixed Point Vector. vi, vii, 60, 63, 66, 90–94, 110, 115–119, 125–129

FPV2 Second approach about FPV. 94, 119–122, 125, 126, 128–130

GB Gigabyte. 84

Gen Generation. 84

GHz Gigahertz. 84

GS Gauss-Seidel's method. 11, 12, 57, 85

GS-NR Gauss-Seidel Newton-Raphson. 85, 87

GSH-FPV-NR GSH-NR method improved by FPV. 92, 93, 125, 127–129

GSH-NR Guided Solution Homotopy. 88–94, 115, 116, 125, 127

HKW Heun-King-Werner's method. 2, 28, 112–114, 126

HVDC High-voltage Direct Current. 145

IC Initial Condition. 95, 97, 102

IEEE Institute of Electrical and Electronics Engineers. 54, 79

LU Lower-upper factorization. 62, 65, 67, 68, 95, 99, 101, 106, 116

MATPOWER Package of open-source Matlab-language M-files (or Octave) for solving steady-state power system simulation and optimization problems. 4, 34, 53, 74–82, 84, 85, 87, 92, 103, 112, 113, 115–118, 122, 125, 126, 129, 147

NPHC Numerical Polynomial Homotopy-based Continuation. 55, 56

NR Newton-Raphson method. vi, vii, x, xii, xiv, 1–4, 12–15, 20, 25, 28, 30, 34, 39, 43, 46, 48, 51–55, 57, 60, 62, 64, 65, 68, 72, 74–76, 79, 80, 84–94, 97–108, 110–122, 125, 127–129, 144, 148, 149, 151

NR-flat NR solver initializating from the flat start guess. 85, 87, 92, 126

NR-MAT NR solver starting from native initial estimate given in MATPOWER. 85, 87, 92, 103, 115, 116, 125, 126

ODE Ordinary Differential Equations. 25, 60–62, 64, 65, 72, 73, 118

OM Optimal Multiplier. 2, 40–42

OM-NR Optimal Multiplier Newton-Raphson. 85, 87

OPF Optimal Power Flow. 56, 59

ORGANON Computational tools for power systems analysis. 29, 53

OS Operating System. 84

PBE Power Balance Equations. 10, 27

PDE Partial Differential Equation. 62

PEGASE Pan European Grid Advanced Simulation and State Estimation. 77, 78

PF Power Flow. 1, 2, 50, 59

PFP Power Flow Problem. vi, vii, 1–7, 10–13, 18, 24, 25, 27, 29, 31, 36, 45, 48–55, 58–61, 63–65, 67, 68, 70–73, 75, 76, 81, 82, 84, 85, 87, 89, 92–98, 101–103, 106, 111, 114, 115, 117, 119, 121, 125, 127–129, 143–145

RAM Random-access Memory. 84

RK Runge-Kutta' formulas. 27, 112, 116

RK2 Runge-Kutta 2^{nd} order' method. 27, 62, 66, 68, 96–99, 101–104, 108, 109, 112–114, 128, 149

RK4 Runge-Kutta 4^{th} order's method. 27, 112, 113, 126

SDPF Synthetic Dynamic Power Flow. 29, 30, 38, 53

SR Senseless Result. 110, 113

SSD Solid-state Drive. 84

SSR Sum of Squares of Residuals. 28

TM Trapezoidal method. 26, 32

UHV Ultra-high Voltage. 21, 23, 24

CHAPTER 1

INTRODUCTION

1.1 BACKGROUND

Power Flow studies are essential for determining the steady-state operating point of electrical power systems. Based on the solution obtained for the problem, it is possible to investigate operational conditions that guarantee the successful operation of the power system under normal conditions, such as supply of energy demand and power generation, proximity of voltage magnitudes to extreme operating values, operation of generators within active and reactive power limits, overload in transmission lines and transformers, contingencies and other information (GLOVER *et al.*, 2012).

The Power Flow Problem (PFP) is expressed as a system of nonlinear algebraic equations. Iterative methods are commonly used to find its solution due to its complex nonlinear characteristics. Among these methods, the classical Newton-Raphson method (NR) has traditionally been adopted as the standard approach (KUNDUR, 1994). The NR method relies on an initial estimate that is ideally assigned close to the solution. However, several factors in today's power systems can introduce significant shifts in operating conditions. Therefore, these factors can lead to serious difficulties in achieving an accurate solution using this method. The widespread integration of renewable energy sources (WENG *et al.*, 2012), control devices (GATTA *et al.*, 2024), frequent reversals of power flows (TARANTO *et al.*, 2022), and load variations are just a few examples of such factors. As a result, the voltage magnitudes and angles within the system can undergo substantial changes.

The dynamic nature of these changes poses a challenge in selecting an appropriate initial estimate for the Power Flow (PF) solver. A common practice is to initialize the PF solver using an initial guess based on the learning of qualified personnel who handle the operation of the system. Another alternative is to use data stored by software in planning studies. It is done, for

example, based on daily (or other scale) system operational results, which are peculiar to each power system area. However, without this "learning", a more general estimation can be done based on a flat start, *i.e.*, all bus voltage phase angles equal to zero, and voltage magnitudes in load buses equal 1 pu. On the other hand, this guess may deviate significantly from the desired solution in the analyzed power system model, and consequently, classical iterative methods may diverge (TOSTADO-VÉLIZ *et al.*, 2020a; TOSTADO-VÉLIZ *et al.*, 2021).

According to Milano (2009), when the solution of the PFP cannot be obtained using conventional methods and the standard flat-start initial guess, the problem is considered ill-conditioned, despite the problem having a valid solution. Consequently, there is a need to develop more robust and accurate techniques for initializing the PF solver in order to enhance its effectiveness in handling diverse operating conditions.

Several researchers have investigated different approaches to address ill-conditioning in the PFP. For example, some studies have proposed modifications to the NR method or other iterative methods such as the Heun-King-Werner's method (HKW), as proposed in Tostado-Véliz *et al.* (2020c). Other studies have focused on preconditioning techniques or optimization-based methods. In Pan *et al.* (2020), it has been reported that the accuracy of calculations involving an Optimal Multiplier (OM) can be significantly improved by introducing additional information, for instance, retaining the higher-order terms in Taylor's expansion series approximations for the PFP equations. This particular assumption has consequently motivated the development of an alternative load flow algorithm that utilizes the NR method with optimized step size (PAN *et al.*, 2020).

Managing a single OM entails the manipulation of deviation magnitudes while ensuring consistent directional changes in the state of the system. Alternative methodologies have been proposed to address ill-conditioned PFP. Notably, techniques grounded in the Continuous Newton's philosophy (CN) have gained attention. These techniques involve adapting numerical integration methods to effectively solve the PFP (MILANO, 2009). This can be interpreted as a dynamic tool.

In this context of the increasing complexity of power systems and the search for more robust solvers, homotopy concepts are suitable (OKUMURA *et al.*, 1991) for solving the problem as they change the original state in search of an easy-to-solve scenario (KU *et al.*, 2011). If the

change is appropriate, a feasible solution presents itself, starting an iterative process, with the help of other solvers, to return to the original scenario that is difficult to solve. In Freitas & Silva (2022), a static homotopy approach was presented for solving a PFP. This approach utilizes two parameters to generate a path starting from an initial guess and leading to the final solution. However, due to the utilization of the NR solver at each step of the path, the computational cost is high, especially for ill-conditioned large-scale systems. Despite the elevated cost, the technique is robust and effective in obtaining a solution for the PFP, even under challenging conditions.

1.2 OBJECTIVE

The main objective of this PhD thesis is to present alternative techniques using homotopy that combine different techniques to efficiently solve the ill-conditioned power flow problem in large-scale systems. The static and dynamic homotopy-based techniques are investigated.

The specific objectives of this PhD thesis are specified as follows:

- Presentation of homotopy-based techniques applied to power systems to solve the large-scale ill-conditioned power flow problem;
- Investigation of both static and dynamical homotopy approaches with some specific characteristics of each method;
- Simulations involving large-scale ill-conditioned power systems to demonstrate the robustness of the techniques to solve difficult convergence problems;
- Investigations of the behavior of the defined method parameters, tests in contingency scenarios, and simulations for cases considering multiple slacks and overloaded systems; and
- Demonstration of the sensitivity of the results for an iterative PFP, departing from an initial estimate based on a flat start. It is emphasized how a homotopy-based technique is beneficial for successfully converging the problem.

The proposed approaches aim to overcome the limitations of traditional methods, such

as the conventional Newton-Raphson method, and provide accurate solutions while avoiding convergence issues. The effectiveness of these approaches is evaluated through experiments on large-scale and ill-conditioned models to contribute to developing more efficient and effective solutions for PFP in complex power systems.

1.3 CONTRIBUTIONS

The main contribution presented by this work is the proposition of methods that allow convergence for ill-conditioned large-scale systems starting from an initial estimate flat start. The methods were tested with real systems available in the MATPOWER database, such as 13k-, 70k-, 82k, and 109k-bus, demonstrating the robustness of the method.

The idea is to handle homotopy functions in both static and dynamic forms. In general, other publications explore only the static form. In this work, detailed studies based on the dynamical approach demonstrate the efficiency of this tool to solve a PFP in combination with the classical NR solver.

The work presents the homotopy technique as a powerful tool for dealing with the problem of multiple slacks in a power system model. It is also adequate for multiple contingency studies since interconnections can generally be disabled and/or activated simultaneously, while the proposed power flow based on homotopy is solved just once. Experiments involving an 82k-bus system illustrate this contribution.

Another relevant point is that the method was developed in the free software MATPOWER (ZIMMERMAN; MURILLO-SÁNCHEZ, 2020), in which adaptations were implemented in an auxiliary script to complement the original and obtain the desired results.

1.4 RELATED PUBLICATIONS

As a result of the research, the work provided the following publications:

(1) FREITAS, F. D.; SILVA, A. L. Flat start guess homotopy-based power flow method guided by fictitious network compensation control. International Journal of Electrical Power & Energy Systems, Elsevier Ltd, v. 142, p. 108311, 11 2022. ISSN 01420615. Available

in: <https://doi.org/10.1016/j.ijepes.2022.108311>. (FREITAS; SILVA, 2022);

(2) LIMA-SILVA, A.; FREITAS, F. D.; FERNANDES, L. F. de J. A homotopy-based approach to solve the power flow problem in islanded microgrid with droop-controlled distributed generation units. Energies, v. 16, p. 5323, 7 2023. ISSN 1996-1073. Available in: <https://www.mdpi.com/1996-1073/16/14/5323>. (LIMA-SILVA *et al.*, 2023);

(3) LIMA-SILVA, A.; FREITAS, F. D. Dynamical homotopy transient-based technique to improve the convergence of ill-posed power flow problem. International Journal of Electrical Power & Energy Systems, Elsevier Ltd, v. 155, p. 109436, 1 2024. ISSN 01420615. Available in: <https://doi.org/10.1016/j.ijepes.2023.109436>. (LIMA-SILVA; FREITAS, 2024a);

(4) FREITAS, F. D.; LIMA-SILVA, A. A power flow homotopy-based solver emanating from a flat start estimate. In: 2023 IEEE Power & Energy Society General Meeting (PESGM). IEEE, 2023. p. 15. ISBN 978-1-6654-6441-3. Available in: <https://ieeexplore.ieee.org/document/10252210/> (FREITAS; LIMA-SILVA, 2023);

(5) LIMA-SILVA, A.; FREITAS, F. D.; FERNANDES, L. F. D. J. Técnica baseada em homotopia com uma rede fictícia para determinação da solução do problema de fluxo de potência em sistemas mal-condicionados. In: Simpósio Brasileiro de Sistemas Elétricos - SBSE. [S.l.: s.n.], 2023. (LIMA-SILVA *et al.*, 2023); and

(6) LIMA-SILVA, A.; FREITAS, F. D. Exploring a dynamic homotopy technique to enhance the convergence of classical power flow iterative solvers in ill-conditioned power system models. Energies, v. 17, p. 4642, 9 2024. ISSN 1996-1073. Available in: <https://www.mdpi.com/1996-1073/17/18/4642>. (LIMA-SILVA; FREITAS, 2024b).

1.5 OUTLINE

This PhD thesis, in addition to Chapter 1 presented previously, is organized as follows:

- Chapter 2 presents the fundamentals for the formation of nonlinear equations that govern the PFP, in addition to detailing classical solvers based on differential ordinary equations, furthermore details the main concepts of homotopy;

- Chapter 3 provides a bibliographical review of the main works published in scientific

journals that use, among others, the homotopy method to solve the PFP;

- Chapter 4 presents the idea of homotopy-based methods emphasizing static and dynamical homotopy, besides the concepts of the proposed Fixed Point Vector homotopy methods;
- Chapter 5 presents the test systems chosen to validate the proposed methods and their main technical characteristics;
- Chapter 6 presents the experiments and results under different performance parameters, such as the number of iterations, computational performance, and contingency studies, applied to each power system model;
- Chapter 7 shows the main conclusions of the thesis; and
- The Appendix A, Appendix B, and Appendix C complement details and tutorial information covered superficially in the main text.

CHAPTER 2

FUNDAMENTALS

This chapter presents the basis of the power flow problem. It aims to show the key equations involved in modeling the problem and address the traditional and other known methods that originated numerical computations in the past but are still used as references for studying the PFP.

Advanced methodologies that treat ill-conditioned problems are also discussed, including the fundamentals of the homotopy method.

2.1 THE POWER FLOW PROBLEM

An energy transmission system is a complex network that allows the transfer of electricity from generation sources to consumers. At its core, it includes several key components and primarily consists of elements like interconnections, device models, loads, generation sources, and various characteristics, including device limits, transformer tap control, and capacitor/reactor switching. Together, these elements allow the formation of a network model, which can be modeled using various mathematical techniques. These elements have their models and can be effectively modeled to create the network equations (KUNDUR, 1994). These models are essential for deriving network equations that describe how power flows through the system, enable engineers to analyze performance, identify potential issues, and develop strategies for improvement.

Considering a portion of a power system defined by a fictitious bus k and the elements that compose it, as illustrated in Figure 2.1, the current injection convention consists of the current injection at bus k ($\overline{I}_k$), the shunt susceptance at bus k (jb_k^{Sh}), admittance between bus k and bus m (y_{km}). Assigning the voltage at bus k as $\overline{V}_k$, by Kirchhoff's first law, the current

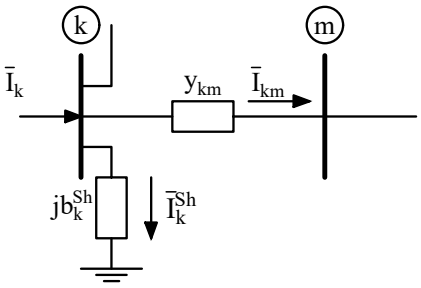

Figure 2.1: Current injection at bus k

injected at bus k is defined by

$$\overline{I}_k = jb_k^{Sh}\overline{V}_k + \sum_{m\in\Omega_k} \overline{I}_{km}, \tag{2.1}$$

in which Ω_k is a set of m buses adjacent to the k bus. Similarly, the current flowing from bus k to bus m can be defined by

$$\overline{I}_{km} = y_{km}\left(\overline{V}_k - \overline{V}_m\right). \tag{2.2}$$

It can be concluded that the current injected into bus k can be defined as

$$\overline{I}_k = \left[jb_k^{Sh} + \sum_{m\in\Omega_k}\left(y_{km} + jb_{km}^{Sh}\right)\right]\overline{V}_k + \sum_{m\in\Omega_k}\left(-y_{km}\right)\overline{V}_m. \tag{2.3}$$

The Kirchhoff's law relating current and voltage modeling these devices at each bus can be put as

$$\left[\overline{\mathbf{I}}\right] = \left[\mathbf{Y}_{bus}\right]\cdot\left[\overline{V}\right]. \tag{2.4}$$

From Equation (2.3), each element of nodal admittance matrix $\mathbf{Y}_{bus}$ may be constructed as

$$\mathbf{Y}_{km} = -y_{km}, \tag{2.5}$$

$$\mathbf{Y}_{kk} = jb_k^{Sh} + \sum_{m\in\Omega_k}\left(y_{km} + jb_{km}^{Sh}\right), \tag{2.6}$$

such that Equation (2.4) can be expressed with its elements (ZANETTA JR., 2006) in matrix form

$$\begin{bmatrix}\overline{\mathbf{I}}_1\\ \overline{\mathbf{I}}_2\\ \vdots\\ \overline{\mathbf{I}}_k\\ \vdots\\ \overline{\mathbf{I}}_N\end{bmatrix} = \begin{bmatrix}\mathbf{Y}_{11} & \mathbf{Y}_{12} & \cdots & \mathbf{Y}_{1m} & \cdots & \mathbf{Y}_{1N}\\ \mathbf{Y}_{21} & \mathbf{Y}_{22} & \cdots & \mathbf{Y}_{2m} & \cdots & \mathbf{Y}_{2N}\\ \vdots & \vdots & \ddots & \vdots & \ddots & \vdots\\ \mathbf{Y}_{k1} & \mathbf{Y}_{k2} & \cdots & \mathbf{Y}_{km} & \cdots & \mathbf{Y}_{kN}\\ \vdots & \vdots & \ddots & \vdots & \ddots & \vdots\\ \mathbf{Y}_{N1} & \mathbf{Y}_{N2} & \cdots & \mathbf{Y}_{Nm} & \cdots & \mathbf{Y}_{NN}\end{bmatrix}\cdot\begin{bmatrix}\overline{V}_1\\ \overline{V}_2\\ \vdots\\ \overline{V}_m\\ \vdots\\ \overline{V}_N\end{bmatrix}. \tag{2.7}$$

Therefore, the current in the k^{th} node, for a given total number of buses N_b, is given by Equation (2.8).

$$\begin{aligned} \overline{I}_k &= Y_{k1}\overline{V}_1 + Y_{k2}\overline{V}_2 + \cdots + Y_{km}\overline{V}_m, \\ \overline{I}_k &= \sum_{m=1}^{N_b} \overline{Y}_{km}\overline{V}_m. \end{aligned} \tag{2.8}$$

The complex power injection at each bus depends on the voltage at the bus, and the injected current (GLOVER *et al.*, 2012) in such a way that

$$\overline{S}_k \ = \ P_k \ + jQ_k = \overline{V}_k \overline{I}_k^*, \tag{2.9}$$

$$P_k \ + jQ_k = \overline{V}_k \left[\sum_{m=1}^{N_b} \overline{Y}_{km}\overline{V}_m \right]^* . \tag{2.10}$$

Moreover, the voltage phasor is $\overline{V}_k = V_k e^{j\theta_k}$, $\overline{V}_m^* = V_m e^{-j\theta_m}$ and $\overline{Y}_{km}^* = G_{km} - jB_{km}$. Then, replacing it in Equation (2.10)

$$P_k \ + jQ_k = V_k \sum_{m=1}^{N_b} (G_{km} - jB_{km}) V_m e^{j(\theta_k - \theta_m)}. \tag{2.11}$$

Knowing that the angular difference is given by $\theta_k - \theta_m = \theta_{km}$ and using the Euler equation given by

$$e^{j\theta_{km}} = \cos\theta_{km} + j\sin\theta_{km}, \tag{2.12}$$

Equation (2.11) can be rewritten as Equation (2.13).

$$P_k \ + jQ_k = V_k \sum_{m=1}^{N_b} V_m (G_{km} - jB_{km}) \left[\cos(\theta_{km}) + j\sin(\theta_{km}) \right]. \tag{2.13}$$

Therefore, separating the imaginary and real components from Equation (2.13), the net active power injected into bus $\#k$, denoted as P_k, and the net reactive power injected into the same bus, denoted as Q_k, can be expressed as Equation (2.14) and Equation (2.15).

$$P_k = V_k \sum_{m=1}^{N_b} V_m \left[G_{km}\cos(\theta_{km}) + B_{km}\sin(\theta_{km}) \right] \qquad k = 1, 2, \ldots, N_b, \tag{2.14}$$

$$Q_k = V_k \sum_{m=1}^{N_b} V_m \left[G_{km}\sin(\theta_{km}) - B_{km}\cos(\theta_{km}) \right] \qquad k = 1, 2, \ldots, N_b. \tag{2.15}$$

Analyzing a bus of a power system, the power injected into this bus $\overline{S}_k$ is the sum of the powers generated $\overline{S}_{Gk}$ and the power consumed $\overline{S}_{Dk}$ in this bus k, that is, $\overline{S}_k = \overline{S}_{Gk} - \overline{S}_{Dk}$. Decomposing the apparent power $\overline{S}_k$ into active $\overline{P}_k$ and reactive power $\overline{Q}_k$

$$\overline{P}_k = \overline{P}_{Gk} - \overline{P}_{Dk}, \tag{2.16}$$

$$\overline{Q}_k = \overline{Q}_{Gk} - \overline{Q}_{Dk}. \tag{2.17}$$

Each bus is associated with four variables: V_k, θ_k, P_k, and Q_k (GLOVER *et al.*, 2012). Two of these variables must be specified to compute an operation point and the power flow in the network. According to the bus type, the others are calculated, which can be verified in Equations (2.14) and (2.15). The slack bus, or $V\theta$-bus type, is a reference point with a predetermined voltage magnitude and angle, contributing to balance system losses. The PQ bus, also called the load bus, is the one where active and reactive power are specified, and the voltage magnitude and phase angle are determined. This bus typically represents a load connection. The PV bus, or controlled voltage bus, is linked to a voltage source, with the voltage phase and reactive power are calculated. Furthermore, it requires consideration of reactive power constraints (QIN, 2017).

Equations (2.14) and (2.15) represent a set of nonlinear equations that serve as the basis for the PFP solution for a system with N_b buses. Rearranging these equations establishes this set of equations according to the number of PV and PQ buses, known as Power Balance Equations (PBE). Its standard form is in the polar coordinates by considering power injection formulation in Equations (2.18) and (2.19),

$$0 = P_k - V_k \sum_{m=1}^{N_b} V_m \left[G_{km} cos(\theta_{km}) + B_{km} sin(\theta_{km}) \right], \quad k \in PQ \text{ or } PV, \tag{2.18}$$

$$0 = Q_k - V_k \sum_{m=1}^{N_b} V_m \left[G_{km} sin(\theta_{km}) - B_{km} cos(\theta_{km}) \right], \quad k \in PQ. \tag{2.19}$$

where a nodal voltage phasor at bus $\#k$ is $\overline{V}_k = V_k \angle \theta_k$, V_k and θ_k are the voltage magnitude and phase angle of $\overline{V}_k$, respectively; $\theta_{km} = \theta_k - \theta_m$ is the angular difference between θ_k and θ_m at buses $\#k$ and $\#m$, respectively. P_k is the net active power injected into bus $\#k$, while Q_k is the net reactive power injected into the same bus; G_{km} and B_{km} are the real and imaginary parts of $\overline{Y}_{km} = G_{km} + jB_{km}$, the complex-valued entry element $\overline{Y}_{km}$ of the system bus admittance matrix.

In Equation (2.18) and Equation (2.19), P_k and Q_k can be put as a function of the voltage magnitude (ZIP model, exponential form, etc.) (KUNDUR, 1994). Also, they can be constrained, where the most usual is the reactive power limits verified in generator models.

The number of buses (N_b) can be defined by the sum of the number of PV buses (N_{PV}) and

PQ buses (N_{PQ}) plus the slack bus. For example, considering an AC network with only one slack bus, the number of bus is

$$N_b = N_{PQ} + N_{PV} + 1. \tag{2.20}$$

However, note that several slack buses can be present in a network, for example, in the case of islanding of the system or in the case of asynchronous networks interconnected by DC link. Knowing that Equation (2.18) is due to the PQ and PV buses, and Equation (2.19) is due just to the PQ buses (ZANETTA JR., 2006), the total number (n) of nonlinear equations to be solved is given by

$$n = 2N_{PQ} + N_{PV}, \tag{2.21}$$

and this set n of equations can be denoted by Equation (2.22), in which $\mathbf{x} = \left[\boldsymbol{\theta}^T \, \boldsymbol{V}^T\right]^T \in \mathbb{R}^n$ is the network state and $\mathbf{f}(\mathbf{x})$ is a map, that is known as mismatch (or residue) of the PFP, of the type $\mathbf{f}(\mathbf{x}) : \mathbb{R}^n \mapsto \mathbb{R}^n$, which is usually solved by numerical methods.

$$\mathbf{f}(\mathbf{x}) = \mathbf{0}. \tag{2.22}$$

2.2 CLASSICAL SOLVERS

Several methods are used to determine the solution of the PFP. The problem is discussed in the sequel.

2.2.1 Gauss-Seidel method

The Gauss-Seidel's method (GS) is an iterative numerical and simple method (AMERON-GEN, 1989) which performs well for solving a load flow in small power systems. In some solvers, the GS method is used as the initial solution (CHATTERJEE; MANDAL, 2017). A noted disadvantage is the number of iterations needed to achieve the desired accuracy; the convergence becomes slower when the system size expands.

Assume a relation between nodal voltage and injected current into a bus. The base equation starts from the relationship between the voltage and current in a bus and the active and reactive

powers injected (STEVENSON JR., 1986).

$$\overline{V}_k \overline{I}_k^* = P_k - jQ_k, \tag{2.23}$$

$$\overline{I}_k = \frac{P_k - jQ_k}{\overline{V}_k^*}, \tag{2.24}$$

$$\frac{P_k - jQ_k}{\overline{V}_k^*} = \overline{Y}_{kk}\overline{V}_k + \sum_{\substack{n=1 \\ n\neq k}}^{N_b} \overline{Y}_{kn}\overline{V}_n. \tag{2.25}$$

The voltage at PQ-bus k can be calculated (ZANETTA JR., 2006) using iterative steps defined by

$$\overline{V}_k^{(i+1)} = \frac{1}{\overline{Y}_{kk}} \left(\frac{P_k - jQ_k}{\left(\overline{V}_k^{(i)}\right)^*} - \sum_{\substack{n=1 \\ n\neq k}}^{N_b} \overline{Y}_{kn}\overline{V}_n^{(i)} \right), \tag{2.26}$$

and the iterative GS method

$$\overline{V}_k^{(i+1)} = \frac{1}{\overline{Y}_{kk}} \left(\frac{P_k - jQ_k}{\left(\overline{V}_k^{(i)}\right)^*} - \sum_{n=1}^{k-1} \overline{Y}_{kn}\overline{V}_n^{(i+1)} - \sum_{n=k+1}^{N_b} \overline{Y}_{kn}\overline{V}_n^{(i)} \right). \tag{2.27}$$

Iterations continue as long as a stopping condition from Equation (2.28) is not met (GLOVER *et al.*, 2012).

$$\left| \frac{\overline{V}_k^{(i+1)} - \overline{V}_k^{(i)}}{\overline{V}_k^{(i)}} \right| < \epsilon \qquad \text{for all} \quad k = 1, 2, \ldots, N. \tag{2.28}$$

2.2.2 Newton-Raphson's method

A classical load flow method known as Newton-Raphson method (NR) or Newton-Fouriers method (MILANO, 2010) is widely used in several PFP studies as a reference method. Well known as a solver for well-conditioned cases (MILANO, 2009), it can solve large-scale systems in a few iterations. The speed of convergence is one of its characteristics since the number of iterations does not depend on the size of the system (TINNEY; HART, 1967). Furthermore, accuracy is an important point for this method, being the precision controlled by a tolerance for the power mismatch (ϵ), for example, in the range of $\epsilon = 1 \times 10^{-8}$ or smaller. This value is widely used as a parameter for testing numerical solvers. Describing this power mismatch in real values, it amounts to an inaccuracy of the calculations obtained of the order of 1 VA for a system based on 100 MVA.

Assuming that a PFP can be modeled by a set of non-linear equations defined by $\mathbf{f}(\mathbf{x})$, the idea is to find the solution $\mathbf{x}_*$ of the set of equations for which $\mathbf{f}(\mathbf{x}) = 0$ starting from an initial guess $\mathbf{x}^{(0)}$.

Let $\mathbf{x}$ be a single variable and $\mathbf{f}(\mathbf{x})$ a single variate function. The Taylor expansion is used as a starting point for the NR method, which is defined by

$$\mathbf{f}(\mathbf{x}) = \sum_{n=0}^{\infty} \frac{\mathbf{f}^{(n)}\left(\mathbf{x}^{(0)}\right)}{n!} \left(\mathbf{x} - \mathbf{x}^{(0)}\right)^n, \tag{2.29}$$

and can be rewritten as

$$\begin{aligned} \mathbf{f}(\mathbf{x}) = \mathbf{f}\left(\mathbf{x}^{(0)}\right) + \mathbf{f}'\left(\mathbf{x}^{(0)}\right)\left(\mathbf{x} - \mathbf{x}^{(0)}\right) + \frac{\mathbf{f}''\left(\mathbf{x}^{(0)}\right)}{2!}\left(\mathbf{x} - \mathbf{x}^{(0)}\right)^2 + \\ \frac{\mathbf{f}'''\left(\mathbf{x}^{(0)}\right)}{3!}\left(\mathbf{x} - \mathbf{x}^{(0)}\right)^3 + \cdots + \frac{\mathbf{f}^{(n)}\left(\mathbf{x}^{(0)}\right)}{n!}\left(\mathbf{x} - \mathbf{x}^{(0)}\right)^n. \end{aligned} \tag{2.30}$$

Considering that higher-order terms have less impact on the total sum, a linear approximation is defined by

$$\mathbf{f}(\mathbf{x}) \approx \mathbf{f}\left(\mathbf{x}^{(0)}\right) + \mathbf{f}'\left(\mathbf{x}^{(0)}\right)\left(\mathbf{x} - \mathbf{x}^{(0)}\right), \tag{2.31}$$

in which $\mathbf{f}'(\mathbf{x}) = \left[\dfrac{\partial \mathbf{f}}{\partial \mathbf{x}}\right]$, then

$$\mathbf{f}(\mathbf{x}) \approx \mathbf{f}\left(\mathbf{x}^{(0)}\right) + \left[\left.\frac{\partial \mathbf{f}}{\partial \mathbf{x}}\right|_{\mathbf{x}^{(0)}}\right]\left(\mathbf{x} - \mathbf{x}^{(0)}\right). \tag{2.32}$$

Given that $\mathbf{f}(\mathbf{x}) = 0$, then

$$0 \approx \mathbf{f}\left(\mathbf{x}^{(0)}\right) + \left[\left.\frac{\partial \mathbf{f}}{\partial \mathbf{x}}\right|_{\mathbf{x}^{(0)}}\right]\left(\mathbf{x} - \mathbf{x}^{(0)}\right), \tag{2.33}$$

and

$$\mathbf{f}\left(\mathbf{x}^{(0)}\right) \approx -\left[\left.\frac{\partial \mathbf{f}}{\partial \mathbf{x}}\right|_{\mathbf{x}^{(0)}}\right]^{-1}\left(\mathbf{x} - \mathbf{x}^{(0)}\right). \tag{2.34}$$

Therefore the new estimate $\mathbf{x}$ can be obtained through the previous estimate $\mathbf{x}^{(0)}$ given from the equation

$$\mathbf{x} \approx \mathbf{x}^{(0)} - \frac{\mathbf{f}\left(\mathbf{x}^{(0)}\right)}{\left.\dfrac{\partial \mathbf{f}}{\partial \mathbf{x}}\right|_{\mathbf{x}^{(0)}}}. \tag{2.35}$$

In the same way, as $\mathbf{x} - \mathbf{x}^{(0)} = \Delta\mathbf{x}$, it is easy to note that

$$\Delta\mathbf{x} \approx -\frac{\mathbf{f}\left(\mathbf{x}^{(0)}\right)}{\left.\dfrac{\partial \mathbf{f}}{\partial \mathbf{x}}\right|_{\mathbf{x}^{(0)}}}, \tag{2.36}$$

and Equation (2.35) can be rewritten as

$$\mathbf{x} \approx \mathbf{x}^{(0)} + \Delta\mathbf{x}. \tag{2.37}$$

Updating in Equation (2.37) is needed because the expression gives only a linear approximation of $\mathbf{f}(\mathbf{x})$. Then, several iterates are necessary until a prescribed precision is reached.

Considering that the nonlinear equations formed by a practical system are defined by multiple variables, Equation (2.36) can be extended to a matrix form. In this case, the derivative function of $\mathbf{f}(\mathbf{x})$ is transformed into a matrix named as Jacobian matrix $\mathbf{J}(\mathbf{x})$, where for $\mathbf{f}(\mathbf{x}) \in \mathbb{R}^n$ and $\mathbf{x} \in \mathbb{R}^n$

$$\mathbf{J}\left(\mathbf{x}^{(i)}\right) = \left.\frac{\partial \mathbf{f}(\mathbf{x})}{\partial \mathbf{x}}\right|_{\mathbf{x}^{(i)}}, \tag{2.38}$$

$$\mathbf{J}\left(\mathbf{x}^{(i)}\right) = \begin{bmatrix} \frac{\partial \mathbf{f}_1(\mathbf{x})}{\partial \mathbf{x}_1} & \frac{\partial \mathbf{f}_1(\mathbf{x})}{\partial \mathbf{x}_2} & \cdots & \frac{\partial \mathbf{f}_1(\mathbf{x})}{\partial \mathbf{x}_n} \\ \frac{\partial \mathbf{f}_2(\mathbf{x})}{\partial \mathbf{x}_1} & \frac{\partial \mathbf{f}_2(\mathbf{x})}{\partial \mathbf{x}_2} & \cdots & \frac{\partial \mathbf{f}_2(\mathbf{x})}{\partial \mathbf{x}_n} \\ \vdots & \vdots & \ddots & \vdots \\ \frac{\partial \mathbf{f}_n(\mathbf{x})}{\partial \mathbf{x}_1} & \frac{\partial \mathbf{f}_n(\mathbf{x})}{\partial \mathbf{x}_2} & \cdots & \frac{\partial \mathbf{f}_n(\mathbf{x})}{\partial \mathbf{x}_n} \end{bmatrix}. \tag{2.39}$$

In summary, the NR method is governed by Equation (2.40). Furthermore, the estimate of the root $\mathbf{x}_*$ computed for the ith iteration is $\mathbf{x}^{(i+1)}$. Hence, it clearly depends on the estimate from the previous iteration $\mathbf{x}^{(i)}$, and the increment $\Delta\mathbf{x}^{(i)}$ computed according to (2.41).

$$\mathbf{x}^{(i+1)} = \mathbf{x}^{(i)} + \Delta\mathbf{x}^{(i)}, \tag{2.40}$$

$$\Delta\mathbf{x}^{(i)} = -\left[\mathbf{J}\left(\mathbf{x}^{(i)}\right)\right]^{-1} \mathbf{f}\left(\mathbf{x}^{(i)}\right). \tag{2.41}$$

After some convergent iterations, the numerical iterative procedure can converge for a result $\mathbf{x}_*$, depending on the initial guess. The control of the convergence process is assessed by verifying the absolute deviations of a given set of variables or mismatch of $\mathbf{f}(\mathbf{x})$. A usual metric is to adopt the $||\cdot||_\infty$. Then, one way is to control the absolute deviations of $\Delta\mathbf{x}^{(i)}$ or of the mismatches of the function (see Equation (2.42)). Then, when $||\cdot||_\infty < \epsilon$ for a specified error ϵ, the method converges. In case this result is not obtained for a fixed number of iterations max_{iter}, the problem is divergent. In this latter case, the problem has no solution, or the initial guess was not adequately assigned to lead to the convergence of the iterates. Therefore, a robust

method (or strategy) is necessary to solve the problem better.

$$\|\mathbf{f}(\mathbf{x}_*)\|_\infty < \epsilon, \text{for } \epsilon > 0, \tag{2.42}$$

$$\|\mathbf{f}(\mathbf{x}_*)\|_\infty = max\left\{|f_1|, \ldots, |f_n|\right\}. \tag{2.43}$$

2.2.2.1 Polar coordinate

All formulations of the NR method shown before followed the formulation in polar coordinates. From Equations (2.18) and (2.19), the objective of the iterative method is to find a state vector $\mathbf{x}$ composed of a module V and an angle θ of voltage that satisfies the equation below, or approximates the result

$$P_k^{sp} - V_k \sum_{m=1}^{N_b} V_m(\mathbf{G}_{km}\cos\theta_{km} + \mathbf{B}_{km}\sin\theta_{km}) = 0, \tag{2.44}$$

$$Q_k^{sp} - V_k \sum_{m=1}^{N_b} V_m(\mathbf{G}_{km}\sin\theta_{km} + \mathbf{B}_{km}\cos\theta_{km}) = 0, \tag{2.45}$$

where the specified active power is defined by P_k^{sp} and the specified reactive power is defined by Q_k^{sp}. Thus the state vector in polar form is defined by

$$\mathbf{x} = \begin{bmatrix} \theta \\ \mathbf{V} \end{bmatrix}. \tag{2.46}$$

Therefore the power mismatches in the iterative process can be defined by

$$\Delta P_k = P_k^{sp} - P(\mathbf{V},\theta), \tag{2.47}$$

$$\Delta Q_k = Q_k^{sp} - Q(\mathbf{V},\theta). \tag{2.48}$$

Applying Equation (2.31), the matrix of power mismatches was defined for each iteration i as

$$\begin{bmatrix} \Delta P^{(i)} \\ \\ \Delta Q^{(i)} \end{bmatrix} = \begin{bmatrix} \dfrac{\partial(\Delta P)}{\partial\theta} & \dfrac{\partial(\Delta P)}{\partial V} \\ \\ \dfrac{\partial(\Delta Q)}{\partial\theta} & \dfrac{\partial(\Delta Q)}{\partial V} \end{bmatrix} \begin{bmatrix} \Delta\theta^{(i)} \\ \\ \Delta V^{(i)} \end{bmatrix}, \tag{2.49}$$

knowing that P^{sp} and Q^{sp} are constants, Equations (2.47) and (2.48) are as follows

$$\begin{bmatrix} \Delta P^{(i)} \\ \\ \Delta Q^{(i)} \end{bmatrix} = - \begin{bmatrix} \dfrac{\partial P}{\partial\theta} & \dfrac{\partial P}{\partial V} \\ \\ \dfrac{\partial Q}{\partial\theta} & \dfrac{\partial Q}{\partial V} \end{bmatrix} \begin{bmatrix} \Delta\theta^{(i)} \\ \\ \Delta V^{(i)} \end{bmatrix}. \tag{2.50}$$

Thus, the increments of the state vector can be calculated for each iteration i as follows

$$\begin{bmatrix} \Delta\theta^{(i)} \\ \\ \Delta V^{(i)} \end{bmatrix} = - \begin{bmatrix} \dfrac{\partial P}{\partial \theta} & \dfrac{\partial P}{\partial V} \\ \\ \dfrac{\partial Q}{\partial \theta} & \dfrac{\partial Q}{\partial V} \end{bmatrix}^{-1} \begin{bmatrix} \Delta P^{(i)} \\ \\ \Delta Q^{(i)} \end{bmatrix}, \tag{2.51}$$

and can be updated at each iteration as follows

$$\theta^{(i+1)} = \theta^{(i)} + \Delta\theta^{(i)}, \tag{2.52}$$

$$V^{(i+1)} = V^{(i)} + \Delta V^{(i)}. \tag{2.53}$$

In the literature, it is common to see the subdivision of the Jacobian matrix $\mathbf{J} = \begin{bmatrix} \frac{\partial P}{\partial \theta} & \frac{\partial P}{\partial V} \\ \frac{\partial Q}{\partial \theta} & \frac{\partial Q}{\partial V} \end{bmatrix}$ into submatrices called H, N, M and L, in which $L = \frac{\partial P}{\partial \theta}$, $N = \frac{\partial P}{\partial V}$, $M = \frac{\partial Q}{\partial \theta}$, and $L = \frac{\partial Q}{\partial V}$ (STEVENSON JR., 1986; KUNDUR, 1994; ZANETTA JR., 2006). Thus, Equation (2.51) can be rewritten as

$$\begin{bmatrix} \Delta\theta^{(i)} \\ \\ \Delta V^{(i)} \end{bmatrix} = - \begin{bmatrix} H & N \\ \\ M & L \end{bmatrix}^{-1} \begin{bmatrix} \Delta P^{(i)} \\ \\ \Delta Q^{(i)} \end{bmatrix}. \tag{2.54}$$

This subdivision into submatrices is justified because the equation of the partial derivatives of the power equations as a function of the variables results in equations in polar coordinates that are easy to implement computationally. Therefore, the submatrices can be defined by

$$H_{km} = \frac{\partial P_k}{\partial \theta_m} = V_k V_m (\mathbf{G}_{km} \sin\theta_{km} - \mathbf{B}_{km} \cos\theta_{km}), \tag{2.55}$$

$$H_{kk} = \frac{\partial P_k}{\partial \theta_k} = -Q_k - V_k^2 B_{kk}, \tag{2.56}$$

$$N_{km} = \frac{\partial P_k}{\partial V_m} = V_k (\mathbf{G}_{km} \cos\theta_{km} + \mathbf{B}_{km} \sin\theta_{km}), \tag{2.57}$$

$$N_{kk} = \frac{\partial P_k}{\partial V_k} = V_k^{-1} (P_k + V_k^2 \mathbf{G}_{kk}), \tag{2.58}$$

$$M_{km} = \frac{\partial Q_k}{\partial \theta_m} = -V_k V_m (\mathbf{G}_{km} \cos\theta_{km} + \mathbf{B}_{km} \sin\theta_{km}), \tag{2.59}$$

$$M_{kk} = \frac{\partial Q_k}{\partial \theta_k} = P_k - V_k^2 \mathbf{G}_{kk}, \tag{2.60}$$

$$L_{km} = \frac{\partial Q_k}{\partial V_m} = V_k (\mathbf{G}_{km} \sin\theta_{km} - \mathbf{B}_{km} \cos\theta_{km}), \tag{2.61}$$

$$L_{kk} = \frac{\partial Q_k}{\partial V_k} = V_k^{-1} (Q_k - V_k^2 \mathbf{B}_{kk}). \tag{2.62}$$

2.2.2.2 Rectangular coordinate

Another way to organize the power flow equations is to use a rectangular form instead of a polar one. All equations must be adjusted, and a new formulation must be defined in this case. In this way, the nodal voltages at buses k and m can be rewritten as

$$\overline{V}_k = V_k e^{j\theta_k} = V_{r_k} + jV_{im_k}, \tag{2.63}$$

$$\overline{V}_m = V_m e^{j\theta_m} = V_{r_m} + jV_{im_m}, \tag{2.64}$$

where V_r and V_{im} are defined as the real and imaginary part of the voltage phasor $\overline{V}$. The active and reactive power injected into a bus k can be written in rectangular form as

$$P_k = \sum_{m=1}^{N_b} \left[V_{r_k}(\mathbf{G}_{km}V_{r_m} - \mathbf{B}_{km}V_{im_m}) + V_{im_k}(\mathbf{G}_{km}V_{im_m} - \mathbf{B}_{km}V_{r_m}) \right], \tag{2.65}$$

$$Q_k = \sum_{m=1}^{N_b} \left[V_{im_k}(\mathbf{G}_{km}V_{r_m} - \mathbf{B}_{km}V_{im_m}) - V_{r_k}(\mathbf{G}_{km}V_{im_m} - \mathbf{B}_{km}V_{r_m}) \right]. \tag{2.66}$$

For PQ-type buses, the power mismatches are given by

$$\Delta P_k = P_k^{sp} - \sum_{m=1}^{N_b} \left[V_{r_k}(\mathbf{G}_{km}V_{r_m} - \mathbf{B}_{km}V_{im_m}) + V_{im_k}(\mathbf{G}_{km}V_{im_m} - \mathbf{B}_{km}V_{r_m}) \right] = 0, \tag{2.67}$$

$$\Delta Q_k = Q_k^{sp} - \sum_{m=1}^{N_b} \left[V_{im_k}(\mathbf{G}_{km}V_{r_m} - \mathbf{B}_{km}V_{im_m}) - V_{r_k}(\mathbf{G}_{km}V_{im_m} - \mathbf{B}_{km}V_{r_m}) \right] = 0. \tag{2.68}$$

A voltage restriction equation is required for a PV-type bus, which is given by $V_k^2 = V_{r_k}^2 + V_{im_k}^2$. The linearization of this equation gives $\Delta V_k^2 = 2V_{r_k}\Delta V_{r_k} + 2V_{im_k}\Delta V_{im_k}$ where $\Delta V_k^2 = (V_k^{sp})^2 - (V_k^{calc})^2$. Thus, the power mismatch matrix considering the voltage constraint equation can be given by

$$\begin{bmatrix} \Delta P_1 \\ \Delta P_2 \\ \vdots \\ \Delta P_k \\ \vdots \\ \Delta P_n \\ \hline \Delta Q_1 \\ \Delta Q_2 \\ \vdots \\ \Delta V_k^2 \\ \vdots \\ \Delta Q_n \end{bmatrix} = - \left[\begin{array}{cccccc|cccccc} H_{11} & H_{12} & \dots & H_{1k} & \dots & H_{1n} & N_{11} & N_{12} & \dots & N_{1k} & \dots & N_{1n} \\ H_{21} & H_{22} & \dots & H_{2k} & \dots & H_{2n} & N_{21} & N_{22} & \dots & N_{2k} & \dots & N_{2n} \\ \vdots & \vdots & \ddots & \vdots & \ddots & \vdots & \vdots & \vdots & \ddots & \vdots & \ddots & \vdots \\ H_{k1} & H_{k2} & \dots & H_{kk} & \dots & H_{kn} & N_{k1} & N_{k2} & \dots & N_{kk} & \dots & N_{kn} \\ \vdots & \vdots & \ddots & \vdots & \ddots & \vdots & \vdots & \vdots & \ddots & \vdots & \ddots & \vdots \\ H_{n1} & H_{n2} & \dots & H_{nk} & \dots & H_{nn} & N_{n1} & N_{n2} & \dots & N_{nk} & \dots & N_{nn} \\ \hline M_{11} & M_{12} & \dots & M_{1k} & \dots & M_{1n} & L_{11} & L_{12} & \dots & L_{1k} & \dots & L_{1n} \\ M_{21} & M_{22} & \dots & M_{2k} & \dots & M_{2n} & L_{21} & L_{22} & \dots & L_{2k} & \dots & L_{2n} \\ \vdots & \vdots & \ddots & \vdots & \ddots & \vdots & \vdots & \vdots & \ddots & \vdots & \ddots & \vdots \\ 0 & 0 & \dots & 2V_{r_k} & \dots & 0 & 0 & 0 & \dots & 2V_{im_k} & \dots & 0 \\ \vdots & \vdots & \ddots & \vdots & \ddots & \vdots & \vdots & \vdots & \ddots & \vdots & \ddots & \vdots \\ M_{n1} & M_{n2} & \dots & M_{nk} & \dots & M_{nn} & L_{n1} & L_{n2} & \dots & L_{nk} & \dots & L_{nn} \end{array}\right] \begin{bmatrix} \Delta V_{r_1} \\ \Delta V_{r_2} \\ \vdots \\ \Delta V_{r_k} \\ \vdots \\ \Delta V_{r_n} \\ \hline \Delta V_{im_1} \\ \Delta V_{im_2} \\ \vdots \\ \Delta V_{im_k} \\ \vdots \\ \Delta V_{im_n} \end{bmatrix} \tag{2.69}$$

Similarly, the submatrices of the Jacobian matrix can be defined by

$$H_{km} = \frac{\partial P_k}{\partial V_{r_m}} = V_{r_k}\mathbf{G}_{km} + V_{im_k}\mathbf{B}_{km}, \tag{2.70}$$

$$H_{kk} = \frac{\partial P_k}{\partial V_{r_k}} = V_{r_k}\mathbf{G}_{kk} + V_{im_k}\mathbf{B}_{kk} + I_{r_k}, \tag{2.71}$$

$$N_{km} = \frac{\partial P_k}{\partial V_{im_m}} = -V_{r_k}\mathbf{B}_{km} + V_{im_k}\mathbf{G}_{km}, \tag{2.72}$$

$$N_{kk} = \frac{\partial P_k}{\partial V_{im_k}} = -V_{r_k}\mathbf{B}_{kk} + V_{im_k}\mathbf{G}_{kk} + I_{im_k}, \tag{2.73}$$

$$M_{km} = \frac{\partial Q_k}{\partial V_{r_m}} = -V_{r_k}\mathbf{B}_{km} + V_{im_k}\mathbf{G}_{km} = N_{km}, \tag{2.74}$$

$$M_{kk} = \frac{\partial Q_k}{\partial V_{r_k}} = -V_{r_k}\mathbf{B}_{kk} + V_{im_k}\mathbf{G}_{kk} - I_{m_k}, \tag{2.75}$$

$$L_{km} = \frac{\partial Q_k}{\partial V_{im_m}} = -V_{r_k}\mathbf{G}_{km} - V_{im_k}\mathbf{B}_{km} = -H_{km}, \tag{2.76}$$

$$L_{kk} = \frac{\partial Q_k}{\partial V_{im_k}} = -V_{r_k}\mathbf{G}_{kk} - V_{im_k}\mathbf{B}_{kk} + I_{r_k}, \tag{2.77}$$

in which $\mathbf{I} = \mathbf{YV} = I_r + jI_{im}$. Therefore, the increments of the state vector can be updated at each iteration as follows

$$V_r^{(i+1)} = V_r^{(i)} + \Delta V_r^{(i)}, \tag{2.78}$$

$$V_{im}^{(i+1)} = V_{im}^{(i)} + \Delta V_{im}^{(i)}. \tag{2.79}$$

2.2.2.3 Current injection

Another way for solving the PFP alternatively to polar and rectangular approaches is using the form known as the current injection method (COSTA *et al.*, 1999; ALVES *et al.*, 2019). Solving the equations in rectangular coordinates using the current injection mode requests a set of N_{PQ} equations for PQ buses and a set of $2N_{PQ}$ equations for the current residuals defined by

$$I'_{r_k} = \sum_{i\in\Omega_k}(\mathbf{G}_{k_i}V_{r_i} - \mathbf{B}_{k_i}V_{im_i}) - \frac{V_{r_k}P_k + V_{im_k}Q_k}{V_{r_k}^2 + V_{im_k}^2}, \tag{2.80}$$

$$I'_{im_k} = \sum_{i \in \Omega_k} (\mathbf{G}_{k_i} V_{im_i} + \mathbf{B}_{k_i} V_{r_i}) - \frac{V_{im_k} P_k + V_{r_k} Q_k}{V_{r_k}^2 + V_{im_k}^2}. \tag{2.81}$$

The imaginary and real current deviations can be defined by

$$\Delta I_{im_k} = \frac{V_{im_k} \Delta P_k - V_{r_k} \Delta Q_k}{V_{r_k}^2 + V_{im_k}^2}, \tag{2.82}$$

$$\Delta I_{r_k} = \frac{V_{r_k} \Delta P_k + V_{im_k} \Delta Q_k}{V_{r_k}^2 + V_{im_k}^2}, \tag{2.83}$$

in which $V_k = \sqrt{V_{r_k}^2 + V_{im_k}^2}$ (COSTA *et al.*, 2001), and the equations can be rewritten as

$$\Delta I_{im_k} = \frac{V_{im_k} \Delta P_k}{V_k^2} - \frac{V_{r_k} \Delta Q_k}{V_k^2}, \tag{2.84}$$

$$\Delta I_{r_k} = \frac{V_{r_k} \Delta P_k}{V_k^2} + \frac{V_{im_k} \Delta Q_k}{V_k^2}, \tag{2.85}$$

with

$$\begin{bmatrix} \Delta I_{im_1} \\ \Delta I_{r_1} \\ \hline \Delta I_{im_2} \\ \Delta I_{r_2} \\ \hline \vdots \\ \hline \Delta I_{im_n} \\ \Delta I_{r_n} \end{bmatrix} = - \left[\begin{array}{cc|cc|c|cc} \mathbf{B}'_{11} & \mathbf{G}'_{11} & \mathbf{B}_{12} & \mathbf{G}_{12} & \dots & \mathbf{B}_{1n} & \mathbf{G}_{1n} \\ \mathbf{G}''_{11} & \mathbf{B}''_{11} & \mathbf{G}_{12} & -\mathbf{B}_{12} & \dots & \mathbf{G}_{1n} & -\mathbf{B}_{1n} \\ \hline \mathbf{B}_{21} & \mathbf{G}_{21} & \mathbf{B}'_{22} & \mathbf{G}'_{22} & \dots & \mathbf{B}_{2n} & \mathbf{G}_{2n} \\ \mathbf{G}_{21} & -\mathbf{B}_{21} & \mathbf{G}''_{22} & \mathbf{B}''_{22} & \dots & \mathbf{G}_{2n} & -\mathbf{B}_{2n} \\ \hline \vdots & \vdots & \vdots & \vdots & \ddots & \vdots & \vdots \\ \hline \mathbf{B}_{n1} & \mathbf{G}_{n1} & \mathbf{B}_{n2} & \mathbf{G}_{n2} & \dots & \mathbf{B}'_{nn} & \mathbf{G}'_{nn} \\ \mathbf{G}_{n1} & -\mathbf{B}_{n1} & \mathbf{G}_{n2} & \mathbf{B}_{n2} & \dots & \mathbf{G}''_{nn} & -\mathbf{B}''_{nn} \end{array}\right] \begin{bmatrix} \Delta V_{r_1} \\ \Delta V_{im_1} \\ \hline \Delta V_{r_2} \\ \Delta V_{im_2} \\ \hline \vdots \\ \hline \Delta V_{r_n} \\ \Delta V_{im_n} \end{bmatrix}. \tag{2.86}$$

The set of submatrices for the constant power model of the Jacobian matrix can be defined by

$$\mathbf{B}'_{kk} = \frac{\partial I'_{im_k}}{\partial V_{r_k}} = \mathbf{B}_{kk} - \frac{Q_k(V_{r_k}^2 - V_{im_k}^2) - 2V_{r_k} V_{im_k} P_k}{V_k^4}, \tag{2.87}$$

$$\mathbf{G}'_{kk} = \frac{\partial I'_{im_k}}{\partial V_{im_k}} = \mathbf{G}_{kk} - \frac{P_k(V_{r_k}^2 - V_{im_k}^2) + 2V_{r_k} V_{im_k} Q_k}{V_k^4}, \tag{2.88}$$

$$\mathbf{B}''_{kk} = \frac{\partial I'_{r_k}}{\partial V_{im_k}} = -\mathbf{B}_{kk} - \frac{Q_k(V_{r_k}^2 - V_{im_k}^2) - 2V_{r_k} V_{im_k} P_k}{V_k^4}, \tag{2.89}$$

$$\mathbf{G}''_{kk} = \frac{\partial I'_{r_k}}{\partial V_{r_k}} = \mathbf{G}_{kk} + \frac{P_k(V_{r_k}^2 - V_{im_k}^2) + 2V_{r_k} V_{im_k} Q_k}{V_k^4}. \tag{2.90}$$

Reactive power residuals form a new state variable, so a new constraint equation is imposed for PV buses.

$$\Delta V_k = \frac{V_{r_k}}{V_k} \Delta V_{r_k} + \frac{V_{im_k}}{V_k} \Delta V_{im_k}, \tag{2.91}$$

where $\Delta V_k = V_k^{sp} - V_k^{calc}$ (ALVES *et al.*, 2019). Therefore the matrix can be adjusted as

$$\begin{bmatrix} \Delta I_{im_1} \\ \Delta I_{im_2} \\ \vdots \\ \frac{V_{im_k}}{V_k^2}\Delta P_k \\ \vdots \\ \Delta I_{im_n} \\ \hline \Delta I_{r_1} \\ \Delta I_{r_2} \\ \vdots \\ \frac{V_{r_k}}{V_k^2}\Delta P_k \\ \vdots \\ \Delta I_{r_n} \\ \hline \Delta V_k \end{bmatrix} = - \begin{bmatrix} \mathbf{B}'_{11} & \mathbf{B}_{12} & \dots & \mathbf{B}_{1k} & \dots & \mathbf{B}_{1n} & \mathbf{G}'_{11} & \mathbf{G}_{12} & \dots & \mathbf{G}_{1k} & \dots & \mathbf{G}_{1n} & 0 \\ \mathbf{B}_{21} & \mathbf{B}'_{22} & \dots & \mathbf{B}_{2k} & \dots & \mathbf{B}_{2n} & \mathbf{G}_{21} & \mathbf{G}'_{22} & \dots & \mathbf{G}_{2k} & \dots & \mathbf{G}_{2n} & 0 \\ \vdots & \vdots & \ddots & \vdots & \ddots & \vdots & \vdots & \vdots & \ddots & \vdots & \ddots & \vdots & \vdots \\ \mathbf{B}_{k1} & \mathbf{B}_{k2} & \dots & \mathbf{B}'_{kk} & \dots & \mathbf{B}_{kn} & \mathbf{G}_{k1} & \mathbf{G}_{k2} & \dots & \mathbf{G}'_{kk} & \dots & \mathbf{G}_{kn} & \frac{V_{r_k}}{V_k^2} \\ \vdots & \vdots & \ddots & \vdots & \ddots & \vdots & \vdots & \vdots & \ddots & \vdots & \ddots & \vdots & \vdots \\ \mathbf{B}_{n1} & \mathbf{B}_{n2} & \dots & \mathbf{B}_{nk} & \dots & \mathbf{B}'_{nn} & \mathbf{G}_{n1} & \mathbf{G}_{n2} & \dots & \mathbf{G}_{nk} & \dots & \mathbf{G}'_{nn} & 0 \\ \hline \mathbf{G}''_{11} & \mathbf{G}_{12} & \dots & \mathbf{G}_{1k} & \dots & \mathbf{G}_{1n} & \mathbf{B}''_{11} & -\mathbf{B}_{12} & \dots & -\mathbf{B}_{1k} & \dots & -\mathbf{B}_{1n} & 0 \\ \mathbf{G}_{21} & \mathbf{G}''_{22} & \dots & \mathbf{G}_{2k} & \dots & \mathbf{G}_{2n} & -\mathbf{B}_{21} & \mathbf{B}''_{22} & \dots & -\mathbf{B}_{2k} & \dots & -\mathbf{B}_{2n} & 0 \\ \vdots & \vdots & \ddots & \vdots & \ddots & \vdots & \vdots & \vdots & \ddots & \vdots & \ddots & \vdots & \vdots \\ \mathbf{G}_{k1} & \mathbf{G}_{k2} & \dots & \mathbf{G}''_{kk} & \dots & \mathbf{G}_{kn} & -\mathbf{B}_{k1} & -\mathbf{B}_{k2} & \dots & \mathbf{B}''_{kk} & \dots & -\mathbf{B}_{kn} & -\frac{V_{im_k}}{V_k^2} \\ \vdots & \vdots & \ddots & \vdots & \ddots & \vdots & \vdots & \vdots & \ddots & \vdots & \ddots & \vdots & \vdots \\ \mathbf{G}_{n1} & \mathbf{G}_{n2} & \dots & \mathbf{G}_{nk} & \dots & \mathbf{G}''_{nn} & -\mathbf{B}_{n1} & -\mathbf{B}_{n2} & \dots & -\mathbf{B}_{nk} & \dots & \mathbf{B}''_{nn} & 0 \\ \hline 0 & 0 & \dots & \frac{V_{r_k}}{V_k} & \dots & 0 & 0 & 0 & \dots & \frac{V_{im_k}}{V_k} & \dots & 0 & 0 \end{bmatrix} \begin{bmatrix} \Delta V_{r_1} \\ \Delta V_{r_2} \\ \vdots \\ \Delta V_{r_k} \\ \vdots \\ \Delta V_{r_n} \\ \hline \Delta V_{im_1} \\ \Delta V_{im_2} \\ \vdots \\ \Delta V_{im_k} \\ \vdots \\ \Delta V_{im_n} \\ \hline \Delta Q_k \end{bmatrix} \tag{2.92}$$

Finally the increment equations (ALVES *et al.*, 2019) are defined by

$$V_r^{(i+1)} = V_r^{(i)} + \Delta V_r^{(i)}, \tag{2.93}$$

$$V_{im}^{(i+1)} = V_{im}^{(i)} + \Delta V_{im}^{(i)}. \tag{2.94}$$

2.2.3 Fast-Decoupled method

A widely used method called Fast Decoupled Power Flow (FDPF), initially proposed by Stott & Alsac (1974), presents fast convergence compared to the full NR solver. Since its conception, different versions have been created. The approach is also known as XB or BX methods (AMERONGEN, 1989). Before explaining the difference between them, it is essential to detail the construction of matrix $\mathbf{B}$.

The transmission line branches are modeled by a conductance $\mathbf{G}$ and a suceptance $\mathbf{B}$ (STOTT; ALSAC, 1974), according to Equation (2.95).

$$\overline{\mathbf{Y}}_{km} = \mathbf{G}_{km} + j\mathbf{B}_{km}. \tag{2.95}$$

Once the line conductance $\mathbf{G}_{km}$ is neglected, the $\overline{\mathbf{Y}}_{km}$ matrix will be represented by $\overline{\mathbf{Y}}_{km} =$

$j\mathbf{B}_{km}$, since only susceptance elements will compose it, being represented by the Equation (2.96).

$$\overline{\mathbf{Y}}_{bus} = j \cdot \begin{bmatrix} \mathbf{B}_{11} & \mathbf{B}_{12} & \cdots & \mathbf{B}_{1m} \\ \mathbf{B}_{21} & \mathbf{B}_{22} & \cdots & \mathbf{B}_{2m} \\ \vdots & \vdots & \ddots & \vdots \\ \mathbf{B}_{k1} & \mathbf{B}_{k2} & \cdots & \mathbf{B}_{km} \end{bmatrix}. \tag{2.96}$$

The decoupled method assumes that the power flow equations have a resistance of the branch small with respect to the reactance $\mathbf{R}_{km} \ll \mathbf{X}_{km}$ and the angular differences are near to zero $\theta_{km} = \theta_k - \theta_m \simeq 0$.

These simplifications are possible by relating the power flow relations ($\mathbf{P} + j\mathbf{Q}$) with the associated voltage drop (ΔV) and its angular opening (θ_{km}). The nonlinear equations that govern the power system are basically given by Equation (2.97) (STEVENSON JR., 1986; ZANETTA JR., 2006; GLOVER *et al.*, 2012).

$$\mathbf{P}_k - j\mathbf{Q}_k = V_k \sum_{m=1}^{N_b} V_m(\mathbf{G}_{km} + j\mathbf{B}_{km}) \left[\cos(\theta_{km}) + j\sin(\theta_{km})\right]. \tag{2.97}$$

Assuming studies with Extra-high Voltage (EHV) and Ultra-high Voltage (UHV) systems, the branch resistances are assumed to be much less than the reactance ($\mathbf{R}_{km} \ll \mathbf{X}_{km}$) (ZANETTA JR., 2006), and the impedance $\mathbf{Z}_{km} = \mathbf{R}_{km} + j\mathbf{X}_{km}$ can be rewritten as admittance $\mathbf{Y}_{km} = \dfrac{1}{\mathbf{R}_{km} + j\mathbf{X}_{km}} = \dfrac{\mathbf{R}_{km}}{\mathbf{R}_{km}^2 + \mathbf{X}_{km}^2} - j\dfrac{\mathbf{X}_{km}}{\mathbf{R}_{km}^2 + \mathbf{X}_{km}^2}$. Neglecting conductance, only the susceptance element $\mathbf{B}$ will remain, as Equation (2.98).

$$\mathbf{B}_{km} = -\frac{\mathbf{X}_{km}}{\mathbf{R}_{km}^2 + \mathbf{X}_{km}^2}. \tag{2.98}$$

Then, Equation (2.97) can be rewritten as

$$\mathbf{P}_k - j\mathbf{Q}_k = V_k \sum_{m=1}^{N_b} V_m[\mathbf{B}_{km}\sin(\theta_{km}) + j\mathbf{B}_{km}\cos(\theta_{km})]. \tag{2.99}$$

Considering the following approximations $\sin(\theta_{km}) \simeq \theta_{km}$ and $\cos(\theta_{km}) \simeq 1$, we have

$$\begin{aligned} \mathbf{P}_k &= \sum_{\substack{m=1 \\ m\neq k}}^{N_b} V_k V_m \mathbf{B}_{km}(\theta_k - \theta_m), \\ \mathbf{Q}_k &= -\sum_{m=1}^{N_b} V_k V_m \mathbf{B}_{km}. \end{aligned} \tag{2.100}$$

In this way, it is possible to note that active power is associated with the angular phase shift ($\mathbf{P}\theta$), and reactive power is associated with the voltage magnitude variation ($\mathbf{QV}$). Evaluating only the active power of Equation (2.100), we can rewrite it as follows:

$$\frac{\mathbf{P}_k}{V_k} = \sum_{\substack{m=1 \\ m\neq k}}^{N_b} V_m \mathbf{B}_{km}\theta_k - \sum_{\substack{m=1 \\ m\neq k}}^{N_b} V_m \mathbf{B}_{km}\theta_m. \tag{2.101}$$

Assuming that $V_m \simeq 1$ and that $\Delta V \ll V$ for incremental values, we have that $\Delta\left(\frac{P}{V}\right) \simeq \frac{\Delta P}{V}$ yielding Equation (2.102) (ZANETTA JR., 2006).

$$\frac{\Delta\mathbf{P}_k}{V_k} = \sum_{\substack{m=1 \\ m\neq k}}^{N_b} \mathbf{B}_{km}\Delta\theta_k - \sum_{\substack{m=1 \\ m\neq k}}^{N_b} \mathbf{B}_{km}\Delta\theta_m. \tag{2.102}$$

From the nodal analysis, considering the neglected shunt elements, the proper element of susceptance is obtained by $B_{kk} = -\sum_{\substack{m=1 \\ m\neq k}}^{N_b} \mathbf{B}_{km}$ and $\frac{\Delta\mathbf{P}_k}{V_k} = -\mathbf{B}_{kk}\Delta\theta_k - \sum_{\substack{m=1 \\ m\neq k}}^{N_b} \mathbf{B}_{km}\Delta\theta_m$. After simplifications, we have $\frac{\Delta\mathbf{P}_k}{V_k} = -\sum_{m=1}^{N_b} \mathbf{B}_{km}\Delta\theta_m$ and writing as matrices

$$\left[\frac{\Delta\mathbf{P}}{V}\right] = -[\mathbf{B}][\Delta\theta]. \tag{2.103}$$

For convenience, the matrix $-[\mathbf{B}]$ in the active power equation is called $[\mathbf{B}']$. In the same way, with $\Delta\left(\frac{Q}{V}\right) \simeq \frac{\Delta Q}{V}$, Equation (2.100) can be rewritten as

$$\frac{\Delta\mathbf{Q}_k}{V_k} = -\sum_{m=1}^{N_b} \mathbf{B}_{km}\Delta V_m, \tag{2.104}$$

and

$$\left[\frac{\Delta\mathbf{Q}}{V}\right] = -[\mathbf{B}][\Delta V]. \tag{2.105}$$

Similarly, the matrix $-[\mathbf{B}]$ in the reactive power equation is called $[\mathbf{B}'']$. Summarizing Equation (2.103) and Equation (2.105) the iterative equations are organized as

$$\begin{aligned} \left[\frac{\Delta\mathbf{P}}{V}\right] &= [\mathbf{B}'][\Delta\theta], \\ \left[\frac{\Delta\mathbf{Q}}{V}\right] &= [\mathbf{B}'']][\Delta V]. \end{aligned} \tag{2.106}$$

The method proposed by Amerongen (1989) considers four different strategies to consider the resistance in the branches in the $\mathbf{Y}_{bus}$ formation named BB, XB, BX, and XX methods. The BB method considers the resistances in $\mathbf{B}'$ and $\mathbf{B}''$. In method XB, resistance is ignored only in matrix $\mathbf{B}'$ formation. In the BX method, resistance is ignored only in the formation of $\mathbf{B}''$. Finally, in the XX method, resistance is disregarded in forming $\mathbf{B}'$ and $\mathbf{B}''$. In summary, among these, the ones that present the best performance are XB and BX (MILANO, 2010). The best performance between XB and BX is associated with generally high $\mathbf{R}/\mathbf{X}$ ratios (AMERONGEN, 1989).

2.2.4 DC Power Flow method

The DC Power Flow method, also known as linear power flow, is an approximate method that only considers the active power distribution throughout the power system. The technique is a good alternative to simplify classical power flow methods, being considered the simplest power system analysis tools (PURCHALA *et al.*, 2005). Therefore, the method has an analytical solution and does not need iterations. Stott *et al.* (2009) enumerate some advantages:

(a) non-iterative solutions;
(b) relatively simple method;
(c) the network data are relatively simple to obtain; and
(d) the results are reasonably accurate for phase angle.

The method considers some simplifications in Equation (2.22) to obtain a set of linear equations (MILANO, 2010). The simplifications keep active power $\mathbf{P}$ and voltage angle θ and neglect reactive power $\mathbf{Q}$ and voltage magnitude V (BIRCHFIELD *et al.*, 2018). Initially, only the nonlinear active power Equation (2.18) is considered, *i.e.*,

$$\mathbf{P}_k = V_k \sum_{m=1}^{N_b} V_m \left[\mathbf{G}_{km} cos(\theta_{km}) + \mathbf{B}_{km} sin(\theta_{km})\right]. \tag{2.107}$$

More specifically, in Extra-high Voltage (EHV) and Ultra-high Voltage (UHV) systems the voltage magnitude is near to 1 *pu* (BIRCHFIELD *et al.*, 2018) in such a way that the following simplification can be applied

$$\overline{V}_k = \overline{V}_m \approx e^{j\theta_k}. \tag{2.108}$$

Furthermore, in EHV and UHV the voltage angle θ_{km} is small such that the angular approximation are small enough that

$$\sin(\theta_{km}) = \sin(\theta_k - \theta_m) \approx \theta_k - \theta_m. \tag{2.109}$$

In addition, the resistance of the lines $\mathbf{R}$ and charging capacitance $\mathbf{B}_c$ are also neglected in the construction of admittance matrix (WOOD *et al.*, 2013; ZIMMERMAN *et al.*, 2011), and in such way that

$$\overline{\mathbf{Y}} = \frac{1}{\mathbf{R} + j\mathbf{X}} \approx \frac{1}{j\mathbf{X}}, \quad \mathbf{B}_c \approx 0. \tag{2.110}$$

The admittance matrix $\overline{\mathbf{Y}}_{bus}$ can be written as

$$\overline{\mathbf{Y}}_{bus} = j \cdot \begin{bmatrix} \mathbf{B}_{11} & \mathbf{B}_{12} & \cdots & \mathbf{B}_{1m} \\ \mathbf{B}_{21} & \mathbf{B}_{22} & \cdots & \mathbf{B}_{2m} \\ \vdots & \vdots & \ddots & \vdots \\ \mathbf{B}_{k1} & \mathbf{B}_{k2} & \cdots & \mathbf{B}_{km} \end{bmatrix}. \tag{2.111}$$

The result leads to the nodal real power injections expressed as a linear function (HONGFU *et al.*, 2014)

$$\mathbf{P}_k = \sum_{m=1}^{N_b} \left[-\mathbf{B}_{km} \cdot (\theta_m - \theta_k) \right]. \tag{2.112}$$

The main disadvantage of DC power flow is the inaccuracy of results, which can lead to a wrong estimate (MILANO, 2010). It is important to know the system to which the simplifications are considered in the study. Despite this, some authors continued to investigate the method and presented works to improve the accuracy of DC power flow formulations (YAN; SEKAR, 2002; STOTT *et al.*, 2009; QI *et al.*, 2012).

2.3 NON-TRADITIONAL METHODS BASED ON SYNTHETIC DYNAMICS

The methods discussed beforehand may have limitations and fail when it comes to determining the PFP solution.

The emergence of more complex electrical networks with more restricted operations contributed to difficulties in determining the solution to the load flow problem. This approach continued to motivate research in the area to focus on unconventional techniques to solve the problem. One line adopted was to seek the solution through a synthetic dynamics approach

based on transformations and adaptations of the algebraic equations of the original problem (MILANO, 2010; JARDIM; STOTT, 2005; TOSTADO-VÉLIZ *et al.*, 2020a). However, always with the aim of calculating the original PFP solution.

Several contributions were proposed to the topic of synthetic dynamic in the power flow problem. Some of them are discussed below.

2.3.1 Euler's method

A technique denominated Continuous Newton's philosophy (CN) was proposed by Hetzler (1997). Following this philosophy, the static problem for solving a set of nonlinear equations via the NR method is formulated as a set of Ordinary Differential Equations (ODE). Then, with this objective, in principle, any numerical integration can be applied to solve the dynamical problem.

A well-known and easy-to-implement numerical integration method is the Forward Euler's method (FE). The equations are similar to NR (a static approach) in such a way that the NR method acts as an FE method with step size $\Delta t = 1$ (HETZLER, 1997). Therefore, by introducing a generic and appropriate integration step Δt into Equation (2.41), for iteration i, the state deviations are given by

$$\Delta \mathbf{x}^{(i)} = \Delta t \cdot \left\{ - \left[\mathbf{J} \left(\mathbf{x}^{(i)} \right) \right]^{-1} \mathbf{f} \left(\mathbf{x}^{(i)} \right) \right\}. \tag{2.113}$$

From Equation (2.40), knowing that $\mathbf{x}^{(i+1)} = \mathbf{x}^{(i)} + \Delta \mathbf{x}^{(i)}$, then

$$\mathbf{x}^{(i+1)} = \mathbf{x}^{(i)} - \Delta t \left[\mathbf{J} \left(\mathbf{x}^{(i)} \right) \right]^{-1} \mathbf{f} \left(\mathbf{x}^{(i)} \right), \quad i = 0,1,\ldots \tag{2.114}$$

The problem formulation according to (2.114) can take several forms considering Δt as an optimal multiplier. In this context, the problem is viewed as the numerical solution at the step i of the ODE $\dot{\mathbf{x}} = - \left[\mathbf{f}_{\mathbf{x}} \right]^{-1} \mathbf{f}(\mathbf{x})$. The problem formulated this way was defined as Continuous Newton's method, and so a problem characterized by a synthetic dynamic (HETZLER, 1997; MILANO, 2009; MILANO, 2010). In this context, other numerical integration techniques can be utilized to solve the problem, noting that the solution of interest is the steady-state one.

Since the initial estimation is often not the solution, it can be viewed as a perturbation in the dynamic problem. Therefore, until reaching the steady state, the intermediary curve

points, defined by $\mathbf{x}^{(i)}$ between the initial point in $\mathbf{x}^{(0)}$ and $\mathbf{x}_*$, are similar to those composing the points of a transient. Thereby, the synthetic dynamic problem can be viewed as solving a transient problem in power systems.

The FE scheme is considered a single-step and explicit integration method because the calculation of the solution $\mathbf{x}^{(i+1)}$ depends on only a single recurrence in the known solution (point) $\mathbf{x}^{(i)}$.

2.3.2 Backward Euler's method

Another single integration scheme is the Backward Euler's method (BE). It was presented in the context of CN power flow topic by Milano (2019). It is an implicit numerical method that depends on the current iteration to calculate the current step. Its standard scheme can be given by

$$\mathbf{x}^{(i+1)} = \mathbf{x}^{(i)} - \Delta t \left[\mathbf{J}\left(\mathbf{x}^{(i+1)}\right)\right]^{-1} \mathbf{f}\left(\mathbf{x}^{(i+1)}\right), \quad i = 0,1,\ldots \tag{2.115}$$

Note that the calculated iteration $\mathbf{x}^{(i+1)}$ depends on itself to compose the terms given by $\mathbf{J}\left(\mathbf{x}^{(i+1)}\right)$ and $\mathbf{f}\left(\mathbf{x}^{(i+1)}\right)$. According to Butcher (2016) the method is promising because it presents a certain stability depending directly on the step size Δt.

2.3.3 Trapezoidal method

The Trapezoidal method (TM) can be viewed as an evolution of Euler's method, representing an average of both FE and BE methods (BISWAS *et al.*, 2013). It is classified as an implicit method because it uses the results of the current iterations to continue calculations until convergence is achieved. Its standard scheme is given by Equation (2.116). According to Sun *et al.* (2024), it may show better accuracy for long time intervals Δt (SUN *et al.*, 2024).

$$\mathbf{x}^{(i+1)} = \mathbf{x}^{(i)} - \frac{\Delta t}{2}\left[\left[\mathbf{J}\left(\mathbf{x}^{(i)}\right)\right]^{-1}\mathbf{f}\left(\mathbf{x}^{(i)}\right) + \left[\mathbf{J}\left(\mathbf{x}^{(i+1)}\right)\right]^{-1}\mathbf{f}\left(\mathbf{x}^{(i+1)}\right)\right], \quad i = 0,1,\ldots \tag{2.116}$$

2.3.4 Runge-Kutta's methods

Similar to the FE method, the Runge-Kutta' formulas (RK) are used to solve dynamical nonlinear equations through numerical integration schemes (SHAMPINE, 1986; KUNDUR, 1994). This method is also employed for a dynamic form of the PFP (MILANO, 2009). It involves additional computation using constants referred to as K_n, for the same iteration.

The Runge-Kutta 2^{nd} order' method (RK2) iterative formula is given by

$$\mathbf{x}^{(i+1)} = \mathbf{x}^{(i)} + \frac{\Delta t(K_1 + K_2)}{2}, \tag{2.117}$$

where the constants are calculated (LOTKIN, 1951; RALSTON, 1962) as

$$\begin{aligned} K_1 &= \mathbf{f}(\mathbf{x}^{(i)}, t^{(i)}), \text{ and} \\ K_2 &= \mathbf{f}(\mathbf{x}^{(i)} + K_1, t^{(i)} + \Delta t), \end{aligned} \tag{2.118}$$

with $t^{(i)}$ as fictitious time related to the iterations, generally not used explicitly in the formulas.

In the same way, classical Runge-Kutta 4^{th} order's method (RK4) is an efficient explicit numerical integration to solve the PBE using the previous state $\mathbf{x}^{(i)}$ to take the next iteration and get the solution to the problem (MILANO, 2009). The update $\mathbf{x}^{(i+1)}$ is composed of previous iteration results and calculated as

$$\mathbf{x}^{(i+1)} = \mathbf{x}^{(i)} + \frac{\Delta t(K_1 + 2K_2 + 2K_3 + K_4)}{6}, \tag{2.119}$$

where the constants are calculated (GALLER; ROZENBERG, 1960) as

$$\begin{aligned} K_1 &= \mathbf{f}(\mathbf{x}^{(i)}, t^{(i)}); \\ K_2 &= \mathbf{f}\left(\mathbf{x}^{(i)} + \frac{K_1}{2}, t^{(i)} + \frac{\Delta t}{2}\right); \\ K_3 &= \mathbf{f}\left(\mathbf{x}^{(i)} + \frac{K_2}{2}, t^{(i)} + \frac{\Delta t}{2}\right); \\ K_4 &= \mathbf{f}(\mathbf{x}^{(i)} + K_3, t^{(i)} + \Delta t). \end{aligned} \tag{2.120}$$

Several methods are proposed in Tostado-Véliz *et al.* (2019a) and are compared with the RK methods. The robustness of the method is assessed considering medium and large-scale ill-conditioned power systems.

2.3.5 Heun and King Werner's method

The Heun-King-Werner's method (HKW) proposed by Tostado-Véliz *et al.* (2020a) can solve ill- and well-conditioned cases. With an approach that combines the Heun method (BUTCHER, 2016) and the King-Werner method (ARGYROS; MAGREÑÁN, 2017), it is suitable for solving nonlinear equations with a convergence greater than NR (MCDOUGALL; WOTHERSPOON, 2014). The Euler method with a step Δt is expandable by the prediction step for an initial estimate of $\mathbf{x}^{(k)}$ given by

$$\mathbf{y}^{(k)} = \mathbf{x}^{(k)} + \Delta t \cdot \mathbf{g}\left(\mathbf{x}^{(k)}\right), \tag{2.121}$$

where

$$\mathbf{g}\left(\mathbf{x}^{(k)}\right) = -\mathbf{J}_{\mathbf{x}}\left(\mathbf{x}^{(k)}\right)^{-1} \cdot \mathbf{f}\left(\mathbf{x}^{(k)}\right). \tag{2.122}$$

Using the King-Werner's method, an intermediate point between $\mathbf{x}^{(k)}$ and $\mathbf{y}^{(k)}$ is calculated generating the estimate $\tilde{\mathbf{x}}^{(k)}$

$$\tilde{\mathbf{x}}^{(k)} = \frac{1}{2}\left(\mathbf{x}^{(k)} + \mathbf{y}^{(k)}\right). \tag{2.123}$$

Then, Equation (2.122) is modified to

$$\mathbf{g}\left(\tilde{\mathbf{x}}^{(k)}\right) = -\mathbf{J}_{\mathbf{x}}\left(\tilde{\mathbf{x}}^{(k)}\right)^{-1} \cdot \mathbf{f}\left(\tilde{\mathbf{x}}^{(k)}\right). \tag{2.124}$$

Therefore, Heun's method is characterized by estimating the next iteration using the following equation

$$\mathbf{x}^{(k+1)} = \mathbf{x}^{(k)} + \frac{\Delta t}{2}\left[\mathbf{g}\left(\tilde{\mathbf{x}}^{(k)}\right) + \mathbf{g}\left(\mathbf{x}^{(k)}\right)\right]. \tag{2.125}$$

The method proposed by Tostado-Véliz *et al.* (2020a) uses an adaptation parameter $\psi^{(k)}$ defined as

$$\psi^{(k)} = \frac{2|SSR^{(k)} - SSR^{(0)}|}{SSR^{(0)}}, \tag{2.126}$$

where the suggested initialization is given by $\psi^{(0)}$ and the Sum of Squares of Residuals (SSR), for $SSR(\cdot) : \mathbb{R}^n \mapsto \mathbb{R}^n$, defined as

$$SSR^{(k)} = \frac{1}{2}\left[\mathbf{f}\left(\mathbf{x}^{(k)}\right)\right]^T \cdot \mathbf{f}\left(\mathbf{x}^{(k)}\right). \tag{2.127}$$

Tostado-Véliz *et al.* (2020a) suggest limiting ψ to a maximum value of 2, where under these conditions, they work like the NR method with $\Delta t = 1$.

The next subsection will examine a different method utilizing a dynamic approach to address the static PFP.

2.4 SYNTHETIC DYNAMIC POWER FLOW

This section discusses a different dynamic technique used to solve the PFP. The objective is not to provide an in-depth analysis of the technique but to evaluate its components to highlight another dynamic scheme for the PFP that differs from the dynamic homotopy approach. The Synthetic Dynamic Power Flow (SDPF) is part of the ORGANON software (see Chaves (2008)) and its detailing is beyond that one discussed in this thesis.

The method analyzed in this section is known as Synthetic Dynamic Power Flow (SDPF) and was proposed by Jardim & Stott (2005). In the problem formulation, the nonlinear equations of the PFP are grouped and modified conveniently to join states, $\mathbf{x}$, with another set of variables called control variable $\mathbf{y}$. The steady-state response of this modified problem is expected to converge to the standard PFP solution. Consequently, like the dynamic homotopy problem, it depends heavily on a numerical integration method for determining its solution.

2.4.1 Description of the method

The main aspect of the method is the introduction of decision variables, also known as controlled variables. As a result, a dynamic characteristic is created so that these variables reach a steady-state, following a dynamic behavior. This aspect is what characterizes the so-called synthetic dynamics of the problem. It can be said that the solution to the problem in a steady-state is what matters, regardless of its transient behavior. Furthermore, the nature of the dynamic aspect introduced into the problem is entirely artificial and can assume infinite configurations, depending on the parameters adopted to represent it.

The differential equations involving the decision variable are of the type (JARDIM; STOTT, 2005)

$$\dot{\mathbf{y}} = \mathbf{z}(\mathbf{x}, \mathbf{y}), \tag{2.128}$$

in which $\mathbf{y}$ is the control variable (decision variable) and $\mathbf{x}$ represents the states.

Equation (2.128) is associated with control in the voltage magnitude in PV buses, limits of equipment, control actions, etc. In the PQ buses, the goal is to deal with mismatches that characterize an equilibrium between the specified power injection into the bus and the power flow to interconnections. Then a set of nonlinear equations characterizes the power balance equations and can be represented by algebraic equations of the form

$$0 = \mathbf{f}(\mathbf{x},\mathbf{y}). \tag{2.129}$$

The problem involves solving a nonlinear algebraic-differential equation set composed of (2.128)-(2.129). An implicit integration method is suggested in (JARDIM; STOTT, 2005) to solve the problem. Following the strategy adopted in that reference, the set of nonlinear equations is discretized for a given step Δt and handled according to the chosen implicit method. Then, a general form for the differential equations can be transformed into a set of algebraic equations organized as follows

$$\begin{aligned} \mathbf{y}_{n+1} &= \beta \Delta t \mathbf{z}(\mathbf{x}_{n+1}, \mathbf{y}_{n+1}) + \mathbf{C}, \\ -\mathbf{y}_{n+1} &+ \beta \Delta t \mathbf{z}(\mathbf{x}_{n+1}, \mathbf{y}_{n+1}) + \mathbf{C} = 0, \end{aligned} \tag{2.130}$$

in which Δt is the integration step, β is a coefficient that depends on the numerical method, and $\mathbf{C}$ is a term that depends on the previous steps, which are intrinsic to the implicit method. The algebraic equations in (2.129) assume the form

$$\mathbf{f}(\mathbf{x}_{n+1},\mathbf{y}_{n+1}) = 0. \tag{2.131}$$

The combination of Equation (2.130) and (2.131) forms a set of nonlinear equations that must be solved simultaneously, for example, by the NR method.

2.4.2 Definition of decision variables and associated dynamic equations

A key aspect of the SDPF method is characterizing the decision control variables. In Jardim & Stott (2005), several options are presented. However, in this thesis, only some variables associated with a power generator are the target of the discussion. For example, the controls of the active power, the terminal voltage, and the reactive power limits. However, other quantities and other components could be explored.

In a PV bus associated with power generation in the PFP, the main control strategy usually used is to control the active power of the generator and its terminal voltage. These two aspects are modeled below.

Jardim & Stott (2005) suggest that power generation can be represented by a classical model (electric circuit), whose PV bus is connected by an internal voltage source through a reactance X_t. In this case, the internal source, represented by a dynamic phasor, is used to form a differential equation associated with a given decision variable. Figure 2.2 illustrates the associated electric circuit when a bus k of type PV is considered.

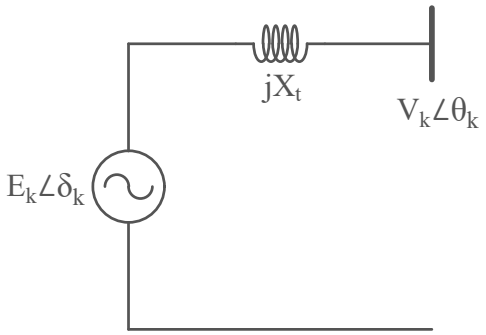

Figure 2.2: Electric circuit with an internal voltage behind a reactance X_t

In the electric circuit in Figure 2.2, the objective is to control the active power produced by the generator at a specified value P_k^{sp} and a specified terminal voltage V_k^{sp}. Then, assuming a dynamic behavior, in steady-state, it is expected that $V_k(t) \to V_k^{sp}$ and $P_k(t) \to P_k^{sp}$. Also, reactive power limits can be controlled by handling the reactive power of the generator, $Q_k(t)$, and its respective limits. In this case, the option to control the voltage $V_k(t)$ must be released.

Following Jardim & Stott (2005) and considering the electric circuit in Figure 2.2, the active power control in a PV bus for a generator k can be associated to the differential equation

$$\dot{\delta}_k = K_{Pk}[P_k^{sp} - P_k(\mathbf{V},\theta,\mathbf{y})], \tag{2.132}$$

in which δ_k is the internal angle of the generation unit, which is determined considering a voltage drop in the generator reactance. K_{Pk} is a positive constant, P_k^{sp} is the power to be controlled on the generator terminal bus, and $P_k(\mathbf{V},\theta,\mathbf{y})$ is the power calculated as a function of the states and control variables.

The terminal voltage control at bus k is based on the dynamic equation

$$\dot{E}_k = K_{Vk}(V_k^{sp} - V_k), \tag{2.133}$$

in which E_k is determined as the internal voltage behind the reactance X_t (see Figure 2.2), the term K_{Vk} is a positive constant, V_k^{sp} is the voltage specified at bus k, and V_k is the voltage variable used to control V_k^{sp}.

If the reactive power limit is activated, an alternative is to release the control of the voltage magnitude and start controlling reactive power in order to keep it within pre-established limits. In this situation, Equation (2.134) is used instead of Equation (2.133) if the limit is violated

$$\dot{E}_k = K_{qk}[Q_k^{sp} - Q_k(\mathbf{V},\theta,\mathbf{y})], \tag{2.134}$$

in which Q_k^{sp} is the violated limit, *i.e.*, $Q_k^{sp} = Q_{min}$ case the violated limit is the minimum value Q_{min} or $Q_k^{sp} = Q_{max}$ case the violated limit is the maximum value Q_{max}.

The reactive power limit must be checked after convergence of the implicit method iterations at each time step n, to verify which equation to use in the step calculation, either Equation (2.133) or Equation (2.134).

The slack bus in the system is considered an infinite bus, in which the angle $\theta_{slack} = 0$ and $V_{slack} = V_\infty$ are defined.

The Trapezoidal method (TM) was used in the variables discretization, traditionally used in electromechanical and electromagnetic transients simulations. Assuming that the reactive power limits meet established conditions, the dynamic equations for a given bus k are

$$\dot{\delta}_k = K_{Pk}[P_k^{sp} - P_k(\mathbf{V},\theta,\mathbf{y})] = -K_{Pk}\Delta P_k, \tag{2.135}$$

$$\dot{E}_k = K_{Vk}(V_k^{sp} - V_k) = -K_{Vk}\Delta V_k, \tag{2.136}$$

where

$$\Delta P_k = P_k(\mathbf{V},\theta,\mathbf{y}) - P_k^{sp}, \tag{2.137}$$

$$\Delta V_k = V_k - V_k^{sp}. \tag{2.138}$$

Using the trapezoidal method, knowing the data at step n, the calculation at step $n+1$ and time-step Δt, gives

$$\delta_k^{(n+1)} = \delta_k^{(n)} - \frac{\Delta t}{2} K_{Pk}(\Delta P_k^{(n+1)} + \Delta P_k^{(n)}), \tag{2.139}$$

$$E_k^{(n+1)} = E_k^{(n)} - \frac{\Delta t}{2} K_{Vk}(\Delta V_k^{(n+1)} + \Delta V_k^{(n)}), \tag{2.140}$$

that generates the nonlinear equations

$$0 = \delta_k^{(n+1)} - \delta_k^{(n)} + \frac{\Delta t}{2} K_{Pk}(\Delta P_k^{(n+1)} + \Delta P_k^{(n)}), \tag{2.141}$$

$$0 = E_k^{(n+1)} - E_k^{(n)} + \frac{\Delta t}{2} K_{Vk}(\Delta V_k^{(n+1)} + \Delta V_k^{(n)}). \tag{2.142}$$

In addition, there are also the algebraic equations of the type

$$\mathbf{f}(\mathbf{x}^{(n+1)}, \mathbf{y}^{(n+1)}) = 0. \tag{2.143}$$

In addition to Equations (2.141), (2.142) and (2.143), the equations due to the internal voltage drop in each generating unit connected to a bus k, of the PV type, must be considered. From the circuit in Figure 2.2, the voltage behind the reactance can be calculated, assuming a current I_k and a terminal voltage $V_k \angle \theta_k$. The relationship between the voltages is

$$E_k \angle \delta_k = V_k \angle \theta_k + jX_t I_k. \tag{2.144}$$

Current I_k can be interpreted as the current injection into bus k due to the generator. It can be calculated using the matrix Y_{bus} and the voltage at each bus of the system as

$$\begin{aligned} I_k &= Y_{bus}(k,:)\mathbf{V} = V_1 Y_{k1} + V_2 Y_{k2} + \ldots + V_{N_b} Y_{kN_b}, \\ I_k &= \sum_{m=1}^{N_b} V_m Y_{km}. \end{aligned} \tag{2.145}$$

Therefore, Equation (2.144) becomes

$$E_k \angle \delta_k = V_k \angle \theta_k + jX_t \sum_{m=1}^{N_b} Y_{km} V_m. \tag{2.146}$$

Splitting Equation (2.146) into real and imaginary parts, it is obtained

$$E_k \cos\delta_k = V_k \cos\theta_k - X_t \sum_{m=1}^{N_b} V_m(\mathbf{G}_{km} \sin\theta_m + \mathbf{B}_{km} \cos\theta_m), \tag{2.147}$$

$$E_k \sin\delta_k = V_k \sin\theta_k + X_t \sum_{m=1}^{N_b} V_m(\mathbf{G}_{km} \cos\theta_m - \mathbf{B}_{km} \sin\theta_m), \tag{2.148}$$

allowing to write the algebraic equations

$$0 = E_k \cos\delta_k - V_k \cos\theta_k + X_t \sum_{m=1}^{N_b} V_m(\mathbf{G}_{km} \sin\theta_m + \mathbf{B}_{km} \cos\theta_m), \quad \forall\ k = 1, \cdots, N_b, \tag{2.149}$$

$$0 = E_k \sin\delta_k - V_k \sin\theta_k - X_t \sum_{m=1}^{N_b} V_m(\mathbf{G}_{km}\cos\theta_m - \mathbf{B}_{km}\sin\theta_m), \quad \forall\ k = 1, \cdots, N_b. \tag{2.150}$$

Therefore, Equations (2.141), (2.142), (2.143), (2.149) and (2.150) form a nonlinear equation system which must be solved in the variables $\mathbf{x}^{(n+1)}$ and $\mathbf{y}^{(n+1)}$, for the time t_{n+1}, given that the states and decision control variables at the step n (time t_n), $\mathbf{x}^{(n)}$ and $\mathbf{y}^{(n)}$, are known.

Assuming that the problem is solved iteratively by the NR method, then in the i^{th} iteration of the step $n+1$ is calculated as

$$\mathbf{x}^{(n+1,i+1)} = \mathbf{x}^{(n+1,i)} + \Delta\mathbf{x}^{(n+1,i)}, \tag{2.151}$$

$$\mathbf{y}^{(n+1,i+1)} = \mathbf{y}^{(n+1,i)} + \Delta\mathbf{y}^{(n+1,i)}. \tag{2.152}$$

Note that δ and E comprise the set of variables $\mathbf{y}$. Thus, considering the slack bus as the number 1 and it has angle zero, the state vector is $\mathbf{x} = [\theta_2 \dots \theta_{Nb}, V_2 \dots V_{Nb}]^T \in \mathbb{R}^{2(N_{PV}+N_{PQ})}$ and $\mathbf{y} = [\delta_1 E_1 \dots \delta_{N_{PV}} E_{N_{PV}}]^T \in \mathbb{R}^{2(N_{PV})}$.

The organization of variables and equations was done by prioritizing the representation usually made in MATPOWER to take advantage of its existing data structure. Thus, the variables were defined as follows

$$\mathbf{x} = \left[\theta_{(PV)}^T \;\vdots\; \theta_{(PQ)}^T \;\vdots\; V_{(PV)}^T \;\vdots\; V_{(PQ)}^T \;\vdots\; \delta^T \;\vdots\; E^T\right]^T. \tag{2.153}$$

The equations were organized as follows:

1) N_{PV} equations of the type (2.141);
2) N_{PQ} equations with active power mismatches at load buses;
3) N_{PV} equations of the type (2.142);
4) N_{PQ} equations with reactive power mismatches at load buses; and
5) $2N_{PV}$ equations of the type (2.149) and (2.150).

Considering the previous modeling, it is possible to write a linearized system of the type

$$\Delta\delta^{(n+1)} + \frac{\Delta}{2} K_P (J_{1PV}\Delta\theta + J_{2PV}\Delta V) = -F_\delta, \tag{2.154}$$

$$J_{1PQ}\Delta\theta + J_{2PQ}\Delta V = -F_{PPQ}, \tag{2.155}$$

$$\Delta E^{(n+1)} + \frac{\Delta}{2} K_V \Delta V = -F_V, \tag{2.156}$$

$$J_{3PQ}\Delta\theta + J_{4PQ}\Delta V = -F_{QPQ}, \tag{2.157}$$

$$a_{11}\Delta E + a_{12}\Delta\delta + a_{13}\Delta\theta + a_{14}\Delta V = -F_{E1}, \tag{2.158}$$

$$a_{21}\Delta E + a_{22}\Delta\delta + a_{23}\Delta\theta + a_{24}\Delta V = -F_{E2}, \tag{2.159}$$

where the mismatches F_δ, F_{PPQ}, F_V, F_{QPQ}, F_{E1}, and F_{E2} are calculated as follows

$$F_\delta = \delta^{(n+1)} + \frac{\Delta}{2}K_P\Delta P^{(n+1)} + (-\delta^{(n)} + \frac{\Delta}{2}K_P\Delta P^{(n)}). \tag{2.160}$$

Given that $\Delta P = P(V,\theta) - P^{sp}$ at a PV bus. Remark that in the illustration of Figure 2.3 that P^{sp} at bus k refers to the power injected into the bus. Thus, if there is generation and a constant load P at the bus, $P^{sp} = P^{ger} - P^{load}$. In the figure, the illustration refers to the case where an active power generation is 1.0 pu in the bus, and the consumption in the bus equals 0.8 pu. Then, it must be considered a power injection of 0.2 pu as P_k^{sp} for the bus.

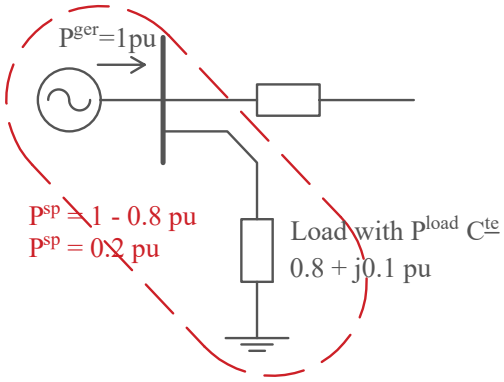

Figure 2.3: Illustration for the definition of the power injected into the bus k in the scenario where in the bus there is both generation and load

Remark that $\Delta P^{(n)}$ in Equation (2.160) must be kept constant at step n since the interest is the iteration to obtain the results at step $n+1$. Other information are:

- F_{PPQ} = mismatch ΔP at PQ buses;
- $F_V = E^{(n+1)} + \frac{\Delta t}{2}K_V\Delta V^{(n+1)} + \left(-E^{(n)} + \frac{\Delta t}{2}K_V\Delta V^{(n)}\right)$ with $\Delta V = V - V^{sp}$ at PV buses;
- F_{QPQ} = mismatch ΔQ at PQ buses; and
- $\begin{bmatrix} F_{E1} \\ F_{E2} \end{bmatrix} = \Big[\text{Equations (2.149) and (2.150)}\Big]$.

Note that the objective is to solve an initial problem for determining the variables in step $n+1$. Assuming that an iterative method is used, an initial estimate is needed for this step. The value of the previous step n was adopted with this aim. Therefore, the initialization for computing the variables in step $(n+1)$ are done considering the variables $\mathbf{x}^{(n+1,0)} = \mathbf{x}^{(n)}$ and $\mathbf{y}^{(n+1,0)} = \mathbf{y}^{(n)}$. Jardim & Stott (2005) suggested initializing the problem by considering a predictor step.

In the case of convergence in step $n+1$ (point t_{n+1}), the time is incremented according to the time-step Δt, and a new point is obtained. The process continues until a steady-state status is reached or a given tolerance is acceptable for the PFP. Also, the divergence can occur, and in this case, other parameters associated with the decision control variable should be set.

Convergence (steady-state) is verified when the error between the specified value of all control variables and the specified values, as well as mismatches in all buses, is less than a prescribed tolerance.

2.4.3 Reactive power control in generators

The reactive power limit in generators is an important issue treated when the PFP is studied. Its study should be considered for several reasons, such as controlling the terminal voltage or other remote bus voltage. The constraint comprises minimum and maximum values, Q_{min}, and Q_{max}, respectively.

According to Jardim & Stott (2005), when a violation of the reactive power limit is detected in a generator, the differential equation $\dot{E}_K = K_{Vk}(V_k^{sp} - V_k)$ used to control the terminal voltage must be replaced by $\dot{E}_k = K_{qk}(Q_k^{sp} - Q_k(\mathbf{x},\mathbf{y})) = -K_{qk}\Delta Q_k$, with $\Delta Q_k = Q_k(\mathbf{x},\mathbf{y}) - Q_k^{sp}$, in which K_{qk} is a positive constant, Q_k^{sp} is the violated limit (Q_{min}, or Q_{max}) and $Q_k(\mathbf{x},\mathbf{y})$ is the reactive power calculated in step n for the generator connected at bus k.

Thereby, applying the trapezoidal rule for numerical integration, the discretization of the equation generates the recurrence equation at the bus k of type PV

$$E_k^{(n+1)} = E_k^{(n)} - \frac{\Delta t}{2} K_{qk}(\Delta Q_k^{(n+1)} + \Delta Q_k^{(n)}), \tag{2.161}$$

producing the algebraic equation

$$0 = E_k^{(n+1)} - E_k^{(n)} + \frac{\Delta t}{2} K_{qk} \Delta Q_k^{(n+1)} + \frac{\Delta t}{2} K_{qk} \Delta Q_k^{(n)}. \tag{2.162}$$

The evaluation of Q_k to compare with the bounds $[Q_{min}, Q_{max}]$ is given by (see Figure 2.4 for illustration)

$$Q_k = \sum_{m=1}^{N_b} Q_{km} + Q_k^{(load)}, \qquad k \in PV \tag{2.163}$$

where Q_{km} is the reactive power flowing from the bus k to m, and

$$\overline{S}_{km} = \overline{V}_k \overline{I}_k^* = \overline{V}_k (Y_{bus}^* V^*) = P_{km} + jQ_{km}, \tag{2.164}$$

$$\overline{S}^{(load)} = P_k^{(load)} + jQ_k^{(load)}. \tag{2.165}$$

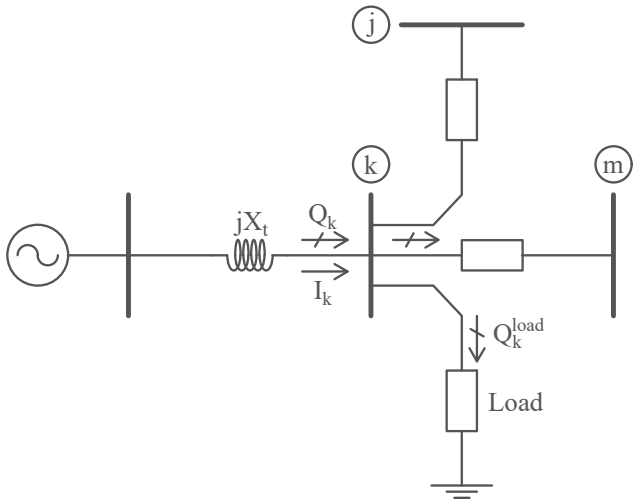

Figure 2.4: Reactive power flow

Therefore, the value of Q_k can be computed as

$$Q_k = imag[V_k (Y_{bus}(k,:) V)^*] + Q_k^{(load)}. \tag{2.166}$$

Considering the PV buses, the linearization of Equation (2.162) generates the mismatch equation

$$\text{Mismatch: } F_{Qlim} = E_k^{(n+1)} - E_k^{(n)} + \frac{\Delta t}{2} K_{qk} \left(\Delta Q_k^{(n+1)} + \Delta Q_k^{(n)} \right), \tag{2.167}$$

and

$$\Delta E_k^{(n+1)} + \frac{\Delta t}{2} K_{qk} (\mathbf{J}_{31PV} \Delta\theta + \mathbf{J}_{32PV} \Delta V) = -F_{Qlim}. \tag{2.168}$$

Remark that the submatrices $\mathbf{J}_{31PV}$ and $\mathbf{J}_{32PV}$ were not part of the Jacobian matrix when bounds were met and are now incorporated to accommodate the bounds violation of Q_k.

Figures 2.5 and 2.6 shows a simplified flowchart for the SDPF. In the flowchart, it is possible to highlight two main loops: an internal and an external. So, the main comments will emphasize their characteristics.

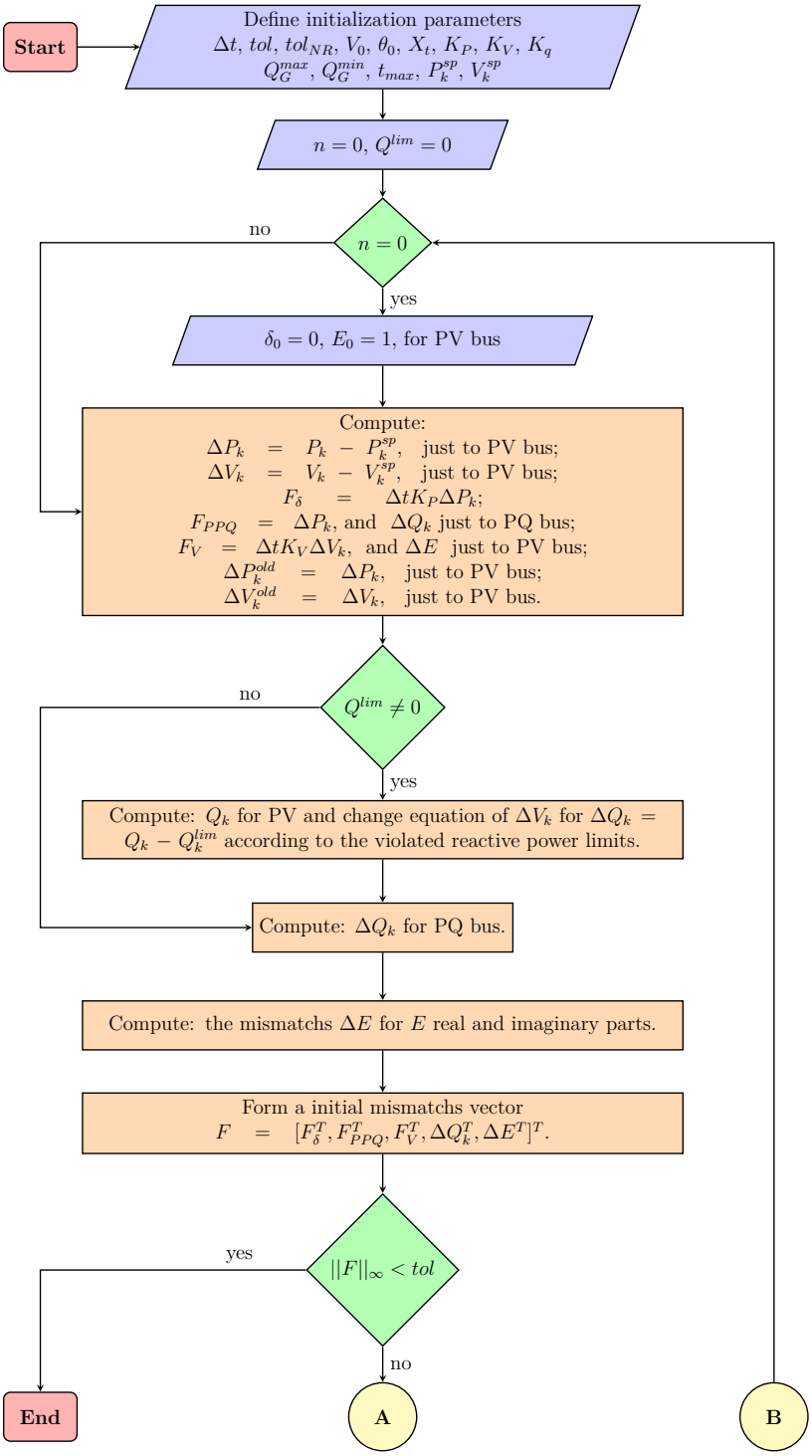

Figure 2.5: Flowchart illustrating the SDPF - Part I

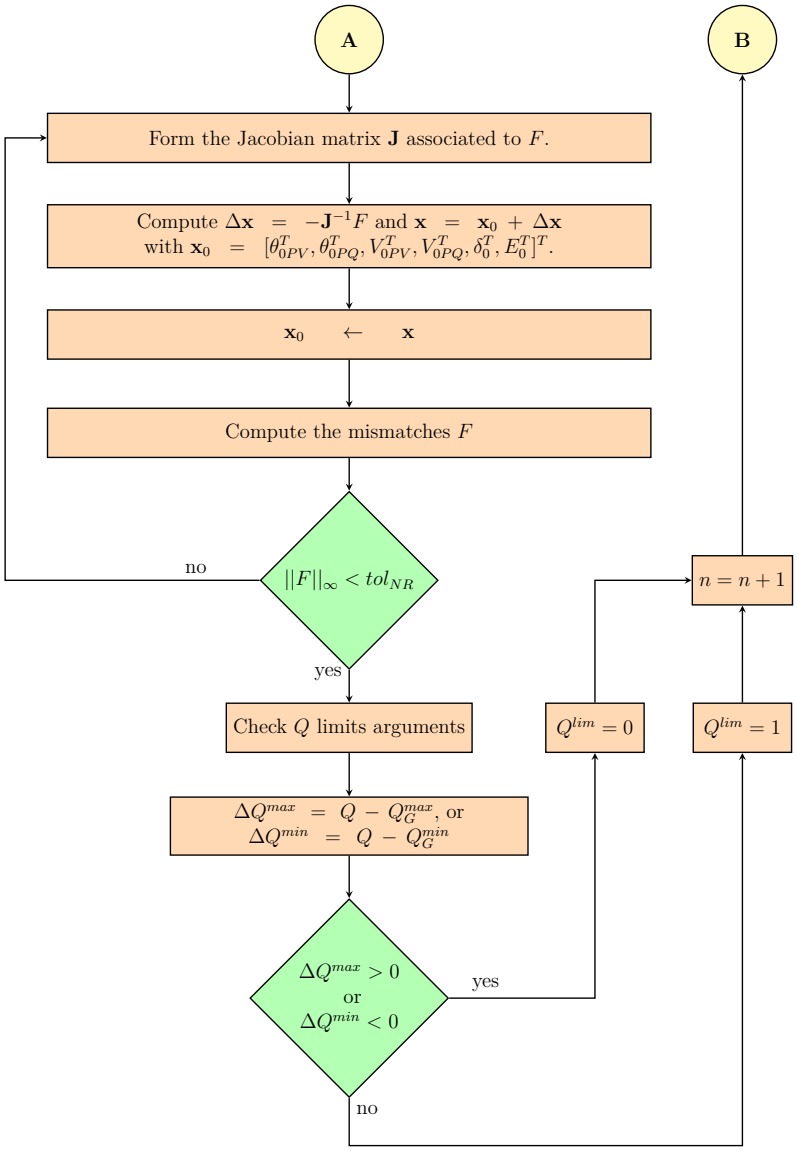

Figure 2.6: Flowchart illustrating the SDPF - Part II

The internal loop is in Figure 2.6, following the direction marked by the letter "A". This loop performs computations of the NR scheme related to the computations of the variables for the step $n + 1$. The convergence is met when the infinite norm of the mismatches is smaller than tol_{NR}. After convergence, the reactive power limits of generators are evaluated. In case of any violation, a flag Q^{lim} is switched to the value 1, but if no violation is verified, the flag is set to zero, as initialized on starting the initial computations. Then the step n is incremented, and the external loop is completed, returning to restart the problem following the path "B" in the flowchart, now in Part - I. This external loop stops when the mismatches F achieve a tolerance tol, indicating a steady-state status.

2.5 IWAMOTO'S METHOD

Another common strategy to address the issue of ill-conditioning encountered in solving the power flow problem was to use an acceleration factor. This factor is applied to the deviation states to compute the updated states during each iteration.

A method proposed by Iwamoto & Tamura (1981) focuses on optimizing the acceleration factor, also known as the Optimal Multiplier (OM). This method utilizes the power flow representation in rectangular coordinates, benefiting from the quadratic characteristics of the problem for its 1-parameter optimization approach (IWAMOTO; TAMURA, 1978). The following provides a brief description of the problem formulation.

Assume the set of nonlinear equations given by Equation (2.169), in which $\mathbf{y}(\mathbf{x})$ is a calculated power vector and $\mathbf{y}^s$ is a specified power vector.

$$\mathbf{y}(\mathbf{x}) = \mathbf{y}^s. \tag{2.169}$$

Considering an m-bus network with input data in rectangular coordinates, then

- vector of nodal voltages: $\mathbf{x} = [\ e_1 \ \ f_1 \ \ e_2 \ \ f_2 \ \ \dots \ \ e_m \ \ f_m\ ]$;
- vector of specified quantities: $\mathbf{y}^s = [\ \mathbf{P}_1^s \ \ \mathbf{Q}_1^s \ \ \mathbf{P}_2^s \ \ |\mathbf{V}_2^s|^2 \ \ \dots \ \ \mathbf{P}_m^s \ \ \mathbf{Q}_m^s\ ]$; and
- vector of calculated variables: $\mathbf{y}(\mathbf{x}) = [\ \mathbf{P}_1(\mathbf{x}) \ \ \mathbf{Q}_1(\mathbf{x}) \ \ \mathbf{P}_2(\mathbf{x}) \ \ |\mathbf{V}_2(\mathbf{x})|^2 \ \dots \ \mathbf{P}_m(\mathbf{x}) \ \ \mathbf{Q}_m(\mathbf{x})\ ]$.

Expanding Equation (2.169) in Taylor series, it is obtained

$$\mathbf{y}^s = \mathbf{y}(\mathbf{x} + \Delta\mathbf{x}), \tag{2.170}$$

where

$$\mathbf{y}^s = \mathbf{y}(\mathbf{x}) + \frac{\partial}{\partial \mathbf{x}}\mathbf{y}(\mathbf{x}) \cdot \Delta\mathbf{x} + \Delta\mathbf{x}^T \cdot \frac{\partial^2}{\partial \mathbf{x}^2}\mathbf{y}(\mathbf{x}) \cdot \Delta\mathbf{x}. \tag{2.171}$$

Considering that the Jacobian is $\mathbf{J} = \dfrac{\partial}{\partial \mathbf{x}}\mathbf{y}(\mathbf{x})$ and

$$\mathbf{y}(\Delta\mathbf{x}) = \Delta\mathbf{x}^T \cdot \frac{\partial^2}{\partial \mathbf{x}^2}\mathbf{y}(\mathbf{x}) \cdot \Delta\mathbf{x}, \tag{2.172}$$

then

$$\mathbf{y}^s = \mathbf{y}(\mathbf{x}) + \mathbf{J} \cdot \Delta\mathbf{x} + \mathbf{y}(\Delta\mathbf{x}). \tag{2.173}$$

Suppose that a scalar μ is inserted into the equation in the same direction as $\Delta\mathbf{x}$ in order to improve convergence and suppose that in some iteration, the state vector $\mathbf{x}$ is named as $\mathbf{x_e}$. Then, the following algebraic equation is formed as

$$\mathbf{y}^s - \mathbf{y}(\mathbf{x_e}) - \mathbf{J} \cdot \mu\Delta\mathbf{x} - \mathbf{y}(\mu\Delta\mathbf{x}) = 0. \tag{2.174}$$

Therefore, Equation (2.172) can be rewritten as

$$\begin{aligned} \mathbf{y}(\mu\Delta\mathbf{x}) &= (\mu\Delta\mathbf{x}^T) \cdot \frac{\partial^2}{\partial\mathbf{x}^2}\mathbf{y}(\mathbf{x}) \cdot (\mu\Delta\mathbf{x}), \\ \mathbf{y}(\mu\Delta\mathbf{x}) &= \mu^2 \cdot \Delta\mathbf{x}^T \cdot \frac{\partial^2}{\partial\mathbf{x}^2}\mathbf{y}(\mathbf{x}) \cdot \Delta\mathbf{x}. \end{aligned} \tag{2.175}$$

Observing Equation (2.172), Equation (2.175) can be rewritten as

$$\mathbf{y}(\mu\Delta\mathbf{x}) = \mu^2 \cdot \mathbf{y}(\Delta\mathbf{x}). \tag{2.176}$$

Hence, Equation (2.174) remains as a second order equation defined with the constants $\mathbf{a}$, $\mathbf{b}$ and $\mathbf{c}$ as a function of μ

$$\mathbf{y}^s - \mathbf{y}(\mathbf{x_e}) + \mu \cdot [-\mathbf{J} \cdot \Delta\mathbf{x}] + \mu^2 \cdot [-\mathbf{y}(\Delta\mathbf{x})] = 0, \tag{2.177}$$

then

$$\mathbf{a} + \mu \cdot \mathbf{b} + \mu^2 \cdot \mathbf{c} = 0, \tag{2.178}$$

where

$$\begin{aligned} \mathbf{a} &= \mathbf{y}^s - \mathbf{y}(\mathbf{x_e}); \\ \mathbf{b} &= -\mathbf{J} \cdot \Delta\mathbf{x}; \\ \mathbf{c} &= -\mathbf{y}(\Delta\mathbf{x}). \end{aligned} \tag{2.179}$$

If μ is an Optimal Multiplier (OM), and $n = 2 \cdot m$, the idea is to adjust the OM size, using the function F defined in Equation (2.180).

$$F = \frac{1}{2} \cdot \sum_{j=1}^{n} \left(\mathbf{a}_i + \mu \cdot \mathbf{b}_i + \mu^2 \cdot \mathbf{c}_i\right)^2. \tag{2.180}$$

The OM μ is adjusted through the minimization of the function F. Then, applying the optimal conditions for Equation (2.180), the condition $\dfrac{\partial}{\partial\mu}F = 0$ must be satisfied. Therefore, resulting in

$$\sum_{i=1}^{n}(\mathbf{a}_i\mathbf{b}_i) + \sum_{i=1}^{n}\left(\mathbf{b}_i^2 + 2 \cdot \mathbf{a}_i\mathbf{c}_i\right) \cdot \mu + 3 \cdot \sum_{i=1}^{n}(\mathbf{b}_i\mathbf{c}_i) \cdot \mu^2 + 2 \cdot \sum_{i=1}^{n}\left(c_i^2\right) \cdot \mu^3 = 0, \tag{2.181}$$

and

$$\mathbf{g}_0 + \mathbf{g}_1 \cdot \mu + \mathbf{g}_2 \cdot \mu^2 + \mathbf{g}_3 \cdot \mu^3 = 0, \tag{2.182}$$

where

$$\begin{aligned}
\mathbf{g}_0 &= \sum_{i=1}^{n} (\mathbf{a}_i \mathbf{b}_i); \\
\mathbf{g}_1 &= \sum_{i=1}^{n} \left(\mathbf{b}_i^2 + 2 \cdot \mathbf{a}_i \mathbf{c}_i\right); \\
\mathbf{g}_2 &= 3 \cdot \sum_{i=1}^{n} (\mathbf{b}_i \mathbf{c}_i); \\
\mathbf{g}_3 &= 2 \cdot \sum_{i=1}^{n} \left(c_i^2\right).
\end{aligned} \tag{2.183}$$

Finally, calculating the OM μ for each iteration and choosing a real solution for it close to one, an updated state deviation vector can be obtained as $\Delta\mathbf{x}^{(r)} \leftarrow \mu^{(r)} \cdot \Delta\mathbf{x}^{(r)}$ and

$$\mathbf{x}^{(r+1)} = \mathbf{x}^{(r)} + \mu \Delta\mathbf{x}^{(r)}. \tag{2.184}$$

2.6 APPROACH BY HOMOTOPY

Using homotopy-based techniques offers an alternative method for addressing ill-conditioned systems, focusing on both static and dynamic approaches. This expands the tool options for power flow research, complementing traditional methods and those that incorporate synthetic dynamics and acceleration factor optimization.

Homotopy methods are robust numerical techniques applied for solving systems of nonlinear algebraic equations as Equation (2.22) (WATSON, 1989; CHIANG; WANG, 2018) for the generic power flow problem. They are also called numerical path-following methods since they depend on a path emanating from an initial state to a final equilibrium point. The problem involves designing an appropriate parameterized nonlinear equations system for a parameter $h \in [0,1]$ (LIAO, 2012). The formulation considers that at the initial state, defined for $h = 0$, the problem is "easy" to solve or has a known solution. In contrast, when $h = 1$, the final state is identical to the "difficult" solution for the problem formulated for finding the roots of $\mathbf{f}(\mathbf{x}) = 0$ (WATSON, 1989).

The homotopy process is generated assuming the inclusion of parameters to gradually modify a nonlinear function (formulation for the "easy" problem, which has a trivial solution),

modifying it until the original function is recovered (the "difficult" problem, which corresponds to finding the zeros of equations such as Equation (2.22)). We also assume in this work that *the trivial solution of the "easy" problem is precisely equal to the initial estimate,* $\mathbf{x}^{(0)}$, for solving the NR problem of the homotopy path.

The homotopy technique applied to a specific problem depends on a homotopy map $\mathbf{G}$ based on the original system of equations $\mathbf{f}(\mathbf{x}) = 0$ and a set of parameter $\mathbf{h}$ according to a modified nonlinear function for an algebraic system (MILANO, 2010)

$$\mathbf{G}(\mathbf{x},\mathbf{h}) = \mathbf{0}, \tag{2.185}$$

in which $\mathbf{h} = [h_1 \ h_2 \ \dots \ h_h]^T$ is the continuation parameter set; a map $\mathbf{G}$ is defined as $\mathbf{G} : \mathbb{R}^{n+n_h} \mapsto \mathbb{R}^n$ and is generated according to the use of $\mathbf{h}$ and the definition of the "easy problem", *i.e.*, for $\mathbf{h} = 0$. The parameter $\mathbf{h}$ is an independent variable such that $\mathbf{G} : \mathbb{R}^n \times \mathbb{R}^{n_h} \mapsto \mathbb{R}^n$.

The expression $\mathbf{G}(\mathbf{x},\mathbf{h})$ comprises generally two parts: one is related to the term that must be preserved when the homotopy parameter assumes the unitary value; and the other is the one that is extinguished for this same parameter value. For a single homotopy parameter $h \in [0,1]$, an example is the classical expression

$$\mathbf{G}(\mathbf{x},\mathbf{h}) = h\mathbf{f}(\mathbf{x}) + (1-h)\mathbf{g}_0(\mathbf{x}) = \mathbf{0}, \tag{2.186}$$

in which $\mathbf{g}_0(\mathbf{x})$ is considered the "easy" solution problem and $\mathbf{f}(\mathbf{x})$ is the target nonlinear equation.

Note that $\mathbf{g}_0(\mathbf{x})$ in Equation (2.186) is a function freely defined by the user, and for each value of h, a system of the nonlinear equation should be solved according to a fixed h. When h is discretized for values 0, h_1, $h_2, \dots, h_n$, we say that the solutions for $\mathbf{G}(\mathbf{x},\mathbf{h})$ corresponding to h_i are associated to a point of the *homotopy path.* Therefore, the path is formed by all solutions obtained using the values h_i, $i = 0,1,2,\dots,n$.

For a simple demonstration of an application of the composition of $\mathbf{G}(\mathbf{x},\mathbf{h})$ to manipulate a network through a single homotopy parameter h, assume that $\mathbf{f}(\mathbf{x}) = \mathbf{f}_1(\mathbf{x}) + \mathbf{f}_2(\mathbf{x})$, *i.e.*, the network equations are composed of two parts $\mathbf{f}_1(\mathbf{x})$ and $\mathbf{f}_2(\mathbf{x})$. For example, the function $\mathbf{G}(\mathbf{x},\mathbf{h})$ can be formed to eliminate the second part, such as in a contingency study. For this claim and using the single homotopy parameter $h \in [0,1]$, the expression is

$$\mathbf{G}(\mathbf{x},\mathbf{h}) = h\mathbf{f}_1(\mathbf{x}) + (1-h)\mathbf{f}_2(\mathbf{x}) + (1-h)\mathbf{g}_0(\mathbf{x}) = \mathbf{0}. \tag{2.187}$$

In Equation (2.187), when $h = 0$ (the "easy" solution problem), the problem consists of solving the equation $\mathbf{f}_2(\mathbf{x}) + \mathbf{g}_0(\mathbf{x}) = 0$, starting from an initial estimate $\mathbf{x}^{(0)}$. Considering that in a contingency scenario, $\mathbf{f}_2(\mathbf{x})$ models a very small part of the network, for example, a transmission line outage or other interconnection, its representation is very simple. Consequently, we can formulate this initial problem as easily solvable.

On the other hand, if the interest is the insertion of a device or control law, we can suppose that initially $\mathbf{f}(\mathbf{x}) = \mathbf{f}_1(\mathbf{x})$ and the term $\mathbf{f}_2(\mathbf{x})$ needs to be added to the original one. Then, the expression for $\mathbf{G}(\mathbf{x},\mathbf{h})$ can be written as

$$\mathbf{G}(\mathbf{x},\mathbf{h}) = h\mathbf{f}_1(\mathbf{x}) + h\mathbf{f}_2(\mathbf{x}) + (1-h)\mathbf{g}_0(\mathbf{x}) = \mathbf{0}. \tag{2.188}$$

In Freitas & Silva (2022), a static homotopy approach was introduced to solve a problem of type Equation (2.185) embedding two parameters, *i.e.*, $n_h = 2$. The parameters were used to drive the solution from a flat start initial estimate, which also coincides with the solution to this starting point of the homotopy path. Modifications that affect only some specific elements of the system admittance matrix according to $\mathbf{h}$ reach the final result at the last point of the homotopy path.

The idea in using $\mathbf{h} = 0$ was to obtain the trivial solution by reorganizing the network elements fictitiously so that each bus met its own consumption and generation demand. The consequence is that there would be no load flow between the buses, and the solution of this system is the same initial estimate of a flat start guess. The networks presented in Figure 2.7 show two didactic examples of how the method works for highlighting changes at the k-bus of type PQ (Figure 2.7(a)) and the k-bus of type PV (Figure 2.7(b)).

Evaluating the system in Figure 2.7(a), it is assumed that bus #1 is the slack-bus, where the voltage magnitude is given, $|\overline{V}_1| = V_{01}$, and as reference bus with $\theta_1 = 0°$; $\overline{V}_1 = V_{01}\angle 0°$, for the bus #m of PV-type with the given voltage magnitude V_{0m}, $\overline{V}_m = V_{0m}\angle 0°$. Considering that the initial estimate is of the type flat start, we have the voltages on the buses of type PQ, $\overline{V}_k$ and $\overline{V}_j$, $\overline{V}_k = \overline{V}_j = 1\angle 0°$. Then, Equation (2.18) and Equation (2.19) can be written for this specific case, as follows

$$\begin{aligned}\Delta P_k = P_k - V_k V_j \left[G_{kj}\cos(\theta_{kj}) + B_{kj}\sin(\theta_{kj})\right] - V_k V_{01}\left[G_{k1}\cos(\theta_{k1}) + B_{k1}\sin(\theta_{k1})\right] - \\ V_k V_{0m}\left[G_{km}\cos(\theta_{km}) + B_{km}\sin(\theta_{km})\right] - V_k V_k\left[G_{kk}\right],\end{aligned} \tag{2.189}$$

$$\Delta Q_k = Q_k - V_k V_j \left[G_{kj}\sin(\theta_{kj}) - B_{kj}\cos(\theta_{kj})\right] - V_k V_{01}\left[B_{k1}\sin(\theta_{k1}) - B_{k1}\cos(\theta_{k1})\right] - V_k V_{0m}\left[G_{km}\sin(\theta_{km}) - B_{km}\cos(\theta_{km})\right] - V_k V_k\left[-B_{kk}\right]. \tag{2.190}$$

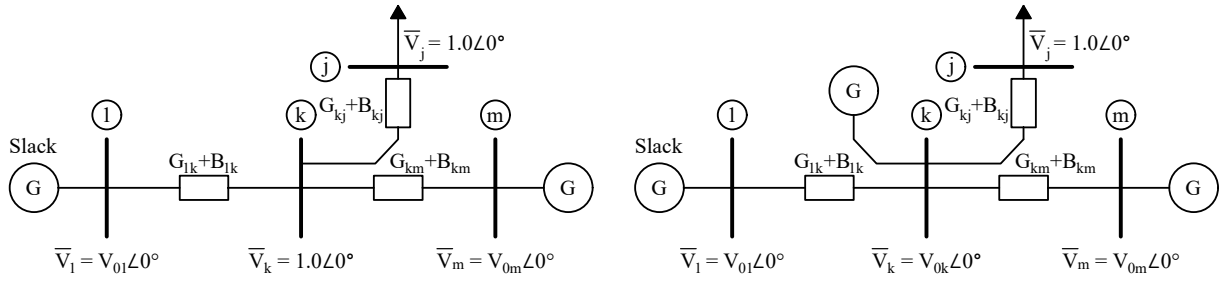

(a) bus #k as PQ-type (b) bus #k as PV-type

Figure 2.7: Schematic diagram to determine the power flow equations at first iteration with flat start guess at a bus #k as PV- and PQ-type

Assuming that $V_k = V_j$, $\sin(\theta_{kj}) = \sin(\theta_{km}) = \sin(\theta_{kk}) = 0$ and $\cos(\theta_{kj}) = \cos(\theta_{kk}) = 1$, Equation (2.189) and Equation (2.190) are transformed to

$$\Delta P_k = P_k - G_{kj} - V_{01}G_{k1} - V_{0m}G_{km} - G_{kk}, \tag{2.191}$$

$$\Delta Q_k = Q_k + B_{kj} + V_{01}B_{k1} + V_{0m}B_{km} + B_{kk}. \tag{2.192}$$

The strategy to reset the mismatches of the equations is to insert a fictitious shunt element g_k in Equation (2.191) and b_k in Equation (2.192) such that it makes the values of ΔP_k and ΔQ_k zero. *i.e.*, fictitious shunt compensation elements are introduced for $\mathbf{h} = 0$. From these equations, the fictitious network elements are defined to make the PFP solution trivial and equal to the initial estimate at the first iteration. Then, the fictitious shunt elements are determined as follows:

$$g_k = P_k - G_{kj} - V_{01}G_{k1} - V_{0m}G_{km} - G_{kk}, \tag{2.193}$$

$$b_k = -(Q_k + B_{kj} + V_{01}B_{k1} + V_{0m}B_{km} + B_{kk}). \tag{2.194}$$

Therefore, when the fictitious shunt elements are inserted into Equation (2.191) and Equation (2.192), the power mismatches become null, as can be seen in (2.195)-(2.196). This means that the state of the system coincides with the PFP's own initial estimate.

$$\Delta P_k = P_k - G_{kj} - V_{01}G_{k1} - V_{0m}G_{km} - (G_{kk} + g_k) = 0, \tag{2.195}$$

$$\Delta Q_k = Q_k + B_{kj} + V_{01}B_{k1} + V_{0m}B_{km} + (B_{kk} + b_k) = 0. \tag{2.196}$$

Proceeding in the same way for the PV-bus in Figure 2.7(b), the difference in relation to the PQ-bus is that the voltage magnitude is known. Then only one variable is unknown and just one fictitious compensation element is necessary. In this case, to reset the mismatch of active power since it is a known value. Considering the magnitude of the specified voltage, $\overline{V}_k = V_{0k}\angle 0°$, the Equation 2.18 and Equation 2.19 will be

$$\Delta P_k = P_k - V_{0k}V_j\left[G_{kj}\cos(\theta_{kj}) + B_{kj}\sin(\theta_{kj})\right] - V_{0k}V_{01}\left[G_{k1}\cos(\theta_{k1}) + B_{k1}\sin(\theta_{k1})\right] - V_{0k}V_{0m}\left[G_{km}\cos(\theta_{km}) + B_{km}\sin(\theta_{km})\right] - V_{0k}V_{0k}G_{kk}. \tag{2.197}$$

For PQ-bus linking the bus #k, $V_j = 1$, $\sin(\theta_{kj}) = \sin(\theta_{km}) = \sin(\theta_{kk}) = 0$ and $\cos(\theta_{kj}) = \cos(\theta_{km}) = \cos(\theta_{kk}) = 1$, Equation (2.197) can be rewritten as

$$\Delta P_k = P_k - V_{0k}G_{kj} - V_{0k}V_{01}G_{k1} - V_{0k}V_{0m}G_{km} - V_{0k}V_{0k}G_{kk}. \tag{2.198}$$

Assuming the same strategy, to get $\Delta P_k = 0$, the shunt element can be defined as

$$g_k = \frac{P_k}{V_{0k}^2} - \frac{1}{V_{0k}}G_{kj} - \frac{V_{01}}{V_{0k}}G_{k1} - \frac{V_{0m}}{V_{0k}}G_{km} - G_{kk}. \tag{2.199}$$

Therefore, the mismatches can be computed as Equation (2.200) and considered zero.

$$\Delta P_k = P_k - V_{0k}G_{kj} - V_{0k}V_{01}G_{k1} - V_{0k}V_{0m}G_{km} - V_{0k}^2\left(G_{kk} + g_k\right) = 0. \tag{2.200}$$

Notably, fictitious elements were inserted only in the PQ- and PV-type buses as shunt elements. The consequence of this is that they will only change the main diagonal in the construction of the admittance matrix $\hat{Y}_{kk}$ (see Equation (2.201) and Equation (2.202)). The amount of the fictitious shunt elements must be removed progressively along the homotopy path until fully extinguished at the end path, which occurs for $\mathbf{h} = 1$.

Note that along the homotopy path, the network gradually changes its configuration, and as a consequence, a new point of operation (solution of the resulting nonlinear equation system) will also be formed. The solution of this new operating point is calculated through an iterative method, such as NR, using the result of the previous point as an initial estimate. This flexibility gives a margin for the user to have a very close estimate for the solution on the next point of the homotopy's path. Therefore, as the homotopy path points are obtained numerically, the

distance between points can be regulated by controlling a step Δh of the homotopy parameter of interest h.

Since network configurations can be modified through a homotopy path with many parameters of the vector $\mathbf{h}$, we assigned the parameter (entry) h_1 to change only the fictitious admittance as described previously. Therefore, assuming that the homotopy parameter h_1 changes in the interval $0 \leq h_1 \leq 1$, we have the construction of the nodal admittance matrix with the fictitious elements as

$$\hat{Y}_{kk} = h_1 Y_{kk} + (1 - h_1)(g_k + jb_k), \;\; k \in PQ, \tag{2.201}$$

$$\hat{Y}_{kk} = h_1 Y_{kk} + (1 - h_1)(g_k), \;\; k \in PV. \tag{2.202}$$

in which Y_{kk} is an admittance of the original network.

The representation of power system didactic example with the fictitious elements (FREITAS; SILVA, 2022) can be seen in Figure 2.8(a) for PQ-type and Figure 2.8(b) for PV-type.

A second strategy to modify the network configuration uses an additional parameter, h_2. Using it simultaneously with h_1 allows for a more extensive change in the network. However, the more parameters for the homotopy path are inserted, the more operating points need to be calculated. As a result, the computational cost will increase. If the user can avoid this maneuver regarding the diversification of the parameters, it may also have a reduced computational cost.

The second strategy to facilitate convergence is modifying the impedance in the branches close to the slack bus, defined as neighborhood Ω_s. The idea was to *reduce the impedance z_{km} linking two buses #k and #m*, by a scaling factor $\delta \leq 1$ in such a way as to artificially increase the load flow capacity in the referred branch. Evidently, this factor must be removed at the end of the homotopy process, for example, by assigning a unitary value for δ. To meet this demand, a new homotopy factor h_2 was defined, and the fictitious impedance was defined as

$$\hat{z}_{km} = h_2 z_{km} + (1 - h_2)\delta z_{km}, \;\; z_{km} \in \Omega_s, \quad \hat{y}_{km} = 1/\hat{z}_{km}. \tag{2.203}$$

Therefore, the modified admittance matrix along the homotopy path must also be formed incorporating the elements $\hat{y}_{km}$, due to the activation of h_2, besides those fictitious shunt admittance due to the contribution of h_1.

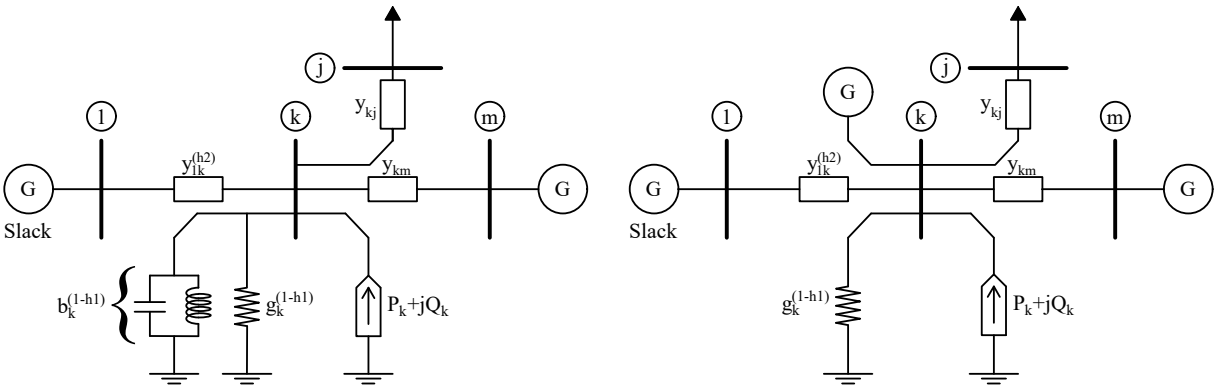

(a) bus #k as PQ-type (b) bus #k as PV-type

Figure 2.8: Fictitious network inserted governed by homotopy parameters h_1 and h_2 at a bus #k as PV- and PQ-type

The homotopy path is formed through the solution of nonlinear algebraic equations, given the parameters h_1 and h_2 for discrete values in the range $0 \leq h_1 \leq 1$ and $0 \leq h_2 \leq 1$, for step-lengths Δh_1 and Δh_2, respectively, *i.e.*, h_{1i}, $i = 0,1,\ldots,N_1$ and h_{2k}, $k = 0,1,\ldots,N_2$. At each path point (i,k), a nonlinear equation system must be solved iteratively using the NR scheme requiring a given number of iterations $iter_{hi,hk}$.

Except for the first point, which has a trivial solution coinciding with the initial estimate $\mathbf{x}^{(0)}$, all others are solved iteratively considering its initial estimate as that point of the homotopy path previously computed by the NR solver. This way, the solution at each point in the path is expected to stay close to its neighbor, providing good conditions for converging the NR's method up to achieving the last one, for $h = 1$.

Therefore, the number of NR solvers for the homotopy path, consequently the global number of iterations, depends on how h_1 and h_2 are discretized. Then, the NR global number of iterations to achieve the final solution of the PFP depends on the step-length Δh for the homotopy parameters. Also, it depends on the number of iterations of the NR solver to determine the nonlinear equation solution solved individually per discrete point. So, for two parameters $\mathbf{h} = [h_1\ h_2]^T$, the global number of iterations, N_{iter} for the homotopy path can be determined as

$$N_{iter} = \sum_{i=1}^{N_1} \sum_{k=1}^{N_2} iter_{(i,k)}, \tag{2.204}$$

where $iter_{(i,k)}$ is the number of iterates for the point i and k to form the homotopy path. Remember that $iter_{(0,0)} = 0$ because it corresponds to the initial point, and no iteration is

necessary since the solution at this point is its own estimate $\mathbf{x}^{(0)}$.

2.7 OVERVIEW

This chapter focused on the theoretical foundation of the PFP. It presented the construction of the well-known active and reactive power balance equations that model the PFP using Ohm's law, which is the starting point for this problem. Since they are nonlinear equations, developing techniques to solve them is crucial, which is an important scientific finding. This theory has evolved over the years and has become more robust to solve more complex problems. It presented classical solvers and others with relevant numerical performance available in the literature to demonstrate their relevance and complexity. These solvers served as a basis for the comparison of the proposed method.

Several techniques were discussed for solving the PFP, such as the classical methods, methods based on synthetic dynamics, optimization, and homotopy.

The theoretical foundation of this chapter aims to establish the numerical basis for understanding the proposed method described in Chapter 4, as well as the reference comparison methods used in Chapter 6. Additionally, the next chapter will provide a review of the literature on PFP, ill-conditioned systems, homotopy methods, and various applications.

CHAPTER 3

STATE OF THE ART

This chapter reviews the power flow problem, emphasizing the issues involving the ill-posed questions that have been detected over the years. The bibliographic survey is far from complete, but it summarizes some issues addressed in the investigation proposed in this work.

The emphasis on the homotopy theme received attention since it provides a key framework for solving the PFP, as studied in this PhD thesis. Therefore, some publications in this field motivated the investigations proposed in the continuation of the work.

3.1 INTRODUCTION

The PFP is a topic that has been studied for a long time. Since the beginning, it has challenged the understanding of mathematical models in solving the nonlinear algebraic equations that govern the power system. In a way, the main challenge was associated with the dimensions of the power system and consequently to estimate the PF solutions. Since the first studies (DUNSTAN, 1948), the topic was investigated considering parameters such as accuracy and speed of methods converging to the solution. Also, there was an interest in decoupling the results of calculations from human intervention, leaving the process automated from digital computing (HENDERSON, 1954; DUNSTAN, 1954; GLIMN; STAGG, 1957).

Generally, the input parameters for modeling the electrical system consist of a set of known values defined by the physical arrangement of the elements in the circuit of the network. After establishing the physical limits considered, parameters such as the resistance and reactance of each transmission line, the voltage ratio and phase shift transformer, the power load and generation, and data on the generation buses are established as input data (DUNSTAN, 1947). Based on the initial information, Kirchhoff's law imposes restrictions, including the principle that the sums of the currents must equal zero. Additionally, considering the equipment limits,

the power flow in each branch of the network is calculated using the voltage values at the terminals (WARD; HALE, 1956).

Since the Massachusetts Institute of Technology used the first network analyzer in 1929, due to the importance of the system for electrical safety, interest in these solvers has grown, and countries have started to invest in these solutions (DUNSTAN, 1947). In the beginning, one of the main advantages was to obtain the solution using digital computers in such a way as to consider all input parameters to obtain an accurate solution (DUNSTAN, 1954; HENDERSON, 1954; WARD; HALE, 1956). An example is the method based on a digital computer proposed by McGillis (1957), which solved the problem using mesh and nodal methods. Another example was proposed by Ness (1959), who restricted the approach proposed by Ward & Hale (1956) only to the convergence problem of nonlinear equations by an iterative method. This followed the analysis method and convergence acceleration technique proposed by Brown & Tinney (1957), obtaining faster convergence for a 6-bus test system. From this work, the methods became more robust as they increasingly relied on the support and advancement of computer technology.

With this technological advancement, many well-known methods have been tested and were used as a reference, such as NR (TINNEY; HART, 1967) and Fast Decoupled load flow (STOTT; ALSAC, 1974). It made it possible to compare performance between methods (GLIMN; STAGG, 1957; TAYLOR; TREECE, 1967) based on parameters such as solving large-scale and overload systems, convergence speed, number of iterations, approximation error, ability to solve well- and ill-conditioned power systems, among others (STOTT, 1974).

Given the complexity of solving the PFP in certain power systems, it was observed that some solvers achieved convergence while others did not. In view of the existence of possible solutions, a distinction needed to be done between well-conditioned and ill-conditioned power systems. There have been instances where the solver diverged or stagnated when using conventional load flow calculation methods, despite the existence of a potential solution; that is, there was no practical load flow solver available to address the PFP (IWAMOTO; TAMURA, 1981). Thus, cases were classified into well-conditioned systems to differentiate them from ill-conditioned cases. This application is crucial when the system's operating state is unknown or when only a poor initial guess is available (DEUFLHARD, 1974). This problem can occur in real situations

such as contingencies, insertion of new equipment into the system, or in power system transients.

The NR method is considered standard in applications for PFP solutions. Therefore, it is regarded as a reference to distinguish well- and ill-conditioned cases (MILANO, 2009; MILANO, 2010). According to Milano (2010), well-conditioned systems exist where the PFP solution exists and are solved by standard NR using the flat start guess as an initial estimate. The flat start guess is the initial estimate in the iterative process with voltage magnitude on the load buses equal to 1 pu and voltage angle equal to 0. According to Milano (2010), the ill-conditioned cases are defined where the PFP solution exists, but they are not found using standard NR solver starting from the flat start guess. From another point of view, Tripathy *et al.* (1982) defined as ill-conditioned systems when the Jacobian matrix has eigenvalues sensitive to small changes in values compared to other less sensitive eigenvalues, for example. From the classification of ill-conditioned cases, a wide range of research and solution proposals have recently opened up, including promising results for large-scale systems.

It is worth highlighting some works that dealt with methods to treat ill-conditioned cases. An approach using high-order Levenberg-Marquardt concepts (POURBAGHER; DERAKHSHANDEH, 2016) and later adding fuzzy rules concepts (DERAKHSHANDEH *et al.*, 2018) was presented to solve ill-conditioned cases with 11-, 57-, 118- and 2383-buses with reliability and high speed. The method was compared with five other solvers, including standard NR and Iwamoto's method. Shahriari *et al.* (2012) use the state space search method to search a low voltage solution and maximum loading point of two ill-conditioned test systems. Oliveira & Freitas (2021) and Freitas & Oliveira (2023b) solved large-scale ill-conditioned cases, including 70k-buses inspired by the Heun-King-Werner methods, presenting superior performance compared to standard NR, Euler, and Runge-Kutta-Broyden hybrid form. Tostado-Veliz *et al.* proposed different approaches to solve ill-conditioned cases such as combining Runge-Kutta Broyden's Load Flow (TOSTADO-VÉLIZ *et al.*, 2018); based on the Adams-Bashforth formulation (TOSTADO-VÉLIZ *et al.*, 2019b); the new approach called Newton-Raphson-Predictor-Corrector (TOSTADO *et al.*, 2019a); using concepts from current injection form (TOSTADO-VÉLIZ *et al.*, 2021); combining approach with Forward-Euler formula and Ralston method (TOSTADO *et al.*, 2019c); based on Gauss-Newton's formulation (TOSTADO *et al.*, 2019b); among other approaches applied to ill-conditioned systems (TOSTADO-VÉLIZ *et al.*, 2020c;

TOSTADO-VÉLIZ *et al.*, 2020a).

Finally, it is also worth highlighting some works that dealt with ill-conditioned systems but using homotopy concepts. With the evolution of models, the methods became robust and solved large-scale test systems. In this context, the homotopy method is suitable as it transforms a difficult-to-solve problem into a feasible solution and progressively returns to the original difficult-to-solve state (KU *et al.*, 2011). Okumura *et al.* (1991) use concepts of predictor step for following the homotopy path and solved an 11-bus test system. Freitas & Silva (2022) fictionally reorganized the entire network so that the initial solution in the homotopy process was trivial. From then on, the original elements were reinserted into the system. At each homotopy step, the NR method was used to find intermediate solutions until the system returned to its original state of complex solution. This method was tested for large-scale test systems with 13k- and 70k-buses and achieved reliable results that motivated exploring homotopy techniques to solve the PFP.

Jardim & Stott (2005) proposed a Synthetic Dynamic Power Flow (SDPF) method inspired by the work proposed by Galloway *et al.* (1970) in 1970. The idea in these works is to embed the power flow equations into a dynamic model and take advantage of the fact that the dynamic response of a stable power system converges to a stable equilibrium point. In the work presented by Galloway *et al.* (1970), great potential for convergence was claimed. However, little attention was paid to the proposal. In 2005, Jardim & Stott (2005) changed the technique and presented a method based on the introduction of decision variables. While Galloway *et al.* (1970) used undamped second-order dynamics to mimic the behavior of synchronous generators, Jardim & Stott (2005) proposed a reliable and efficient first-order dynamics. The nature of the dynamic aspect introduced into the problem is entirely artificial and can assume infinite configurations, depending on the parameters adopted to represent it. In 2008, Chaves (2008) presented an MSc thesis, exploring the discovery in Jardim & Stott (2005) to investigate the operation point of two small test systems for different initial conditions and verifying the ill-conditioning influence. The technique was implemented into a production-grade software called ORGANON (JARDIM, 2005), whose script is not accessible as it is the MATPOWER software (ZIMMERMAN *et al.*, 2011).

3.2 HOMOTOPY AND POWER FLOW

Over time, the homotopy method has been shown to be highly effective in solving nonlinear equations (LI, 1997). Since it was presented in 1935 by Hu (1959), the idea has proven capable of facilitating the path to solutions and has been applied in different areas of study, such as science, finance, and engineering (LIAO, 2012). Recently, it has been applied in different fields of science (MEHTA *et al.*, 2016) such as physics, chemistry, and biology in different works (MEHTA, 2011; MANIATIS; MEHTA, 2012). However, it was restricted to evaluating the relationship between the homotopy methods and the nonlinear equations that govern the PFP. So, a bibliographical search was actually carried out in a scientific database to understand the evolution of scientific works and the latest publications on the topic. Initially, the homotopy and power flow themes were related to collecting works with these related themes. This research and previous work related to these latest publications have been carried out over the last four years. This survey verified the main techniques, methods, and real cases applied to solve the problem. The main idea was to verify how homotopy helps with difficult-to-solve problems, such as load flow.

3.2.1 New approaches to solve nonlinear equations

The work presented by Echavarren *et al.* (2023) introduces a second-order formulation of the Newton-Raphson method. This method utilizes homotopy techniques to solve the PFP through the reformulation of the equations. An important point is that the initial estimates start from the flat start guess. One of the difficulties of the method is computing successive derivatives to create the second-order update state vector, which leads to more significant computational time effort. The method was tested for the IEEE 39-bus test network and reduced the number of iterations compared to the NR method, even in four variations of load scenarios. The applied homotopy methodology with the second-order approach was more accurate, robust, and stable than NR.

Some publications employ numerical methods and homotopy to make the hybrid method more efficient. Tostado *et al.* (2019c) proposed a novel approach that combined homotopy and the numerical Newton method to solve ill-conditioned systems. They used the Forward-

Euler and Ralston method to propose the idea without being affected by the initial guess and validated the method in systems such as 3012-bus and 9241-bus systems. Mehta *et al.* (2016) proposed a homotopy continuation technique named the Numerical Polynomial Homotopy-based Continuation (NPHC) method that used complex-valued solutions to find convergence to the physical real form solution. In Freitas & Silva (2022), the static homotopy approach is employed to solve the PFP by assuming a fictitious network. At each point along the homotopy path, the fictitious network is gradually removed until it vanishes completely at the end of the path.

Another approach considered the development of electrical generation through renewable energies, such as photovoltaic, wind, and fuel cells (CHIANG *et al.*, 2014). The so-called Distributed Generation (DG) started to be considered in PFP studies that demand solvers incorporating these characteristics (ZHAO *et al.*, 2013; CHIANG; WANG, 2018). In this same direction, Lima-Silva *et al.* (2023) proposed a homotopy numerical method to solve a PFP with DG inserted in the grid. The method proved to be advantageous over the traditional NR when considering different load scenarios for 6-, 38-, and 69-bus distribution test systems.

The methods already developed using homotopy are also widely studied as a reference for performance comparison (KU *et al.*, 2011; CHANDRA *et al.*, 2017; ALI *et al.*, 2023a; BALUEV *et al.*, 2024). To present a brief history of some numerical methods applications in PFP applications, we show some important works on the subject that have been published over time in Table 3.1. It is important to note that, over time, electrical systems have become more complex and larger. In this context, the evolution of solvers needed to keep up with this evolution, as shown by the growth of the systems tested, and the increase in the number of buses.

3.2.2 Power systems stability studies

The homotopy method also helps in stability studies, where it is essential to know all possible solutions of the nonlinear equations of a power system, whether stable or unstable (LEE; CHIANG, 2004). Lindberg *et al.* (2023) presented a new method to calculate all real solutions of a lossless system with all PV buses. Through parameter homotopy continuation,

this work presents advantages over other homotopy methods, reaching solutions more quickly by exploiting the symmetry between the system's equations. However, they tested only with didactic models such as a 3-bus system.

In the same way, Ali *et al.* (2023a) and Ali *et al.* (2023b) use homotopy concept to find all solution boundaries, delimiting in regions for a system, and Chandra *et al.* (2017) uses a NPHC, independent of the initial guess, a 3-bus and another 10-bus system with renewable generation, to provide the operator a voltage stability studies.

3.2.3 Optimal power flow

The Optimal Power Flow (OPF) studies are an essential tool for the safe operation of the electrical grid. Operators depend on numerical simulators to predict optimal dispatch meeting system constraints. In this sense, many works address issues for evaluating the system's available resources.

The homotopy approach, as described by Nair *et al.* (2022), assesses algorithm performance by modeling the power system in both Cartesian and polar coordinates. It compares parameters such as the number of iterations and computational performance, which change based on the size of the system. The approach considers power systems ranging from 9 to 25k buses.

Park *et al.* (2020) employed the OPF post-contingency approach for a Polish network simulating an online outage. Three models were tested using two homotopy parameters, achieving good performance and guaranteeing global convergence under established initial conditions.

Agarwal *et al.* (2021) seek global convergence for large-scale systems. Other methods utilize homotopy to adapt OPF solvers to the increasing integration of renewable energy sources (MCNAMARA *et al.*, 2022). They also take into account the time-dependent constraints of energy storage systems in large power networks, such as those with 70k-buses (AGARWAL; PILEGGI, 2022).

3.2.4 Three-phase power flow

The homotopy method approach is also applied to three-phase power flow (PANDEY *et al.*, 2017). Pandey & Pileggi (2020) proposed a method that uses NR and GS, associated with homotopy concepts, to guarantee convergence in large-scale transmission and distribution systems since the continuation methods (GOLDGEISSER; GREEN, 2000) are also appropriate for this approach.

Table 3.1: Summary of different approaches about PFP and tested cases

Reference	**Main contribution**	**Size of tested systems (buses)**
Dunstan (1947)	Establishes certain principles and methods that facilitate the handling of problems of power flow in networks	5 and 24
Dunstan (1948)	Load flow studies computing a complete set of coefficients describing the effects network using just a desk calculating machine	5 and 10
Henderson (1954)	Presents an iterative method employed for solving power flow problems on an automatic digital computer	15
Ward & Hale (1956)	Describe the network connections and impedances in the form of a list of node basis parameters	6
Glimn & Stagg (1957)	Automatic calculation of load flows performed by the Gauss-Seidel method	30 and 80
McGillis (1957)	Solved the load-flow problem by mesh and nodal method with an IBM digital computer	7 and 38
Brown & Tinney (1957)	Present the acceleration methods and discuss their effectiveness	13 and 50
Ness (1959)	Worked for faster convergence to reduce the time required to run a load flow	6
Tinney & Hart (1967)	Present a classical power flow solution by Newton's method that works efficiently for large problems	7, 500 and 1k
Taylor & Treece (1967)	Load flow analysis by the Gauss-Seidel method	-
Stott (1974)	Describes a fast decoupled load flow method	14, 30, 57, 118, 205 and other

Table 3.1 – continued from previous page

Reference	**Main contribution**	**Size of tested systems (buses)**
Iwamoto & Tamura (1981)	Developed a load flow calculation method for ill-conditioned power systems	11 and 43
Tripathy *et al.* (1982)	Present the K.M. Brown's method to solve ill-conditioned load-flow problems	11, 13, 43, 30 and 57
Okumura *et al.* (1991)	Use concepts of predictor step for following the homotopy path	11
Milano (2009)	Proposes an entire family of numerically efcient algorithms for solving ill-conditioned power flow cases	1254
Milano (2010)	Presents different methods which any well-assessed numerical method can be used to solve a PFP	2, 14 and other
Zhao *et al.* (2013)	Presents a homotopy method for power flow analysis of distribution networks with DGs modeled as P-V nodes	13, 37, 123, 1101, and 8500
Chiang *et al.* (2014)	Presents a homotopy power flow method considering distributed generation	13, 123, 1101 and 8500
Mehta *et al.* (2016)	Proposed a homotopy continuation named the Numerical Polynomial Homotopy-based Continuation	5, 10, 11, 12, 13 and 14
Tostado-Véliz *et al.* (2018)	Combined Runge-Kutta and Broyden's approach for solving ill-conditioned power systems	11, 13, 20, 43, 30, 57, 118, 300
Tostado *et al.* (2019c)	Proposed two novel load flow techniques combining Forward-Euler and Ralston method	118, 300, 312, 9241, and 13659
Tostado-Véliz *et al.* (2020b)	Proposed a method based on Newton-Cotes formula for solving ill-conditioned systems	3012, 3375, 6024, 9961, 13659 and 27318
Tostado-Véliz *et al.* (2021)	Presented a novel method for Ill-conditioned systems using current injection	500, 2383, 2737, 3012, 3120, 3375 and 6468
Freitas & Silva (2022)	Fictionally reorganized the entire network so that the initial solution in the homotopy process was trivial	9, 300, 1888, 1951, 3012, 3375, 6515, 13659, and 70k
Echavarren *et al.* (2023)	Presents the second-order formulation for the Newton-Raphson method	39

Table 3.1 – continued from previous page

Reference	Main contribution	Size of tested systems (buses)
Lima-Silva & Freitas (2024a)	Proposed a hybrid technique to solve the ill-posed power flow problem	300, 3012, 3375, 13659 and 70000
Baluev *et al.* (2024)	Studied the safety and stability of power flow evaluating the operating states proximity to the loadability limits	14, 30, 64, 118, and 300
Lima-Silva & Freitas (2024b)	Present a dynamic homotopy technique to calculate a preliminary result for a power flow employing integration techniques	18482, 27318, 36964, 54636 and 109272

3.3 OVERVIEW

This chapter presented a literature review related to the topics homotopy and PF. We have verified various recent works that address the topic in different contexts. In these works, the concept of homotopy is utilized to divide the solution path into parts and reach the real solution of the original problem. In general, the latest works can be grouped by common themes, such as approaches to solving nonlinear PF equations, studies related to voltage stability of an electrical network, studies to determine the OPF according to network constraints, and a three-phase PFP approach.

The next chapter presents a different approach to treating the homotopy problem applied to the PFP. Both, static and dynamic structure approaches, are investigated as a new alternative to solve the PFP in large-scale ill-conditioned power system models.

CHAPTER 4

PROPOSED METHODS

4.1 INTRODUCTION

This chapter presents the proposed dynamic homotopy formulation for solving the large-scale ill-conditioned PFP.

The idea is to start from an initial flat start estimate to obtain an easily solvable state necessary to implement the homotopy concepts. The dynamical homotopy has advantages over other available methods because in just a few steps, during the dynamic homotopy, it can arrive at an initial estimate suitable for initializing traditional methods, such as NR.

Both the static and dynamic homotopy-based techniques are addressed.

The static homotopy approach presented in Chapter 2 is modified in the current chapter, and an alternative model for the problem is introduced. Besides, two dynamic homotopy approaches with different characteristics are proposed. In both cases, the objective is to calculate a solution with low precision for the PFP and use it as an initial estimate for use by a traditional iterative method. The first dynamic homotopy method is based on a combination of a Fixed Point Vector (FPV) solution and the mismatched equations of the original PFP. The second approach has an additional part concerning the static homotopy-based method because it introduces a new fictitious part composed of a compensation network that is removed along the homotopy process.

4.2 DYNAMICAL HOMOTOPY

The PFP formulation in this section is organized as a nonlinear system of Ordinary Differential Equations (ODE) and explores the homotopy principle. The idea is to use the analogy with the power system transient studies. The initial estimate, $\mathbf{x}^{(0)}$, for the iterative PFP numerical

computation behaves precisely like a disturbance at the beginning of a transient, in which it is calculated from zero up to a unitary parameter value.

To model the problem according to Equation (2.185), we assume a single homotopy parameter, *i.e.*, $n_h = 1$.

Suppose a 1-parameter homotopy problem, where Equation (2.185) is related according to an embedding parameter $h = t$, in analogy to the time t for a physical system. Considering this analogy, the homotopy parameter t will be designated as "time" from this point. Then, performing the computation of the differential of the multivariate function $\mathbf{G}(\mathbf{x},t)$ in Equation (2.185), the state vector $\mathbf{x}$ is dependent on the parameter t and the following expression is obtained

$$d\mathbf{G}(\mathbf{x},t) = \frac{\partial \mathbf{G}}{\partial \mathbf{x}} d\mathbf{x}(t) + \frac{\partial \mathbf{G}}{\partial t} dt = 0, \tag{4.1}$$

generating the nonlinear system of ODEs

$$\frac{d\mathbf{G}(\mathbf{x},t)}{dt} = \frac{\partial \mathbf{G}}{\partial \mathbf{x}} \frac{d\mathbf{x}(t)}{dt} + \frac{\partial \mathbf{G}}{\partial t} = 0, \tag{4.2}$$

for the initial state $\mathbf{x}(0) = \mathbf{x}^{(0)}$.

Therefore, the initial estimate $\mathbf{x}^{(0)}$ for the PFP is viewed as the initial boundary condition (disturbance) at the beginning of the transient. On the other hand, as it is not the solution of the algebraic equations $\mathbf{f}(\mathbf{x}) = \mathbf{0}$, $\mathbf{x}^{(0)}$ can be interpreted as a "perturbation" for the transient problem. Then, the PFP consists in solving the ODE, giving

$$\mathbf{G}_x \frac{d\mathbf{x}(t)}{dt} = -\mathbf{G}_t, \;\; \mathbf{x}(0) = \mathbf{x}^{(0)}, \tag{4.3}$$

where $\mathbf{G}_x$ stands for $\mathbf{G}_x(\mathbf{x},t) = \dfrac{\partial \mathbf{G}(\mathbf{x},t)}{\partial \mathbf{x}}$ and $\mathbf{G}_t$, for $\mathbf{G}_t(\mathbf{x},t) = \dfrac{\partial \mathbf{G}(\mathbf{x},t)}{\partial t}$.

In Equation (4.3), $\mathbf{G}_x$ is assumed to be nonsingular for all t, and the objective is to determine a path curve $\gamma(t)$, $0 \leq t \leq 1$, associated with the states at each t. Therefore, the PFP solution $\mathbf{x}_*$ consists in determining the result at the final point of the curve, $\gamma(1)$. In the case of some t, the Jacobian $\mathbf{G}_x$ may be singular (the situation for a saddle point), and the resolution of the problem fails. The path does not reach the final state at $t = 1$ in this situation. Therefore, divergence is verified analogously with an unstable system. However, this weakness does not imply that the "difficult" problem has no solution.

Therefore, the homotopy problem can be transformed into a "dynamical" problem (MILANO, 2010), also analogous to Newton's continuous problem as proposed in Milano (2009),

Milano (2010) and Milano (2019) to solve nonlinear equations. The problem can be extended for a multi-parameter homotopy problem according to the number of parameters defined in $\mathbf{h}$. A nonlinear Partial Differential Equation (PDE) system should be solved in this case. However, only ODEs will be the focus of this thesis.

The ODE (4.3) can be solved by a numerical integration method. The most traditional is the Forward Euler's method (FE) for an initial condition $\mathbf{x}(0)$ for computing the states at regular step-size, Δt, until a final discrete time, t_f. For the homotopy path, $t_f = 1$. The FE solver applied to Equation (4.3) gives the states in the discrete-time $t_{k+1} = (k+1)\Delta t$

$$\begin{aligned} \mathbf{x}(k+1) &= \mathbf{x}(k) - \Delta t[G_x]^{-1}\mathbf{G}_t, \quad k = 0,1,\ldots \\ \mathbf{x}(k+1) &= \mathbf{x}(k) - \Delta t[\mathbf{G}_x(\mathbf{x}(k),t_k)]^{-1}\mathbf{G}_t(\mathbf{x}(k),t_k), \quad k = 0,1,\ldots \end{aligned} \tag{4.4}$$

An implicit form represented by the BE is given by

$$\begin{aligned} \mathbf{x}(k+1) &= \mathbf{x}(k) - \Delta t[\mathbf{G}_x]^{-1}\mathbf{G}_t, \quad k = 0,1,\ldots \\ \mathbf{x}(k+1) &= \mathbf{x}(k) - \Delta t[\mathbf{G}_x(\mathbf{x}(k+1),t_{k+1})]^{-1}\mathbf{G}_t(\mathbf{x}(k+1),t_{k+1}), \quad k = 0,1,\ldots \end{aligned} \tag{4.5}$$

Another explicit integration method, but requiring additional computations for the same iterate, is the Runge-Kutta 2^{nd} order' method (Euler modified), given by

$$\mathbf{x}(k+1) = \mathbf{x}(k) + \frac{\Delta t}{2}[\mathbf{K}_1 + \mathbf{K}_2], \;\; k = 0,1,\ldots \tag{4.6}$$

where

$$\begin{aligned} \mathbf{K}_1 &= -[\mathbf{G}_x(\mathbf{x}(k),t_k)]^{-1}\mathbf{G}_t(\mathbf{x}(k),t_k), \\ \mathbf{K}_2 &= -[\mathbf{G}_x(\mathbf{x}(k) + \Delta t\mathbf{K}_1,t_k)]^{-1}\,\mathbf{G}_t(\mathbf{x}(k) + \Delta t\mathbf{K}_1,t_k). \end{aligned} \tag{4.7}$$

Unlike the static problem discussed in static homotopy, the dynamical homotopy problem as presented in Equation (4.2) and solved via explicit schemes such as the Euler or other method, does not require solving a nonlinear equation system in the $(k+1)^{th}$ path point, because the implementation of the technique is part of a recurrence scheme. Even using implicit methods, such as BE, it will be demonstrated through experiments that solving nonlinear equations is unnecessary to obtain an adequate solution for the implicit scheme. In the case of Equation (4.4), it needs a primary computational burden to perform the operation $[\mathbf{G}_x]^{-1}\mathbf{G}_t$. Therefore, it involves only one computation of a Jacobian matrix and its associated LU factorization, besides mismatches. On the other hand, for the static problem, a certain number of iterates is needed to solve the NR method. The RK2 in Equation (4.6) needs the computation of $\mathbf{K}_1$ and $\mathbf{K}_2$, requiring two LU factorizations.

4.2.1 Homotopy "easy" function definition

Considering a 1-parameter homotopy map (2.185), the equation $\mathbf{G}(\mathbf{x},t)$ can be represented as the static homotopy path expression (4.8), starting from the "easy" solution, $t = 0$, and evolving to the target function in $t = 1$.

$$\mathbf{G}(\mathbf{x},t) = t\mathbf{f}(\mathbf{x}) + (1-t)\mathbf{g}_0(\mathbf{x}) = \mathbf{0}. \tag{4.8}$$

In Equation (4.8), $\mathbf{g}_0(\mathbf{x})$ is a function chosen in order to provide an easy solution for $t = 0$ in Equation (4.8). A difficult task is to establish the function $\mathbf{g}_0(\mathbf{x})$. In the sequence, we propose schemes based on the initial estimate, similar to the disturbance state on starting a transient.

4.2.2 Fixed point vector homotopy function

The goal is to obtain the mismatch vector $\mathbf{f}(\mathbf{x})$ at the final $t = 1$ such that $||\mathbf{f}(\mathbf{x})|| < \epsilon$, with sufficiently small ϵ.

An alternative to the easy function $\mathbf{g}_0(\mathbf{x})$, it is to use the Fixed Point Vector (FPV) homotopy function (LIU; KUO, 2011), *i.e.*, $\mathbf{g}_0(\mathbf{x}) = K(\mathbf{x} - \mathbf{x}^{(0)})$, in which K is a user defined constant.

For this situation, considering the practical PFP, at the beginning of the homotopy path, at $t = 0$, the initial estimate will be defined as a *flat start* estimate, *i.e.*, phase angle zero for all nodal buses, and unitary magnitude in the PQ buses (Voltage magnitudes of controlled buses are kept constant and are not modified by the homotopy scheme). So, for the states θ and $\mathbf{V}$,

$$\mathbf{G}(\mathbf{x},0) = \mathbf{g}_0(\mathbf{x}) = K\begin{bmatrix}\theta \\ \mathbf{V} - \mathbf{V}_0\end{bmatrix} = \mathbf{0}, \tag{4.9}$$

$\mathbf{V}_0$ is a vector with all entries 1 and K is a parameter established according to the system model.

From Equation (4.9), we conclude that for $t = 0$, $\mathbf{x}(0) = \mathbf{x}^{(0)}$, *i.e.*, $\theta = 0$ and $\mathbf{V} = \mathbf{V}_0$.

According to Equation (4.8) and Equation (4.9), we have the general equations

$$\frac{\partial \mathbf{G}}{\partial \mathbf{x}} = t\frac{\partial \mathbf{f}}{\partial \mathbf{x}} + (1-t)\frac{\partial \mathbf{g}_0}{\partial \mathbf{x}}, \text{ where } \begin{cases} \left.\dfrac{\partial \mathbf{f}}{\partial \mathbf{x}}\right|_{\mathbf{x}(t)} = \mathbf{J}(\mathbf{x}(t)), \\ \dfrac{\partial \mathbf{g}_0}{\partial \mathbf{x}} = K\mathbf{I}, \end{cases} \tag{4.10}$$

and

$$\mathbf{G}_x = \left.\frac{\partial \mathbf{G}}{\partial \mathbf{x}}\right|_{\mathbf{x}(t)} = t\mathbf{J}(\mathbf{x}(t)) + (1-t)K\mathbf{I}, \;\; t = k\Delta t, \quad \text{k=0,1,2,...}$$
$$\mathbf{G}_t = \left.\frac{\partial \mathbf{G}}{\partial t}\right|_{\mathbf{x}(t)} = \mathbf{f}(\mathbf{x}(t)) - \mathbf{g}_0(\mathbf{x}(t)), \tag{4.11}$$

in which $\mathbf{J}(\mathbf{x}(t))$ is the Jacobian matrix of the PFP; $\mathbf{I}$ is the identity matrix; and for a constant step-size, Δt, the discrete-time evolves as $t = 0, \Delta t, 2\Delta t, \ldots, 1$, with $\Delta t \leq 1$. Assume that the notation $\mathbf{x}(k)$ corresponds to the discrete state vector computed for the parameter $t = k\Delta t$.

According to Equation (4.11), $\mathbf{G}_x$ depends on the original PFP Jacobian matrix $\mathbf{J}(\mathbf{x}(t))$ and the constant K. The parameter t acts in the direction to recover the original Jacobian matrix when t changes from zero to 1. The vector $\mathbf{G}_t$ depends only on the mismatch function $\mathbf{f}(\mathbf{x}(t))$ and the function of deviations from the flat start initialization, $\mathbf{g}_0(\mathbf{x}(t))$. We can conclude that the matrices $\mathbf{G}_x$ and $\mathbf{G}_t$ are similar to those necessary to implement the algorithm to solve the traditional PFP. Once they are computed according to Equation (4.11), the ODE in Equation (4.2) can be solved by a numerical integration scheme such as Equation (4.4), Equation (4.5) or Equation (4.6).

In practice, for the PFP application, the constant K should be chosen as a small positive value in order to avoid high diagonal values in the original system Jacobian matrix with the increment of t.

A small step Δt_0 in general is sufficient to start adequately the simulations and reach successful convergence at $t = 1$. However, for $t > \Delta t_0$, a larger step $\Delta t \gg \Delta t_0$ is mandatory. This procedure avoids the computations of many intermediary points with step Δt_0 up to the final result in $t = 1$. Furthermore, it increases the computational cost of obtaining the total number of points until this final point is reached.

The proposed dynamical scheme is suitable to solve ill-posed nonlinear systems since the *introduction of the function* $\mathbf{g}_0(\mathbf{x})$ *works as a term to attenuate the ill-conditioning of the Jacobian matrix* of the original PFP.

Depending on the adopted integration method to solve Equation (4.2) and the time-step Δt, the result accuracy in $t = 1$ is low. Then, we propose to *use the result computed by numerical integration in* $t = 1$ *and refine it by applying the NR scheme.* The hybrid process following this strategy is expected to improve the original PFP solution when the result determined by the

homotopy transient-based approach has been computed successfully.

The technique is symbolically summarized through the Algorithm 1. On implementing the Algorithm 1, step 6 requires a reduced number of iterations since the result provided by the dynamical homotopy at $t = 1$ gives an initial estimate that provides fast convergence for the NR solver. Then, the proposed technique efficiently solves ill-conditioned large-scale PFP.

Algorithm 1 Homotopy transient-based approach and improvement by the NR solver

Require: Flat start estimate $\mathbf{x}^{(0)}$; Δt_0; $\Delta t > \Delta t_0$; K; tolerance $\epsilon = 10^{-8}$ pu; and grid data.
Ensure: Solution of the PFP, $\mathbf{x}_*$, *i.e.*, states of the system $\mathbf{x}_* = \left[\boldsymbol{\theta}^T \;\; \boldsymbol{V}^T\right]^T$.

1: Define an integration method for computing the initial step in t_1 and do $k = 0$; define the number of points whose states need to be calculated, $N \geq 2$, according to the assigned Δt.
2: Introduce $\mathbf{x}(0) = \mathbf{x}^{(0)}$ (similar to a disturbance in $t = 0$) and compute $\mathbf{x}(1)$ with time-step Δt_0 for the point t_1 using an explicit or implicit scheme.
3: **for** $k = 1,2,\ldots,N$ **do**
4: Compute $\mathbf{x}(k+1)$ with (constant or not) time-step Δt_k for the point t_{k+1} using one of schemes (4.4), (4.5) or (4.6), given $\mathbf{x}(k)$ has been successfully calculated; remember that for the last point to compute $\mathbf{x}(N)$, the time-step should be adjusted to $(\Delta t_k - \Delta t_0)$, in reason that in the last point, t was fixed in 1.
5: **end for**
6: Use the state vector $\mathbf{x}(N)$ computed in step 4 as a guess to solve the PFP by utilizing the classical NR solver and determine $\mathbf{x}_*$ with high accuracy ϵ.

4.3 PERFORMANCE OF THE SOLVERS IN THE FIRST TIME-STEP

Based on the proposed dynamic homotopy methodology, its performance will be investigated in the next steps, mainly on the importance of the first stage where the low accuracy initial states are calculated.

Assume that the homotopy pathway starts at $t = 0$ with the initial state $\mathbf{x}(\mathbf{0}) = \mathbf{x}^{(0)}$, defined by the ODE's initial condition, it then evolves through time instants t_k, spaced by a time-step Δt_k, where $k = 0,1,2,\ldots,N$ and N is the number of time-steps, until $t_k = 1$. The procedure allows for variable time steps Δt_k along the pathway, which can result in reduced accuracy for large time steps. However, at each time step, at least one LU factorization needs to be performed, because it is necessary to perform a computation of the type $\Phi(\mathbf{x}^{(k)},t_k) = -[\mathbf{G}_x(\mathbf{x}^{(k)},t_k)]^{-1}\mathbf{G}_t(\mathbf{x}^{(k)},t_k)$, which increases the computational cost. Therefore, various aspects need to be analyzed in order to determine an appropriate method for computing

the solution of the nonlinear equation systems $\mathbf{f}(\mathbf{x}) = 0$ at the end of the homotopy pathway.

Given a time-step Δt_0, the homotopy pathway can diverge from the exact path point for the first time-step, at $t_1 = \Delta t_0$, depending on the choice of the $\mathbf{g}_0(\mathbf{x})$ and Δt_0. The analysis below concerns the choice based on the fixed point function, FPV, as defined previously, *i.e.*, $\mathbf{g}_0(\mathbf{x}) = K(\mathbf{x}-\mathbf{x}^{(0)})$. The first point, $t_1 = \Delta t_0$, on the pathway will be calculated to demonstrate that even though Δt_0 is very small, using an explicit integration solver at this time may not be appropriate, especially for ill-conditioned systems.

Let the FE solver be used to compute the states in the step $t_1 = \Delta t_0 \ll 1$. Then, for $\mathbf{x}(0) = \mathbf{x}^{(0)}$ and $t = 0$, $\mathbf{G}_x(\mathbf{x}(0),0) = K\mathbf{I}$ and $\mathbf{G}_t(\mathbf{x}(0),0) = \mathbf{f}(\mathbf{x}^{(0)})$. It implies from Equation (4.4) that the increment $\mathbf{x}(t_1) - \mathbf{x}^{(0)} = -\Delta t_0[K\mathbf{I}]^{-1}\mathbf{f}(\mathbf{x}^{(0)}) = -\frac{\Delta t_0}{K}\mathbf{f}(\mathbf{x}^{(0)})$, *i.e.*, the deviation $\Delta\mathbf{x}(0) = \mathbf{x}(t_1) - \mathbf{x}^{(0)}$ is proportional to the mismatch $\mathbf{f}(\mathbf{x}^{(0)})$. However, in the case of ill-conditioned systems, $||\mathbf{f}(\mathbf{x}^{(0)})|| \gg 1$ and the ratio $\Delta t_0/K$ needs to be set at a very small value. On the other hand, this strategy leads to small deviations $\Delta\mathbf{x}(0)$, causing slow convergence, with stagnation or leading to early divergence of the homotopy problem. The error increases when using an explicit integration method that requires the calculation of intermediary points, such as RK2. This is because computations involving the mismatch $\mathbf{f}(\mathbf{x}(0))$ are even more involved. Additionally, the error increases because it depends on the partial results of the type $\mathbf{x}(0) + K_1\mathbf{f}(\mathbf{x}(0))$, as in the case of RK2. Therefore, it is necessary to establish a proper method to calculate t_1 with a very small time-step.

Now, let the BE scheme be used to compute the states in the instant $t_1 = \Delta t_0 \ll 1$. From Equation (4.5), the increment is $\mathbf{x}(t_1) - \mathbf{x}_0 = -\Delta t_0[\Delta t_0\mathbf{J}(\mathbf{x}(t_1)) + (1 - \Delta t_0)K\mathbf{I}]^{-1}\mathbf{f}(\mathbf{x}(t_1))$ and the unknown is $\mathbf{x}(t_1)$, which arises in the two sides of the equation. Considering the time-step $\Delta t_0 \ll 1$, a fixed-point iteration technique can be applied to the expression to obtain $\mathbf{x}(t_1)$. Assume that, in its i^{th} iterate, the unknown is the variable $\mathbf{x}^{(i)}(t_1)$. In this work, to minimize computations involving the inverse of $\mathbf{G}_x$, it was suggested to calculate just one iteration i and assigning $\mathbf{x}^{(0)}(t_1) = \mathbf{x}^{(0)}$ to compute $\mathbf{x}^{(1)}(t_1)$, the final result of interest, for a simplified result. Then, the updated result yields

$$\begin{aligned}\Delta\mathbf{x}(0) = -[\mathbf{J}(\mathbf{x}^{(0)}) + \frac{(1-\Delta t_0)}{\Delta t_0}K\mathbf{I}]^{-1}\mathbf{f}(\mathbf{x}^{(0)}) \approx -[\mathbf{J}(\mathbf{x}^{(0)}) + \frac{K}{\Delta t_0}\mathbf{I}]^{-1}\mathbf{f}(\mathbf{x}^{(0)}) = \\ = -[\mathbf{J}(\mathbf{x}^{(0)}) + \delta\mathbf{I}]^{-1}\mathbf{f}(\mathbf{x}^{(0)}),\end{aligned} \tag{4.12}$$

in which $\delta = K/\Delta t_0$.

Interestingly, in Equation (4.12), the original PFP ill-conditioned Jacobian $\mathbf{J}(\mathbf{x}^{(0)})$ of the initial iteration was modified by the introduction of the small-perturbation factor δ for this step t_1. According to Freitas & Oliveira (2023a), the small perturbation factor allows an adequate conditioning procedure to solve the original ill-posed PFP. Also, in the function of the assignment of δ and Δt_0, the factor K is determined as $K = \delta\Delta t_0$. Therefore, it is not necessarily equal to unity.

Another form to achieve a good result when the time step t_1 is very small, given $\mathbf{x}^{(0)}$, is by solving Equation (4.8) for a specific t_1. In this scenario, only the states are considered as variables. Then, an approximation for the states at t_1 can be obtained by solving the algebraic equation $\mathbf{G}(\mathbf{x}) = \Delta t_0\mathbf{f}(\mathbf{x}) + (1 - \Delta t_0)K(\mathbf{x} - \mathbf{x}^{(0)}) = 0$, assuming a linear approximation for $t_1 \ll 1$. According to (GARCIA; ZANGWILL, 1981), a linear approximation of $\mathbf{G}(\mathbf{x})$ around $\mathbf{x}^{(0)}$ gives

$$\mathbf{G}(\mathbf{x} + \Delta\mathbf{x}) \approx \mathbf{G}(\mathbf{x}^{(0)}) + \mathbf{G}_x(\mathbf{x}^{(0)})\Delta\mathbf{x} = 0. \tag{4.13}$$

Considering that $t_1 = \Delta t_0$ for computing (4.13), then $\mathbf{G}(\mathbf{x}^{(0)}) \neq \mathbf{0}$, $\mathbf{G}_x(\mathbf{x}^{(0)}) = \Delta t_0\mathbf{J}(\mathbf{x}^{(0)}) + (1 - \Delta t_0)KI$, and $\mathbf{G}(\mathbf{x}^{(0)}) = \Delta t_0\mathbf{f}(\mathbf{x}^{(0)}) + (1 - \Delta t_0)K(\mathbf{x}^{(0)} - \mathbf{x}^{(0)}) = \Delta t_0\mathbf{f}(\mathbf{x}^{(0)})$. Then, the linear approximation in (4.13) gives the deviation

$$\Delta\mathbf{x} = \mathbf{x} - \mathbf{x}^{(0)} = -[\mathbf{G}_x(\mathbf{x}^{(0)})]^{-1}\mathbf{G}(\mathbf{x}^{(0)}) = [\Delta t_0\mathbf{J}(\mathbf{x}^{(0)}) + (1 - \Delta t_0)KI]^{-1}\Delta t_0\mathbf{f}(\mathbf{x}^{(0)}). \tag{4.14}$$

Note that, after some algebraic handling, the result in (4.14) is identical to that in (4.12), and the result obtained by the linear approximation and through the BE solver agrees. Hence, using these two forms for approximating the states at the time $t_1 = \Delta t_0$ provides results close to the homotopy pathway. These approximations can be used as initial conditions at t_1 for numerical integration methods for the homotopy pathway. Particularly, explicit techniques are unable to yield satisfactory results without this initialization.

For $t_1 < t_k \leq 1$, the remaining points should preferably be calculated with integration steps Δt much larger than the initial one Δt_0. This requirement is reinforced by the need to minimize the number of computations of $\Phi(\mathbf{x}(t_k),t_k)$ at each step t_k. However, explicit methods may be more sensitive to the high integration step. On the other hand, an implicit method requires iterations to obtain the result in the integration step itself and admits a large time-step. In one way or another, the goal is to minimize performing LU factorizations until the final result

at $t = 1$ is reached, as these factorizations require the highest computational costs. In explicit methods of the FE and RK2 types, at least 1 LU factorization is performed to obtain the result in one step. In the implicit BE method, only 1 LU iteration is proposed to be used in this work to obtain the result. However, this approach yields an approximate result for the step due to the need for more iterations to achieve high precision. It is suggested that the results of the homotopy problem at step $t = 1$ in this work may be inaccurate regarding the error requirements needed for the PFP, based on the characteristics of the methods. The result obtained from the integration process is only considered to be a rough estimate of the exact solution to the load flow problem. Hence, a conventional method such as NR or its NR fast decoupled (FDXB) (see Kundur (1994) and Zimmerman *et al.* (2011) for details of the decoupled method), is a good approach to improve the solution obtained from dynamic homotopy.

Therefore, a compromise must be sought between the expected result at the end of the dynamic homotopy simulation horizon and the expected accuracy of the PFP solution. Considering that it is not reasonable to use an exaggerated number of time-steps in the simulation because the dynamic homotopy process would be very computationally expensive, an alternative would provide an approximation of the result in time $t = 1$. However, at this point, an approximate solution for the states may be unaccepted and would need to be refined. In simpler terms, in this scenario, the homotopy method changes the initial estimate $\mathbf{x}^{(0)}$ to a new state $\hat{\mathbf{x}}^{(0)} = \mathbf{x}(t)|_{t=1}$. The transformed state is expected to be within an attraction region and should give a good starting point for convergence, even for a numerical method like the classical NR and FDXB methods.

The idea is to use the dynamic homotopy method to determine an approximate solution for the PFP, starting from a flat start estimate, equivalent to an improvement in the region of attraction in the original problem. From this result, the PFP solution can be calculated with high precision. Furthermore, this new starting point, $\mathbf{x}(t)|_{t=1}$, can be used by other iterative techniques different from the traditional NR.

4.4 FICTITIOUS NETWORK COMPENSATION TO IMPROVE THE DYNAMIC HOMOTOPY PATH

Due to the characteristics of certain networks, such as overloaded systems, isolated subsystems, and large networks, the initialization of the homotopy process can have a divergence problem. Another alternative homotopy function was investigated to circumvent this weakness, and another method to implement the dynamical homotopy was proposed.

In this case, the proposal is to *combine in the homotopy function also the insertion of fictitious elements*, proposed by Freitas & Silva (2022), to avoid power flow between the buses at the beginning of the homotopy process when $h = 0$. The static process is based on inserting a compensation network connecting constant impedances to the buses.

To illustrate the procedure of compensation network insertion, let a bus k be interconnected with their respective adjacent buses i and j. A shunt load or generation connected to bus k is assumed, forming a power injection given by the active power specified P^{sp} and reactive power specified Q^{sp}, where the specified apparent power is given by $\overline{S}_k^{sp} = P_k^{sp} + jQ_k^{sp}$. Figure 4.1 illustrates a one-line diagram for this representation.

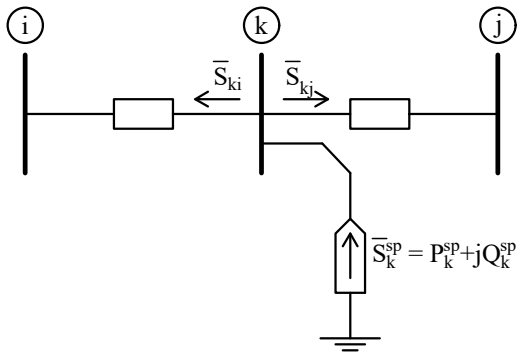

Figure 4.1: Original network without fictitious power injection inserted at bus k

Assuming that the initial estimate is the flat start type, $\theta_m = 0 \quad \forall m$, and $V_m = 1\ pu$ in PQ buses and $V_m = V_m^{sp}$ in PV or Vθ buses.

When starting the homotopy process, at $h = 0$, the objective is to start with a constant impedance load, which is adjusted to avoid power flow between interconnections. Consequently, the method depends on converting the load to an impedance $\overline{Z}^{cte}$ at each bus k. The impedance is set to avoid power $\overline{S}_{km}$ between two bus k and m so that the voltage at bus k, for $h = 0$, is

precisely equal to the estimate $V_k^{(0)}$ for the PFP. Figure 4.2 illustrates the scheme when $h = 0$, given that there is a compensation impedance $\overline{Z}_{ck}^{cte}$.

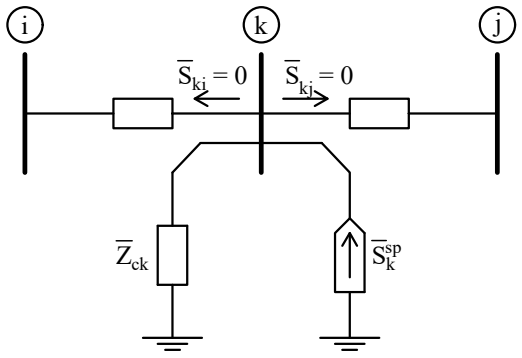

Figure 4.2: Network with a fictitious impedance inserted at bus k to enforce the power flow between interconnections $i-k$ and $k-j$ equal to zero and supply the load $\overline{S}_k^{sp} = P_k^{sp} + jQ_k^{sp}$ when $h = 0$

Considering the equilibrium balance equations at bus k and the flat start initialization and the compensation load, then, at $h = 0$, it becomes

$$\Delta P_k = \left[\left(V_k^2 \mathbf{G}_{kk} + V_k \sum_{\substack{m=1 \\ m \neq k}}^{N_b} V_m \mathbf{G}_{km} \right) - P_k^{sp} \right] + V_k^2 g_k, \tag{4.15}$$

$$\Delta Q_k = \left[\left(-V_k^2 \mathbf{B}_{kk} - V_k \sum_{\substack{m=1 \\ m \neq k}}^{N_b} V_m \mathbf{B}_{km} \right) - Q_k^{sp} \right] + V_k^2 b_k, \tag{4.16}$$

in which $\overline{y}_k = \dfrac{1}{\overline{Z}_k} = g_k + jb_k$ is the fictitious shunt admittance connected to the bus k and which needs to be removed along the evolution of the homotopy parameter h. Therefore, g_k and b_k are adjusted to generate zero mismatches at $h = 0$, and this objective can be achieved through the following setting

$$g_k = \left(-\mathbf{G}_{kk} - \frac{1}{V_k} \sum_{\substack{m=1 \\ m \neq k}}^{N_b} V_m \mathbf{G}_{km} \right) + \frac{1}{V_k^2} P_k^{sp}, \tag{4.17}$$

$$b_k = \left(\mathbf{B}_{kk} + \frac{1}{V_k} \sum_{\substack{m=1 \\ m \neq k}}^{N_b} V_m \mathbf{B}_{km} \right) + \frac{1}{V_k^2} Q_k^{sp}. \tag{4.18}$$

Now, for $h > 0$, the power balance equations are modified as follows, depending on the homotopy parameter h. For a specific bus k, according to the type of bus (PQ or PV), the

mismatches are dependent on h and calculated as

$$\mathbf{G}_k(\mathbf{x},h) = \begin{bmatrix} \Delta P_k \\ \\ \Delta Q_k \end{bmatrix} = \begin{bmatrix} \left[\left(V_k \sum_{m=1}^{N_b} V_m (\mathbf{G}_{km} cos(\theta_{km}) + \mathbf{B}_{km} sin(\theta_{km}) \right) - P_k^{sp} \right] + (1-h) V_k^2 g_k \\ \\ \left[\left(V_k \sum_{m=1}^{N_b} V_m (\mathbf{G}_{km} sin(\theta_{km}) - \mathbf{B}_{km} cos(\theta_{km}) \right) - Q_k^{sp} \right] + (1-h) V_k^2 b_k \end{bmatrix}, \tag{4.19}$$

with $0 \leq h \leq 1$.

Solving successive PFPs in (4.19) varying h from zero up to the unitary value and using the initializations of the previously calculated states for h, the solution of the PFP is obtained.

Note that at each point $h > 0$, it is necessary to use the associated Jacobian matrix $\mathbf{J}(\mathbf{x}) = \dfrac{\partial \mathbf{f}(\mathbf{x})}{\partial \mathbf{x}}$ calculated by using (4.20) of the original PFP. It is calculated without network compensation and separated into four submatrices to better explain its influence on a general homotopy Jacobian, $\mathbf{J}_h$, which is determined from $\mathbf{G}(\mathbf{x},h)$ instead of only $\mathbf{f}(\mathbf{x})$.

$$\mathbf{J}(\mathbf{x}) = \begin{bmatrix} \mathbf{J}_{11} & \mathbf{J}_{12} \\ \\ \mathbf{J}_{21} & \mathbf{J}_{22} \end{bmatrix}. \tag{4.20}$$

Thus, using $\mathbf{G}(\mathbf{x},h)$ from Equation (4.19), the submatrices associated to the Jacobian matrix $\mathbf{J}_h$ modified by h are calculated as follows

PQ and PV buses
$$\begin{cases} \mathbf{J}_{h_{11}} = \dfrac{\partial \Delta P_k(\mathbf{x},h)}{\partial \theta_k} = \mathbf{J}_{11}, & \text{(not affected by } h) \\ \\ \mathbf{J}_{h_{12}} = \dfrac{\partial \Delta P_k(\mathbf{x},h)}{\partial V_k} = \mathbf{J}_{12} + (1-h)(2V_k g_k), & \text{(only the diagonal element of original } \mathbf{J}_{12} \text{ is affected)} \end{cases}$$

Only PQ buses
$$\begin{cases} \mathbf{J}_{h_{21}} = \dfrac{\partial \Delta Q_k(\mathbf{x},h)}{\partial \theta_k} = \mathbf{J}_{21}, & \text{(not affected by } h) \\ \\ \mathbf{J}_{h_{22}} = \dfrac{\partial \Delta Q_k(\mathbf{x},h)}{\partial V_k} = \mathbf{J}_{22} + (1-h)(2V_k b_k). & \text{(only the diagonal element of original } \mathbf{J}_{22} \text{ is affected)} \end{cases}$$

Thus, by computing the Jocobian $\mathbf{J}_h$ according to the parameter h and the mismatches in Equation (4.19), the increments are determined as

$$\Delta \mathbf{x} = -\mathbf{J}_h^{-1} \mathbf{G}(\mathbf{x},h). \tag{4.21}$$

Therefore, using an iterative method such as NR (or others alike), the updated values of the states $\mathbf{x}$ can be calculated for a given h, but following an idea of static approach, since the points in the homotopy pathway are precisely determined unless there is tolerance.

The procedure described previously is related to the static homotopy problem in which a fictitious power flow problem is solved at each point of the homotopy path. However, only the latter point is of practical interest because it is the solution that was sought for the original PFP. Then, in the next steps, the objective is to modify the static homotopy problem discussed and embed it into an efficient dynamic homotopy scheme to determine an approximate solution for the homotopy path and improve it using a conventional iterative technique.

Following the notation adopted for the homotopy parameter when the dynamical homotopy is studied, the parameter h will be replaced again by t. This way, considering the dynamic homotopy approach, the following differential equations are involved:

$$\begin{aligned} d\mathbf{G} &= \frac{\partial \mathbf{G}}{\partial \mathbf{x}} d\mathbf{x} + \frac{\partial \mathbf{G}}{\partial t} dt, \\ \frac{d\mathbf{G}}{dt} &= \frac{\partial \mathbf{G}}{\partial \mathbf{x}} \cdot \frac{d\mathbf{x}}{dt} + \frac{\partial \mathbf{G}}{\partial t} = 0, \\ \mathbf{G}_{\mathbf{x}} \frac{d\mathbf{x}}{dt} &= -\mathbf{G}_t. \end{aligned} \tag{4.22}$$

in which $\mathbf{G}_{\mathbf{x}}$ is exactly the same matrix used in the static approach. However, the term $\dfrac{d\mathbf{G}}{dt}$ is calculated as

$$\frac{\partial \mathbf{G}}{\partial t} = \begin{bmatrix} \dfrac{\partial(\Delta P_k(\mathbf{x},t))}{\partial t} \\ \\ \dfrac{\partial(\Delta Q_k(\mathbf{x},t))}{\partial t} \end{bmatrix} = - \begin{bmatrix} V_k^2 g_k \\ \\ V_k^2 b_k \end{bmatrix}. \tag{4.23}$$

Therefore, since the terms $\mathbf{G}_{\mathbf{x}}$ and $\mathbf{G}_t$ are known, the ODE in (4.22) can be promptly solved. However, the dependence in (4.23) is verified only for the voltage magnitudes. Then, a modification in the homotopy function is proposed in the next subsection to consider also the voltage angles in $\mathbf{G}_t$.

4.4.1 Modifying the dynamical homotopy equation

In some cases, a more robust initialization is needed to address the ill-conditioning that can arise when using the dynamic homotopy technique. One approach to dealing with this problem

is to modify the homotopy function in Equation (4.19), integrating its superior convergence properties into the dynamic homotopy problem. This modification is justified as the convergence for specific issues can be hindered when exploring the dynamic homotopy derived from (4.8). The change also includes the initial estimate and modifies the weighting of ΔP_k and ΔQ_k previously with t, for bus k. Then, a new homotopy function can be proposed as follows.

$$\mathbf{G}(\mathbf{x},t) = t[\mathbf{f}(\mathbf{x}) + (1-t)\mathbf{f}_1(\mathbf{x})] + (1-t)\mathbf{g}_0(\mathbf{x}), \tag{4.24}$$

where the traditional power balance equations for a bus k of type PQ are

$$\mathbf{f}_k(\mathbf{x}) = \begin{bmatrix} V_k^2\mathbf{G}_{kk} + V_k \sum_{m\neq k}^{N_b} V_m[\mathbf{G}_{km}\cos\theta_{km} + \mathbf{B}_{km}\sin\theta_{km}] - P_k^{sp} \\ \\ -V_k^2\mathbf{B}_{kk} + V_k \sum_{m\neq k}^{N_b} V_m[\mathbf{G}_{km}\sin\theta_{km} - \mathbf{B}_{km}\cos\theta_{km}] - Q_k^{sp} \end{bmatrix}, \tag{4.25}$$

and the compensation term adopted in the static homotopy for the bus k of type PQ is

$$\mathbf{f}_{1k}(\mathbf{x}) = \begin{bmatrix} V_k^2 g_k \\ \\ V_k^2 b_k \end{bmatrix}. \tag{4.26}$$

The initialization of the dynamic homotopy problem still uses the flat start estimation of the PFP. Then, with $\mathbf{x}^{(0)}$, *i.e.*, $\theta_k^{(0)} = 0$ for PQ and PV buses and $V_k^{(0)} = 1$ pu for PQ buses, the easy function continues to be defined as

$$\mathbf{g}_0(\mathbf{x}) = K \begin{bmatrix} \theta \\ \\ \mathbf{V} - 1 \end{bmatrix}. \tag{4.27}$$

For the conditions in (4.24), the matrix $\mathbf{G}_\mathbf{x}$ is modified to

$$\mathbf{G}_\mathbf{x} = t\left(\frac{\partial \mathbf{f}}{\partial \mathbf{x}} + (1-t)\frac{d\mathbf{f}_1}{d\mathbf{x}}\right) + (1-t)K\mathbf{I}, \tag{4.28}$$

with $\dfrac{\partial \mathbf{f}}{\partial \mathbf{x}} = \mathbf{J}(\mathbf{x})$, the Jacobian of the original PFP, while $\dfrac{\partial \mathbf{f}_1}{\partial \mathbf{x}}$ is calculated only for V_k in PQ buses. Hence, changes are verified only for the element $\dfrac{\partial(\Delta P_k)}{\partial V_k} = 2V_k g_k$ and $\dfrac{\partial(\Delta Q_k)}{\partial V_k} = 2V_k b_k$. It is worth noting that K must be set at a reduced value in Equation (4.28) because it affects the diagonal values of $\mathbf{G}_x$. So, from Equation (4.24) the function $\mathbf{G}_t$ is also determined, yielding

$$\begin{aligned} \mathbf{G}_t = \frac{\partial \mathbf{G}}{\partial t} &= \mathbf{f}(\mathbf{x}) + \mathbf{f}_1(\mathbf{x}) - 2t\mathbf{f}_1(\mathbf{x}) - \mathbf{g}_0(\mathbf{x}) = \\ &= \mathbf{f}(\mathbf{x}) + (1-2t)\mathbf{f}_1(\mathbf{x}) - \mathbf{g}_0(\mathbf{x}). \end{aligned} \tag{4.29}$$

Therefore, with the matrices $\mathbf{G}_\mathbf{x}$ and $\mathbf{G}_t$ calculated from (4.28) and (4.29), respectively, the ODE in (4.22) is solved by a numerical integration method.

4.5 OVERVIEW

In this chapter, the homotopy approaches were presented in both static and dynamic methods. Two dynamical homotopy-based schemes were proposed, and peculiar characteristics demonstrate the difference between the two techniques. The results of these strategies have low precision since the implementation prioritizes a low computational cost in this step. Then, the states obtained from the dynamic homotopy are refined and adopted as an initial estimate for finding a more accurate solution through a traditional scheme such as the NR method. Therefore, the proposal can be viewed as a two-step hybrid method. Other methods based on static homotopy were discussed.

A detailed description of all techniques was addressed. They were implemented computationally and adapted in a version of the MATPOWER software (ZIMMERMAN *et al.*, 2011), basically through modifications in one of its functions (scripts available in Zimmerman & Murillo-Sánchez (2016)) which integrate the tool package.

In the next sections, several test systems are detailed, and experiments are performed to demonstrate the techniques' performance qualities.

CHAPTER 5

TEST SYSTEMS

5.1 INTRODUCTION

This section details the various test systems used in the experiments described in the next chapter. Different types of systems based on their size and loading characteristics are highlighted. One example is a very large model system that consists of three islands. This system was originally studied in MATPOWER (ZIMMERMAN *et al.*, 2011), which was analyzed with three slack buses. In the next chapter, we aim to demonstrate, using the homotopy technique, that systems like this can be represented as a single synchronous equivalent network.

Most of the simulated test cases were extracted from MATPOWER (ZIMMERMAN; MURILLO-SÁNCHEZ, 2020), which contains a vast library of real and synthetic power systems.

The main idea was to explore some well-conditioned cases for initial tests, including overloaded test systems. However, the main interest is to study those of ill-conditioned type cases, *i.e.*, those ones where a solution for the PFP exists, but cannot be solved by a classical NR method starting from the initial flat start estimate. In particular, large-scale test systems are of great interest.

5.2 GROUP OF CASES

In summary, five groups of cases were chosen to be tested, as will be highlighted below.

i) Native ill-conditioned MATPOWER study cases

   (a) `case3012wp`;
   (b) `case3375wp`;
   (c) `case13659pegase`; and
   (d) `case_ACTIVSg70k`.

ii) Synthetic systems created by replication process

   (a) `case18482`;
   (b) `case27318`;
   (c) `case36964`;
   (d) `case54636`; and
   (e) `case109272`.

iii) Well-conditioned power systems

   (a) `case300`.

iv) Overloaded and well-conditioned power systems

   (a) `case69limit`;
   (b) `case141limit`;
   (c) `case_ACTIVSg500limit`; and
   (d) `case_ACTIVSg2000limit`.

v) Multiple slacks ill-conditioned power system

   (a) `case82k`.

5.2.1 Native ill-conditioned MATPOWER study cases

These cases are native from MATPOWER, available in the program's database (ZIMMERMAN; MURILLO-SÁNCHEZ, 2020). Tests were performed to identify the ill-conditioned situation of each test system, verifying if the solution of the PFP is obtained through an NR scheme based on a flat start guess. Table 5.1 summarizes the main physical characteristics of the systems highlighting figures of number of buses, generators, loads, shunts, branches, and transformers. The latter column shows the slack-bus power generation (S_{Slack}) just to check the convergence to the correct result. The results are calculated based on the initial estimate provided in the MATPOWER databank. This estimate is closer to the PFP solution and will serve as a reference for evaluating the cases in the next chapter, where the initialization will use a flat start guess.

The `case3012wp` is a native MATPOWER case data (ZIMMERMAN; MURILLO-SÁNCHEZ, 2020) with 3012-buses representing the Polish 400 kV, 220 kV, and 110 kV network during peak

Table 5.1: Quantification of the main elements characterizing a selected native ill-conditioned MATPOWER study case

CASE	Buses	Generators	Loads	Shunts	Branches	Transformers	S_{slack}
`case3012wp`	3,012	502	2,271	9	3,572	201	8.2135 + j0.6083
`case3375wp`	3,375	596	2,434	9	4,161	383	6.8986 + j0.6439
`case13659pegase`	13,659	4,092	5,544	8,754	20,467	5,713	0.7687 + j0.1581
`case_ACTIVSg70k`	70,000	10,390	32,460	3,477	88,207	16,855	13.2478 + j0.7668

hours in winter 2007–2008. In the same way, the `case3375wp` represents the Polish 400 kV, 220 kV, and 110 kV networks with 3375-buses during winter 2007-2008 evening peak conditions, but including some equivalents of the German, Czech, and Slovak networks.

The `case13659pegase` is available in MATPOWER data bank (ZIMMERMAN; MURILLO-SÁNCHEZ, 2020) representing a large and complex European high-voltage transmission network with 13659-buses (FLISCOUNAKIS *et al.*, 2013; JOSZ *et al.*, 2016). Its data does not correspond to reality but is used as a test model for planning and operation that simulates European grid data. The data stems from the Pan European Grid Advanced Simulation and State Estimation (PEGASE) project, part of the 7^{th} Framework Program of the European Union. Their main voltage levels in decreasing order are: 750 kV, 400 kV, 380 kV, 330 kV, 220 kV, 154 kV, 150 kV, 120 kV, and 110 kV. The low voltage levels range from 27 kV to 400 V and are used to model step-up transformers that connect generators to the high-voltage network.

The `case_ACTIVSg70k` is one of the biggest case data available in MATPOWER (ZIMMERMAN; MURILLO-SÁNCHEZ, 2020) with 70,000-buses. It is a synthetic system of the Eastern United States. Figure 5.1 exhibits a map illustrating its hypothetical geographical scope[1]. The grid has voltage levels with 765 kV, 500 kV, 345 kV, 230 kV, 161 kV, 138 kV, 115 kV, 100 kV and 69 kV. It was created with algorithms described in Birchfield *et al.* (2017), similar to the local network (see Birchfield *et al.* (2018) for additional details).

5.2.2 Synthetic systems created by replication process

Some ill-conditioned MATPOWER base cases were combined by Tostado-Véliz *et al.* (2019c) to validate novels ill-conditioned power-flow techniques. The purpose was to create large systems and increase the complexity of available tested systems. Table 5.2 summarizes the cha-

[1] Available in: <https://electricgrids.engr.tamu.edu/>

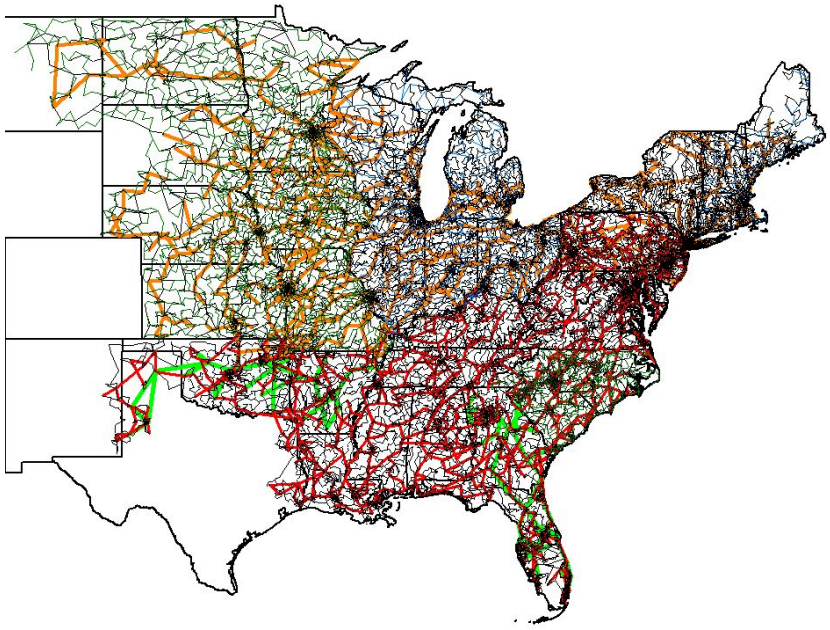

Figure 5.1: Picture of the oneline diagram for the synthetic `case_ACTIVSg70k` covering part of the USA map

racteristics of how these new synthetic power systems turned out.

Table 5.2: Characteristics in numbers for some elements of five synthetic ill-conditioned power systems

CASE	Buses	Generators	Loads	Shunts	Branches	Transformers	S_{slack}
`case18482`	18,482	2,890	9,790	14,654	32,113	2,638	23.6193 + j7.1130
`case27318`	27,318	8,184	11,088	17,508	40,935	11,426	1.1141 + j0.1248
`case36964`	36,964	5,780	19,580	29,308	64,227	5,276	20.8768 + j7.2080
`case54636`	54,636	16,368	22,176	35,016	81,871	22,852	1.8052 + j0.0589
`case109272`	109,272	32,736	44,352	70,032	163,743	45,704	3.1883 - j0.0702

The `case18482` and `case36964`, available in Tostado-Véliz *et al.* (2019c), are synthetic cases resulting from the manipulation of the original MATPOWER data bank `case9241pegase`. For these cases, the test system models were set by carrying out replications of the same system by two and four times, and performing appropriate adjustments in the interconnections of the final networks. Then the resulting cases were:

- `case18482` = `case9241pegase` × 2;
- `case36964` = `case9241pegase` × 4.

The `case9241pegase` represents in size and complexity the European high voltage transmission network, but not exactly the real system. This data comes from PEGASE project (FLISCOUNAKIS *et al.*, 2013; JOSZ *et al.*, 2016). Its main voltage levels in decreasing order are 750 kV, 400 kV, 380 kV, 330 kV, 220 kV, 154 kV, 150 kV, 120 kV, and 110 kV.

Similarly to the manipulation with the model represented by `case9241pegase`, the `case27318`, `case54636`, and `case109272`, available in Tostado-Véliz *et al.* (2019c), are also synthetic cases resulting from the multiplication of the original MATPOWER `case13659pegase` as follows:

- `case27318` = `case13659pegase` × 2;
- `case54636` = `case13659pegase` × 4;
- `case109272` = `case13659pegase` × 8.

The main characteristics of `case13659pegase` are available in Section 5.2.1.

5.2.3 Well-conditioned power systems

The power flow problem presented in this section has a convergent solution for the test systems when using a flat start estimation to run the NR scheme. Then, following the understanding verified in Milano (2009), the system models are well-conditioned.

The `case300` is a classic IEEE case available in MATPOWER that is widely used for validating load flow algorithms. It was developed in 1993 by the IEEE Test Systems Task Force under the direction of Mike Adibi[2]. Their main bus voltage levels in decreasing order are: 345 kV, 230 kV, 138 kV, 115 kV, 86 kV, 66 kV, 27 kV, 20 kV, 16.6 kV and 13.6 kV. Table 5.3 summarizes the main figures of the system. The latter column in the table shows the slack-bus power generation (S_{slack}) just for the purpose of convergence checking and reference for validating other results.

Table 5.3: Figures of elements of the 300-bus

CASE	Buses	Generators	Loads	Shunts	Branches	Transformers	S_{slack}
`case300`	300	69	201	29	411	107	4.5595 + j0.3884

[2]Available in: <http://labs.ece.uw.edu/pstca/pf300/pg_tca300bus.htm>

5.2.4 Overloaded and well-conditioned power systems

The information in this subsection comprises well-conditioned test systems but with an elevated loading level limit (see other details in Tostado-Véliz *et al.* (2019d)). They were generated from native MATPOWER systems to increase the load level near the maximum operational limit point. The strategy followed for this objective was to increase the active power injected into the generation buses, in steps of 0.0001 pu, until the NR method had divergence, starting from the flat start estimate. On identifying the divergence, the data of the operational point previous to the step with guaranteed convergence was then retained. Table 5.4 summarizes the characteristics of the overloaded and well-conditioned systems.

Table 5.4: Figures of elements of the overloaded and well-conditioned power systems

CASE	Buses	Generators	Loads	Shunts	Branches	Transformers	S_{slack}
`case69limit`	69	1	48	0	68	0	0.403 + j0.280
`case141limit`	141	1	84	0	140	0	1.252 + j0.784
`case_ACTIVSg500limit`	500	90	200	15	597	131	8.878 + j1.209
`case_ACTIVSg2000limit`	2,000	544	1,125	149	3,206	861	12.522 + j1.811

The `case69limit` is a portion of a distribution system for which data are available at Baran & Wu (1989) and Das (2008) with some modifications as branch flow limits disabled, *i.e.*, set to 0 (instead of 999) and generator limits for Q_{min}, Q_{max}, P_{max} magnitudes set to 10 (instead of 999). The voltage system is 12.7 kV.

The `case141limit` is a 141-bus distribution system for the zone of the metropolitan area of Caracas, in Venezuela (KHODR *et al.*, 2008), with some modifications such as doubled load at bus 53 (100 kVA instead of 50 kVA) and set BASE_KV to 12.47 kV (instead of 12.5). Its working voltage is 12.5 kV.

The `case_ACTIVSg500limit` is a synthetic 500-bus system located in the northwestern part of the United States state of South Carolina designed with a 345 kV and 138 kV transmission network. This model fictitiously simulates the mentioned region electrical network (BIRCHFIELD *et al.*, 2017).

Likewise, the `case_ACTIVSg2000limit` is a synthetic 2000-bus system located in the state of Texas, United States, designed with 500 kV, 230 kV, 161 kV, and 115 kV transmission networks. This model fictitiously simulates the electrical area for the region (BIRCHFIELD *et al.*, 2017).

5.2.5 Multiple slacks ill-conditioned power system

Usually, most electrical networks are considered to operate as a synchronous system area. However, when areas are interconnected by DC links, the operation can be of type asynchronous (KUNDUR, 1994). In this case, the power flow is solved assuming more than one slack bus. In the next chapter, it will be demonstrated that the problem can be solved synthetically by considering only one slack bus. Given these aspects, a more complex system is presented in this section and used in the next chapter to determine the solution of the PFP for its operation point.

The test system represents a case with distinct slack buses and will be labeled `case82k`. Also, it is a native case found in the MATPOWER data bank called as `case_SyntheticUSA`. It represents three isolated areas with their respective slack buses. Table 5.5 summarizes the main data of this case scenario.

Table 5.5: Figures highlighting the main characteristics of the 82k-bus three slacks power system

CASE	Buses	Generators	Loads	Shunts	Branches	Transformers	S_{slack}
`case82k`	82,000	13,419	37,755	3,952	104,121	20,696	9.5001 + j0.6799 23.0181 + j3.3767 8.0378 + j0.9838

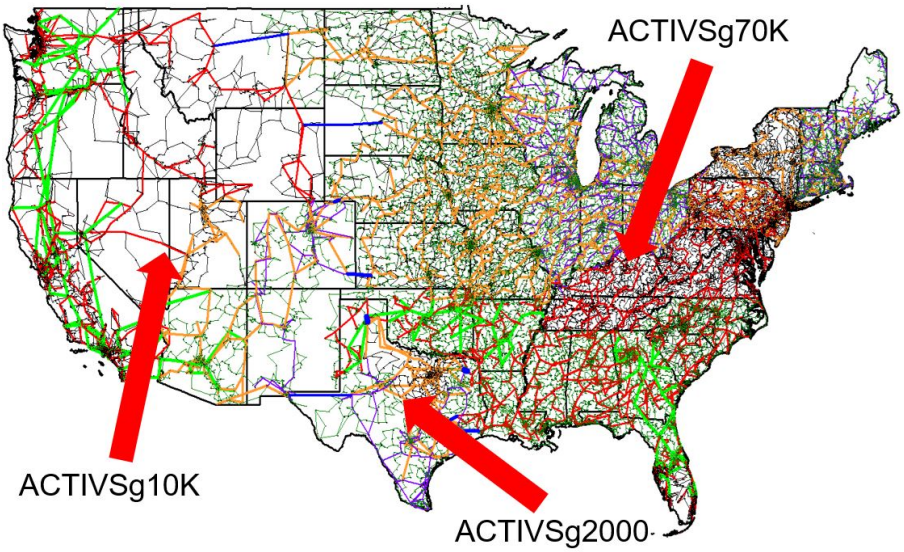

Figure 5.2: Oneline diagram for the synthetic `case82k`

The `case82k` is a synthetic United States case, that comprises data from an electrical grid

that spans the geographic map of the USA, as illustrated[3] in Figure 5.2. It combines three distinct cases, namely `case_ACTIVSg70k` from the eastern United States, `case_ACTIVSg10k` from the western United States, and `case_ACTIVSg2k` from Texas. The AC voltage levels of the transmission network are 765 kV, 500 kV, 345 kV, 230 kV, 161 kV, 138 kV, 115 kV, 100 kV, 69 kV, 24 kV, 22 kV, 20 kV, 18 kV and 13.8 kV. The three isolated systems are connected by nine DC lines. An algorithm described by Birchfield *et al.* (2017) simulates the transmission system models but without modeling any actual lines (BIRCHFIELD *et al.*, 2018). Figure 5.3 illustrates the interconnection between buses and branches of each of the three areas of the system. This figure presents the representation of interconnections between the buses using the branches and has no equivalence with the physical representation of the system.

5.3 OVERVIEW

This chapter presented five test system groups that were characterized as follows: four original ill-conditioned MATPOWER study cases, five synthetic ill-conditioned, one well-conditioned, four of type overloaded and well-conditioned, and one with multiple slacks and ill-conditioned. In this list, tests on `case13659pegase`, `case_ACTIVSg70k`, and `case54636` will illustrate examples to demonstrate how close the initial voltage estimates given by MATPOWER are to the solution. This pattern led to the search for a PFP solution that relies on a more independent initial estimation for iterative techniques, such as the classical flat start estimation, whose application through the homotopy technique will be discussed in the next chapter.

[3]Available in: <https://electricgrids.engr.tamu.edu/>

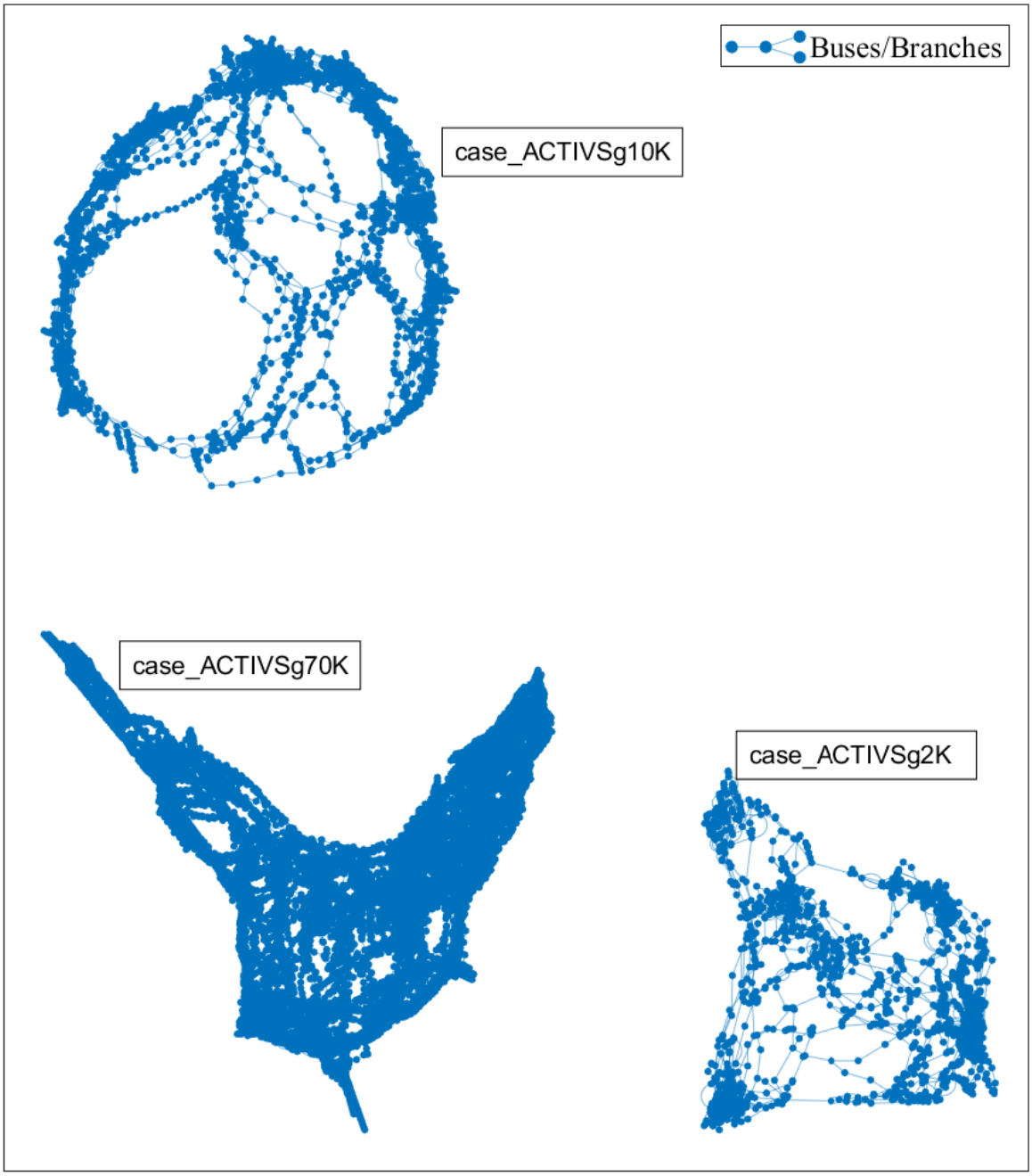

Figure 5.3: Three areas of the `case82k` illustrated by graph connections constructed from the native MATPOWER data bank

CHAPTER 6

EXPERIMENTS AND RESULTS

6.1 INTRODUCTION

This chapter presents experiments and results related to the application of homotopy-based PFP approaches. Both static and dynamic homotopy techniques are evaluated.

Two static homotopy approaches are discussed, highlighting their characteristics and limitations. Additionally, two dynamic homotopy-based schemes are tested for their effectiveness in solving the power flow problem. Each approach is examined for its numerical performance and the key aspects inherent to it.

Multiple experiments are conducted on large-scale, ill-conditioned power system models, as presented in Chapter 5, to verify the effectiveness of the proposed methods. Additionally, contingency cases are evaluated to assess the efficiency of the dynamical homotopy-based method.

All simulations employ MATPOWER's database. For any system running the NR method with MATPOWER's database initial estimate, the PFP always converges. Then, the results of the PFP executed for this situation are taken as a reference for comparison with the accuracy of the proposed numerical schemes in this work. The simulations were carried out using a personal computer, Intel(R) Core(TM) i7-8565U 8^{th} Gen, 256 GB SSD CPU, 1.80 GHz, 16 GB RAM, 64-bit OS.

6.2 IMPACT OF THE INITIAL ESTIMATE FOR THE CLASSICAL NR METHOD

This section presents two examples of initial estimates used in the native cases of MATPOWER. The aim is to emphasize the question of the initial guess adopted by MATPOWER (reference solution of the PFP) and the flat start adopted in further simulations to demonstrate the effectiveness of the proposed techniques of this PhD thesis. The systems represented by

case13659pegase, case_ACTIVSg70k, and case54636 were tested.

To illustrate how far MATPOWER's initial estimates are from the PFP solution, Figure 6.1 shows in plots the initial estimates (red dashed) and the PFP solution (black) for the bus nodal voltage magnitudes and angles for the 13,659-bus, Figure 6.1(a) and 6.1(b); 70,000-bus, Figure 6.1(c) and 6.1(d); and 54,636-bus model, Figure 6.1(e) and 6.1(f). Note the proximity of the solution and the initial estimate (see, for example, the details in the zoom region). These aspects explain the convergence in all cases of the classical NR method when the native MATPOWER database is used.

However, when the initial estimate is changed to flat start, divergence from the iterative process occurs when the classical NR method is used to determine the PFP solution, as will be detailed later. The results confirm the ill-conditioning of the systems represented by the data in case3012wp, case3375wp, case13659pegase, case_ACTIVSg70k, case18482, case27381, case36964, case54636, case82k and case109272. Therefore, the simulations in the sequence are based on experiments using ill-conditioning cases such as these and others.

6.3 TESTS CONSIDERING THE CLASSICAL NR WITH DIFFERENT STRATEGIES OF INITIALIZATIONS

Before introducing a new method, the classical schemes were used to solve the PFP, considering the test systems covered in the previous chapter.

This section discusses simulations and results assessed with the classical NR solver when computed in four different strategies of initializations. The goal is to demonstrate the poor performance of the NR method when applied without adequate initialization or adequate system conditioning. First, tests were performed considering the native initial estimate (NR-MAT) given in MATPOWER (ZIMMERMAN; MURILLO-SÁNCHEZ, 2020); second, the simulations assumed the classical NR solver, but with initialization entirely of the type flat start (NR-flat); third, the simulations considered an estimate with a flat start but modified by using an Optimal Multiplier (OM-NR) solver as defined in Equation (2.184); finally, for the last simulations the NR solver uses initial estimate which is the result of two iterations of the Gauss-Seidel (GS) solver (GS-NR). The GS solver departs from the flat start guess. When the GS computes more

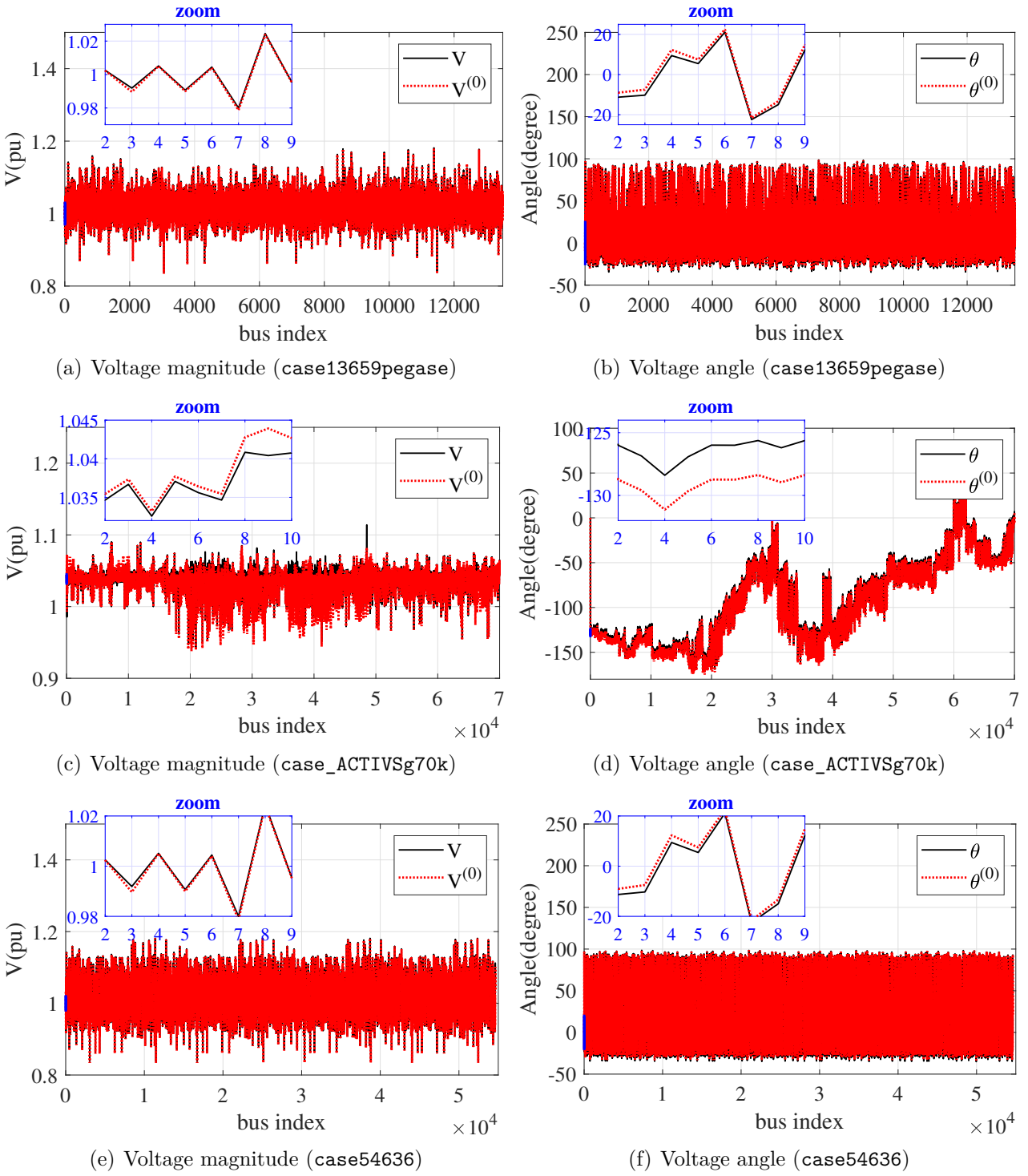

(a) Voltage magnitude (`case13659pegase`)

(b) Voltage angle (`case13659pegase`)

(c) Voltage magnitude (`case_ACTIVSg70k`)

(d) Voltage angle (`case_ACTIVSg70k`)

(e) Voltage magnitude (`case54636`)

(f) Voltage angle (`case54636`)

Figure 6.1: Illustrative plots for comparison between the initial voltage estimate $V^{(0)}$, available on MATPOWER data bank, and the final states V (solution of the PFP) for the `case13659pegase`, `case_ACTIVSg70k` and `case54636`

than two iterations, the results delivered for the NR cause divergence for the NR solver for all cases. Seven ill-conditioned cases were used in the experiments. Table 6.1 exhibits the number of iterations when occurring convergence according to the case and strategy.

Table 6.1: Performance for the strategies NR-MAT, NR-flat, OM-NR and GS-NR

CASE	NR-MAT	NR-flat	OM-NR	GS-NR
`case3012wp`	3	x	x	3
`case3375wp`	4	x	x	4
`case13659pegase`	5	x	15*	7*
`case_ACTIVSg70k`	6	x	x	x
`case18482`	6	x	x	x
`case54636`	5	x	x	x
`case109272`	5	x	x	x

x: divergence; * unstable point.

From Table 6.1, it is verified that when the simulations are performed with the NR solver with a flat start (NR-flat), all results of the PFP are divergent. On the other hand, only the approach with MATPOWER's initialization (NR-MAT) presented convergence for all test systems. Despite this, three iterations are required for the smallest system and five for the highest one. This occurs even with an initial estimate that is very close to the solution. When the strategies OM-NR and GS-NR were used, both diverged for the `case_ACTIVSg70k`. Also, both converged for simulations for the `case13659pegase` for a different operation point.

In Table 6.1, except for the (NR-flat) solver, the worst performance was verified for the OM-NR approach, which converged for just one case, albeit to an unstable operation point. The GS-NR, despite having better performance than the OM-NR solver, presented inadequate results for four larger systems. Hence, using the Gauss-Seidel result for initializing the PFP provides an inadequate partial solution for the classical NR solver in case of ill-conditioned large-scale system models.

6.4 STATIC HOMOTOPY APPROACH SIMULATIONS

This section presents two approaches to the static homotopy problem. The main difference between them is the introduction of a fixed point vector in one of the homotopy functions, besides an artificial compensation network to drive the solution of the homotopy problem from a flat start point until the PFP solution or a result close to the high precision states.

6.4.1 Homotopy function without a FPV term

In Chapter 2, the static homotopy approach was presented as a two-parameter problem (h_1 and h_2) based on introducing a fictitious compensation network, as proposed in Freitas & Silva (2022). The problem depends on the homotopy parameter $h = h_1$ (see Equations (2.201)-(2.202)) and its step Δh to define the discrete points along the homotopy path. Also, it was introduced a parameter h_2 to control the insertion of a scaling factor for impedance, $\delta \leq 1$. This factor acts artificially reinforcing interconnections in the neighborhood of the slack bus (see Equation (2.203)). The insertion of δ is then controlled by this second homotopy parameter, h_2, used to activate the factor δ for $0 \leq h_1 < 1$, and remove it when $h_1 = 1$ since this factor is not part of the original network. This second homotopy parameter was introduced to reinforce connections near the slack bus along the homotopy process, *i.e.*, for $0 \leq h_1 < 1$. We suppose that links near the slack bus are subject to power flow fluctuations along iterations, supposedly due to actions to regulate the system losses.

The same idea was presented again in Chapter 4, but in the form outlined in Equation (4.19). This formulation includes a slight modification in its computational implementation regarding the point $h = 1$ in the homotopy pathway. This is the main difference compared to the technique described previously.

In this formulation, the factor δ is implicitly present in the elements of the matrix Y_{bus}, which consists of entries $Y_{km} = G_{km} + jB_{km}$, even when $h_1 = 1$. As a result, this modified matrix accounts for compensations due to changes related to δ, making the parameter h_2 unnecessary.

However, for the new problem formulation, when $h_1 = 1$, it is essential to remove the effect of the artificial scaling factor δ to restore the original network. This is achieved by running the Newton-Raphson method (NR) again, using the original admittance matrix without the influence of δ and the states obtained for the last point of the homotopy path (still under the effect of δ).

In this new version of the homotopy function, the load (or generation) compensation is introduced directly in Equation (4.19) through constant impedance powers $V_k^2 g_k$ and $V_k^2 b_k$ at the bus k, which are removed as h_1 increases.

The previously described problem was referred to as Guided Solution Homotopy (GSH-NR)

because it employs the Newton-Raphson method (NR) to compute the states at each point along the homotopy pathway. The final point in the old version ($h_1 = 1$ and $h_2 = 1$) represents the solution for PFP. An example of this method and how the global iterates are computed for the solver can be found in Appendix A.

A first version of the GSH-NR was proposed in Freitas & Silva (2022). In this version, the factor δ is removed when the last point of the homotopy path is reached. For this situation, the parameter h_2 is switched from 0 to 1, indicating that all impedances possibly modified by $\delta < 1$ must be restored, and so the original admittance matrix. Then, the artificial network is still found for $h_1 = 1 - \Delta h$, and is switched to the original network, *i.e.*, for $\delta = 1$, when $h_1 = 1$. The states on the previous point are used as an initial estimate for finding the final states in the homotopy pathway $h_1 = 1$. The flowchart in Figure 6.2 shows the procedure for setting parameters and the computation logic leading to the final solution of the PFP for the first version of the GSH-NR scheme, as outlined in Chapter 2. It is hoped that at the end of the homotopy process, the result is the PFP high precision solution.

A second version of the GSH-NR, as outlined in Equation (4.19), was developed and illustrated in the flowchart in Figure 6.3. The key distinction in this approach is that the compensated network, and so matrix Y_{bus}, is modified by the scaling factor δ only before commencing the homotopy process. This process entails the adjustment of the admittance matrix while ensuring it remains invariant with respect to δ until the conclusion of the homotopy process. Additionally, the calculation of the PFP along the homotopy path is performed with a relaxed tolerance tol_1, in which tol_1 is significantly larger than a tolerance tol_2. This latter is a small value that ensures a highly precise solution for the power flow. To meet this requirement, the final result from the homotopy process is improved by running a Newton-Raphson method (NR) solver with the specified tolerance tol_2. Consequently, the total number of iterations needed to reach the final solution for the PFP, including those required by the GSH-NR solver, in addition to the iterations needed for the high-precision execution of the NR solver.

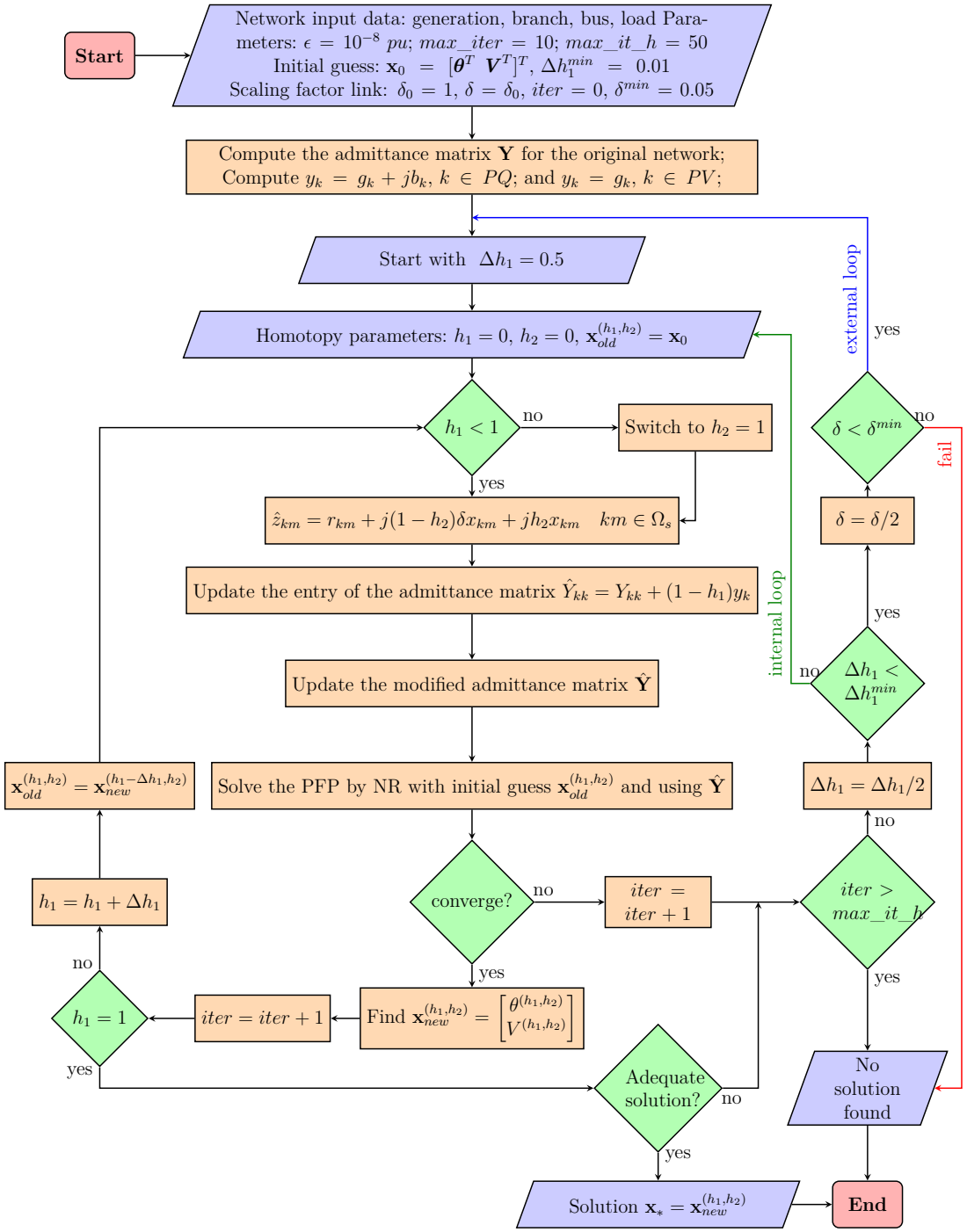

Figure 6.2: Flowchart illustrating the main procedure aspects of the GSH-NR solver (first version)

6.4.2 Homotopy function with a FPV term

Furthermore, this thesis proposes a modification in the GSH-NR scheme by presenting a new approach to utilizing the homotopy parameter h within the homotopy function, as shown in Equation (4.24). In this new homotopy function, an FPV term was introduced for the compensation approach defined through GSH-NR. The compensated mismatches are now

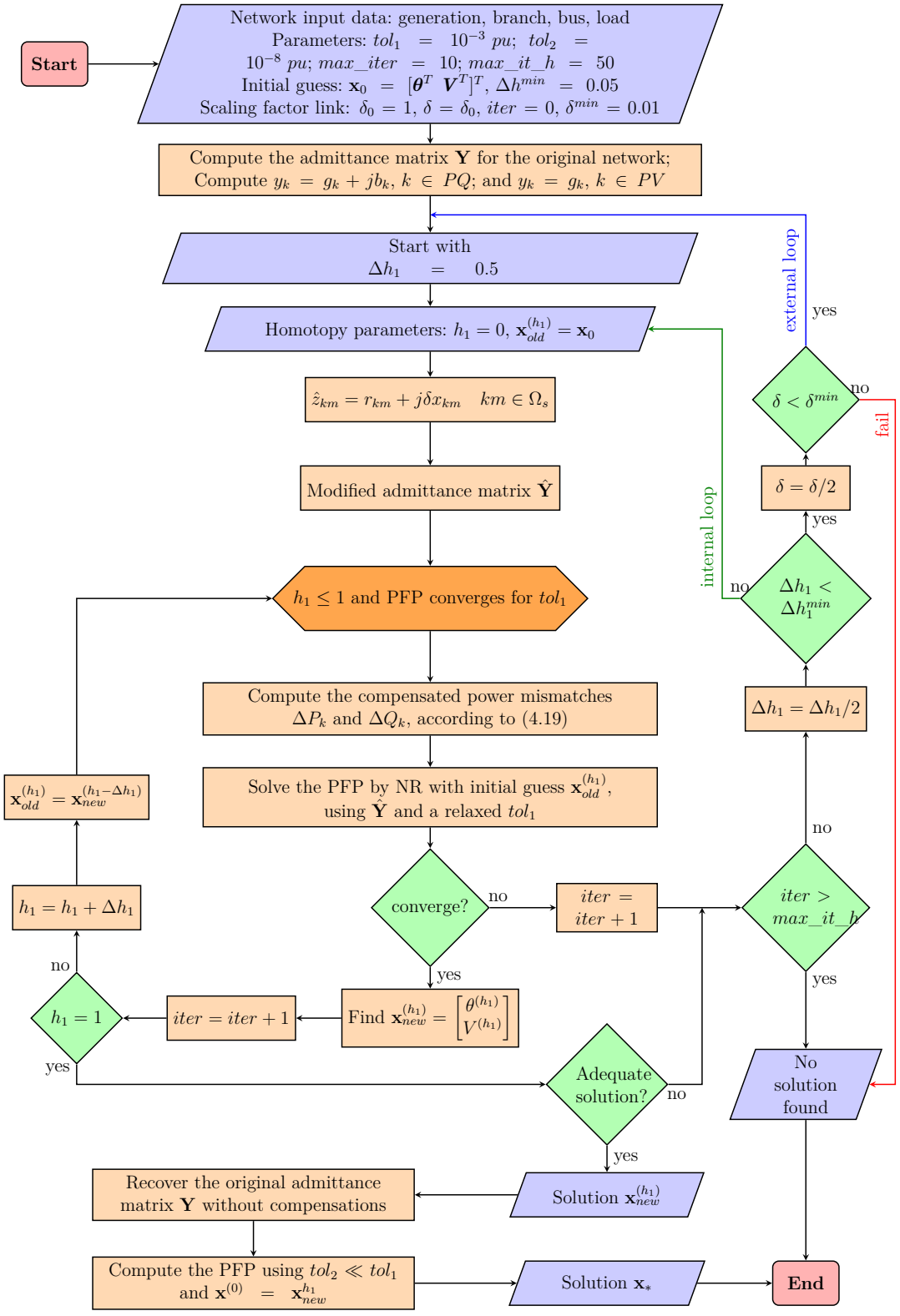

Figure 6.3: Flowchart illustrating the main procedure aspects of the GSH-NR solver (second version)

weighted by h, while the FPV is weighted by $(1 - h)$. Remark that for smaller values of h, the main weight is driven for the FPV term in relation to the mismatches of the compensated network. Because of the inclusion of the FPV term and the use of the GSH-NR idea, the

technique was called GSH-FPV-NR. In this new solver, an additional parameter, K, must be introduced to include the term FPV.

Referring to the flowchart in Figure 6.3, the only modification needed to implement this new solver is to change the box immediately after initiating the homotopy loop for $h_1 \leq 1$, using Equation (4.24) in place of Equation (4.19). However, a value for the parameter K must be specified. Based on recent experiments for the cases of dynamical homotopy (see for examples results in Lima-Silva & Freitas (2024b) and Lima-Silva & Freitas (2024a), values in the range $10^{-4} \leq K \leq 10^{-2}$ are suggested.

6.4.3 Experiments with the static homotopy approaches

Simulations were conducted to identify the PFP solution for various test systems using GSH-NR and GSH-FPV-NR. Concerning the GSH-NR solver, results presented are exclusively for the GSH-NR version that follows the algorithm illustrated in the flowchart in Figure 6.3. This choice was made because no significant differences were observed when implementing the algorithm from the flowchart at Figure 6.2.

Table 6.2 summarizes the results of simulations for the NR method with initialization defined in MATPOWER (close to the solution), the NR method with flat start estimate, the GSH-NR, and the GSH-FPV-NR. The $tol_1 = 10^{-3}$ and $tol_2 = 10^{-8}$ were used for the latter. The second column in the table exhibits the iterates, required for convergence for the NR solver when it uses the initial estimate assigned in MATPOWER (NR-MAT). But, for the initialization of type flat start (NR-flat), the convergence is successful only for the 300-bus system, requiring 5 iterations (see the 3^{rd} column). Using the GSH-NR solver needed the parameters adjusted following the flowchart at Figure 6.2, *i.e.*, Δh_1 and δ and and the PFP solution was obtained according to the number of iterations in 6^{th} column. The GSH-FPV-NR, besides these parameters, also needed K (see 9^{th} column). The number of iterations for convergence is presented in the 10^{th} column. In the MATPOWER data bank, all cases represent test systems with just one slack bus, except the `case82k`, which has three slack buses. To use the homotopy algorithm, we modified the slack status in areas 2 and 3 for the type of PV or PQ, and just a single slack in area 1 was established (see Appendix B for further details). For the slack bus in area 1 supplying the removed slacks

in the other areas, fictitious interconnections were assigned between each two buses. In the case of `case82k`, synthetic transformers composed of a complex tap and a reactance were introduced for each connection. So, the system was treated as a single synchronous network.

Table 6.2: Performance of Newton-Raphson (NR) and two static homotopy approaches

	NR		GSH-NR			GSH-FPV-NR			
CASE	NR-MAT	NR-flat	Δh_1	δ	iter_{NR}	Δh_1	δ	K	iter_{NR}
`case3012wp`	3	x	0.25	1.0	20	1.0	0.01	1×10^{-4}	10
`case3375wp`	4	x	0.25	1.0	20	1.0	0.01	1×10^{-4}	11
`case13659pegase`	5	x	0.25	0.125	22	0.5	0.01	1×10^{-4}	15
`case_ACTIVSg70k`	6	x	0.125	1.0	41	0.25	1.0	1×10^{-4}	24
`case18482`	6	x	0.5	1	10	0.5	0.5	1×10^{-2}	11
`case27318`	5	x	0.25	0.125	25	0.5	0.1	1×10^{-2}	13
`case36964`	6	x	0.125	1	27	0.25	0.5	1×10^{-2}	18
`case54636`	5	x	0.01	0.01	x	0.5	0.1	1×10^{-2}	17
`case109272`	5	x	0.01	0.01	x	0.25	0.1	1×10^{-2}	19
`case300`	5	5	0.5	1.0	8	0.5	1.0	1×10^{-4}	8
`case82k`	6	x	0.01	0.01	x	0.25	1.0	1×10^{-4}	24

x: divergence.

The GSH-NR method, applied to the `case_ACTIVSg70k`, a large model, required a total of 41 NR iterations along the entire homotopy path to achieve the PFP solution (see the 6^{th} column). When the GSH-FPV-NR is used, only 24 iterations are required. The GSH-NR solver was unable to find a solution for other large-scale ill-conditioned systems, such as those represented by cases `case54636`, `case109272`, and `case82k`. Conversely, the GSH-FPV-NR effectively solved all cases studied, showcasing its outstanding performance in addressing large-scale ill-conditioned systems, including the modified 3-slack buses (3 isolated areas) of `case82k`.

6.5 EXPERIMENTS USING THE DYNAMIC HOMOTOPY APPROACH

The dynamic homotopy approach grounded on the FPV homotopy function which was implemented to reduce the computational burden of the PFP, followed by a refinement of the result with the NR method. This investigation was prompted by the observation that, although the simulations with the GSH-NR demonstrated high accuracy and efficiency, the number of iterations required to solve the `case_ACTIVSg70k` system was considered excessive. Additionally, some cases experienced divergence. Also, although the GSH-FPV-NR has demonstrated

a high quality of convergence for studied cases in relation to GSH-NR, an elevated number of iterates still motivates interest in improving its performance. But, considering it embedded into a dynamic approach as well. Remember that the homotopy path points in the static approach are each calculated by an NR scheme.

Considering the dynamic aspects, integration methods need to be investigated due to the dynamic nature of the problem. Unlike static approaches, which primarily rely on Newton-Raphson method (NR), dynamic solvers depend on numerical integration methods. The quality and performance of these methods are crucial for achieving successful convergence of the PFP. Then, varied experiments were carried out. Furthermore, the initialization of the dynamic homotopy technique demands reduced integration steps and the employment of appropriate integration methods. Given these aspects, several studies needed to be carried out to verify the best performance of the dynamical homotopy numerical scheme.

6.5.1 Investigation of the dynamic homotopy scheme initialization

This subsection aims to investigate the initial behavior of the dynamic homotopy approach based on the FPV easy function definition and the equations of the PFP. Because of this characterization, the technique will be called only FPV to differ from the other approach to be discussed later, but named FPV2. Considerations will be dedicated to studies involving the initial steps and the performance of the implicit and explicit integration methods for performing this initialization scheme. With this objective, considering a didactic case, a generic example was presented in Appendix C. Furthermore, experiments and results on various poorly conditioned large-scale power system models are assessed. The goal is to show how effective the proposed method is in accurately finding the solution of the PFP by utilizing the desired performance of the dynamic homotopy-based technique.

6.5.1.1 Simulations to assess the performance of the integration solvers

Experiments were assessed to demonstrate the performance of the dynamic homotopy solver's to improving the convergence of the classical NR scheme. The studies initially prioritized the characteristics of integration methods, focusing on the influence of the time-step size.

All simulations involving the integration methods require a small time-step to compute the initial step $t_1 = \Delta t_0$, starting from $t_0 = 0$. This dependence can be physically explained by the smallest "time constant" associated with the system's dynamics under study. For the simulations in this work, the initial time-step, Δt_0, is a factor for investigations since ensuring an adequate result for the dynamical homotopy-based technique is a key aspect for evaluating the efficiency of the method. Therefore, the discrete points in the path curve, $\gamma(t)$, $0 \leq t \leq 1$, are $t_0 = 0$, $t_1 = \Delta t_0$, and $t_{k+1} = \Delta t_0 + k\Delta t_k$, $k = 1, \cdots, (N-1)$. The initial point at $t_0 = 0$ gives the Initial Condition (IC) with states $\mathbf{x}(0) = \mathbf{x}^{(0)}$, which also coincides with the original initial estimation for the PFP. N represents the number of points beyond the initial point 0 in the homotopy pathway. It must be chosen and meet the restriction, which avoids $t_k > 1$. Therefore, if necessary, the final point t_N must be set in the unitary value and the time-step properly reduced. For instance, in the extreme case where $\Delta t_0 = 0.005$ and $\Delta t_1 = 1.0$ were specified, the definition of the time instants t_k (or steps) would be as follows: $t_1 = \Delta t_0 = 0.005$, $t_2 = \Delta t_0 + \Delta t_1 = 1.005$, with $N = 2$ points plus $t_0 = 0$. However, as $t_2 > 1$, the point must be readjusted to give $t_2 = 1$. In this case, the time-step must be reduced to $\Delta t_1 = 0.995$ instead of $\Delta t_1 = 1.0$. The variable N represents the number of points on the homotopy pathway where the states $\mathbf{x}(t_k)$, $k = 1, \cdots, N$ need to be computed. Using a numerical integration method that minimizes N is beneficial because computing each point requires an LU factorization of the matrix $\mathbf{G}(\mathbf{x}(t_k))$ (refer to Equations (4.12) and (4.14) for more details). This aspect becomes more evident in the following simulations for computing states only at the instant t_1, which suggests the use of an implicit method for ill-posed systems.

6.5.1.2 Experiments for the first time-step

In the context of the dynamic homotopy scheme, it is important to determine the states for the initial step when $t_1 = \Delta t_0$. This evaluation impacts the setting of the factor K in the definition of the "easy" function $\mathbf{g}_0(\mathbf{x})$ and, consequently, the conditioning of the state derivative matrix, $\mathbf{G}_x(\mathbf{x},t)$.

Assume that the PFP is of the type ill-conditioned. In reason of the nature of this type of nonlinear system, the mismatches for the initial estimate generally present $||\mathbf{f}(\mathbf{x}^{(0)})|| \gg 1$. At the beginning of the homotopy pathway, the starting point is initially known due to IC and given

by $t_0 = 0$, $\mathbf{x}(0) = \mathbf{x}^{(0)}$. Then, the states $\mathbf{x}(t_1)$ in the point defined by $t_1 = \Delta t_0$ can be calculated in the sequence by $\mathbf{x}(t_1) = \mathbf{x}(t_1) + \Delta\mathbf{x}(0)$. Considering the dynamical homotopy-based problem, a numerical integration technique should be used to determine $\Delta\mathbf{x}(0)$.

Based on the first approximated states, $\mathbf{x}(t_1)$, calculated at t_1, divergence along the homotopy pathway may already be verified. Then, it is fundamental to study the numerical behavior of the states for this point. The states $\mathbf{x}(t_1)$ were calculated for a small Δt_0 following this strategy. For these simulations, the initial time-step was fixed at 0.005, giving $t_1 = 0.005$. To demonstrate the ineffectiveness of explicit integration methods in this situation, we applied the FE and BE solvers to compute the states at t_1. The value 0.0001 was assigned for K in the function $\mathbf{g}_0(\mathbf{x})$. Initially, as presented in Section 4.3 and considering the FE solver, the deviation concerning the initial states, $\mathbf{x}(0) = \mathbf{x}^{(0)}$, is $\Delta\mathbf{x}(0) = \mathbf{x}(t_1) - \mathbf{x}(0) = -(0.005/0.0001)\mathbf{f}(\mathbf{x}^{(0)}) = -50\mathbf{f}(\mathbf{x}^{(0)})$. This result demonstrates that the numerical pattern of $||\Delta\mathbf{x}(0)||$ contributes to amplifying and propagating the characteristics of the ill-conditioning of the original PFP. This is justified because, for ill-conditioned systems, as stated before, $||\mathbf{f}(\mathbf{x}^{(0)}||$ is generally very large. Then, it is unacceptable to compute the state for the instant t_1 as $\mathbf{x}(t_1) = \mathbf{x}(0) - 50\mathbf{f}(\mathbf{x}^{(0)})$, as it will cause a numerical explosion of the norm $||\mathbf{f}(\mathbf{x}(t_1))||$. On the other hand, incrementing K, for example, setting it into a unitary value, results in small increments $\Delta\mathbf{x}(0) = \mathbf{x}(t_1) - \mathbf{x}(0) = -0.005\mathbf{f}(\mathbf{x}^{(0)})$. However, this result yields a greatly reduced variation $\Delta\mathbf{x}(0)$, proportional to mismatches, likely without significantly changing the states in t_1. When using the RK2 scheme, the result becomes even worse because not only we need to directly evaluate the states at t_1 to compute K_1 (as required for FE), but it also needs an additional evaluation to calculate K_2 using an inadequate computed K_1, refer to Equation (4.7). Therefore, we conclude that using FE or RK2 (explicit integration techniques) would significantly increase the error, rendering the solution ineffective for computing the states across the homotopy pathway.

In contrast, when considering the BE solver (or even a linear approximation of the homotopy function as calculated by using Equation (4.14)) at t_1, the deviation $\Delta\mathbf{x}(0)$ is calculated using Equation (4.12). Using the same values adopted for the explicit integration analysis, $K = 0.0001$ and $\Delta t_0 = 0.005$, a small scaling factor increment $\delta = K/\Delta t_0 = 0.0001/0.005 = 0.02$ is calculated, and provides a "perturbation term" $\delta\mathbf{I}$ to be added to the diagonal of the initial

PFP Jacobian matrix in Equation (4.12). Note that the Jacobian matrix is the same as the one for the first iteration of a standard iterative technique, such as the NR scheme. Therefore, the adjustment of δ is a function of K and Δt_0. So, this procedure is expected to effectively mitigate the ill-conditioning of the Jacobian matrix during the dynamic simulation at time t_1. However, only the setting of δ is insufficient since large Δt_0 can also make the convergence process unfeasible, as shown in simulations later. Therefore, the investigations considering these aspects should be considered to achieve results for successfully solving the dynamic homotopy problem for time instants $t_k > t_1$, even when Δt_k is substantial. Ultimately, this will establish a robust starting point for the NR solver and other iterative schemes.

6.5.1.3 Time-step change investigation

Based on the previous findings and descriptions, other experiments were carried out using the FE, RK2, and BE solvers, but starting from the point t_1 instead of $t_0 = 0$. With this objective, the states in the point t_1 were calculated only with the BE solver (or using a linear approximation of the homotopy function as calculated by using Equation (4.14)). Then, they were employed as IC for further studies with FE, RK2, and BE solvers. This procedure aligns with adopting only an implicit integration technique to compute the states initially in the instant t_1, according to the description forwarded in Section 6.5.1.2.

Therefore, it was assumed that the simulations must start from the point whose states $\mathbf{x}(t_1)$ were calculated at time t_1 using the initial point $t_0 = 0$, where the IC is $\mathbf{x}(0) = \mathbf{x}^{(0)}$. For this previous result, only the BE solver or a linear approximation of the homotopy problem (see Equation (4.14)) was used to obtain it.

Then, from this part of the work, the adopted Initial Condition (IC) for FE, RK2, and BE solvers are considered starting in the point defined in the homotopy pathway by t_1, ($\mathbf{x}(t_1)$,t_1).

The numerical integration solvers calculate points with $t_k > t_1$, $k = 1, \cdots, N-1$. To evaluate the performance of the three numerical integration solvers, initial simulations with $t_2 = 2\Delta t_0$ were assumed. Experience has shown that setting t_2 in large time steps, unless using the implicit method, results in premature convergence failures of the explicit methods.

To compare the performance of the implicit method (BE) with the explicit methods (FE

and RK2), simulations using two different types of time steps for $t_k > t_2$ were also carried out. In the first set of experiments, an elevated constant time-step was used to compute the last point in $t_N = 1$. In the second set, it was modified to be a variable time-step that increases over time.

Tables 6.3–6.5 exhibit simulation results, respectively, for the solvers FE, RK2, and BE, when $\Delta t_0 = 0.005$ (used for determining t_1 and t_2) is adopted; and $\Delta t = 0.5$ (large time-step), used for $t > t_2$. The value $K = 0.0001$ was adopted in the simulations. The second row in the tables indicates either the discrete-time for the dynamic homotopy calculations (2^{nd} to 6^{th} columns) or the iterations for the NR solver (columns 7^{th} to 9^{th}), which uses the result in $t = 1$ of the dynamic homotopy problem, *i.e.*, $\hat{\mathbf{x}}^{(0)}$, as an initial estimate. Depending on the solver used, the results of the infinite-norm of the PFP mismatches, $||\mathbf{f}(\mathbf{x})||_\infty$, are shown in 2^{nd} to 9^{th} columns, based on the case defined in the 1^{st} column.

Table 6.3: Norm evolution for the FE solver combined with the NR solver for an initial time-step $\Delta t_0 = 0.005$ and large time-step for $t > 0.01$

CASE/Time	$\|\|\mathbf{f}(\mathbf{x})\|\|_\infty$ of the Solver					$\|\|\mathbf{f}(\mathbf{x})\|\|_\infty$ NR		
t or *iter*	0.0	0.005	0.01	0.51	1.0	1	2	3
`case18482`	532	65	9.7	2×10^3	2×10^3	-	-	-
`case27318`	200	25	1.2	27	2×10^7	-	-	-
`case36964`	532	65	3.5	2×10^3	3×10^5	-	-	-
`case54636`	200	25	1.2	27	1×10^9	-	-	-
`case109272`	200	25	1.2	27	1×10^9	-	-	-
`case69limit`	0.012	2×10^{-4}	1×10^{-5}	5×10^{-4}	2×10^{-5}	2×10^{-8}	3×10^{-12}	-
`case141limit`	0.006	2×10^{-4}	9×10^{-6}	5×10^{-4}	2×10^{-5}	4×10^{-8}	1×10^{-11}	-
`case500limit`	13	1.2	0.02	0.9	1.0	8×10^{-3}	2×10^{-6}	4×10^{-13}
`case2000limit`	54	3.9	0.8	210	7×10^3	-	-	-

Table 6.3 refers to a significant time-step immediately following the instant $t_2 = 0.01$. From the computed norms, it is verified that the FE solver is unable to furnish an adequate estimate $\hat{\mathbf{x}}^{(0)}$ for the NR solver in $t = 1$, when employed to solve the dynamic homotopy problem for the large-scale ill-conditioned base cases. However, when applied to small systems, even considering the loading in the limit (69-, 141-, and 500-bus cases), it provided an appropriate starting, which converged with no more than three additional iterations. However, a failure of convergence occurred for the 2000-bus system. This is the largest model among those with studied stressed conditions.

The explicit technique implemented for the RK2 solver performs similarly to the FE sol-

Table 6.4: Norm evolution for the RK2 solver combined with the NR solver for an initial time-step $\Delta t_0 = 0.005$ and large time-step for $t > 0.01$

CASE/Time	$\|\|\mathbf{f}(\mathbf{x})\|\|_\infty$ of the Solver					$\|\|\mathbf{f}(\mathbf{x})\|\|_\infty$ NR		
t or *iter*	0.0	0.005	0.01	0.51	1.0	1	2	3
`case18482`	532	65	33	3×10^{7}	1×10^{11}	-	-	-
`case27318`	200	25	13	6×10^{5}	1×10^{10}	-	-	-
`case36964`	532	65	33	3×10^{9}	2×10^{14}	-	-	-
`case54636`	200	25	13	7×10^{5}	1×10^{10}	-	-	-
`case109272`	200	25	13	1×10^{7}	5×10^{12}	-	-	-
`case69limit`	0.012	2×10^{-4}	1×10^{-4}	9×10^{-5}	5×10^{-5}	1×10^{-9}	-	-
`case141limit`	0.006	2×10^{-4}	8×10^{-5}	4×10^{-4}	2×10^{-4}	7×10^{-9}	-	-
`case500limit`	13	1.2	0.6	1×10^{4}	5×10^{3}	-	-	-
`case2000limit`	54	3.9	1.9	1×10^{4}	4×10^{4}	-	-	-

ver. However, in some cases (see Table 6.4), the performance is even worse, as there was no convergence for smaller systems. This behavior is because RK2 requires an intermediate LU factorization to reach the instant of interest, according to the defined time-step Δt. Since the method reaches large errors in $t = t_2 = 0.01$, these errors propagate and lead to erroneous results in the following steps. From Tables 6.3 and 6.4, in $t_3 = 0.51$, results with a norm at least 10^4 are observed. Although the FE solver also shows erratic computation, the norms are smaller than those found by the RK2 solver (for reference, see the 5^{th} column in both tables). However, neither FE nor RK2 performed satisfactorily and gave adequate starting states $\hat{\mathbf{x}}^{(0)}$ for running the NR solver.

The results shown in Table 6.5 indicate that the BE method successfully converged for all test cases. This demonstrates that the single implicit method is suitable for solving the dynamic homotopy problem, even when using elevated time steps. When initiated with the results obtained by the dynamic homotopy-based technique, the NR solver required at most three iterations for convergence (see 7^{th}, 8^{th}, and 9^{th} columns in the table for the results of the iterations using NR solver, starting with the states computed by the BE dynamic homotopy-based scheme for $t = 1$), regardless of the system studied.

In the upcoming experiments, the methods were evaluated, extending the time steps for $t_k > t_2$. The specific time points $t_1 = 0.005$, $t_2 = 0.01$, $t_3 = 0.02$, $t_4 = 0.12$, $t_5 = 0.62$, and $t_6 = 1.0$ were established. It should be noted that the time step $\Delta t_4 = t_5 - t_4 = 0.5$ is considered large. Again, the infinite norms of the mismatches were observed for the dynamic homotopy and

Table 6.5: Norm evolution for the BE solver combined with the NR solver for an initial time-step $\Delta t_0 = 0.005$ and large time-steps for $t > 0.01$

CASE/Time	$\|\|\mathbf{f}(\mathbf{x})\|\|_\infty$ of the Solver					$\|\|\mathbf{f}(\mathbf{x})\|\|_\infty$ NR		
t or *iter*	0.0	0.005	0.01	0.51	1.0	1	2	3
`case18482`	532	65	33	7.2	3.7	0.04	1.5×10^{-5}	1×10^{-11}
`case27318`	200	25	13	0.5	0.25	0.1	2.5×10^{-5}	7×10^{-12}
`case36964`	532	65	33	6.9	3.6	0.27	6×10^{-4}	4×10^{-9}
`case54636`	200	25	13	0.5	0.25	0.1	3×10^{-5}	7×10^{-12}
`case109272`	200	25	13	0.5	0.25	0.1	3×10^{-5}	7×10^{-12}
`case69limit`	0.012	2×10^{-4}	1×10^{-4}	2×10^{-6}	5×10^{-7}	5×10^{-12}	-	-
`case141limit`	0.006	2×10^{-4}	8×10^{-5}	1×10^{-6}	5×10^{-7}	6×10^{-11}	-	-
`case500limit`	13	1.2	0.6	0.02	9×10^{-3}	1×10^{-6}	2×10^{-13}	-
`case2000limit`	54	3.9	2	2.8	1.5	0.01	8×10^{-7}	9×10^{-13}

NR solvers. Considering the similar profiles verified for the mismatch norms of `case109272`, `case54636`, and `case27318` and based on the findings in Tables 6.3–6.5, only the results for the largest system is shown for these specific experiments, *i.e.*, the `case109272`. Similarly, the same remark is made for the experiments involving the `case36964` and `case18482`, being considered only the former. Just the largest system was considered concerning the limit loading cases. Given the explanations regarding the selected systems, the new simulation results are presented in Table 6.6.

In Table 6.6, the mismatch norm was computed for each point defined by a specific time instant t_k, according to the employed solver. Also, only the result for three iterations of the NR solver for refining the result is exhibited in the table (see 10^{th} to 12^{th} columns).

Table 6.6: Evolution of norms with reduced initial time steps and progressive increments in computing the dynamic homotopy results, followed by three iterations of the NR solver considering the integration methods FE, RK2, and BE

CASE	Solver/Time	$\|\|\mathbf{f}(\mathbf{x})\|\|_\infty$ of the Solver							$\|\|\mathbf{f}(\mathbf{x})\|\|_\infty$ for NR		
	t or *iter*	0.0	0.005	0.01	0.02	0.12	0.62	1.0	1	2	3
	FE	532	65	3.5	0.7	5.7	57	114	28	5	0.2
`case36964`	RK2	532	65	33	16	9.6	4.2	2.6	0.2	3×10^{-4}	1×10^{-9}
	BE	532	65	33	16	4.0	1.4	0.9	0.09	9×10^{-5}	1×10^{-10}
	FE	200	25	1.2	0.02	0.07	0.3	0.17	0.03	6×10^{-4}	2×10^{-9}
`case109272`	RK2	200	25	13	6.3	1.2	0.5	0.3	0.19	2×10^{-4}	2×10^{-9}
	BE	200	25	13	6.3	1.1	0.2	0.1	0.02	1×10^{-6}	1×10^{-11}
	FE	55	3.9	0.8	0.7	3.6	58	91	16	1.0	6×10^{-3}
`case2000limit`	RK2	55	3.9	1.9	1.0	5.0	5.5	3.4	0.2	3×10^{-4}	1×10^{-9}
	BE	55	3.9	1.9	1.0	1.0	0.3	0.2	5×10^{-4}	3×10^{-9}	-

The results from Table 6.6 show that all solvers now exhibit favorable convergence perfor-

mance, except for the explicit FE solver in the `case36964` and `case2000limit`. In fact, they achieved convergence after two and one more additional iteration, respectively. The BE solver once again performed well in obtaining an initial result for the NR solver at $t = 1$. The RK2 solver also performed well, almost as well as BE, but with slightly lower performance in the system with high loading.

One drawback of the experiments highlighted in Table 6.6 is that additional computations were required because two more time points t_k were necessary compared to the first part of the experiments shown in Tables 6.3–6.5. Despite this, no significant improvement was observed in reducing the number of iterations in the refinement process using the NR solver. It is important to note that a new LU factorization of the Jacobian matrix is required at each time point added, increasing the computational cost of the process.

6.5.1.4 Changes in the time-step and factor K

In Section 6.5.1.3, the simulations were carried out using the parameters $K = 0.0001$ and $\Delta t_0 = 0.005$. In the present subsection, new experiments are conducted modifying these parameters to evaluate their impact on the performance of the dynamical homotopy-based technique. Both the initial time-step Δt_0 and the factor K, the latter composing the "easy" function $\mathbf{g}_0(\mathbf{x})$, were multiplied by a scaling factor ten when compared to the previous values. So, the new values are $\Delta t_0 = 0.05$ and $K = 0.001$. This way, the perturbation parameter in Equation (4.12) $\delta = K/\Delta t_0 = 0.02$ was kept in the same value despite different values for Δt_0 and K. Still, the dynamic of the time simulation due to the numerical integration process was modified. The upcoming investigations will focus on determining whether the initial result, $\hat{\mathbf{x}}^{(0)}$, generated by the dynamical homotopy solver is suitable for initializing the NR method. Additionally, the decoupled form, known as FDXB scheme, will be utilized to accurately compute the results for the PFP under these new conditions.

Several simulations were carried out. The goal is always to minimize the number of points across the homotopy pathway because each point in the path demands a LU factorization of the matrix $\mathbf{G}_x(\mathbf{x}(t))$. The dynamical homotopy-based technique used the NR and FDXB solvers to refine the solution. Again, in the instant t_1, the states $\mathbf{x}(t_1)$ were always obtained using only

the BE scheme.

In the first simulation, the homotopy pathway was set with the points defined by the instants t_k {0, 0.05, 1.0}. A very large time-step, $\Delta t_1 = 0.95$, is verified for determining t_2. Therefore, it is necessary to compute the states for the two points $t_1 = 0.05$ and $t_2 = 1.0$ to reach an approximate state $\hat{\mathbf{x}}^{(0)}$ at the latter instant. Again, the simulations were performed with the solvers FE, RK2, and BE, using IC departing from $\mathbf{x}(t_1)$. For this scenario, only the BE scheme could provide an approximate result, which led to the successful convergence of the NR or the FDXB solvers.

In a second set of experiments, the homotopy pathway now was set with four points and defined by the instants t_k for three different forms: {0, 0.05, 0.1, 1.0}; {0, 0.05, 0.15, 1.0}; and {0, 0.05, 0.20, 1.0}. Again, among FE, RK2, and BE schemes, only the latter was able to provide an approximate result for the successful convergence of the NR or the FDXB solvers.

Another set of experiments investigated the homotopy pathway using five points. The values of t_1 and t_2 were held constant at 0.05 and 0.1, respectively, while only the value of t_3 was changed, with t_4 set at 1 as the final path point. The experiments considered the following time instants t_k for three different path options: {0, 0.05, 0.1, 0.20, 1.0}; {0, 0.05, 0.1, 0.25, 1.0}; and {0, 0.05, 0.1, 0.30, 1.0}. The simulations considered for these options allow us to obtain a suitable approximation of states $\hat{\mathbf{x}}^{(0)}$ to the NR or FDXB solvers. So, convergent solutions with high accuracy for all PFP were calculated to a test system with explicit and implicit schemes. The results concerning the `case109272`, `case36964`, and `case_ACTIVSg2000limit` are discussed in the sequel. Figure 6.4 depicts plots indicating the evolution of the infinite norm of the PFP mismatches for the three test systems when the NR solver is initialized by an explicit (FE or RK2) or implicit (BE) integration scheme. The homotopy pathway has five points, but only the instant t_3 was modified along the simulations, being assigned the values 0.20 and resulting in Figure 6.4(a); 0.25, for Figure 6.4(b); and 0.30, for Figure 6.4(c). In the plots, the norms are associated with results obtained through the dynamical homotopy-based methods and the NR scheme's iterations. Then, the term "Iterations" in the axis of abscissa means index k of a time instant t_k when the visualization occurs from 0 to 4 and means effective iteration of the NR solver for an index greater than 4. In the plot legends, the mnemonics "109k", "36k", and "lim" refer to identification for the `case109272`, `case36964`, and

`case_ACTIVSg2000limit`, respectively. Still, from the plots, the norm results for the index 0 in the abscissa axis correspond to the infinite norm of the mismatches for the original estimate of the PFP, which is initialized with a flat start. The result for index 4 is associated with the instant $t_4 = 1$, the latest point of the homotopy pathway, and also to the approximate states $\hat{\mathbf{x}}^{(0)}$. This is then used as an initial estimate for the NR solver.

The plots in Figure 6.4 indicate that the performance of the dynamical homotopy-based schemes provided convergence for the NR solvers with a number of iterations closer to each system, except for the case where $t_3 = 0.25$ and the FE scheme was employed. Another remark is that the RK2 scheme for more elevated t_3 presented a performance similar to BE. Then, this similarity is expected to remain stronger by increasing the number of points for the homotopy pathway. However, this procedure must be avoided since the objective is to minimize the number of points of the homotopy pathway, aiming to reduce the computational cost in the global PFP resolution.

Table 6.7 shows the required global mean CPU time (dynamical homotopy-based plus NR scheme actions) to perform the simulations for obtaining the PFP solution according to the experiments used to generate the plots in Figure 6.4. Other experiments include simulations with the power flow executed using the native initial estimate provided by the MATPOWER data bank (NR-MAT), which this work uses as a reference framework. The initial estimate in this condition is closer to the known solution. All other mean CPU times result from the computations in which the PFP starts using a flat start guess.

From Table 6.7 it is verified that the explicit integration method FE scheme has almost the same computational burden as BE. However, a comparison is made for the simulation with many points. It was shown that only the BE works properly for smaller points. Then, it is expected to have better BE performance than FE. The RK2 scheme requires more CPU time. This is because RK2 involves the computations of constants K_1 and K_2, while the simplified scheme implemented for the BE is almost similar to FE. Similar to FE, RK2 does not work well for a small number of points, as happens in the BE scheme. Therefore, the results in the table confirm that the BE solver is suitable for use in the dynamic homotopy-based technique. Consequently, the results show that the CPU time can be even smaller when the BE scheme is used with fewer points in the homotopy pathway.

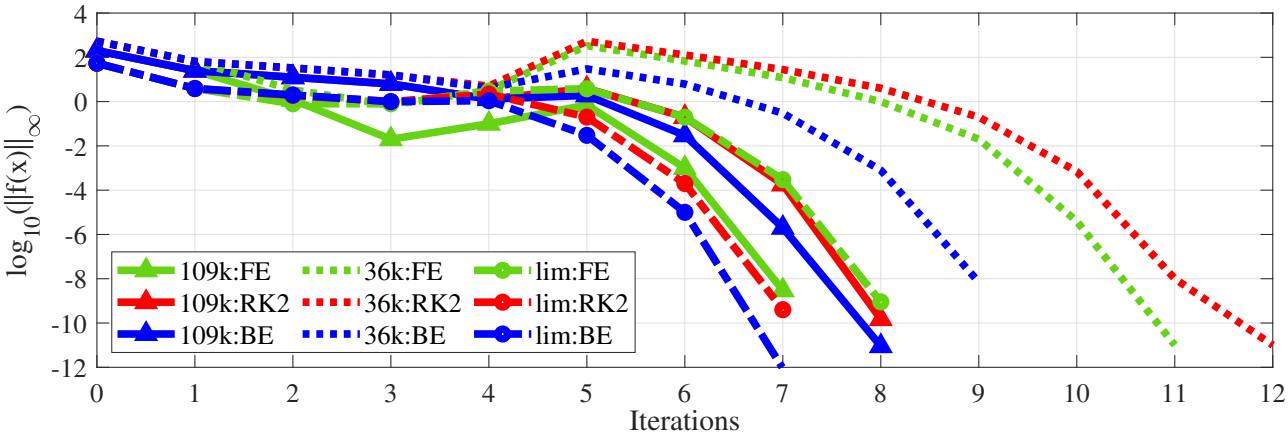

(a) Pathway with $t_3 = 0.20$

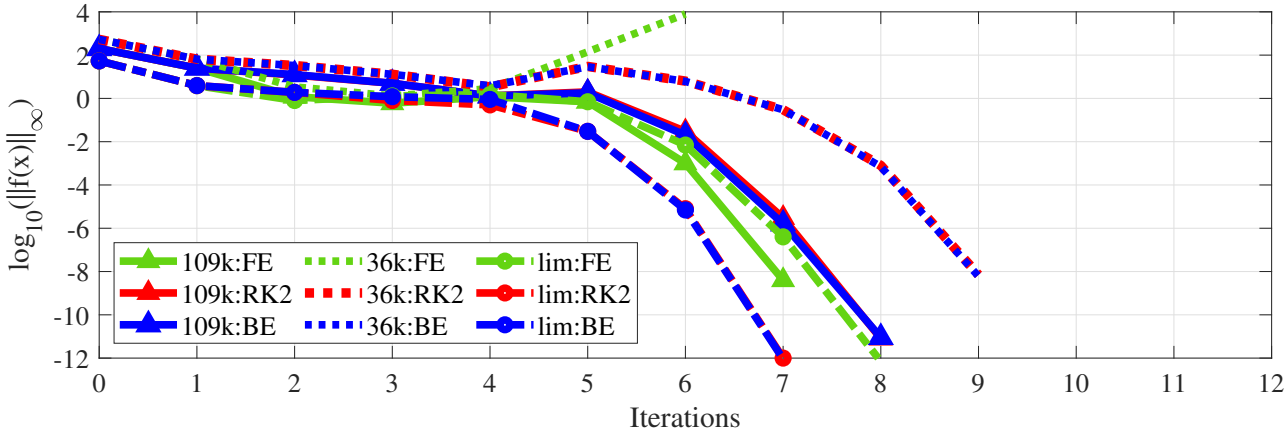

(b) Pathway with $t_3 = 0.25$

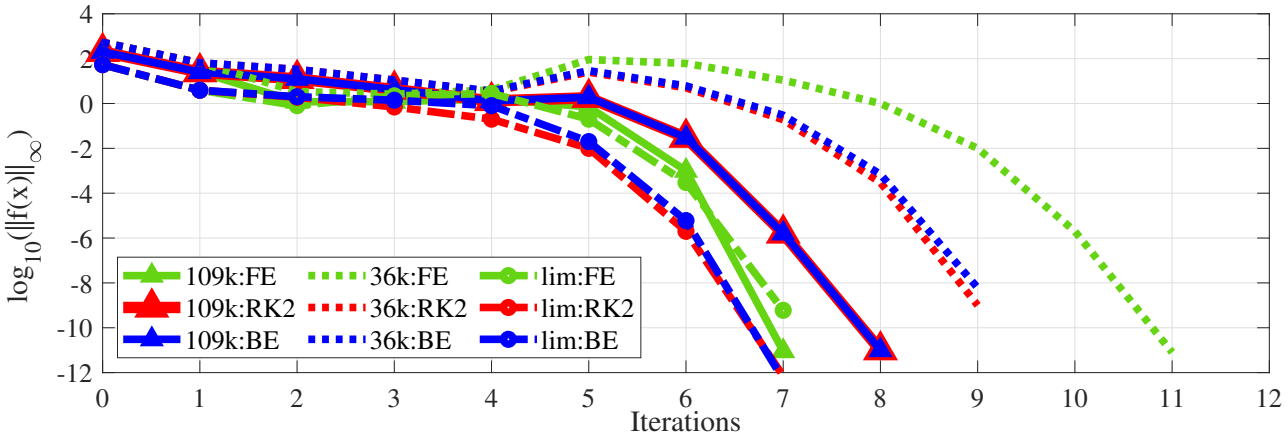

(c) Pathway with $t_3 = 0.30$

Figure 6.4: Plots indicating the evolution of the infinite norm of the PFP mismatches for three test systems when the NR solver is initialized by an explicit (FE or RK2) or implicit (BE) integration scheme, considering the homotopy pathway with five points, but only the instant t_3 is changed

We can observe that from the results of the several sets of experiments performed with proportional increment for Δt_0 and K, only the BE scheme was able to present a suitable approximation to the NR solver for all situations. The schemes FE and RK2 had an adequate

Table 6.7: Mean CPU time in seconds for running experiments whose results were presented in the plots of Figure 6.4

METHOD	t_3	CASES					
		`case109272`		`case36964`		`case_ACTIVSg2000limit`	
NR-MAT	-	3.8889	(100%)	1.8862	(100%)	0.3100	(100%)
FE	0.20	5.6750	(146%)	3.3580	(178%)	0.2120	(68%)
	0.25	5.6500	(145%)	fail	(-)	0.2340	(75%)
	0.30	6.6210	(170%)	3.3680	(179%)	0.2240	(72%)
RK2	0.20	8.9580	(230%)	4.3800	(232%)	0.2550	(82%)
	0.25	8.7950	(226%)	3.5900	(190%)	0.2610	(84%)
	0.30	9.2150	(237%)	3.6770	(195%)	0.2270	(73%)
BE	0.20	6.6550	(171%)	2.7160	(144%)	0.1890	(61%)
	0.25	6.6540	(171%)	2.7110	(144%)	0.2500	(81%)
	0.30	6.5690	(169%)	2.7860	(148%)	0.2900	(94%)

performance only for a larger number of points in the homotopy pathway. Yet, it required considerably small time steps for the initial time instants. This requirement was not essential when using the implicit BE method, except when considering the instant t_1. It was verified that when many points of the homotopy pathway are used, all integration methods provide almost similar performance for searching a good initialization $\hat{\mathbf{x}}^{(0)}$. On the other hand, a large number of points must only be used if obtaining an adequate solution is unfeasible; that is not the situation verified since the implicit scheme BE proved to be efficient for starting the NR and FDXB solvers even with three points (say, instants $\{0;\ t_1;\ 1.0\}$) in the homotopy pathway.

The simulations were also assessed by increasing the values of K to 0.002 and Δt_0 to 0.1 while keeping the perturbation δ at 0.02. However, the large value of Δt_0 did not contribute effectively to determining a suitable approximation of states $\hat{\mathbf{x}}^{(0)}$, which made it impossible to properly initialize the NR and FDXB schemes. When using the dynamical homotopy-based scheme for simulation, it is crucial to take into account not just the parameter δ, but also the initial time-step Δt_0 to obtain a suitable initialization $\hat{\mathbf{x}}^{(0)}$. Once this is achieved, the factor K can be calculated.

The influence of the time-step length was investigated for the largest power system model. Figure 6.5 exhibits results for the backward Euler's integration method simulations for a given constant K. For these experiments, K was set at 0.00015.

Two types of fixed time-step lengths, Δt_0 and Δt, were admitted again. The former was

fixed at the beginning of the transient in a small value because of the selected explicit integration method. So, Δt_0 was fixed in 0.005, while the user can assign Δt according to the study.

For the experiments and plots shown in Figure 6.5, the constant values for Δt were assigned in the values 1.0, 0.5, 0.25, 0.1, and 0.01. The computation of the last point, in $t = 1$, is performed for a reduced step-time $(\Delta t - \Delta t_0)$ to prevent t exceeding the value 1.

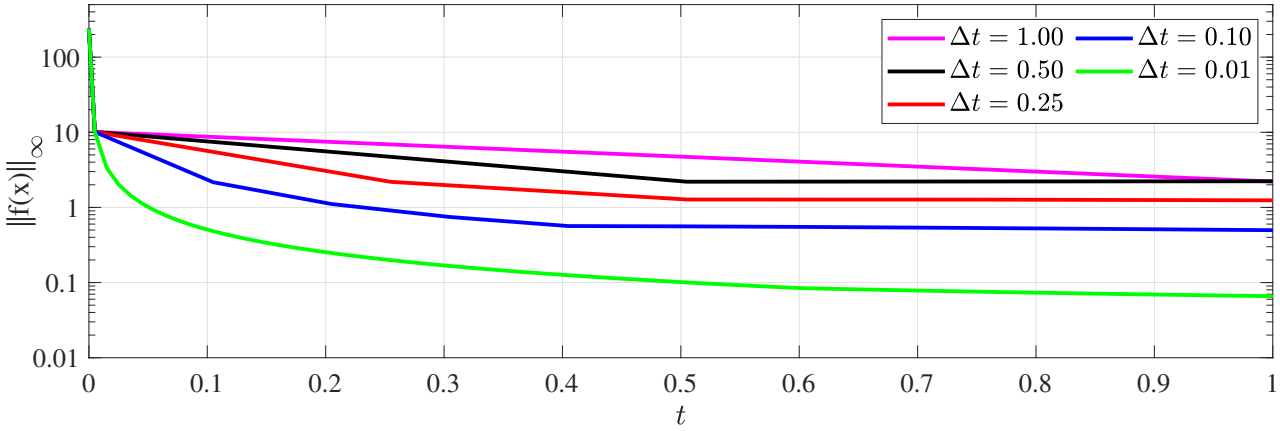

Figure 6.5: Euler's method results for $\Delta t_0 = 0.005$, $K = 0.00015$ and different Δt for the mismatch of the case_ACTIVSg70k

In order to achieve high accuracy in the numerical integration process shown in Figure 6.5, it is necessary to use a significantly smaller time step Δt to obtain a more accurate transient at the time $t = 1$ (as depicted by the green curve). Hence, the best performance was achieved with a value of 0.01 among the different time step lengths tested. This means that more time points are needed in the time range between 0 and 1. However, using more time points requires more LU factorizations, increasing the computational time for the PFP. The question is whether the accuracy of the result obtained at time 1.0 is sufficient for the refined result produced by the NR solver to converge adequately. Hence, based on the plots, it may be acceptable to compute an imprecise solution at the end of the transient at $t = 1$ and employ this estimate as the initial approximation for the NR method to obtain a highly accurate solution.

The choice of Δt_0 and Δt for calculating the curve points in the numerical integration method influences the determination of the norm value in $t = 1$. Consequently, it may impact the result that the NR method will refine at the end. The following experiments (see Figure 6.6) intend to show results explaining the choice of the Δt_0 value. When using the Backward Euler's method, very high or very low values of this parameter may lead to significant mismatches at $t = 1$.

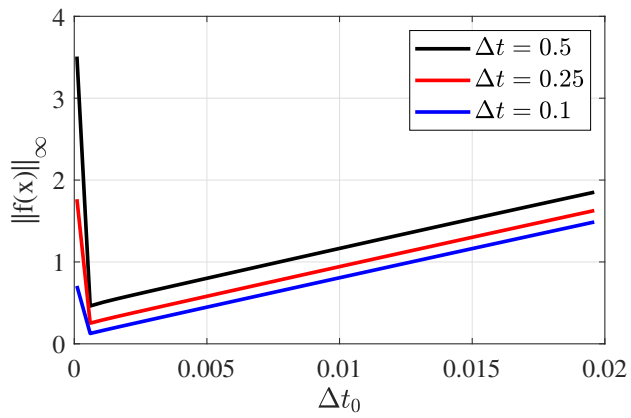

(a) `case3012wp`: Norm in $t = 1$, where $||\mathbf{f}(x^{(0)})||_\infty = 818$, $K = 0.005$

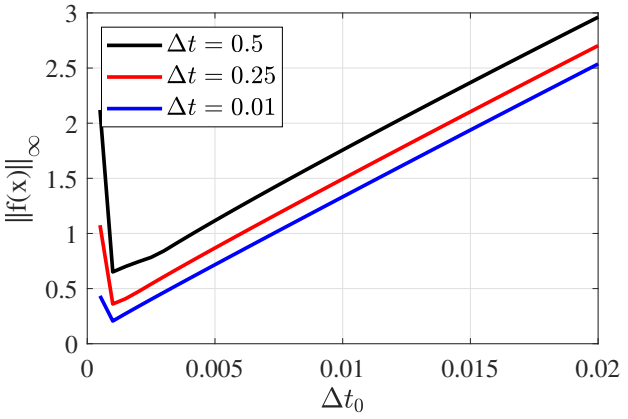

(b) `case3375wp`: Norm in $t = 1$, where $||\mathbf{f}(x^{(0)})||_\infty = 1449$, $K = 0.005$

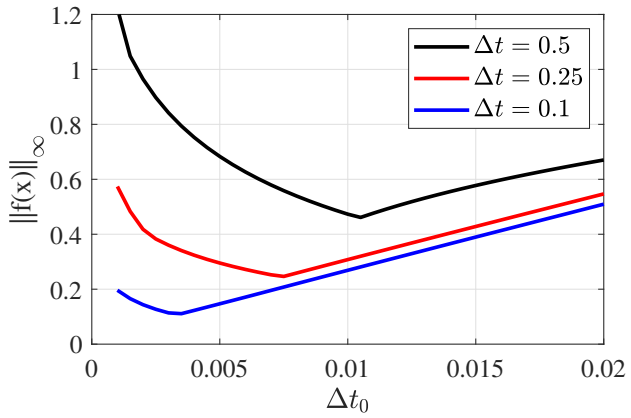

(c) `case13659pegase`: Norm in $t = 1$, where $||\mathbf{f}(x^{(0)})||_\infty = 201$, $K = 0.005$

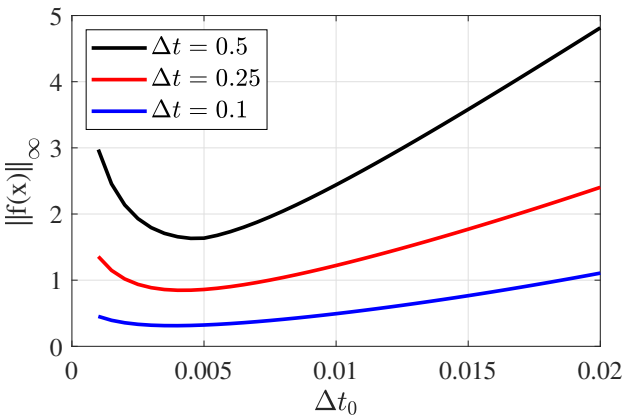

(d) `case_ACTIVSg70k`: Norm in $t = 1$, where $||\mathbf{f}(x^{(0)})||_\infty = 239$, $K = 0.00015$

Figure 6.6: Norm of mismatches calculated by the homotopy transient-based technique for the ill-posed systems, in $t = 1$, as a function of Δt_0, for specific step-lengths Δt and a given K

To demonstrate the influence of Δt_0 and Δt in the dynamical homotopy-based approach, the experiments were performed in the four ill-conditioned systems, *i.e.*, `case3012wp`, `case3375wp`, `case13659pegase`, and `case_ACTIVSg70k`. Again, the initial time-step was assigned to compute the instant t_1 of the curve; and a constant time-step Δt is given to determine the other discrete points t_i of the transient curve up to $t = 1$.

To assess the sensitivity of selecting Δt_0, the experiments were conducted by varying its value from 0 to 0.02. The norm was verified of $\mathbf{f}(\mathbf{x})$ for a given K and three different Δt values: 0.5, 0.25, and 0.01.

The norm value of the homotopy numerical integration result in $t = 1$ was monitored and plotted. This is the value of interest to be refined by the NR solver. The four test systems' results are exhibited in Figure 6.6 as several plots. The initial norm value, computed for

$\mathbf{x}^{(0)}$ (initial maximum mismatch), ranges from 201 for the `case13659pegase` to 1449 for the `case3375wp`. Despite these very high values, the norms at the end of the transient, in $t = 1$, reach values below the unity for certain values of time-step Δt_0, even in the worst case for the time-step Δt selected. Other studies were carried out with different values for K, and similar results profiles were obtained for the Δt_0 value ranges.

Another set of experiments using FPV-BE$_{(\mathrm{NR})}$ and FPV-RK2$_{(\mathrm{NR})}$ were carried out modifying the time-step Δt from 0.1 to 1.0, keeping K constant 1×10^{-4}.

Table 6.8 details the data and obtained results for the two largest models. In the 2^{nd} and 3^{rd} columns, the values for K and Δt are indicated. Further columns show the number of transient curve points and iterations for refining the solution by the NR solver. The results indicate that the dynamic homotopy-based approach, using BE method, achieved satisfactory convergence for systems, as demonstrated in the 6^{th} column of the table. However, the solver for RK2 fails to yield appropriate results for refining the solution in certain Δt values, as evidenced by the total iterates showing SR.

Variable monitoring was assessed to verify the evolution of a state along the homotopy transient (dotted line) and the NR scheme iterations (full line) in refining the low-precision solution obtained by the homotopy transient-based approach. The parameters in this simulation are those used in Table 6.8. Therefore, $K = 1 \times 10^{-4}$ and Δt changes according to the data in 3^{rd} column. The solvers BE and RK2 were considered. The simulations were carried out in the `case109272`. The voltage magnitude and angle in bus #6 were monitored and visualized in Figure 6.7 and Figure 6.8. The plots' dotted lines represent the homotopy transient produced by the points using the BE and RK2 solvers. The full lines begin where the dotted lines end in the plot. For better clarification, consider the step-length $\Delta t = 1$ and the voltage magnitude and angle curves. For this example, the dotted lines reach point 2 in the "Iterations" scale. The result is due to the starting from flat start (bus #6 is a PQ-type), contributing to $V(0) = V^{(0)} = 1$ pu and $Angle(0) = Angle^{(0)} = 0°$. The next points are computed for $t_1 = \Delta t_0$ and $t_2 = (\Delta t - \Delta t_0)$. The t_2 in the plots corresponds to "Iterations(2)". The dotted plot ends and starts the full line plot, corresponding to the NR solver effective iterations. This latter part of the plot goes from Iterations(2) to Iterations(6). Visualizing these transitions for all Δt is better exhibited in the angle curves. A similar procedure can be explained for other Δt.

Table 6.8: Performance of FPV homotopy function varying the time-step Δt keeping $K = 1 \times 10^{-4}$

			Test #3: FPV-BE$_{(NR)}$			Test #4: FPV-RK2$_{(NR)}$		
CASE	K	Δt	iter$_{BE}$	iter$_{NR}$	iter$_{T}$	iter$_{RK2}$	iter$_{NR}$	iter$_{T}$
	1×10^{-4}	1.0	2	4	6	2	5	7
	1×10^{-4}	0.5	3	3	6	3	4	7
case13659pegase	1×10^{-4}	0.25	5	3	8	5	4*	SR
	1×10^{-4}	0.125	9	3	12	9	4	13
	1×10^{-4}	0.1	11	3	14	11	4	15
	1×10^{-4}	1.0	2	5	7	2	x	SR
	1×10^{-4}	0.5	3	4	7	3	x	SR
case_ACTIVSg70k	1×10^{-4}	0.25	5	4	9	5	5	10
	1×10^{-4}	0.125	9	4	13	9	4	13
	1×10^{-4}	0.1	11	4	15	11	4	15
	1×10^{-4}	1.0	2	4	6	2	7*	SR
	1×10^{-4}	0.5	3	4	7	3	6*	SR
case36964	1×10^{-4}	0.25	5	4	9	5	5*	SR
	1×10^{-4}	0.125	9	3	12	9	4*	SR
	1×10^{-4}	0.1	11	3	14	11	4	15
	1×10^{-4}	1.0	2	4	6	2	5	7
	1×10^{-4}	0.5	3	3	6	3	4	7
case109272	1×10^{-4}	0.25	5	3	8	5	4*	SR
	1×10^{-4}	0.125	9	3	12	9	4	13
	1×10^{-4}	0.1	11	3	14	11	4	15

x: divergence; * unstable point; SR: senseless result.

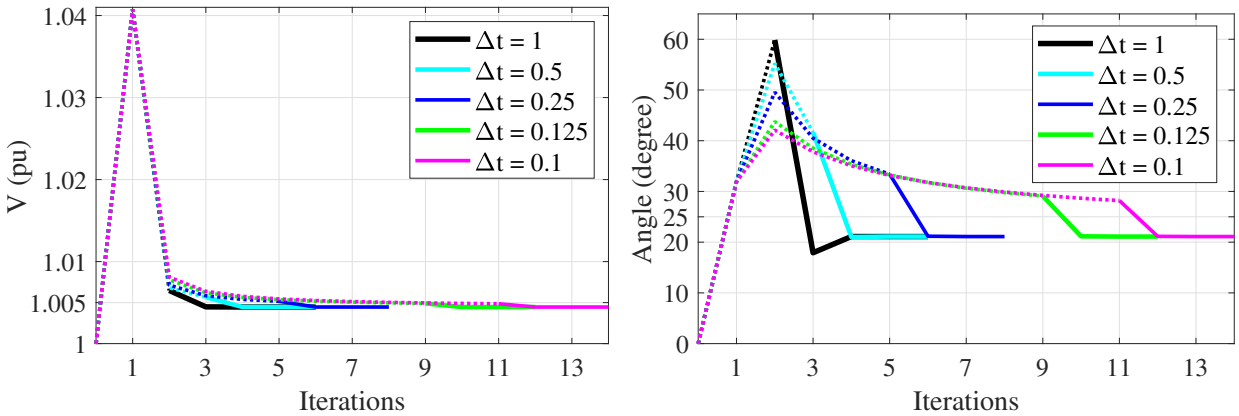

(a) Test #3: FPV-BE$_{(NR)}$ (b) Test #3: FPV-BE$_{(NR)}$

Figure 6.7: Bus-6 of case109272, with different Δt solved by backward Euler's method (dotted line) and Newton-Raphson's method (solid line)

Note that the converged values occur for the same values in the visualization of the plots, regardless of the time-step Δt.

In Figure 6.8, similar results are shown for test using the RK2 solver. However, for the

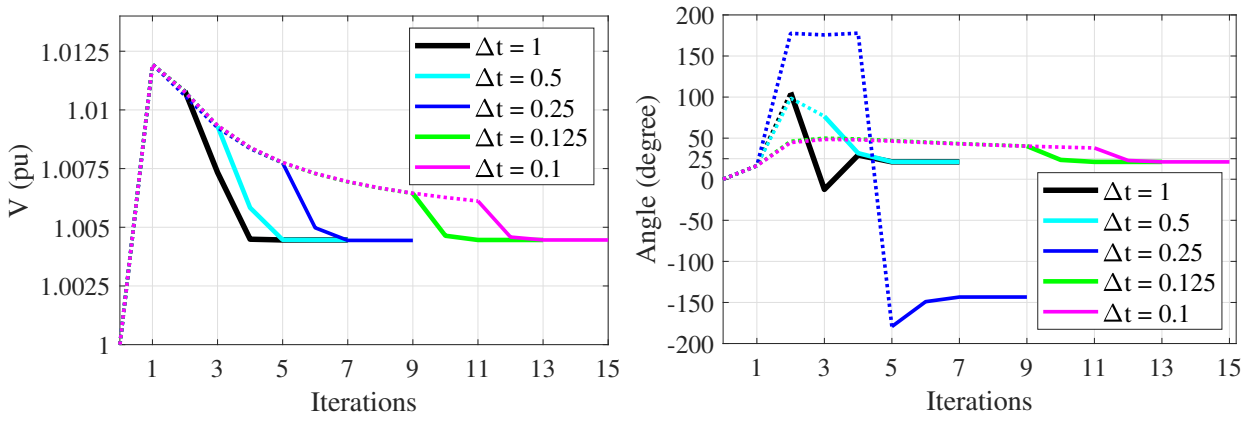

(a) Test #4: FPV-RK2$_{(NR)}$ (b) Test #4: FPV-RK2$_{(NR)}$

Figure 6.8: Bus-6 of `case109272`, with different Δt solved by Runge-Kutta's method (dotted line) and Newton-Raphson's method (solid line)

case $\Delta t = 0.25$ (blue plots), there is evidence of incorrect convergence of the NR. Although the voltage magnitude converges to the correct value after refining the result, the same result was not obtained for the angle. We can see that the NR solver for "Iterations(5)" starts from a value of approximately -175 degrees and converges to about -150 degrees, which is far from the correct value of approximately 25 degrees. The result confirms the evidence mark "SR" assigned in Table 6.8 when $\Delta t = 0.25$ is used.

In the next set of experiments, the backward Euler's and second-order Runge-Kutta's methods were employed for other numerical integration strategies involving options of discrete time t_i, $i = 0,1,\ldots,N$, and time-step lengths Δt_0, Δt, and changing in the parameter K. Experiments were carried out for different test systems. Tables 6.9, 6.10, 6.11, 6.12, and 6.13 depict the simulations results.

Table 6.9 exhibits results in which Δt is kept constant in 0.25, while K is changed in the range 1×10^{-7} to 1×10^{-2}. It is verified that values of K smaller than 1×10^{-4} are inappropriate for Euler's solver. For the `case_ACTIVSg70k`, values greater than 1×10^{-3} also lead to convergence failure. From the table, again, was concluded by the adequate convergence of the NR solver when backward Euler's dynamic homotopy scheme is employed, even for small time-step Δt.

Figure 6.9(a) shows a plot for magnitude and Figure 6.9(b) phase angle of nodal voltage in some buses of the 70,000-bus system with a step $\Delta t_0 = 0.005$, $\Delta t = 0.25$, and $K = 10^{-4}$, using the Euler's method for the FPV homotopy approach. The transient response of a state reaches

Table 6.9: Performance of FPV homotopy function varying K for a step $\Delta t = 0.25$

			Test #5: FPV-BE$_{(NR)}$			Test #6: FPV-RK2$_{(NR)}$		
CASE	K	Δt	iter$_{BE}$	iter$_{NR}$	iter$_{T}$	iter$_{RK2}$	iter$_{NR}$	iter$_{T}$
case13659pegase	1×10^{-2}	0.25	5	4	9	5	5*	SR
	1×10^{-3}	0.25	5	3	8	5	5*	SR
	1×10^{-4}	0.25	5	3	8	5	4*	SR
	1×10^{-5}	0.25	5	4*	SR	5	4*	SR
	1×10^{-6}	0.25	5	3*	SR	5	4	9
	1×10^{-7}	0.25	5	x	SR	5	4*	SR
case_ACTIVSg70k	1×10^{-2}	0.25	5	x	SR	5	x	SR
	1×10^{-3}	0.25	5	4	9	5	5	10
	1×10^{-4}	0.25	5	4	9	5	5	10
	1×10^{-5}	0.25	5	x	SR	5	x	SR
	1×10^{-6}	0.25	5	x	SR	5	x	SR
	1×10^{-7}	0.25	5	x	SR	5	x	SR
case36964	1×10^{-2}	0.25	5	4	9	5	x	SR
	1×10^{-3}	0.25	5	4	9	5	5	10
	1×10^{-4}	0.25	5	4	9	5	5*	SR
	1×10^{-5}	0.25	5	x	SR	5	x	SR
	1×10^{-6}	0.25	5	x	SR	5	x	SR
	1×10^{-7}	0.25	5	x	SR	5	x	SR
case109272	1×10^{-2}	0.25	5	4	9	5	7*	SR
	1×10^{-3}	0.25	5	3	8	5	SR	SR
	1×10^{-4}	0.25	5	3	8	5	4*	SR
	1×10^{-5}	0.25	5	3*	SR	5	4*	SR
	1×10^{-6}	0.25	5	3*	SR	5	4*	SR
	1×10^{-7}	0.25	5	x	SR	5	4*	SR

x: divergence; * unstable point; SR: senseless result.

an accurate result for the voltage magnitude basically for the two points of the transient-based approach (see dotted curves Figure 6.9(a)). The phase angles (see dotted curves in Figure 6.9(b)) need refinement that the NR solver provides. The accuracy of the states is improved by the NR method (solid lines). Again, the contribution of the transient-based result participation on calculating the PFP solution is surprisingly good since we are dealing with an ill-conditioned and large-scale system. We emphasize that the pure NR solver cannot solve the PFP when departing straightforwardly from a flat start estimation.

Experiments with different steps Δt_i along the points of the transient-based curve were carried out. The step lengths $\Delta t_0 = 0.005$, $\Delta t_1 = 0.025$, and $\Delta t_2 = 0.97$ were adopted to obtain the three points $t_1 = 0.005$, $t_2 = 0.03$, $t_3 = 1$. Table 6.10 depicts the results for $K = 10^{-4}$

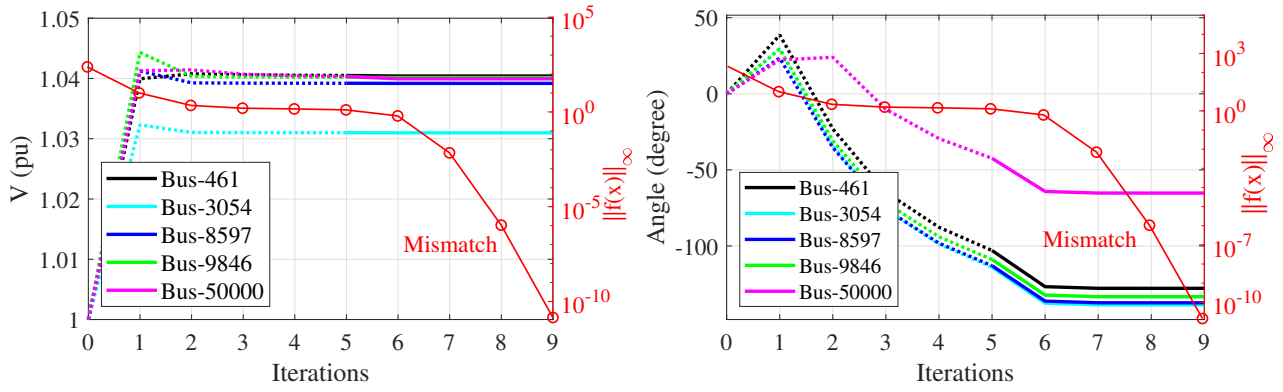

(a) Voltage Magnitude Test #5: FPV-BE$_{(\mathrm{NR})}$ (b) Voltage angle Test #5: FPV-BE$_{(\mathrm{NR})}$

Figure 6.9: Trajectories along the homotopy process for the bus voltage `case_ACTIVSg70k`, with the first iterates obtained applying the transient-based approach with Euler's method (dotted line) for $\Delta t = 0.25$ and $K = 1 \times 10^{-4}$ and the others points refined with Newton-Raphson's method (solid line)

two cases. Considering only the largest system, the RK2 scheme presented convergence for the transient-based stage. In the refinement phase, the NR solver demanded 5 iterates for convergence. In tests with smaller points, the convergence was impossible with just 2 points. However, the BE method performed better than the RK scheme, requiring 3 discrete points in the transient-based stage and just 4 iterations in the refining NR scheme.

Table 6.10: Performance of the FPV for three different time-steps, $\Delta t_0 = 0.005$, $\Delta t_1 = 0.025$, and $\Delta t_2 = 0.97$

			FPV-BE$_{(\mathrm{NR})}$			FPV-RK2$_{(\mathrm{NR})}$		
CASE	K	Δt	iter$_{\mathrm{BE}}$	iter$_{\mathrm{NR}}$	iter$_{\mathrm{T}}$	iter$_{\mathrm{RK2}}$	iter$_{\mathrm{NR}}$	iter$_{\mathrm{T}}$
case13659pegase	1×10^{-4}	Δt_1 and Δt_2	3	3	6	3	4	7
case_ACTIVSg70k	1×10^{-4}	Δt_1 and Δt_2	3	4	7	3	5	8

Simulations that also consider several methods were assessed. The aim was to use other methods different from the NR solver as done in the previous simulations. For these experiments were considered some ill-conditioned systems available on MATPOWER, some ill-conditioned systems available on Tostado-Véliz *et al.* (2019c), and stressed power systems available on Tostado-Véliz *et al.* (2019d). Here, the experiments for obtaining the low-precision solution via dynamic homotopy method were carried out by employing the BE method and RK2, both with time-step $\Delta t = 1$. With these partial results, the methods NR, FDXB (NR fast decoupled), HKW, and RK4 were used to refine the low-accuracy results.

Table 6.11 shows the results in terms of iterations for the convergent cases. The 2^{nd} column in the table is the number of iterations required for the NR solver to reach the convergence,

Table 6.11: Number of total iterations (iter_T), with $\Delta t = 1$, solved by FPV-BE and FPV-RK2 with high accuracy step as NR, FDXB, HKW, RK4

CASE	NR	FPV-BE$_{(\text{NR})}$		FPV-RK2$_{(\text{NR})}$		FPV-BE$_{(\text{FDXB})}$		FPV-RK2$_{(\text{FDXB})}$		FPV-BE$_{(\text{HKW})}$		FPV-RK2$_{(\text{HKW})}$		FPV-BE$_{(\text{RK4})}$		FPV-RK2$_{(\text{RK4})}$	
	MAT	K	iter_T	K	iter_T	K	iter_T	K	iter_T	K	iter_T	K	iter_T	K	iter_T	K	iter_T
case3012wp	3	1×10^{-2}	5	1×10^{-2}	6	1×10^{-2}	21	1×10^{-2}	25	1×10^{-2}	10	1×10^{-2}	10	1×10^{-2}	24	1×10^{-2}	30
case3375wp	4	1×10^{-2}	5	1×10^{-2}	6	1×10^{-2}	21	1×10^{-2}	25	1×10^{-2}	10	1×10^{-2}	10	1×10^{-2}	25	1×10^{-2}	31
136590pegase	5	1×10^{-4}	6	1×10^{-3}	8	1×10^{-2}	33	1×10^{-2}	21	1×10^{-2}	SR	1×10^{-2}	SR	1×10^{-4}	25	1×10^{-2}	29
ACTIVSg70k	6	1×10^{-3}	7	1×10^{-3}	10*	1×10^{-3}	36	1×10^{-3}	37	1×10^{-2}	SR	1×10^{-2}	SR	1×10^{-3}	26	1×10^{-3}	31*
case18482	6	1×10^{-2}	6	1×10^{-3}	6	1×10^{-2}	35	1×10^{-2}	43	1×10^{-2}	8	1×10^{-3}	8	1×10^{-2}	25	1×10^{-2}	30
case27318	5	1×10^{-4}	6	1×10^{-4}	7	1×10^{-3}	31	1×10^{-2}	31	1×10^{-4}	9	1×10^{-2}	9	1×10^{-4}	25	1×10^{-2}	29
case36964	6	1×10^{-3}	6	1×10^{-3}	10*	1×10^{-2}	35	1×10^{-2}	43	1×10^{-4}	8	1×10^{-3}	12*	1×10^{-3}	26	1×10^{-2}	32*
case54636	5	1×10^{-4}	6	1×10^{-4}	7	1×10^{-4}	31	1×10^{-2}	31	1×10^{-4}	9	1×10^{-2}	9	1×10^{-4}	25	1×10^{-2}	29
case109272	5	1×10^{-4}	6	1×10^{-4}	7	1×10^{-3}	31	1×10^{-2}	31	1×10^{-4}	9	1×10^{-2}	9	1×10^{-4}	25	1×10^{-2}	29
case300	5	1×10^{-2}	6	1×10^{-2}	6	1×10^{-2}	29	1×10^{-2}	21	1×10^{-2}	9	1×10^{-2}	9	1×10^{-2}	23	1×10^{-2}	26
case69limit	4	1×10^{-2}	4	1×10^{-2}	5	1×10^{-4}	22	1×10^{-4}	32	1×10^{-2}	5	1×10^{-2}	6	1×10^{-5}	11	1×10^{-3}	16
case141limit	3	1×10^{-2}	4	1×10^{-2}	5	1×10^{-5}	16	1×10^{-2}	26	1×10^{-2}	5	1×10^{-2}	6	1×10^{-5}	11	1×10^{-2}	16
500limit	3	1×10^{-2}	5	1×10^{-2}	5	1×10^{-4}	14	1×10^{-2}	15	1×10^{-4}	5	1×10^{-2}	8	1×10^{-4}	16	1×10^{-2}	25
2000limit	3	1×10^{-2}	6	1×10^{-2}	6	1×10^{-3}	24	1×10^{-2}	26	1×10^{-2}	8	1×10^{-2}	9	1×10^{-3}	21	1×10^{-2}	27

$\star$: $\Delta t = 0.25$

assuming initial conditions assigned in the MATPOWER. From the 3^{th} column to 18^{th}, there are results concerning the NR, FDXB, HKW and RK4. We can observe that the NR, FDXB, and RK4 solver converges for all test systems when the low-accuracy result is obtained by the EU and RK2 approach. Similar results are verified for the RK4 and HKW solvers, but when the HKW is used as the method for the low-accuracy, the method presents Senseless Result (SR) for tested systems `case136590pegase` and `case_ACTIVSg70k`. Figure 6.10 illustrate `case18482` from Table 6.11 with different mismatches along the convergence curve.

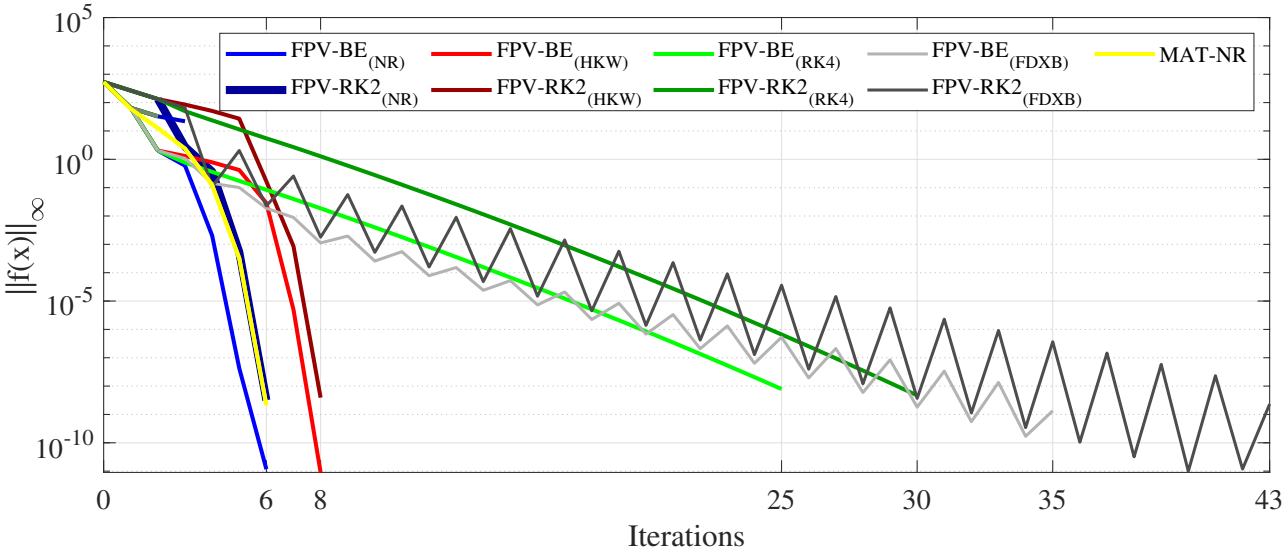

Figure 6.10: Mismatches regarding approaches of nine simulations presented in Table 6.11 for the `case18482`

Simulations were performed for the high time-step dynamic homotopy process for all ill-conditioned test systems. In this experiments, a time-step $\Delta t = 1$ was used for the homotopy path curve $\gamma(t)$, $0 \leq t \leq 1$, and $K = 1 \times 10^{-4}$. Then, considering the initial time-step

Δt_0, the homotopy path has $N = 2$ points. The BE method was employed to determine the solution of the dynamic homotopy at the point $k = 2$ or approximately $t = 1$. The states obtained in this point were used as initial estimates for the NR solver. The combination of all results was presented in plots of some states and the power mismatch for each iteration in the combined processes. Figure 6.11 exhibits the plots of some states and the power mismatch along the iterations for the 109,272-bus system. Figure 6.11(a) is the voltage magnitude, and Figure 6.11(b) is the phase angle for the buses 2 to 6. It is possible to observe the evolution of the mismatch $||\mathbf{f}(\mathbf{x})||_\infty$ as the states start from the initial flat voltage estimate and, at each iteration, converge to the solution of the problem. The dotted-line in the plot represents two iterations of BE method, which in the second iteration has voltage magnitude with low accuracy, on the order of 1×10^0 pu. Also, the mismatch is in order 1. From the second iteration in the plot, it is activated the NR solver demands only four iterations to reach convergence (see dotted lines for the states), and the mismatch falls from 1 to smaller than 10^{-8} pu.

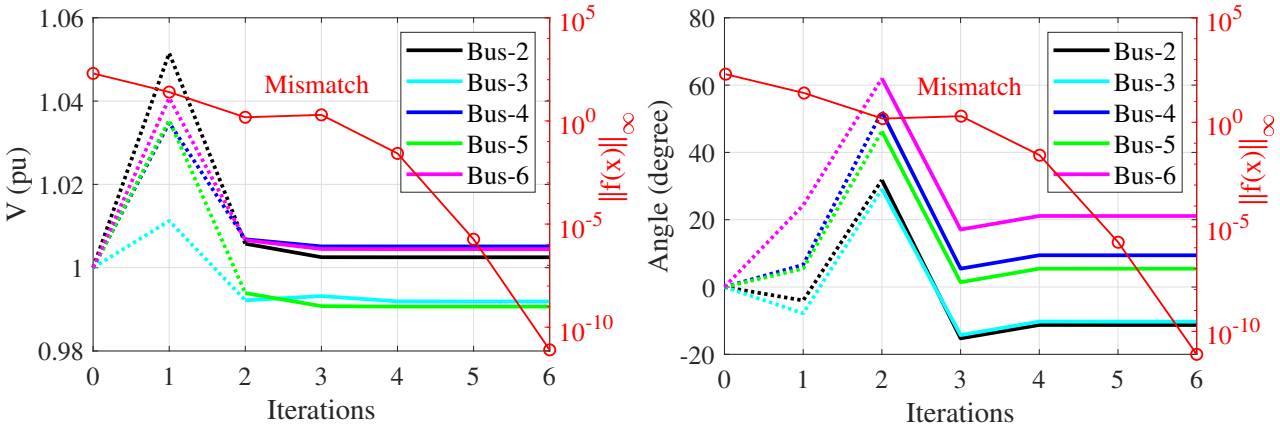

(a) Voltage magnitude for $\Delta t = 1.0$ and $K = 1 \times 10^{-4}$ (b) Voltage angle for $\Delta t = 1.0$ and $K = 1 \times 10^{-4}$

Figure 6.11: `case109272`, BE method (dotted line) and Newton-Raphson's method (solid line)

We can state that although the initial method obtained low accuracy, this step expanded the attraction region. And the NR solver acted to find an accurate solution to the PFP.

Furthermore, to demonstrate the importance of adjusting the homotopy steps appropriately, the `case36964`, for instance, converges with seventeen iterations in total with the parameters $\Delta t = 0.1$ using RK2 and HKW. The first ten iterations follow the homotopy steps and are solved in this case using RK2. The last seven iterations seek high accuracy using the HKW method, thus totaling seventeen iterations. Figure 6.12(a) demonstrates the convergence to the correct solution, represented by the asterisk element (*) in the figure. However, with $\Delta t = 0.5$, despite

obtaining the desired mismatch, it converges to the wrong solution. Note that the voltage angle of each bus in Figure 6.12(b) does not converge to the correct answer, represented by the asterisk (*).

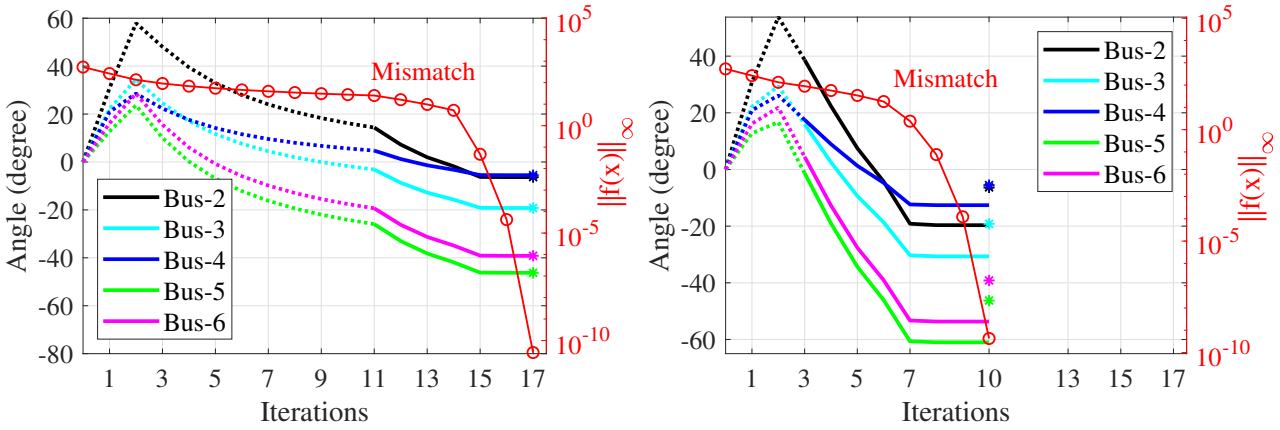

(a) Voltage angle for $\Delta t = 0.1$ converging on the right solution

(b) Voltage angle for $\Delta t = 0.5$ converging on the wrong solution

Figure 6.12: `case36964`, Runge-Kutta second-order method (dotted line) and Heun-King-Werner method (solid line)

6.5.2 Execution time for some solver using FPV

The performance of the proposed method was evaluated by measuring the execution time of calculations for simulations on the two tested systems (13,659- and 70k-bus systems). The experiments were assessed for the static homotopy method (GSH-NR), for the dynamical FPV homotopy approach combined with the refined solution of the NR method, as done in Test #1 and Test #6. Additionally, the CPU time demanded computing the PFP solution by the NR method, NR-MAT, having the initialization used in MATPOWER was performed. Table 6.12 shows the execution time in seconds in the 2^{nd}, 3^{rd}, 4^{th}, and 5^{th} columns. It is confirmed that

Table 6.12: Mean CPU Time in seconds for running experiments considering the two largest test systems

CASE	GSH-NR	Test #1: FPV-BE$_{(NR)}$	Test #6: FPV-RK2$_{(NR)}$	NR-MAT
case13659pegase	1.9750	0.6870 (35%)	1.4840 (75%)	0.5000 (25%)
case_ACTIVSg70k	25.0740	4.4300 (18%)	9.4080* (38%)	3.0100 (12%)

*$K = 1 \times 10^{-3}$

the GSH-NR method (see 2^{nd} column for the percent base of time) is by far the most expensive. In contrast, the CPU time for the NR solver with initialization given in MATPOWER is the

one that requires less computational time (5^{th} column). However, the proposed transient-based approach plus refinement of the solution by the NR method (see 3^{rd} column) has a computational cost almost similar to the MATPOWER's reference burden when Euler's scheme is employed. Therefore, although the RK's scheme presents a computational demand smaller than the GSH-NR, it is greater than Euler's transient-based FPV homotopy approach. This fact is justified because, in addition to giving less LU factorization per calculated point, the Euler method furnishes a better approximation of the low-accuracy solution for the initialization of the NR method in the refinement step. All simulations were performed using $K = 1 \times 10^{-4}$, except the `case_ACTIVSg70k` with Test #6: FPV-RK2$_{(\text{NR})}$ (3^{rd} line and 4^{th} column) that uses $K = 1 \times 10^{-3}$. Notwithstanding, we emphasize that MATPOWER's calculation uses an initial estimate assigned in the neighborhood of the solution. At the same time, the other results are obtained from a flat start estimate, which does not allow for convergence for the NR method without the transient-based approximated states for tested systems.

The CPU time for the NR solver with initialization given in MATPOWER is the one that requires less computational time (2^{nd} method) as can be seen at Table 6.13. However, the pro-

Table 6.13: Mean CPU Time in seconds for running experiments considering some test systems

	CASES									
METHOD	case109272		case54636		case36964		case27318		case18482	
NR-MAT	3.8889	(100%)	2.1236	(100%)	1.8862	(100%)	0.8912	(100%)	0.8241	(100%)
FPV-BE$_{(\text{NR})}$	4.2730	(110%)	2.1840	(103%)	1.7260	(92%)	1.1430	(128%)	0.9040	(110%)
FPV-RK2$_{(\text{NR})}$	6.3920	(164%)	3.1070	(146%)	4.1100	(218%)	1.6240	(182%)	1.1630	(141%)
FPV-BE$_{(\text{FDXB})}$	2.6890	(69%)	1.4070	(66%)	1.0840	(57%)	0.7560	(85%)	0.6250	(76%)
FPV-RK2$_{(\text{FDXB})}$	4.1690	(107%)	2.0840	(98%)	1.5890	(84%)	1.0600	(119%)	0.9160	(111%)
FPV-BE$_{(\text{HKW})}$	9.1300	(235%)	4.5840	(216%)	2.9980	(159%)	2.2600	(254%)	1.4240	(173%)
FPV-RK2$_{(\text{HKW})}$	9.9470	(256%)	4.6800	(220%)	5.2420	(278%)	2.3260	(261%)	1.6950	(206%)
FPV-BE$_{(\text{RK4})}$	66.7260	(1716%)	31.7030	(1493%)	26.6220	(1411%)	15.7050	(1762%)	12.2930	(1492%)
FPV-RK2$_{(\text{RK4})}$	79.5310	(2045%)	38.9190	(1833%)	28.9193	(1533%)	19.0950	(2143%)	14.7610	(1791%)

posed transient-based approach plus refinement of the solution by the NR method (see 2^{nd} and 3^{rd} method) has a computational cost almost similar to the MATPOWER's reference burden when Euler's scheme is employed. It is worth highlighting the FDXB method (see 4^{th} method), which has a lower computational cost than the reference method (NR-MAT), despite obtaining the result with many iterations. Therefore, although the RK's scheme presents a computational demand smaller than the GSH-NR, it is greater than Euler's transient-based FPV homotopy approach. This fact is justified because, in addition to giving less LU factorization per calculated point, Euler's method furnishes a better approximation of the low-accuracy solution for

the initialization of the NR method in the refinement step. Notwithstanding, we emphasize that MATPOWER's calculation uses an initial estimate assigned in the neighborhood of the solution. At the same time, the other results are obtained from a flat start estimate, which does not allow for convergence for the NR method without the transient-based approximated states.

6.6 CONTINGENCY STUDIES

This subsection presents contingency studies considering simulations with the proposed dynamical homotopy-based technique (FPV) applied for the PFP. The type of simulations is more stringent and agrees with practical situations where high loading of the networks is inherent. Experiments were carried out only in the system (70k-bus model), given the greater complexity of the electrical grid. The single contingency based on the traditional load rejection, generation rejection, or transmission line (interconnection) removal was assessed.

The experiments consisted in performing contingencies in the ten most considerable power rejected loads/generations or power interruption transmission line outages of the 70k-bus system, followed by running the PFP for three strategies:

i) using the MATPOWER's initial estimate as given in its database;
ii) using the dynamical homotopy-based technique, however only for the base case and applying the result as an initial estimate (refinement by using the classical NR) for the network under contingency; and
iii) performing the dynamical homotopy-based technique under the network in contingency, followed by the refinement of the inaccurate solution by the classical NR.

All computed states for the case of load and generation rejections successfully converged for the three strategies investigated. However, concerning the interconnection contingencies, all the strategies presented similar results for the PFP solution, including the three contingencies that had divergence. Table 6.14 exhibits the ten interconnections of the 70k-bus system with the highest transmission apparent power (4^{th} column) for the base case (2^{nd} and 3^{rd} columns show the interconnection buses) and the PFP convergence status (5^{th} column) according to the removal of a given interconnection.

Table 6.14: Ten most loading interconnections and contingency convergence status

Case	bus k	bus m	S_{km}(MVA)	Convergence
#1	59757	59774	3221	yes
#2	27110	27113	3137	yes
#3	29761	29768	2887	no
#4	26773	26323	2541	yes
#5	59774	59926	2452	yes
#6	24583	24590	2178	no
#7	32502	32508	2155	yes
#8	25706	25709	2093	yes
#9	23638	23645	2092	no
#10	25707	25709	2077	yes

From Table 6.14, the contribution of the dynamical homotopy-based technique to the successful convergence in case of contingencies is evident. In the situations of divergence, as in the cases #3, #6, and #9, the results agree with those obtained using the NR solver with a very close initial estimate given in MATPOWER's database.

6.7 EXPERIMENTS ON THE DYNAMIC HOMOTOPY APPROACH THAT CONSIDERS BOTH NETWORK COMPENSATION AND FPV FUNCTION

This section presents the results of experiments for the dynamic homotopy approach consisting of both network compensation and FPV function. Information, such as the experience obtained from the dynamic homotopy problem with FPV but without the compensation network, is employed in this section. One of them is the employment of learning acquired in the experiments considering the problem without the compensation network. For these, the range of values of K in the easy function $\mathbf{g}_0(\mathbf{x})$ are very useful in the investigations of this section.

Another important conclusion from previous results was that which characterizes an integration method studied. The simulations indicated the BE method as the most suitable for implementing the numerical resolution schemes investigated for the synthetic ODE associated with the power flow problem. Therefore, it will be the only method used in the following simulations.

This section will use the idea already applied to the dynamic homotopy technique without the compensation network to find a low-precision solution at the homotopy path point at $t = 1$.

Then, with the approximate results, an iterative solver, such as NR, will refine the PFP solution with high numerical precision.

6.7.1 Simulations for obtaining high-precision Solution

Experiments were carried out for some ill-conditioned test systems. The objective was first to execute the FPV2 solver to determine the approximated PFP solution at the end of the dynamic homotopy step in $h = 1$. With this aim, an initial time-step was assigned, Δt_0, and increasing it along the homotopy pathway until it reached the final step in $t = 1$. And, at each step t_i, the states were calculated adopting the BE scheme. With these states, a norm for the compensated system is calculated using the scaling factor δ. Table 6.15 depicts the results for the test systems indicated in the 1^{st} column. The table has information on the results for both the FPV2 and NR solvers. From the 2^{nd} to 13^{th} columns, the results refer to the FPV scheme and time instant from 0 to 1, being informed of the respective norms calculated from the states in these points. The last four columns of the table give results obtained for each iteration of the NR solver when it uses the states obtained by the FPV2 in the point $t = 1$. We emphasize that the network in this point is still under the possible influence of the scaling factor δ in the computation of the admittance matrix Y_{bus}. However, when the NR scheme is applied, this effect is no longer considered because the original admittance matrix is assumed. From the 14^{th} to 16^{th} columns, the table yields information regarding the first iterations of the NR. In the last column, the final norm of the converged PFP solution is indicated, and in what iteration was obtained (see the number in parenthesis). The simulations were performed by using $K = 0.0001$ and $\delta = 1$.

Table 6.15: FPV2-BE$_{(\mathrm{NR})}$, $K = 0.0001$, $\delta = 1$

CASE/Time	$\|\|\mathbf{f}(\mathbf{x})\|\|_\infty$ of the Solver												$\|\|\mathbf{f}(\mathbf{x})\|\|_\infty$ NR			
Δt or *iter*	0.0	5×10^{-6}	1×10^{-4}	5×10^{-4}	15×10^{-4}	0.150	0.150	0.150	0.150	0.150	0.150	0.098	1	2	3	last
t	0.0	5×10^{-6}	1.05×10^{-4}	6.05×10^{-4}	0.0021	0.1521	0.3021	0.4521	0.6021	0.7521	0.9021	1				
`case3012wp`	818	818	818	817	815	589	469	347	220	90	44	128	1.326	0.049	2×10^{-5}	1×10^{-11}(4)
`case3012wp`	1449	1449	1448	1448	1445	1057	849	632	405	169	78	236	2.356	0.051	3×10^{-5}	1×10^{-11}(4)
`case_ACTIVSg70k`	239	239	239	239	238	167	131	95	59	24	12	35	6.7426	2.3028	0.0846	6×10^{-10}(5)
`case82k`	1×10^6	1×10^6	1×10^6	1×10^6	1×10^6	1×10^6	8×10^5	6×10^5	3×10^5	1×10^5	1×10^5	2×10^5	3×10^4	1×10^3	1.226	2×10^{-10}(6)

Results in Table 6.15 indicate convergence for the system investigated, including the `case82k`. Note that the norms for the simulations with the FPV2 are elevated in the point $t = 1$. Notably for the `case82k` whose norm is very high. However, despite this, the NR solver still achieves

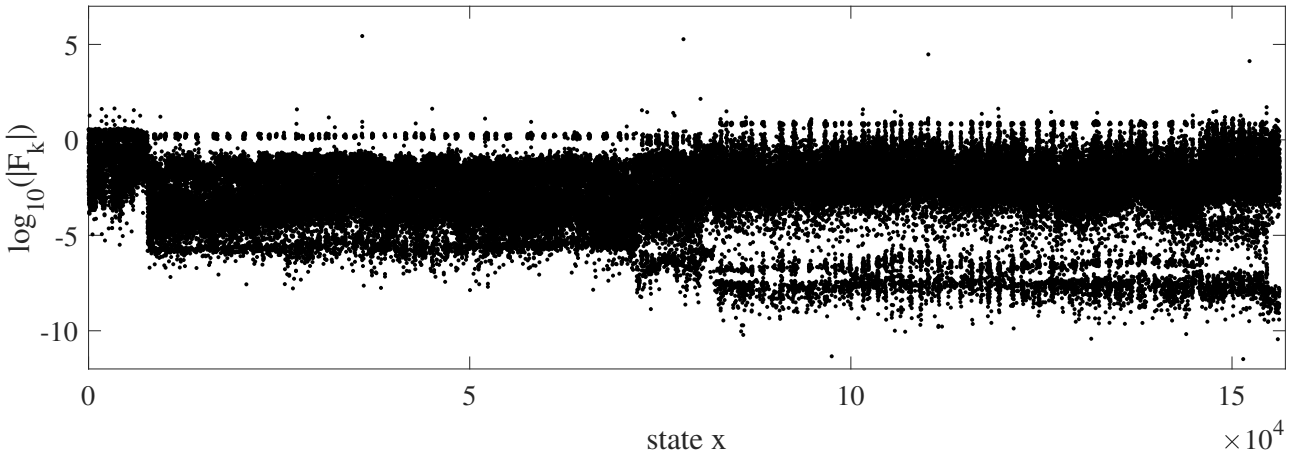

Figure 6.13: Absolute power mismatches computed at the final of the dynamic homotopy by using the FPV2 scheme for the `case82k`

convergence with six iterations. Despite this result of FPV2, a deeper investigation was conducted using the partial states calculated by the FPV2 scheme and the high accuracy refining determined by the NR method. Figure 6.13 shows the distribution of the mismatches (residues) as a function of the states (angle in PV and PQ buses and voltage magnitude in PQ buses) when computed with the result only due to the FPV2 solution. Clearly, only four states have very high norms in the order that are determined after the execution of the FPV2 solver. Most of the points are characterized by good precision, which is reflected in the initial estimate that is handled by the NR solver in Table 6.15. This behavior is also observed when the difference between the high precision states and those calculated in the FPV2 stage is observed. To have this comparison, Figure 6.14 shows results for voltage angle (Figure 6.14(a)) and magnitude (Figure 6.14(b)) for the `case82k`. The proximity between a low- and high-precision curve is measured by calculating the deviation from one value from another.

Comparing both Figure 6.14(a) and Figure 6.14(b), the error is significant whether the difference reaches an elevated value different from zero. This behavior is more evident for voltage angle and magnitude in the last states in the plots. However, most of the plot points indicate good agreement between the low- and high-precision results. This is evidence that despite the elevated norm in Table 6.15, the initialization of the NR solver by the states obtained by the FPV2 solver is appropriate.

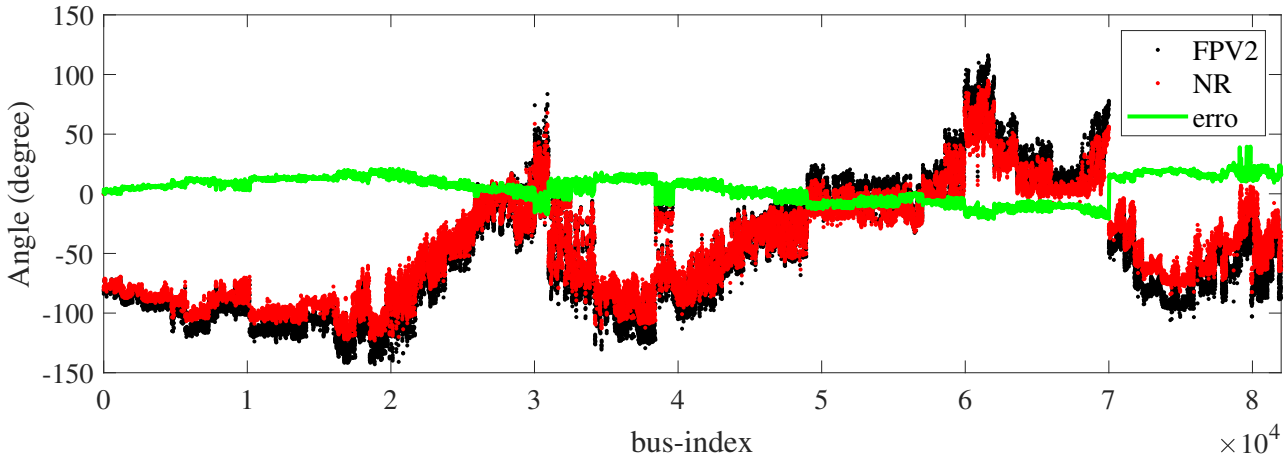

(a) Angle approximation at the end of the homotopy path, $h = 1$, and refined result

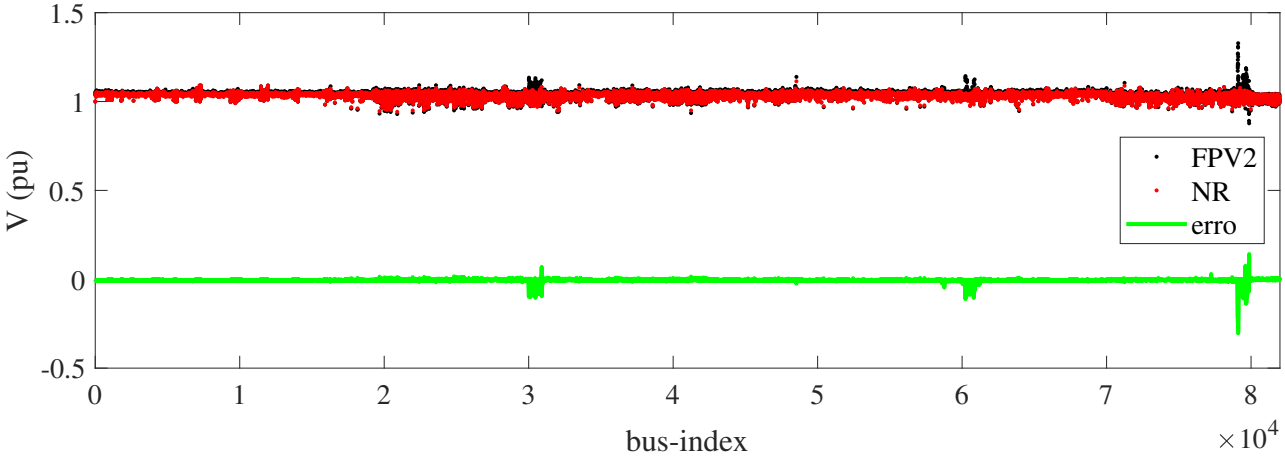

(b) Voltage magnitude approximation at the end of the homotopy path, $h = 1$, and refined result

Figure 6.14: Results obtained for voltage magnitude and phase angle using FPV2 and refined result by the NR solver for the `case82k`

6.7.2 Simulations evidencing the influence of the scaling factor δ on the results

To illustrate the influence of the parameter δ in the results determined by the FPV2 (as well as for other homotopy-based techniques used as a tool for solving the PFP), simulations were performed in the test system represented by the `case13659pegase`. The simulations with $\delta = 0.1$ (the stable case) and $\delta = 1$ (the unstable case) were considered for this aim. The Dynamic homotopy solver was executed for various time steps, and the time and the infinite norm correspondence were observed. Table 6.16 exhibits the instant of time from the point $t_1 = 1 \times 10^{-6}$ until $t = 1$. In the simulations, $K = 1$ was used. The last four columns of the table give the infinite norm of mismatches of the three initial iterates and the last one. The parenthesis at the side of the norm is the total number of iterations required for the NR solver to solve the PFP using the approximation determined by the FPV2 solver. When $\delta = 0.1$, the slack

bus generates $S_g = 0.7687 + j0.1581$ pu. The result agrees with those found in MATPOWER's reference solution. However, for $\delta = 0.1$, the slack bus generates $S_g = 1.5639 + j14.5971$ pu, characterizing an abnormal operation point due to the very high reactive power generated by the slack bus for the specific system.

Table 6.16: FPV2-BE$_{(\mathrm{NR})}$, $K = 0.0001$, and values for $\delta = 0.1$ and $\delta = 1$

CASE/Time	$\|\|\mathbf{f}(\mathbf{x})\|\|_\infty$ of the Solver												$\|\|\mathbf{f}(\mathbf{x})\|\|_\infty$ NR			
Δt or *iter*	5×10^{-6}	1×10^{-4}	5×10^{-4}	15×10^{-4}	0.150	0.150	0.150	0.150	0.150	0.150	0.150	0.0993	1	2	3	last
t	5×10^{-6}	1.05×10^{-4}	2.05×10^{-4}	7.05×10^{-4}	7.2×10^{-4}	0.1507	0.3007	0.4507	0.6007	0.7507	0.9007	1				
case13659pegase*	201	201	201	201	201	149	120	90	59	25	27	35	2.0	0.5	6×10^{-4}	8×10^{-10}(4)
case13659pegase**	201	201	201	201	201	149	120	90	59	92	43	68	37	5	1.3	8×10^{-12}(6)

* for $\delta = 0.1$ and ** for $\delta = 1$

Results in Table 6.16 indicate that two scaling factors were used in the simulations for executing the FPV2 scheme, and two sets of distinct states were, in fact, calculated in the point $t = 1$. The NR solver presented convergence for both situations. The results for $\delta = 0.1$ led to a voltage-stable solution, while $\delta = 1$ generated an unstable set of voltage solutions. This set of unstable voltages was identified by measuring the angular difference between two interconnections. The result was considered unstable when this difference was superior to ninety degrees in absolute value.

In fact, the result for different scaling factors is expected because, for an assigned δ, one correspondent set of states is obtained. Even though they are different in the point $t = 1$, what would be awaited was that any result could be satisfactory enough to start the NR solver adequately. However, this is not true, and in some cases, it is necessary to assign $\delta < 1$ to obtain convergence of the NR when the result of the FPV2 is used as a guess.

To reinforce the impact of δ in the results determined by the dynamic homotopy-based solver, other results are shown in terms of plots of voltage magnitude and angle, the error between the values refined and with low accuracy of the FPV2-NR as well as, the mismatches determined at the end of the FPV2 solver execution. The results are shown from Figures 6.15 until 6.18. The case of unstable solution is evident in Figure 6.17 that highlight very high angular displacement between converged and approximate angles. In the case of stable solutions as in Figure 6.15(a), the error is twenty degrees. With relation to the voltage magnitude is not simple a straightforward conclusion based on the plots whether a case present stable or unstable solution.

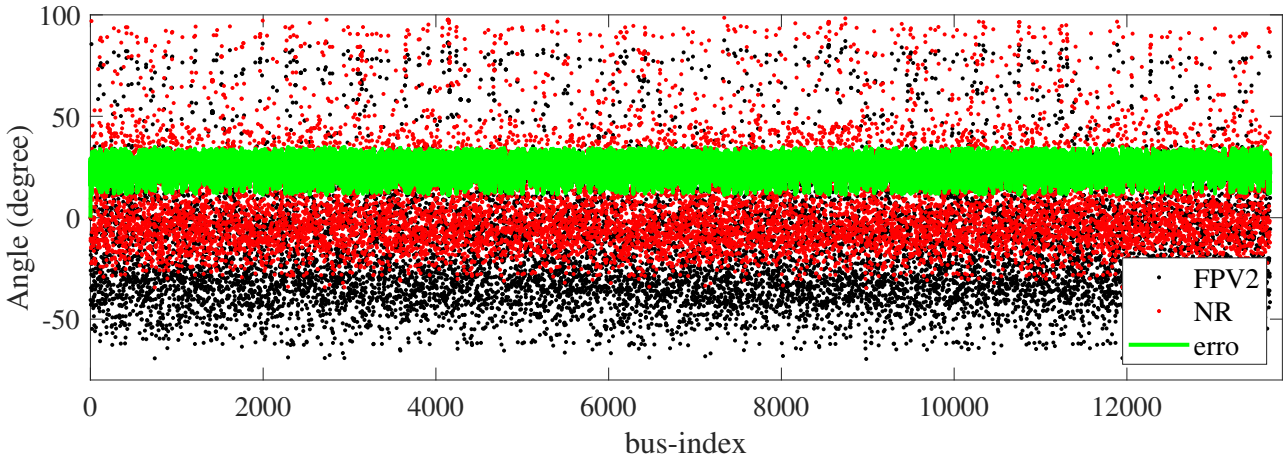

(a) Angle approximation at the end of the homotopy, $h = 1$, and refined result

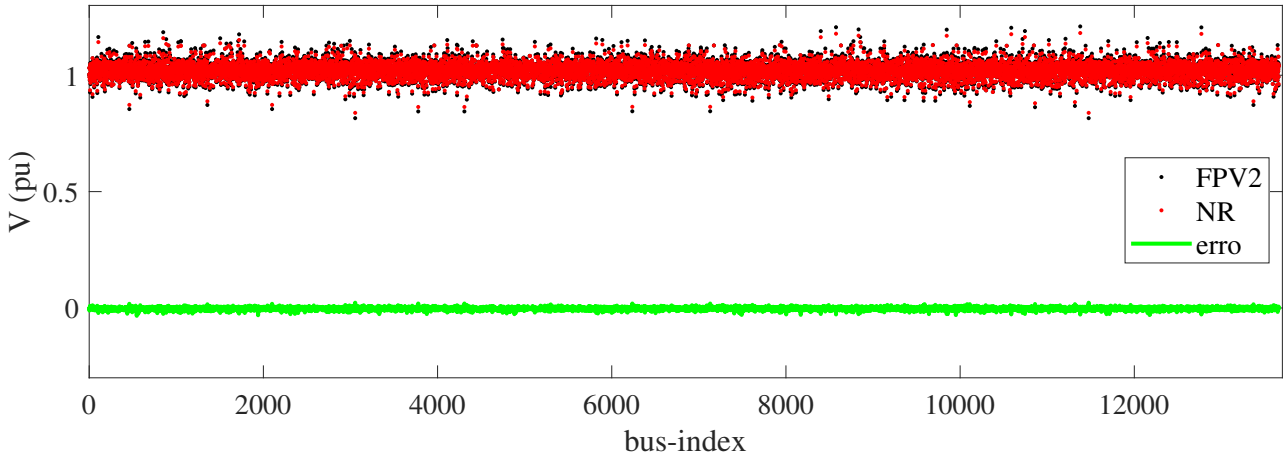

(b) Voltage magnitude approximation at the end of the homotopy, $h = 1$, and refined result

Figure 6.15: Results obtained for voltage magnitude and phase angle using FPV2 and refined result by the NR solver for the `case13659pegase`

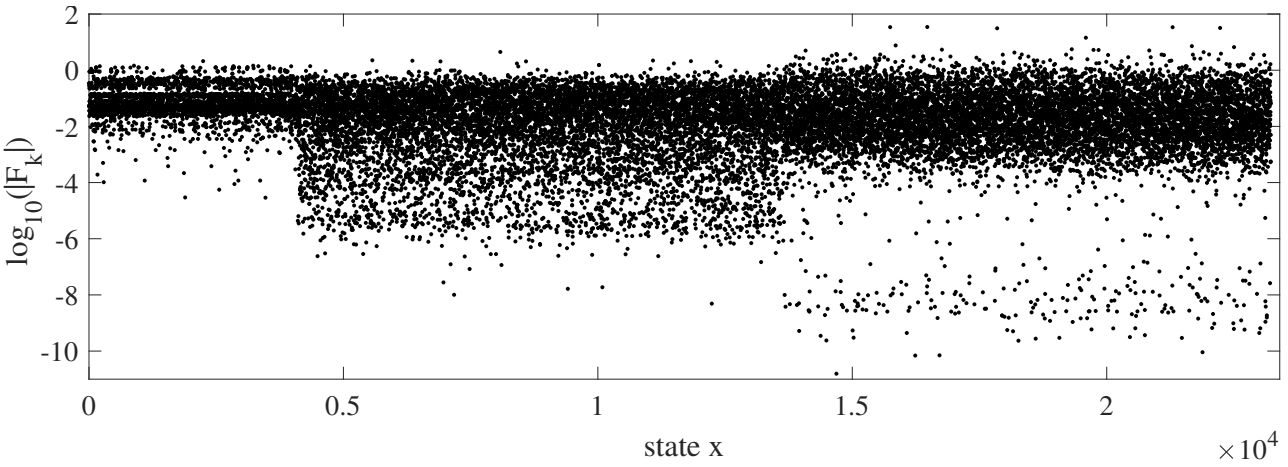

Figure 6.16: Absolute power mismatches computed at the final of the dynamic homotopy by using the FPV2 scheme for the `case13659pegase` when $\delta = 0.1$

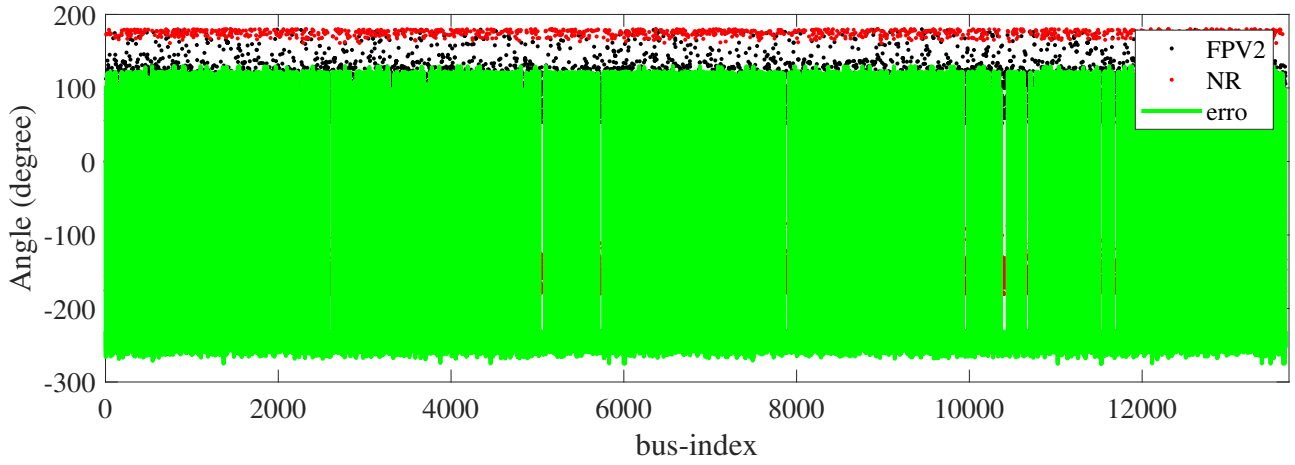

(a) Angle approximation at the end of the homotopy, $h = 1$, and refined result

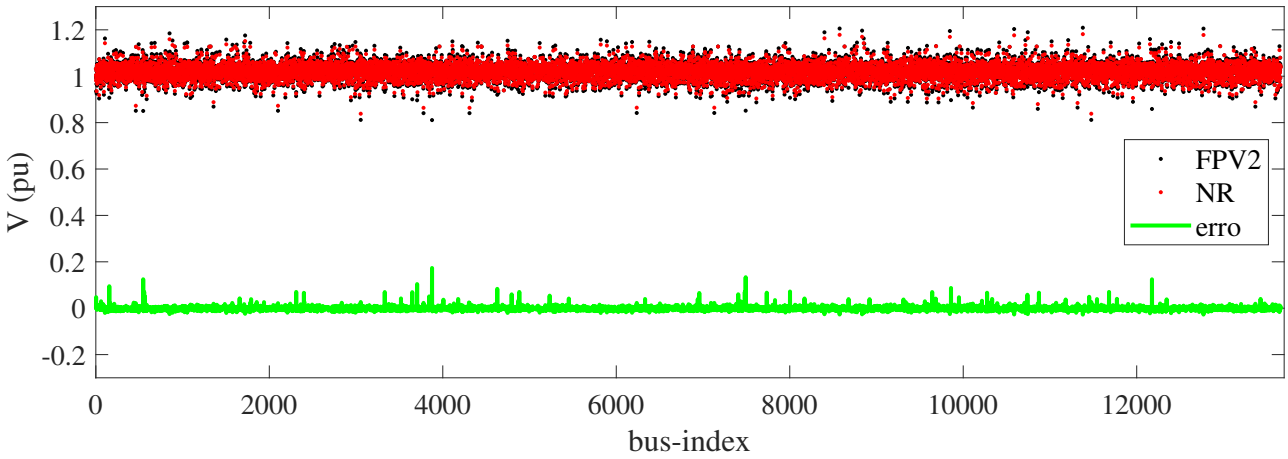

(b) Voltage magnitude approximation at the end of the homotopy, $h = 1$, and refined result

Figure 6.17: Results obtained for voltage magnitude and phase angle using FPV2 and refined result by the NR solver for the `case13659pegase`

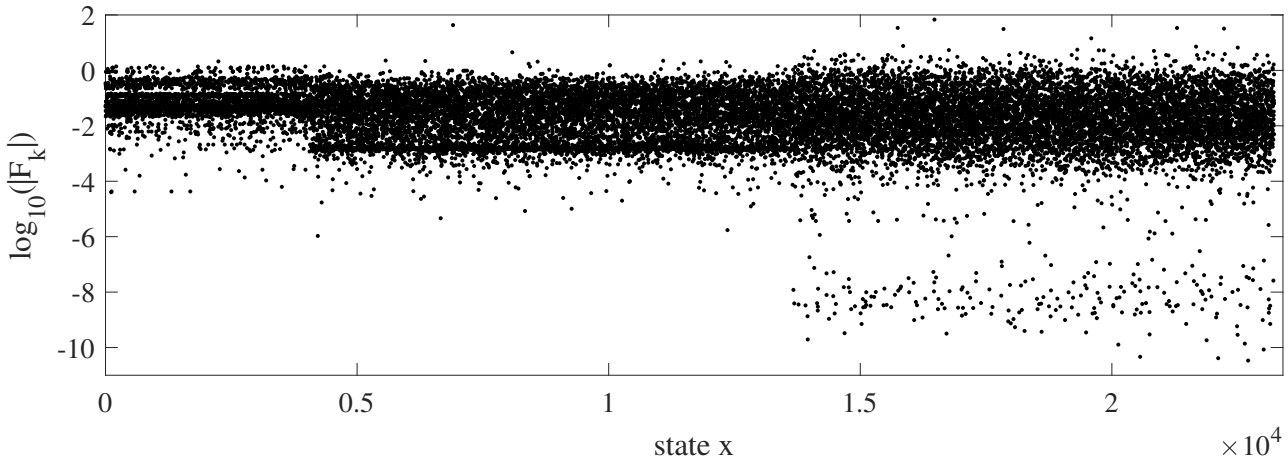

Figure 6.18: Absolute power mismatches computed at the final of the dynamic homotopy by using the FPV2 scheme for the `case13659pegase` when $\delta = 1$

6.7.3 Execution time

The computational time of two large-scale systems was measured to verify the algorithms' performance at Table 6.17. Four methods were tested for the cases that had convergence. The

performance was evaluated for the two static homotopy methods, GSH-NR and GSH-FPV-NR, and the two dynamic homotopy-based techniques, FPV-BE$_{(NR)}$ and FPV2-BE$_{(NR)}$. The performance comparison in figures of CPU time is shown in percentages in parentheses in front of their respective times in seconds. All three methods evaluated outperformed the old method GSH-NR presented in Freitas & Silva (2022) for the test system studied. The FPV-BE$_{(NR)}$ method stood out, as it consumed only 18% of GSH-NR for the `case_ACTIVSg70k`. The FPV2 solver had a performance similar to the static approach GSH-FPV-NR. However, the advantage of both techniques is that they obtain a solution of the PFP for the complex case formed by the three slack buses, namely the `case82k` and others.

Table 6.17: Mean CPU time in seconds for the computational burden of methods used on two large-scale test systems, where the methods were convergent for a solution

CASE	GSH-NR	GSH-FPV-NR	FPV-BE$_{(NR)}$	FPV2-BE$_{(NR)}$
`case13659pegase`	1.9750	1.9211 (97%)	0.6870 (35%)	1.7730 (90%)
`case_ACTIVSg70k`	25.0740	15.3466 (61%)	4.4300 (18%)	17.2930 (69%)

6.8 OVERVIEW

This chapter presented experiments and results to verify the performance of the homotopy-based methods. The simulations use the test systems presented in Chapter 5. The tests consider two static homotopy approaches, namely GSH-NR and GSH-FPV-NR. Also, two dynamic homotopy schemes were presented, simply called FPV and FPV2.

The NR methods, starting from the MATPOWER initial estimate and flat start guess, and the GSH-NR method, starting from the flat start estimate, were used as a comparison reference.

The simulation results highlighted the effectiveness of the GSH-FPV-NR scheme in addressing situations where the GSH-NR fails. Regarding the dynamic homotopy approach, although the FPV2 scheme required the most computational resources compared to the FPV, it demonstrated more robust performance by successfully resolving a complex case where an isolated system transitions into a synchronous network.

Computational performance was evaluated for both FPV-BE$_{(NR)}$ and FPV-RK2$_{(NR)}$ variants. Both models performed comparably to the NR-MAT method, which begins with the

MATPOWER estimate. This highlights the versatility of the schemes, which can achieve solutions at a reasonable computational cost, even when starting from a poor initial estimate. Additionally, the performance was assessed with various numerical solvers at different high-accuracy stages, including FDXB, HKW, and RK4. The methodology demonstrated its effectiveness in expanding the attraction region of the tested methods. Notably, the computational time was similar to that of the NR-MAT method, even when starting from a flat initial estimate. In the case of FPV-BE$_{(\mathrm{FDXB})}$, it exhibited superior performance compared to NR-flat.

Several experiments were presented to demonstrate the effectiveness of the implicit integration method for solving the numerical problem when dynamical homotopy-based techniques are employed. The BE solver performed adequately for the simulations, which was the technique used when the FPV2 scheme was adopted. Experiments were carried out in large-scale ill-conditioned systems, including models of 70k-, 82k-, and 109k-buses.

The tests showed that the integration method's time step, Δt, directly affects the total number of iterations required. As Δt decreases, the number of steps during the dynamical homotopy stage increases, causing the final estimate for the second stage to be closer to the actual solution. Consequently, Newton-Raphson's method converges with fewer iterations. Another test highlighted the importance of the K parameter in achieving a highly accurate solution. The proper definition of this value is crucial for ensuring convergence.

Lastly, the FPV method was also tested in a contingency situation. It was shown that dynamic homotopy schemes help achieve the correct power flow solution, even when considering independent systems with multiple slack buses.

CHAPTER 7

CONCLUSION

This PhD thesis proposed homotopy-based techniques arranged in a way to solve algebraic nonlinear equations and model the power flow problem in large-scale ill-conditioned power system models. Despite the PF being a static problem, the homotopy-based problems were formulated to consider both the static and dynamic approaches. All the homotopy-based solvers assumed that the PFP is solved starting from a flat start guess. Then, when a static approach is considered, the flat start guess is the initial point of the homotopy pathway. However, for a dynamic method, the flat start guess is interpreted as the boundary condition for the synthesized differential equations.

Concerning the static homotopy-based techniques, a method presented in Freitas & Silva (2022) was studied, called GSH-NR, and a modification of it performed in this PhD thesis to solve a more complex problem that was not solved by the original GSH-NR technique. In common, the strategies are based on artificial compensation of the power grid at the starting point of the homotopy path. Compensation is done through the connection of shunt impedances at each bus in the system that absorb (or generate) the power of the bus itself so that there is no initial flow in any interconnection. Thus, there is no need to solve a PFP at the starting point because the solution is the initial estimate of the iterative load flow problem. Along the homotopy process, the fictitious impedances are disconnected progressively, and their amount is regulated by the homotopy parameter until it achieves the unitary value. This new proposal was characterized by the insertion of modifications on the homotopy function of a term based on a Fixed Point Vector (FPV) and weights in the function defined for GSH-NR. Thus, the method was defined as GSH-FPV-NR.

While the GSH-NR was conceived to search for a solution at the end of the homotopy pathway, the GSH-FPV-NR determines a low-precision solution at this point, which an iterative solver, such as NR, refines for high precision.

The dynamic homotopy-based techniques proposed in this work use an FPV term for generating the "easy" function of the homotopy function. A first and simpler homotopy function was proposed based on only the combination of algebraic equations of the original PFP and the FPV component. Then, it was labeled simply as FPV. It does not use an artificial compensation of the network along the dynamic homotopy process. A second proposal was investigated, assuming the replacement of the algebraic equations of the original PFP in the first proposal by the equations of the GSH-FPV-NR scheme, keeping the inclusion of the term FPV. By this proposal, the solver was called FPV2. This second scheme is more robust because it takes into account the qualities and properties of the GSH-FPV-NR, and so the procedure of artificial network compensation. On the other hand, it demanded a computational burden greater than the FPV scheme.

The solution obtained for the dynamic homotopy-based technique is an approximation because the integration methods employ large time-step lengths. Smaller steps would lead to the computation of many discrete points in the homotopy path curve without great impact in the final point since the interest at this specific point is to obtain a rough result. In contrast, it could be computationally expensive compared with the static techniques.

The Static homotopy solvers require the resolution of algebraic nonlinear equations along the homotopy path, while the dynamic homotopy-based technique depends on the determination of results along the homotopy path but whose resolution is done by numerical integration techniques. In this sense, implicit and explicit integration techniques were investigated for the problems. The schemes FE and RK2 were studied as explicit and BE as implicit methods. Experiments demonstrated better performance for the implicit method, being the recommended and the only one used for simulations with the FPV2 solver. Several experiments were carried out considering the determination of the initial step on the dynamical solver since, at this point, the numerical results can significantly impact the subsequent points on the homotopy path. Besides, the definition of these subsequent points influences the process convergence and the associated computational burden.

The solvers GSH-FPV-NR, FPV, and FPV2 determined an adequate low-precision solution of the PFP, which was improved by an iterative scheme such as NR. For the FPV solver, the study was also extended to include refinement with the FDXB scheme.

Experiments were performed to demonstrate the effectiveness of the techniques in various test systems with different characteristics. The solver GSH-FPV-NR presented convergence for all test systems. To the dynamic homotopy solver, the FPV technique demanded a computational burden for finding a solution almost similar to that obtained by the MATPOWER despite using an initial estimation closer to the solution. However, the FPV2 demanded a substantial CPU time, compared with the FPV, to solve the same problem.

An interesting aspect of this work was to address homotopy-based techniques, whether static or dynamic, for solving problems with several slack buses. For this strategy, a formulation considering islanding systems can be explored. As an application, contingency studies were carried out using only the FPV approach applied to the 70k-bus system. Furthermore, a problem was carried out in which the test system presented three slack buses.

In summary, the proposed methodology in this work demonstrates:

- to be suitable for dealing with ill-conditioned and large-scale power system models;
- to use an idea of an artificial compensation network and a dynamic approach to find an approximation of the states of PFP and improve it by using the classical NR solver or other classical solvers;
- that can be implemented in the MATPOWER free software, requiring only a few modifications in the Jacobian matrix and mismatches of solutions that are already directly calculated by the program;
- that the dynamic approach differs from the static homotopy approach because the solution in the homotopy parameter for the unitary value approximates states for $\mathbf{f}(\mathbf{x}) = \mathbf{0}$, whose result is used to improve the PFP results; and
- to be a promising tool for studying contingency and system islanding in power systems.

RECOMMENDATIONS FOR FUTURE RESEARCH

The planned objectives for the new work directions are to extend the application of homotopy to recent studies on the impact on load flow considering equipment limits studies.

Furthermore, it intends to study the applications developed considering a new scenario with a power system with several slack buses replaced by a strategy where a phase-shift device allows working with a single slack bus. This procedure can be useful for islanding studies, interconnections with DC link, contingency studies, etc.

- Investigate other strategies to search for new improvements in the static and dynamic homotopy-based approaches, considering new alternatives to define a homotopy function;
- Research on other integration methods aiming to improve the performance of the dynamic homotopy problem, as well as the use of an adaptive time-step according to the error verified along the homotopy integration process;
- Carry out supplementary tests involving the homotopy-based techniques to take into account diversified cases of contingencies and control of devices or a given quantity;
- Implement the main aspects of the Synthetic Dynamic Power Flow for large-scale systems and verify the joint application with homotopy concepts; and
- Perform additional investigations on the FPV2 approach to implement an optimized code to the algorithm.

REFERENCES

AGARWAL, A.; PANDEY, A.; PILEGGI, L. Fast AC steady-state power grid simulation and optimization using prior knowledge. In: *2021 IEEE Power & Energy Society General Meeting (PESGM)*. IEEE, 2021. p. 1–5. ISBN 978-1-6654-0507-2. ISSN 19449933. Disponível em: <https://ieeexplore.ieee.org/document/9637903/>. Cited in page 56.

AGARWAL, A.; PILEGGI, L. Large scale multi-period optimal power flow with energy storage systems using differential dynamic programming. *IEEE Transactions on Power Systems*, IEEE, v. 37, p. 1750–1759, 5 2022. ISSN 0885-8950. Disponível em: <https://ieeexplore.ieee.org/document/9549701/>. Cited in page 56.

ALI, M.; ALI, M. H.; GRYAZINA, E.; TERZIJA, V. Calculating multiple loadability points in the power flow solution space. *International Journal of Electrical Power & Energy Systems*, Elsevier Ltd, v. 148, p. 108915, 1 2023. ISSN 01420615. Disponível em: <https://doi.org/10.1016/j.ijepes.2022.108915>. Cited 2 times in pages 55 and 56.

ALI, M.; GRYAZINA, E.; DYMARSKY, A.; VOROBEV, P. Calculating voltage feasibility boundaries for power system security assessment. *International Journal of Electrical Power and Energy Systems*, Elsevier Ltd, v. 146, n. November 2022, p. 108739, 2023. ISSN 01420615. Disponível em: <https://doi.org/10.1016/j.ijepes.2022.108739>. Cited in page 56.

ALVES, G. O.; PEREIRA, J.; GATTA, P. O. L.; FILHO, J. P.; TOMIM, M. A new governor power flow formulation based on the current injections method. *International Journal of Electrical Power Energy Systems*, Elsevier Ltd, v. 104, p. 705–715, 1 2019. ISSN 01420615. Disponível em: <https://doi.org/10.1016/j.ijepes.2018.07.031>. Cited 2 times in pages 18 and 20.

AMERONGEN, R. van. A general-purpose version of the fast decoupled load flow. *IEEE Transactions on Power Systems*, v. 4, n. 2, p. 760–770, 5 1989. ISSN 08858950. Disponível em: <http://ieeexplore.ieee.org/document/193851/>. Cited 3 times in pages 11, 20, and 23.

ARGYROS, I. K.; MAGREÑÁN, Á. A. *Iterative methods and their dynamics with applications: A contemporary study*. [S.l.]: CRC Press, 2017. Cited in page 28.

BALUEV, D.; ALI, M.; GRYAZINA, E. State of the art approach for comprehensive power system security assessmentreal case study. *International Journal of Electrical Power and Energy Systems*, Elsevier Ltd, v. 155, n. PB, p. 109594, 2024. ISSN 01420615. Disponível em: <https://doi.org/10.1016/j.ijepes.2023.109594>. Cited 2 times in pages 55 and 59.

BARAN, M.; WU, F. Optimal capacitor placement on radial distribution systems. *IEEE Transactions on Power Delivery*, v. 4, p. 725–734, 1989. ISSN 08858977. Disponível em: <http://ieeexplore.ieee.org/document/19265/>. Cited in page 80.

BIRCHFIELD, A. B.; XU, T.; GEGNER, K. M.; SHETYE, K. S.; OVERBYE, T. J. Grid structural characteristics as validation criteria for synthetic networks. *IEEE Transactions on Power Systems*, v. 32, p. 3258–3265, 7 2017. ISSN 0885-8950. Disponível em: <http://ieeexplore.ieee.org/document/7725528/>. Cited 3 times in pages 77, 80, and 82.

BIRCHFIELD, A. B.; XU, T.; OVERBYE, T. J. Power flow convergence and reactive power planning in the creation of large synthetic grids. *IEEE Transactions on Power Systems*, v. 33, n. 6, p. 6667–6674, 11 2018. ISSN 0885-8950. Disponível em: <https://ieeexplore.ieee.org/document/8333771/>. Cited 3 times in pages 23, 77, and 82.

BISWAS, B. N.; CHATTERJEE, S.; MUKHERJEE, S. P.; PAL, S. A discution on Euler method: A review. *Electronic Journal of Mathematical Analysis and Applications*, v. 1, p. 2090–792, 2013. Disponível em: <https://journals.ekb.eg/article_309811_cb4e94d217da1b8e29e3c9294ccd8e0a.pdf>. Cited in page 26.

BROWN, R. J.; TINNEY, W. F. Digital solutions for large power networks. *Transactions of the American Institute of Electrical Engineers. Part III: Power Apparatus and Systems*, v. 76, n. 3, p. 347–351, 4 1957. ISSN 0097-2460. Disponível em: <http://ieeexplore.ieee.org/document/4499563/>. Cited 2 times in pages 51 and 57.

BUTCHER, J. C. *Numerical methods for ordinary differential equations*. 3rd. ed. United Kingdon: John Wiley & Sons, 2016. Cited 2 times in pages 26 and 28.

CHANDRA, S.; MEHTA, D.; CHAKRABORTTY, A. Locating power flow solution space boundaries: A numerical polynomial homotopy approach. *arXiv preprint arXiv:1704.04792*, p. 1–9, 2017. Disponível em: <http://arxiv.org/abs/1704.04792>. Cited 2 times in pages 55 and 56.

CHATTERJEE, S.; MANDAL, S. A novel comparison of Gauss-Seidel and Newton-Raphson methods for load flow analysis. In: *2017 International Conference on Power and Embedded Drive Control (ICPEDC)*. IEEE, 2017. p. 1–7. ISBN 978-1-5090-4679-9. Disponível em: <http://ieeexplore.ieee.org/document/8081050/>. Cited in page 11.

CHAVES, S. B. *Análise estática e dinâmica de sistemas de potência via aplicativo computacional integrado: ORGANON*. Dissertação (Mestrado) — Universidade Federal Fluminense, Niterói, RJ, 2008. Cited 2 times in pages 29 and 53.

CHIANG, H.-D.; WANG, T. Novel homotopy theory for nonlinear networks and systems and its applications to electrical grids. *IEEE Transactions on Control of Network Systems*, v. 5, p. 1051–1060, 9 2018. ISSN 2325-5870. Disponível em: <https://ieeexplore.ieee.org/document/7862794/>. Cited 3 times in pages 42, 55, and 143.

CHIANG, H.-D.; ZHAO, T.-Q.; DENG, J.-J.; KOYANAGI, K. Homotopy-enhanced power flow methods for general distribution networks with distributed generators. *IEEE Transactions on Power Systems*, School of Electrical and Computer Engineering, Cornell University, Ithaca, NY 14853, United States, v. 29, n. 1, p. 93–100, 1 2014. ISSN 0885-8950. Disponível em: <http://ieeexplore.ieee.org/document/6588949/>. Cited 2 times in pages 55 and 58.

COSTA, V. da; MARTINS, N.; PEREIRA, J. Developments in the newton raphson power flow formulation based on current injections. *IEEE Transactions on Power Systems*, v. 14, p. 1320–1326, 1999. ISSN 08858950. Disponível em: <http://ieeexplore.ieee.org/document/801891/>. Cited in page 18.

COSTA, V. da; PEREIRA, J.; MARTINS, N. An augmented newtonraphson power flow formulation based on current injections. *International Journal of Electrical Power Energy Systems*, v. 23, p. 305–312, 5 2001. ISSN 01420615. Disponível em: <https://doi.org/10.1016/S0142-0615(00)00045-4>. Cited in page 19.

DAS, D. Optimal placement of capacitors in radial distribution system using a Fuzzy-GA method. *International Journal of Electrical Power & Energy Systems*, Elsevier, v. 30, p. 361–367, 7 2008. ISSN 01420615. Disponível em: <https://doi.org/10.1016/j.ijepes.2007.08.004>. Cited in page 80.

DERAKHSHANDEH, S. Y.; POURBAGHER, R.; KARGAR, A. A novel fuzzy logic Levenberg-Marquardt method to solve the ill-conditioned power flow problem. *International Journal of Electrical Power and Energy Systems*, Elsevier, v. 99, n. February, p. 299–308, 2018. ISSN 01420615. Disponível em: <https://doi.org/10.1016/j.ijepes.2018.01.019>. Cited in page 52.

DEUFLHARD, P. A modified Newton method for the solution of ill-conditioned systems of nonlinear equations with application to multiple shooting. *Numerische Mathematik*, v. 22, n. 4, p. 289–315, 8 1974. ISSN 0029-599X. Disponível em: <http://link.springer.com/10.1007/BF01406969>. Cited in page 51.

DUNSTAN, L. A. Machine computation of power network performance. *Transactions of the American Institute of Electrical Engineers*, v. 66, n. 1, p. 610–624, 1 1947. ISSN 0096-3860. Disponível em: <http://ieeexplore.ieee.org/document/5059485/>. Cited 3 times in pages 50, 51, and 57.

DUNSTAN, L. A. The general solution method of power network analysis. *Transactions of the American Institute of Electrical Engineers*, v. 67, n. 1, p. 631–639, 1 1948. Disponível em: <http://ieeexplore.ieee.org/document/5059722/>. Cited 2 times in pages 50 and 57.

DUNSTAN, L. A. Digital load flow studies. *Transactions of the American Institute of Electrical Engineers. Part III: Power Apparatus and Systems*, v. 73, n. 1, p. 825–832, 1 1954. ISSN 0097-2460. Disponível em: <http://ieeexplore.ieee.org/document/4498891/>. Cited 2 times in pages 50 and 51.

ECHAVARREN, F. M.; ROUCO, L.; BENÍTEZ, A.; SIGRIST, L. Power flow algorithm using a second-order differentation approach. In: *2023 IEEE Belgrade PowerTech*. IEEE, 2023. p. 01–06. ISBN 978-1-6654-8778-8. Disponível em: <https://ieeexplore.ieee.org/document/10202924/>. Cited 2 times in pages 54 and 58.

FLISCOUNAKIS, S.; PANCIATICI, P.; CAPITANESCU, F.; WEHENKEL, L. Contingency ranking with respect to overloads in very large power systems taking into account uncertainty, preventive, and corrective actions. *IEEE Transactions on Power Systems*, v. 28, p. 4909–4917, 11 2013. ISSN 0885-8950. Disponível em: <https://ieeexplore.ieee.org/document/6488772/>. Cited 2 times in pages 77 and 78.

FREITAS, F. D.; LIMA-SILVA, A. A power flow homotopy-based solver emanating from a flat start estimate. In: *2023 IEEE Power & Energy Society General Meeting (PESGM)*. IEEE, 2023. p. 1–5. ISBN 978-1-6654-6441-3. Disponível em: <https://ieeexplore.ieee.org/document/10252210/>. Cited in page 5.

FREITAS, F. D.; OLIVEIRA, L. N. de. Conditioning step on the initial estimate when solving ill-conditioned power flow problems. *International Journal of Electrical Power and Energy Systems*, v. 146, p. 108772, March 2023. ISSN 0142-0615. Disponível em: <https://doi.org/10.1016/j.ijepes.2022.108772>. Cited 2 times in pages 67 and 148.

FREITAS, F. D.; OLIVEIRA, L. N. de. Two-step hybrid-based technique for solving ill-conditioned power flow problems. *Electric Power Systems Research*, Elsevier B.V., v. 218, p. 1–10, 11 2023. ISSN 03787796. Disponível em: <https://doi.org/10.1016/j.epsr.2023.109178>. Cited in page 52.

FREITAS, F. D.; SILVA, A. L. Flat start guess homotopy-based power flow method guided by fictitious network compensation control. *International Journal of Electrical Power & Energy Systems*, Elsevier Ltd, v. 142, p. 108311, 11 2022. ISSN 01420615. Disponível em: <https://doi.org/10.1016/j.ijepes.2022.108311>. Cited 14 times in pages 3, 5, 44, 47, 53, 55, 58, 69, 88, 89, 125, 127, 143, and 144.

GALLER, B. A.; ROZENBERG, D. P. A generalization of a theorem of Carr on error bounds for Rung-Kutta procedures. *Journal of the ACM*, v. 7, p. 57–60, 1 1960. ISSN 0004-5411. Disponível em: <https://dl.acm.org/doi/10.1145/321008.321015>. Cited in page 27.

GALLOWAY, R.; TAYLOR, J.; HOGG, W.; SCOTT, M. New approach to power-system load-flow analysis in a digital computer. In: IET. *Proceedings of the Institution of Electrical Engineers*. 1970. v. 117, n. 1, p. 165–169. Disponível em: <https://digital-library.theiet.org/doi/10.1049/piee.1970.0034>. Cited in page 53.

GARCIA, C. B.; ZANGWILL, W. I. *Pathway to solution, fixed points and equilibria*. [S.l.]: prentice-Hall, 1981. Cited in page 67.

GATTA, P. O. L.; NETTO, N. A. R. L.; FILHO, J. A. P. A new model for the hierarchical response of control devices in the power flow problem. *Electrical Engineering*, 11 2024. ISSN 0948-7921. Disponível em: <https://link.springer.com/10.1007/s00202-024-02845-3>. Cited in page 1.

GLIMN, A. F.; STAGG, G. W. Automatic calculation of load flows. *Transactions of the American Institute of Electrical Engineers. Part III: Power Apparatus and Systems*, v. 76, n. 3, p. 817–825, 4 1957. ISSN 0097-2460. Disponível em: <http://ieeexplore.ieee.org/document/4499665/>. Cited 3 times in pages 50, 51, and 57.

GLOVER, J. D.; SARMA, M. S.; OVERBYE, T. J. *Power system analysis & design*. 5th. ed. Stamford, USA: Cengage Learning, 2012. Cited 5 times in pages 1, 9, 10, 12, and 21.

GOLDGEISSER, L.; GREEN, M. Using continuation methods to improve convergence of circuits with high impedance nodes. In: *2000 IEEE International Symposium on Circuits and Systems. Emerging Technologies for the 21st Century. Proceedings (IEEE Cat No.00CH36353)*. Presses Polytech. Univ. Romandes, 2000. v. 4, p. 181–184. ISBN 0-7803-5482-6. Disponível em: <http://ieeexplore.ieee.org/document/858718/>. Cited in page 57.

HENDERSON, J. M. Automatic digital computer solution of load flow studies. *Transactions of the American Institute of Electrical Engineers. Part III: Power Apparatus and Systems*, v. 73, p. 1696–1702, 1 1954. ISSN 0097-2460. Disponível em: <http://ieeexplore.ieee.org/document/4499023/>. Cited 3 times in pages 50, 51, and 57.

HETZLER, S. M. A continuous version of Newton's method. *The College Mathematics Journal*, v. 28, p. 348–351, 11 1997. ISSN 0746-8342. Disponível em: <https://www.tandfonline.com/doi/full/10.1080/07468342.1997.11973888>. Cited in page 25.

HONGFU, W.; XIANGHONG, T.; ZHIQIANG, Z.; CHONG, G.; HAO, Y.; SHIXIA, M. An improved DC power flow algorithm with consideration of network loss. In: *2014 International Conference on Power System Technology*. IEEE, 2014. p. 455–460. ISBN 978-1-4799-5032-4. Disponível em: <http://ieeexplore.ieee.org/document/6993704/>. Cited in page 24.

HU, S. T. *Homotopy theory*. Wayne State University, Detroit, MI: Academic Press, 1959. Cited in page 54.

IWAMOTO, S.; TAMURA, Y. A fast load flow method retaining nonlinearity. *IEEJ Transactions on Power and Energy*, v. 98, p. 192–198, 1978. ISSN 0385-4213. Disponível em: <https://ieeexplore.ieee.org/abstract/document/4181598>. Cited in page 40.

IWAMOTO, S.; TAMURA, Y. A load flow calculation method for ill-conditioned power systems. *IEEE Transactions on Power Apparatus and Systems*, PAS-100, p. 1736–1743, 4 1981. ISSN 0018-9510. Disponível em: <http://ieeexplore.ieee.org/document/4110791/>. Cited 3 times in pages 40, 51, and 58.

JARDIM, J. *Manual of ORGANON - Introduction methodology, vol. 3*. [S.l.]: Version 1.1, 2005. Cited in page 53.

JARDIM, J.; STOTT, B. Synthetic dynamics power flow. In: *IEEE Power Engineering Society General Meeting, 2005*. San Francisco, CA, USA: [s.n.], 2005. v. 1, p. 479–484. Cited 6 times in pages 25, 29, 30, 31, 36, and 53.

JOSZ, C.; FLISCOUNAKIS, S.; MAEGHT, J.; PANCIATICI, P. AC power flow data in MATPOWER and QCQP format: iTesla, RTE Snapshots, and PEGASE. *arXiv preprint arXiv:1603.01533*, p. 1–7, 3 2016. Disponível em: <http://arxiv.org/abs/1603.01533>. Cited 2 times in pages 77 and 78.

KHODR, H.; OLSINA, F.; JESUS, P. D. O.-D.; YUSTA, J. Maximum savings approach for location and sizing of capacitors in distribution systems. *Electric Power Systems Research*, v. 78, p. 1192–1203, 7 2008. ISSN 03787796. Disponível em: <https://doi.org/10.1016/j.epsr.2007.10.002>. Cited in page 80.

KU, C. Y.; YEIH, W.; LIU, C. S. Dynamical Newton-like methods for solving ill-conditioned systems of nonlinear equations with applications to boundary value problems. *CMES - Computer Modeling in Engineering and Sciences*, v. 76, p. 83–108, 2011. ISSN 15261492. Disponível em: <https://www.researchgate.net/publication/258769087>. Cited 3 times in pages 2, 53, and 55.

KUNDUR, P. *Power system stability and control*. New York: McGraw-hill, 1994. Cited 7 times in pages 1, 7, 10, 16, 27, 68, and 81.

LEE, J.; CHIANG, H.-D. A singular fixed-point homotopy method to locate the closest unstable equilibrium point for transient stability region estimate. *IEEE Transactions on Circuits and Systems II: Express Briefs*, v. 51, p. 185–189, 4 2004. ISSN 1057-7130. Disponível em: <http://ieeexplore.ieee.org/document/1288423/>. Cited in page 55.

LI, T. Y. Numerical solution of multivariate polynomial systems by homotopy continuation methods. *Acta Numerica*, v. 6, p. 399–436, 1997. Disponível em: <https://www.cambridge.org/core/journals/acta-numerica>. Cited in page 54.

LIAO, S. *Homotopy analysis method in nonlinear differential equations*. [S.l.]: Springer, 2012. Cited 2 times in pages 42 and 54.

LIMA-SILVA, A.; FREITAS, F. D. Dynamical homotopy transient-based technique to improve the convergence of ill-posed power flow problem. *International Journal of Electrical Power & Energy Systems*, Elsevier Ltd, v. 155, p. 109436, 1 2024. ISSN 01420615. Disponível em: <https://doi.org/10.1016/j.ijepes.2023.109436>. Cited 3 times in pages 5, 59, and 92.

LIMA-SILVA, A.; FREITAS, F. D. Exploring a dynamic homotopy technique to enhance the convergence of classical power flow iterative solvers in ill-conditioned power system models. *Energies*, v. 17, p. 4642, 9 2024. ISSN 1996-1073. Disponível em: <https://www.mdpi.com/1996-1073/17/18/4642>. Cited 3 times in pages 5, 59, and 92.

LIMA-SILVA, A.; FREITAS, F. D.; FERNANDES, L. F. D. J. Técnica baseada em homotopia com uma rede fictícia para determinação da solução do problema de fluxo de potência em sistemas mal-condicionados. In: *Simpósio Brasileiro de Sistemas Elétricos - SBSE*. [S.l.: s.n.], 2023. Cited in page 5.

LIMA-SILVA, A.; FREITAS, F. D.; FERNANDES, L. F. de J. A homotopy-based approach to solve the power flow problem in islanded microgrid with droop-controlled distributed generation units. *Energies*, v. 16, p. 5323, 7 2023. ISSN 1996-1073. Disponível em: <https://www.mdpi.com/1996-1073/16/14/5323>. Cited 2 times in pages 5 and 55.

LINDBERG, J.; ZACHARIAH, A.; BOSTON, N.; LESIEUTRE, B. The distribution of the number of real solutions to the power flow equations. *IEEE Transactions on Power Systems*, IEEE, v. 38, p. 1058–1068, 3 2023. ISSN 0885-8950. Disponível em: <https://ieeexplore.ieee.org/document/9763344/>. Cited in page 55.

LIU, C. S.; KUO, C. L. A dynamical Tikhonov regularization method for solving nonlinear ill-posed problems. *CMES - Computer Modeling in Engineering and Sciences*, v. 76, p. 109–132, 2011. ISSN 15261492. Disponível em: <https://cdn.techscience.cn/files/CMES/2011/v76n2/cmes.2011.076.109.pdf>. Cited in page 63.

LOTKIN, M. On the accuracy of Runge-Kutta's method. *Mathematical tables and other aids to computation*, JSTOR, v. 5, n. 35, p. 128–133, 1951. Disponível em: <https://www.jstor.org/stable/2002436>. Cited in page 27.

MANIATIS, M.; MEHTA, D. Minimizing Higgs potentials via numerical polynomial homotopy continuation. *The European Physical Journal Plus*, v. 127, p. 91, 8 2012. ISSN 2190-5444. Disponível em: <http://link.springer.com/10.1140/epjp/i2012-12091-1>. Cited in page 54.

MCDOUGALL, T. J.; WOTHERSPOON, S. J. A simple modification of Newton's method to achieve convergence of order $1 + \sqrt{2}$. *Applied Mathematics Letters*, Elsevier Ltd, v. 29, p. 20–25, 2014. ISSN 08939659. Disponível em: <http://dx.doi.org/10.1016/j.aml.2013.10.008>. Cited in page 28.

MCGILLIS, D. Nodal iterative solution of power-flow problem using IBM 604 digital computer. *Transactions of the American Institute of Electrical Engineers. Part III: Power Apparatus and Systems*, v. 76, n. 3, p. 803–809, 4 1957. ISSN 0097-2460. Disponível em: <http://ieeexplore.ieee.org/document/4499663/>. Cited 2 times in pages 51 and 57.

MCNAMARA, T.; PANDEY, A.; AGARWAL, A.; PILEGGI, L. Two-stage homotopy method to incorporate discrete control variables into AC-OPF. *Electric Power Systems Research*, Elsevier B.V., v. 212, n. April, p. 108283, 2022. ISSN 03787796. Disponível em: <https://doi.org/10.1016/j.epsr.2022.108283>. Cited in page 56.

MEHTA, D. Numerical polynomial homotopy continuation method and string vacua. *Advances in High Energy Physics*, v. 2011, p. 1–15, 2011. ISSN 1687-7357. Disponível em: <http://www.hindawi.com/journals/ahep/2011/263937/>. Cited in page 54.

MEHTA, D.; NGUYEN, H. D.; TURITSYN, K. Numerical polynomial homotopy continuation method to locate all the power flow solutions. *IET Generation, Transmission & Distribution*, v. 10, p. 2972–2980, 9 2016. ISSN 1751-8687. Disponível em: <https://onlinelibrary.wiley.com/doi/10.1049/iet-gtd.2015.1546>. Cited 3 times in pages 54, 55, and 58.

MILANO, F. Continuous Newton's method for power flow analysis. *IEEE Transactions on Power Systems*, v. 24, p. 50–57, 2 2009. ISSN 0885-8950. Disponível em: <http://ieeexplore.ieee.org/document/4682629/>. Cited 8 times in pages 2, 12, 25, 27, 52, 58, 61, and 79.

MILANO, F. *Power system modelling and scripting*. Spain: Springer Berlin Heidelberg, 2010. 556 p. ISSN 1612-1287. ISBN 978-3-642-13668-9. Disponível em: <http://link.springer.com/10.1007/978-3-642-13669-6>. Cited 9 times in pages 12, 23, 24, 25, 43, 52, 58, 61, and 62.

MILANO, F. Implicit continuous Newton method for power flow analysis. *IEEE Transactions on Power Systems*, v. 34, n. 4, p. 3309–3311, 7 2019. ISSN 0885-8950. Disponível em: <https://ieeexplore.ieee.org/document/8698293/>. Cited 2 times in pages 26 and 62.

NAIR, A. S.; ABHYANKAR, S.; PELES, S.; RANGANATHAN, P. Computational and numerical analysis of AC optimal power flow formulations on large-scale power grids. *Electric Power Systems Research*, Elsevier B.V., v. 202, n. December 2020, p. 107594, 2022. ISSN 03787796. Disponível em: <https://doi.org/10.1016/j.epsr.2021.107594>. Cited in page 56.

NESS, J. E. V. Iteration methods for digital load flow studies. *Transactions of the American Institute of Electrical Engineers. Part III: Power Apparatus and Systems*, v. 78, n. 3, p. 583–586, 4 1959. Disponível em: <http://ieeexplore.ieee.org/document/4500383/>. Cited 2 times in pages 51 and 57.

OKUMURA, K.; TERAI, K.; KISHIMA, A. Solution of ill-conditioned load flow equation by homotopy continuation method. In: *1991., IEEE International Sympoisum on Circuits and Systems*. Kyoto, Japan: IEEE, 1991. p. 2897–2899. ISBN 0-7803-0050-5. Disponível em: <http://ieeexplore.ieee.org/document/176150/>. Cited 3 times in pages 2, 53, and 58.

OLIVEIRA, L. N. de; FREITAS, F. D. Computational impacts of freezing the jacobian matrix in the HKW method for power flow applied to ill-conditioned systems. In: *2021 Workshop on Communication Networks and Power Systems (WCNPS)*. IEEE, 2021. p. 1–6. ISBN 978-1-6654-1078-6. Disponível em: <https://ieeexplore.ieee.org/document/9626286/>. Cited in page 52.

PAN, Z.; WU, J.; DING, T.; LIU, J.; WANG, F.; TONG, X. Load flow calculation for droop-controlled islanded microgrids based on direct Newton-Raphson method with step size optimisation. *IET Generation, Transmission & Distribution*, Institution of

Engineering and Technology, v. 14, p. 4775–4787, 11 2020. ISSN 1751-8687. Disponível em: <https://onlinelibrary.wiley.com/doi/10.1049/iet-gtd.2019.1722>. Cited in page 2.

PANDEY, A.; JEREMINOV, M.; HUG, G.; PILEGGI, L. Improving power flow robustness via circuit simulation methods. In: *2017 IEEE Power & Energy Society General Meeting*. IEEE, 2017. p. 1–5. ISBN 978-1-5386-2212-4. ISSN 19449933. Disponível em: <http://ieeexplore.ieee.org/document/8273753/>. Cited in page 57.

PANDEY, A.; PILEGGI, L. Steady-state simulation for combined transmission and distribution systems. *IEEE Transactions on Smart Grid*, IEEE, v. 11, p. 1124–1135, 3 2020. ISSN 1949-3053. Disponível em: <https://ieeexplore.ieee.org/document/8784416/>. Cited in page 57.

PARK, S.; GLISTA, E.; LAVAEI, J.; SOJOUDI, S. Homotopy method for finding the global solution of post-contingency optimal power flow. In: *2020 American Control Conference (ACC)*. Denver, CO, USA: IEEE, 2020. v. 2020-July, p. 3126–3133. ISBN 978-1-5386-8266-1. ISSN 07431619. Disponível em: <https://ieeexplore.ieee.org/document/9147711/>. Cited in page 56.

POURBAGHER, R.; DERAKHSHANDEH, S. Y. Application of high-order Levenberg-Marquardt method for solving the power flow problem in the ill-conditioned systems. *IET Generation, Transmission & Distribution*, v. 10, p. 3017–3022, 9 2016. ISSN 1751-8695. Disponível em: <https://onlinelibrary.wiley.com/doi/10.1049/iet-gtd.2016.0064>. Cited in page 52.

PURCHALA, K.; MEEUS, L.; DOMMELEN, D. V.; BELMANS, R. Usefulness of DC power flow for active power flow analysis. In: *IEEE Power Engineering Society General Meeting*. IEEE, 2005. v. 1, p. 2457–2462. ISBN 0-7803-9157-8. Disponível em: <http://ieeexplore.ieee.org/document/1489581/>. Cited in page 23.

QI, Y.; SHI, D.; TYLAVSKY, D. Impact of assumptions on DC power flow model accuracy. In: . IEEE, 2012. p. 1–6. ISBN 978-1-4673-2308-6. Disponível em: <http://ieeexplore.ieee.org/document/6336395/>. Cited in page 24.

QIN, N. *Voltage control in the future power transmission systems*. Denmark: Springer, 2017. ISBN 978-3-319-69886-1. Cited in page 10.

RALSTON, A. Runge-Kutta methods with minimum error bounds. *Mathematics of Computation*, v. 16, p. 431–437, 1962. ISSN 0025-5718. Disponível em: <https://www.ams.org/mcom/1962-16-080/S0025-5718-1962-0150954-0/>. Cited in page 27.

SHAHRIARI, A.; MOKHLIS, H.; BAKAR, A. H. A.; KARIMI, M.; ILLIAS, H. A. Application of state space search method to find a low voltage solution for ill-conditioned system. *Przeglad Elektrotechniczny*, v. 88, n. 12 A, p. 247–250, 2012. Disponível em: <https://eprints.um.edu.my/7809/>. Cited in page 52.

SHAMPINE, L. F. Some practical Runge-Kutta formulas. *Mathematics of Computation*, v. 46, p. 135–150, 1986. ISSN 0025-5718. Disponível em: <https://www.ams.org/mcom/1986-46-173/S0025-5718-1986-0815836-3/>. Cited in page 27.

STEVENSON JR., W. D. *Elementos de análise de sistemas de potência*. 2. ed. São Paulo: McGraw-Hill, Inc, 1986. Cited 3 times in pages 12, 16, and 21.

STOTT, B. Review of load-flow calculation methods. *Proceedings of the IEEE*, v. 62, n. 7, p. 916–929, 1974. ISSN 0018-9219. Disponível em: <https://ieeexplore.ieee.org/document/1451474>. Cited 2 times in pages 51 and 57.

STOTT, B.; ALSAC, O. Fast decoupled load flow. *IEEE Transactions on Power Apparatus and Systems*, PAS-93, p. 859–869, 5 1974. ISSN 0018-9510. Disponível em: <http://ieeexplore.ieee.org/document/4075431/>. Cited 2 times in pages 20 and 51.

STOTT, B.; JARDIM, J.; ALSAC, O. DC power flow revisited. *IEEE Transactions on Power Systems*, v. 24, p. 1290–1300, 8 2009. ISSN 0885-8950. Disponível em: <http://ieeexplore.ieee.org/document/4956966/>. Cited 2 times in pages 23 and 24.

SUN, Z.; REN, G.; XU, S.; MA, G.; JATSKEVICH, J. Six-step operation with multistep predictive control using the trapezoidal method for traction PMSM drives. *IEEE Transactions on Power Electronics*, Institute of Electrical and Electronics Engineers Inc., v. 39, p. 3486–3497, 3 2024. ISSN 0885-8993. Disponível em: <https://ieeexplore.ieee.org/document/10323201/>. Cited in page 26.

TARANTO, G. N.; PONTES, C. E.; CAMPELLO, T. M.; ALMEIDA, V. A.; GRAHAM, J.; ESMERALDO, P. C.; SCHICONG, M. Power flow control for an embedded HVDC link to integrate renewable energy in Brazil. *Electric Power Systems Research*, Elsevier Ltd, v. 211, p. 108504, 10 2022. ISSN 03787796. Disponível em: <https://doi.org/10.1016/j.epsr.2022.108504>. Cited in page 1.

TAYLOR, D.; TREECE, J. Load flow analysis by the Gauss-Seidel method. In: *Symp. on Power Systems Load Flow Analysis*. [S.l.: s.n.], 1967. Cited 2 times in pages 51 and 57.

TINNEY, W.; HART, C. Power flow solution by Newton's method. *IEEE Transactions on Power Apparatus and Systems*, PAS-86, p. 1449–1460, 11 1967. ISSN 0018-9510. Disponível em: <http://ieeexplore.ieee.org/document/4073219/>. Cited 3 times in pages 12, 51, and 57.

TOSTADO, M.; KAMEL, S.; JURADO, F. Developed Newton-Raphson based predictor-corrector load flow approach with high convergence rate. *International Journal of Electrical Power and Energy Systems*, Elsevier, v. 105, p. 785–792, 1 2019. ISSN 01420615. Disponível em: <https://doi.org/10.1016/j.ijepes.2018.09.021>. Cited in page 52.

TOSTADO, M.; KAMEL, S.; JURADO, F. An effective load-flow approach based on Gauss-Newton formulation. *International Journal of Electrical Power and Energy Systems*, Elsevier, v. 113, p. 573–581, 3 2019. ISSN 01420615. Disponível em: <https://doi.org/10.1016/j.ijepes.2019.06.006>. Cited in page 52.

TOSTADO, M.; KAMEL, S.; JURADO, F. Several robust and efficient load flow techniques based on combined approach for ill-conditioned power systems. *International Journal of Electrical Power and Energy Systems*, Elsevier, v. 110, n. February, p. 349–356, 2019. ISSN 01420615. Disponível em: <https://doi.org/10.1016/j.ijepes.2019.03.035>. Cited 3 times in pages 52, 54, and 58.

TOSTADO-VÉLIZ, M.; ALHARBI, T.; ALRUMAYH, O.; KAMEL, S.; JURADO, F. A novel power flow solution paradigm for well and ill-conditioned cases. *IEEE Access*, v. 9, p. 112425–112438, 2021. Disponível em: <https://ieeexplore.ieee.org/abstract/document/9505675>. Cited in page 2.

TOSTADO-VÉLIZ, M.; KAMEL, S.; JURADO, F. Development of combined Runge-Kutta Broyden's load flow approach for well- and ill-conditioned power systems. *IET Generation, Transmission & Distribution*, v. 12, p. 5723–5729, 11 2018. ISSN 1751-8695. Disponível em: <https://onlinelibrary.wiley.com/doi/10.1049/iet-gtd.2018.5633>. Cited 2 times in pages 52 and 58.

TOSTADO-VÉLIZ, M.; KAMEL, S.; JURADO, F. Comparison of various robust and efficient load-flow techniques based on Runge-Kutta formulas. *Electric Power Systems Research*, v. 174, p. 105881, 9 2019. ISSN 03787796. Disponível em: <https://doi.org/10.1016/j.epsr.2019.105881>. Cited in page 27.

TOSTADO-VÉLIZ, M.; KAMEL, S.; JURADO, F. Development of different load flow methods for solving large-scale ill-conditioned systems. *International Transactions on Electrical Energy Systems*, v. 29, p. e2784, 4 2019. ISSN 2050-7038. Disponível em: <https://onlinelibrary.wiley.com/doi/10.1002/etep.2784>. Cited in page 52.

TOSTADO-VÉLIZ, M.; KAMEL, S.; JURADO, F. *Matpower Ill-conditioned systems v1*. Zenodo, 2019. Disponível em: <https://doi.org/10.5281/zenodo.3514739>. Cited 4 times in pages 77, 78, 79, and 112.

TOSTADO-VÉLIZ, M.; KAMEL, S.; JURADO, F. *Matpower Limit cases v1*. Zenodo, 2019. Disponível em: <https://doi.org/10.5281/zenodo.3491654>. Cited 2 times in pages 80 and 112.

TOSTADO-VÉLIZ, M.; KAMEL, S.; JURADO, F. An efficient power-flow approach based on Heun and King-Werner's methods for solving both well and ill-conditioned cases. *International Journal of Electrical Power and Energy Systems*, Elsevier, v. 119, p. 105869, 1 2020. ISSN 01420615. Disponível em: <https://doi.org/10.1016/j.ijepes.2020.105869>. Cited 5 times in pages 2, 25, 28, 52, and 53.

TOSTADO-VÉLIZ, M.; KAMEL, S.; JURADO, F. A powerful power-flow method based on composite Newton-Cotes formula for ill-conditioned power systems. *International Journal of Electrical Power and Energy Systems*, Elsevier, v. 116, p. 105558, 2020. ISSN 01420615. Disponível em: <https://doi.org/10.1016/j.ijepes.2019.105558>. Cited in page 58.

TOSTADO-VÉLIZ, M.; KAMEL, S.; JURADO, F. A sixth order power flow technique for large-scale well and ill-conditioned cases. *IET Generation, Transmission & Distribution*, 2020. [Preprint]. Cited 3 times in pages 2, 52, and 53.

TOSTADO-VÉLIZ, M.; KAMEL, S.; JURADO, F. Power flow solution of ill-conditioned systems using current injection formulation: Analysis and a novel method. *International Journal of Electrical Power & Energy Systems*, v. 127, p. 106669, 5 2021. ISSN 01420615. Disponível em: <https://doi.org/10.1016/j.ijepes.2020.106669>. Cited 2 times in pages 52 and 58.

TRIPATHY, S. C.; PRASAD, G. D.; MALIK, O. P.; HOPE, G. S. Load-flow solutions for ill-conditioned power systems by a Newton-like method. *IEEE Power Engineering Review*, PER-2, p. 25–26, 10 1982. ISSN 0272-1724. Disponível em: <https://ieeexplore.ieee.org/document/5519878/>. Cited 2 times in pages 52 and 58.

WARD, J. B.; HALE, H. W. Digital computer solution of power-flow problems. *Transactions of the American Institute of Electrical Engineers. Part III: Power Apparatus and Systems*, v. 75, n. 3, p. 398–404, 1956. Cited 2 times in pages 51 and 57.

WATSON, L. T. Globally convergent homotopy methods: A tutorial. *Applied Mathematics and Computation*, v. 31, p. 369–396, 5 1989. ISSN 00963003. Disponível em: <https://doi.org/10.1016/0096-3003(89)90129-X>. Cited in page 42.

WENG, Z. X.; SHI, L. B.; XU, Z.; YAO, L. Z.; NI, Y. X. N.; BAZARGAN, M. Effects of wind power variability and intermittency on power flow. In: *IEEE Power and Energy Society General Meeting*. San Diego, CA, USA: [s.n.], 2012. p. 1–7. Disponível em: <https://ieeexplore.ieee.org/abstract/document/6344727>. Cited in page 1.

WOOD, A. J.; WOLLENBERG, B. F.; SHEBLÉ, G. B. *Power generation, operation, and control*. [S.l.]: John Wiley & Sons, 2013. Cited in page 24.

YAN, P.; SEKAR, A. Study of linear models in steady state load flow analysis of power systems. In: *2002 IEEE Power Engineering Society Winter Meeting. Conference Proceedings (Cat. No.02CH37309)*. IEEE, 2002. v. 1, p. 666–671. ISBN 0-7803-7322-7. Disponível em: <http://ieeexplore.ieee.org/document/985087/>. Cited in page 24.

ZANETTA JR., L. C. *Fundamentos de sistemas elétricos de potência*. [S.l.]: Editora Livraria da Física, 2006. Cited 6 times in pages 8, 11, 12, 16, 21, and 22.

ZHAO, T.-Q.; DENG, J.-J.; KOYANAGI, K. Homotopy-enhanced power flow methods for general distribution networks with distributed generators. In: *2013 IEEE International Symposium on Circuits and Systems (ISCAS2013)*. School of Electrical Engineering and Automation, Tianjin University, Tianjin, China: IEEE, 2013. p. 1536–1539. ISBN 978-1-4673-5762-3. Disponível em: <http://ieeexplore.ieee.org/document/6572151/>. Cited 2 times in pages 55 and 58.

ZIMMERMAN, R. D.; MURILLO-SÁNCHEZ, C. E. Matpower 6.0 users manual. *Power Systems Engineering Research Center*, v. 9, 2016. Cited in page 74.

ZIMMERMAN, R. D.; MURILLO-SÁNCHEZ, C. E. *Matpower*. 2020. Cited 5 times in pages 4, 75, 76, 77, and 85.

ZIMMERMAN, R. D.; MURILLO-SANCHEZ, C. E.; THOMAS, R. J. Matpower: Steady-state operations, planning, and analysis tools for power systems research and education. *IEEE Transactions on Power Systems*, v. 26, p. 12–19, 2 2011. ISSN 0885-8950. Disponível em: <http://ieeexplore.ieee.org/document/5491276/>. Cited 5 times in pages 24, 53, 68, 74, and 75.

APPENDIX A

THE 2-PARAMETER HOMOTOPY STATIC PROBLEM

Suppose we have an original network and another that is modified by the two parameters of homotopy h_1 and h_2, with discrete values h_{1i}, $i = 0,1,2,\ldots,N_1$ and h_{2k}, $k = 0,1,2,\ldots,N_2$. The original network is modified along the homotopy path, through changes in h_1 and h_2. The changes emanate from a flat start guess, $\mathbf{x}^{(0)}$, which also coincides with the solution for the starting homotopy path point, denoted by $\mathbf{x}^{[0,0]}$, when $h_1 = h_2 = 0$, up to reach a final state in the path, labeled $\mathbf{x}^{[N_1,N_2]}$, for $h_1 = h_2 = 1$. Figure A.1 illustrates a hypothetical homotopy path sketch for the case when $N_1 = 8$ and $N_2 = 1$. In this example, the initial solution of the path is $x^{[0,0]} = x^{(0)}$, while the last point is the solution $\mathbf{x}_*$ for the algebraic equation $\mathbf{f}(\mathbf{x}) = 0$ of the original network.

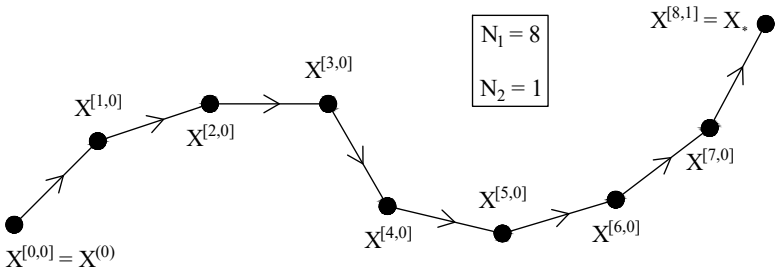

Figure A.1: Illustration for a hypothetical homotopy path sketch for two parameters h_1 and h_2, where $N_1 = 8$ and $N_2 = 1$

The key modification on the network involves operations in the diagonal of the admittance matrix and impedances connecting the slack bus. The changes in the diagonal are performed through the insertion of fictitious shunt admittances adequately adjusted to give flat start solution for the initial point of the homotopy problem. This specific control is performed by modifying only the parameter h_1. Supplementary, the network is modified through the insertion of reinforcement in impedances near the slack bus neighborhood for improving the convergence along the homotopy path. This specific reinforcement, case necessary, is introduced

by a scaling factor δ multiplying an impedance which is regulated by the homotopy parameter h_2. The process occurs as described in the sequence.

Let $\bar{Y}_{kk}$ be a diagonal entry of the original admittance matrix $\mathbf{Y}_{BUS}$. Then, a convex homotopy (CHIANG; WANG, 2018) is adopted as follows. Firstly, the homotopy parameter, h_1, $0 \leq h_1 \leq 1$, is applied to compute a fictitious and parametric dependent diagonal element as

$$\hat{Y}_{kk} = h_1 \bar{Y}_{kk} + (1 - h_1)(g_k + jb_k), \;\; k \in PQ \; bus \text{ when } h_2 = 0, \tag{A.1}$$

in which for PV-bus, b_k is set to zero and no change is needed for the slack bus.

The parameter h_2 is used to modify the impedances $z_{km} \in \Omega_s$ of interconnections around the slack bus and assumes only two values, $h_2 = 0$ or $h_2 = 1$ (*i.e.*, N_2 is always equals 1). The homotopy process produces the modified impedance

$$\hat{z}_{km} = h_2 z_{km} + (1 - h_2)\delta z_{km} \tag{A.2}$$

in which $\delta \in \mathbb{R}$, $0 < \delta \leq 1$ is a factor introduced artificially by the user. This procedure acting with h_2 helps to artificially reinforce links with the slack bus and so strengthen the interconnections when large changes of power flow are required due to a given value of the other parameter h_1. But, it is removed for $h_1 = 1$ because the reinforcement is no longer necessarily justified by the fact that the point in the homotopy path $\mathbf{x}^{[N_1-1,0]}$ is closer to the final point $\mathbf{x}^{[N_1,1]}$. Changes on other interconnections with h_2 are unnecessary since the generation at the other buses supply artificially changes in the loads due to the modification in h_1. Therefore changes in the interconnections also follow what was planned to keep the equilibrium load-generation. However, losses can be different and need to be compensated by the slack bus in high amounts or even with the reverse flow along the generation of the homotopy path by solving a PFP for a required point.

Then, considering

- the inclusion of the fictitious shunt admittances for modifying a diagonal entry $\hat{Y}_{kk}$; and
- the value of branch admittances $\hat{y}_{km} = 1/\hat{z}_{km} \in \Omega_s$, (see Freitas & Silva (2022) for details), and modified as $\hat{z}_{km} = \delta z_{km}$, with $\delta \leq 1$, when $h_2 < 1$ and $\delta = 1$ for $h_2 = 1$,

an updated admittance matrix $\hat{\mathbf{Y}}_{BUS}$ is calculated with the changes promoted by h_1 and h_2

and used for the execution of the PFP via the NR method along the homotopy path. Note that $\hat{\mathbf{Y}}_{BUS} = \mathbf{Y}_{BUS}$ for $h_1 = 1$ and $h_2 = 1$.

Assuming that $N_1 = N$, then the total number of points at the homotopy path which requires the solution computation of a PFP is N. The justification is based on the fact that the initial point has solution $\mathbf{x}^{[0,0]}$ exactly equal to the initial estimate $\mathbf{x}^{(0)}$, according to the suggestion in Freitas & Silva (2022). Hence, the solution for the initial point is trivial, $\mathbf{x}^{[0,0]} = \mathbf{x}^{(0)}$. The intermediate path homotopy points up to $(N-1)$ are modified only by changes in h_1 and considering $\hat{z}_{km} = \delta z_{km}$. In the last point, h_2 is switched to 1, while h_1 also has reached the unitary value (*i.e.*, $N_1 = N$) and $\hat{z}_{km} = z_{km}$. Therefore, N points along the homotopy path need to be calculated. Following this interpretation, the total iterations for the NR solvers to generate the homotopy path is $iter_h = N \sum_{i=1}^{N} iter_{hi}$, where $iter_{hi}$ is the number of iterations for convergence with tolerance ϵ_h of the NR solver at the point i of the homotopy path.

APPENDIX B

EXAMPLE CONSIDERING MULTIPLE SLACKS NETWORK TOPOLOGY

Homotopy is a robust tool for modeling several types of statuses of components as well as controlling laws. Among the applications is modeling multiple slacks in isolated systems in just one fictitious equivalent slack, which is interesting for studies of system islanding. Other applications include contingencies, such as situations where interconnections are open or closed for some reason, modeling of asynchronous HVDC, etc.

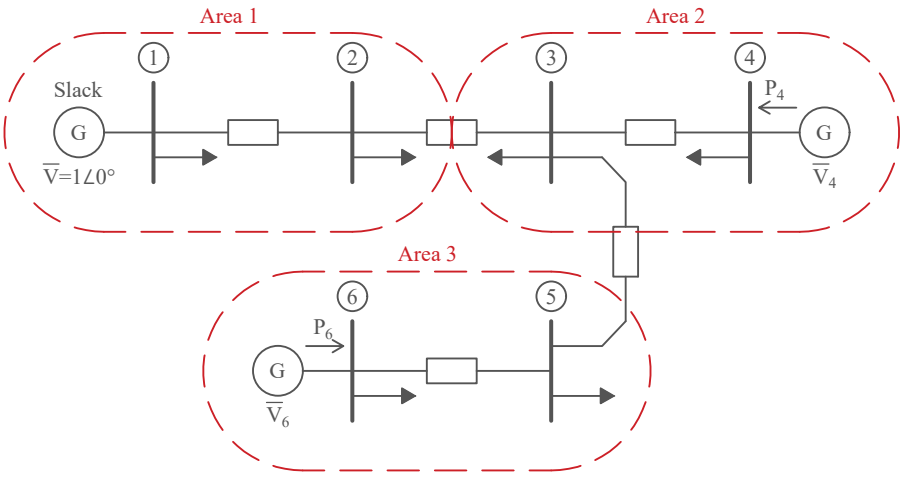

Figure B.1: Synchronous system represented by three interconnected areas

Figure B.1 exhibits an online diagram of a synchronous system composed of three connected areas. Contingencies resulting in the permanent opening of the interconnections 2-3 and 3-5 simultaneously lead to the electrical separation of the three regions. In principle, as the system initially had only one slack bus, conventional techniques for solving a power flow would require two other slack buses. However, applying homotopy, even with the opening of the interconnections, it is possible to simulate fictitious connections between area 1, where, for example, was defined as slack. This way, the execution of the PFP would follow the same pattern as a conventional power flow with just an area or synchronous system. Figure B.2,

based on an online diagram, illustrates the possibility of a new configuration for the artificial system resulting from the fictitious connections.

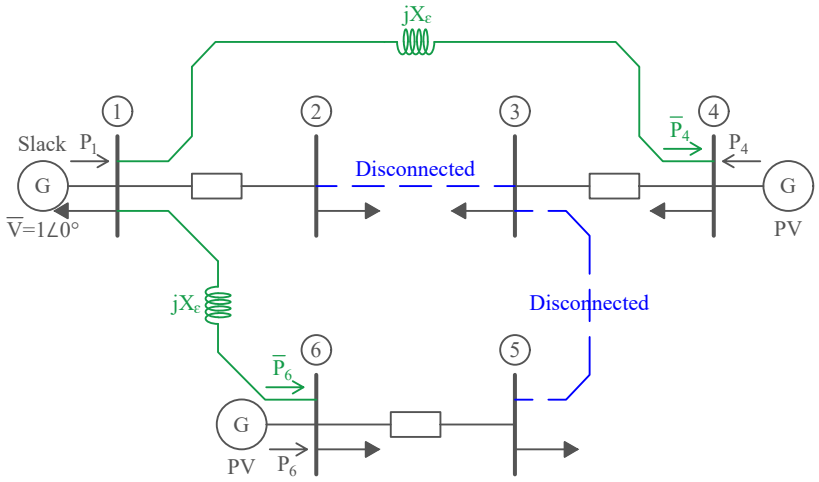

Figure B.2: System represented by three disconnected areas and fictitious reactance connecting the isolated areas

The isolated system analyzed from the point of view of a synthetic synchronous grid can be interpreted as follows. According to the online diagram in Figure B.2, after islanding, although the slack bus generates active power $P_T = P_1 + \overline{P}_4 + \overline{P}_6$, as a matter of fact, only $P_{g1} = P_1$ is the effective generation for the isolated area 1. In the situation of area 2, the effective generation P_4 must be complemented by the artificial active power $\overline{P}_4$. Therefore, physically, generation at bus 4 must be $P_{g4} = P_4 + \overline{P}_4$. This result for P_{g4} would be the power generation to compensate for the lack of a slack bus in the area. However, In this case, it must be verified whether the generation in the area meets the required conditions. In a negative case, load shedding must be implemented in the area. A similar remark can be made for the generation in bus 6. In all cases, the slack buses in areas 2 and 3 were transformed into PV buses, keeping the same specified magnitude voltage. But another alternative would also be to use them as PQ buses. In this case, the voltage magnitude is free to change.

For the situation where the objective is the disconnection of circuits, the configuration network changes can be done using homotopy by setting the desired admittance to be turned off as $y_{km} = g_{km} + jb_{km}$, $\hat{y}_{km}(1-h)y_{km}$ while the connection between slack and the other PV bus, as $\hat{\mathbf{x}}_\varepsilon = h\mathbf{x}_\varepsilon$.

Three isolated areas were connected for the grid represented in the original `case82k`. Modifications were performed to assign just one slack bus in area 1. The other original slack buses

in areas 2 and 3 were converted into PV or PQ buses. To preserve the same voltage assigned to the slacks in areas 2 and 3, they were replaced by a transformer with complex taps and reactance X_t instead of only single reactances. In the original system, for the purpose of the changing, the voltages assigned to the three slack buses were $\overline{V}_1 = 1.0\angle 0^o$, $\overline{V}_2 = 1.043\angle 67.91^o$, and $\overline{V}_3 = 1.043\angle -49.41^o$. Then, the suggested transformers in the interconnections were:

- link 1 - 2: $x_\varepsilon = 10^{-6}$; $tap = (1/1.043)\angle -67.91^o$;
- link 1 - 3: $x_\varepsilon = 10^{-6}$; $tap = (1/1.043)\angle 49.41^o$.

The taps' information is according to MATPOWER's input branch data $k - m$, where the notation for tap is $a : 1$, and the complex tap a is referenced at the side of bus k.

APPENDIX C

A GENERIC TUTORIAL EXAMPLE OF DYNAMIC HOMOTOPY INITIALIZATION

To better understand the application of the concepts, a tutorial example from Freitas & Oliveira (2023a) was proposed before applying the details to large-scale ill-conditioned power system models. The problem consists of finding the roots of the nonlinear equation generic system represented by $f_1(x_1,x_2) = x_1^2 + x_2^2 - 2x_1x_2 - 1 = 0$, $f_2(x_1,x_2) = x_1 + x_2 - 2 = 0$, $\mathbf{f}(x_1,x_2) = [f_1(x_1,x_2) \;\; f_2(x_1,x_2)]^T$, and $\mathbf{x} = [x_1 \; x_2]^T$.

In order to iteratively solve the system, an initial estimate $\mathbf{x}^{(0)} = [1 \;\; 1]^T$ is assigned. Note that at this point, the Jacobian matrix is singular. However, in the neighborhood of $\mathbf{x}^{(0)}$, the singularity disappears for other points. Then, to eliminate the singularity at $\mathbf{x}^{(0)}$, it was proposed by Freitas & Oliveira (2023a) to replace one of the variable values with the same value incremented by a small value ϵ, for example, $x_2^{(0)} = 1-\epsilon$. The Newton-Raphson solver has been found to not converge without the added perturbation. Additionally, achieving convergence may be difficult depending on the specific value of ϵ. However, the dynamic homotopy-based technique addresses this issue by incorporating the explicit and implicit integration methods we have previously discussed, along with any necessary adjustments.

Two different approaches were used for simulations: one using only the classical NR scheme, starting from $\mathbf{x}^{(0)}$; and the other using a combination of the dynamic homotopy-based method and the NR solver. By this latter, the NR solver uses $\hat{\mathbf{x}}^{(0)} = \mathbf{x}(t)|_{t=1}$ as the initial guess, which was obtained previously by a dynamic homotopy numerical scheme.

When the NR is used starting directly from $\mathbf{x}^{(0)}$, it was investigated with different values of ϵ to modify only the entry $\mathbf{x}_2^{(0)}$.

In the hybrid approach, an integration method is initially used to calculate a partial result at $t = 1$, generating $\hat{\mathbf{x}}^{(0)} = \mathbf{x}(t)|_{t=1}$. This partial result is used as a guess for the classical NR

solver to compute the high-accuracy solution $\mathbf{x}_*$.

The integration methods FE, BE, and RK2, were used as proposed previously. In all dynamic homotopy simulations, the initial time step $\Delta t_0 = 0.01$ produces the first step $t_1 = 0.01$. The subsequent steps $t_k > t_1$, $k = 2,3,\ldots$ were determined by a constant time step, denoted as Δt. Two different types of simulations were run with constant values for Δt: 0.5 and 0.125. In addition, the value of K was varied, with the following values: 0.005, 0.01, and 0.05. For all simulations using dynamic homotopy, the results were initially computed at time t_1 using only the BE solver, or equivalently, by using the linear approximation for the static homotopy equation. Then, the states obtained at time t_1 were used as the starting point for the FE, BE, and RK2 numerical integration solvers for $t_k > t_1$, $k = 2,3,\ldots$ with a given Δt. Figure C.1 illustrates the mismatch plots for the simulations. In Figure C.1(a), the plots for results were obtained using only the NR solver, while the other subfigures exhibit the plot visualizations for the hybrid approach, considering constant step-time $\Delta t = 0.5$. Convergence was achieved for all simulations and, after using the NR solver, reached the refined values $x_{1_*} = 1.5$ and $x_{2_*} = 0.5$ with a tolerance for the mismatch of 10^{-5}.

The analysis of the results shows that when the NR solver departs directly from the original estimate $\mathbf{x}^{(0)}$ with $x_2^{(0)} = 1 + \epsilon$, the mismatches initially experience a sudden increase for any perturbation value ϵ, and then gradually decrease with each iteration. A minimum of 9 to 11 iterations were necessary to achieve a tolerance of 10^{-5} in these experiments. In the hybrid approach (refer to Figures C.1(b), C.1(c) and C.1(d)), the NR solver utilizes the result obtained for the point when $t = 1$. The discrete intermediate points in the plots for the range 0 to 1 refer to results obtained from the dynamic homotopy solvers. With the enhancements introduced by the homotopy solvers, the Newton-Raphson solver exhibits improved convergence behavior, consistently achieving convergence within a maximum of 8 iterations across a range of values for the parameter K. This enhanced performance is observed when the NR solver is utilized in conjunction with the FE, BE, and RK2 solvers. In all cases, the best performance was observed with the BE (implicit form) solver, which required no more than 3 iterations to reach a solution. The explicit forms (FE and RK2) also achieved the solution with fewer iterations than the NR solver properly when starting directly from $\mathbf{x}^{(0)}$.

Another set of experiments was accomplished to verify the influence of the time-step Δt,

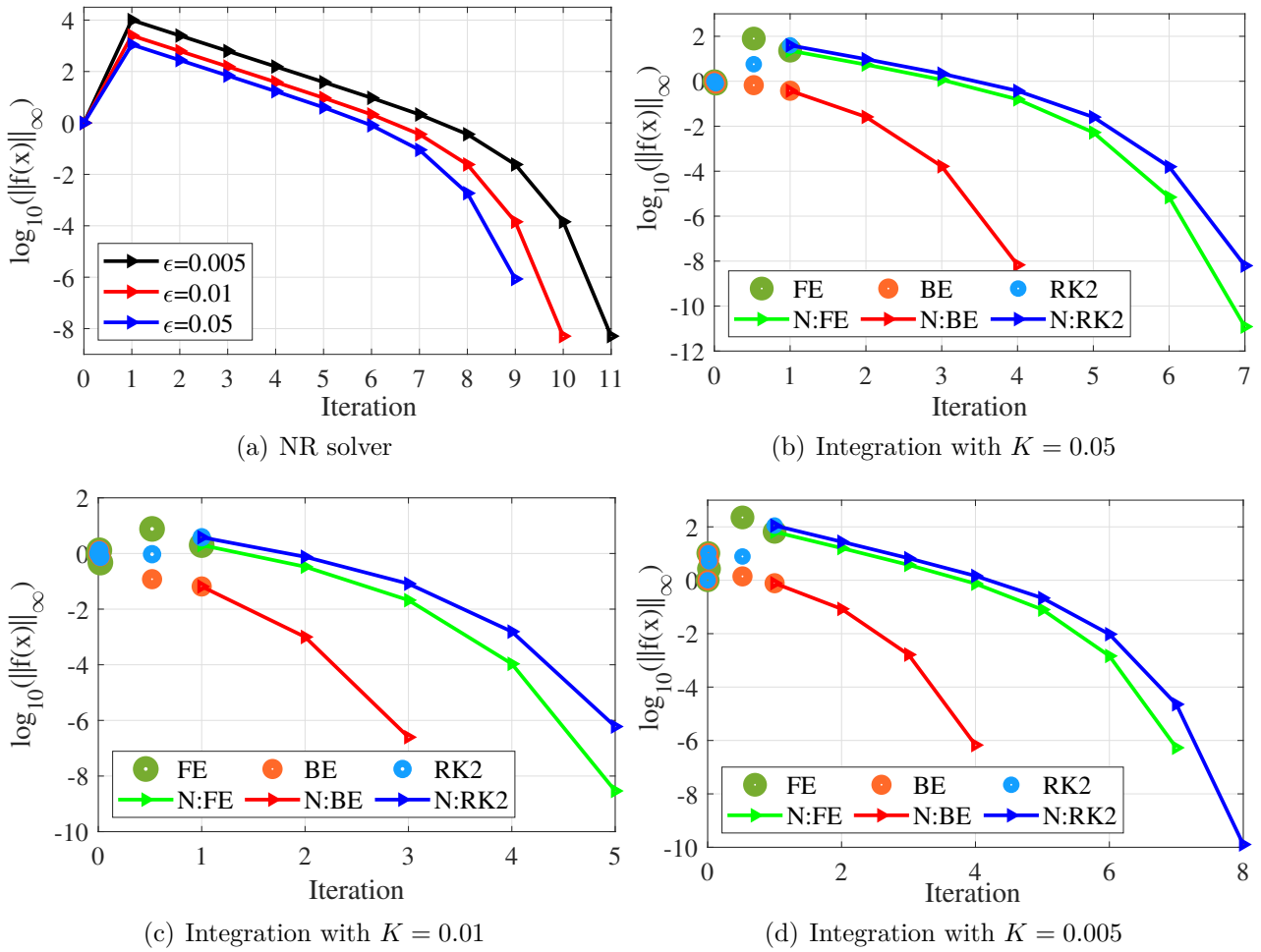

(a) NR solver

(b) Integration with $K = 0.05$

(c) Integration with $K = 0.01$

(d) Integration with $K = 0.005$

Figure C.1: Results determined by using only NR and a combination of dynamic homotopy, with $\Delta t = 0.5$, and the NR solver

keeping the same step initial, $t_1 = 0.01$, and using $K = 0.05$. For this case, a constant value $\Delta t = 0.125$ was set. Figure C.2 depicts plots for the hybrid approach involving the experiments.

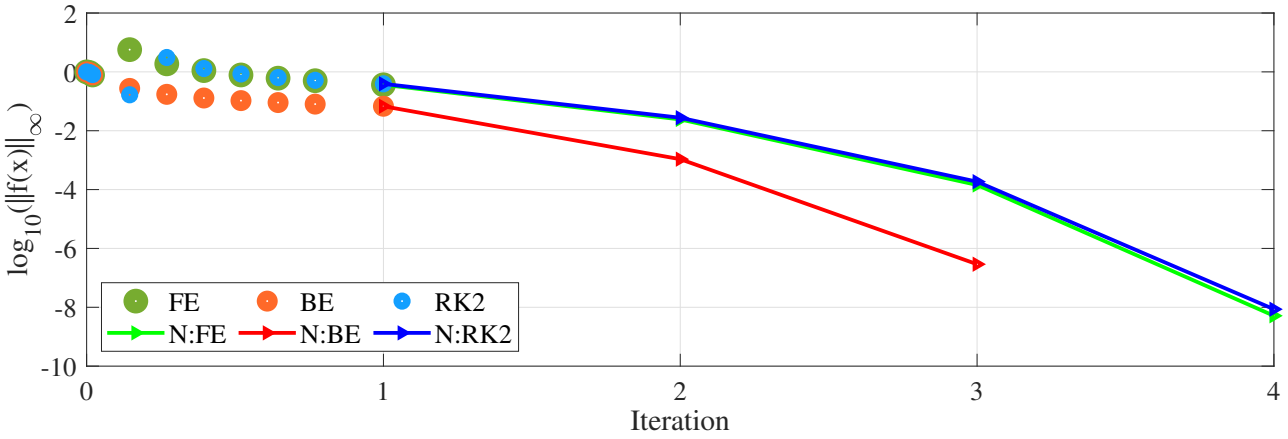

Figure C.2: Integration solver performance when a smaller time-step $\Delta t = 0.125$ was adopted after the step $t_1 = 0.01$

From Figure C.2, we can confirm that the behavior observed in the results shown in Figure C.1 was maintained. However, the explicit solvers now require fewer iterations to achieve a highly accurate solution using the NR method. The BE solver did not show a significant improvement compared to its performance with a high time-step size, but it still outperformed the other dynamic homotopy solvers.